MICELLAR AGGREGATION AND CHARGE EFFECTS ON SOLUBILIZATION

By

YUNG SHING YANG

A thesis submitted in partial fulfillment of the requirements for the degree of

DOCTOR OF PHILOSOPHY

(Pharmacy)

at the

UNIVERSITY OF WISCONSIN-MADISON

1980

MICELLAR AGGREGATION AND CHARGE EFFECTS ON SOLUBILIZATION

A thesis submitted to the Graduate School of the University of Wisconsin-Madison in partial fulfillment of the requirements for the degree of Doctor of Philosophy

by

YUNG SHING YANG

Degree to be awarded: December 19 80 May 19____ August 19____

Approved by Thesis Reading Committee:

Pampati Mukerjee
Major Professor

September 30, 1980
Date of Examination

George Zografi

Kenneth A. Connors

Robert M. Berdahl
Dean, Graduate School

MICELLAR AGGREGATION AND CHARGE EFFECTS ON SOLUBILIZATION

by YUNG SHING YANG

(Under the supervision of Professor Pasupati Mukerjee)

This dissertation is concerned with some investigations on the self-association of surfactants and the solubilization of additives. The main subjects of study were (a) the charge effects on the interactions of some indicator dyes and similar molecules with some long chain surfactants, bile salts, and hydrophilic polymers, (b) the pattern of self-association of some phenothiazine derivatives, and (c) the mutual interactions of long chain hydrocarbon and fluorocarbon surfactants in mixed micelles.

The dissociation constants (K) of two cationic indicator dyes, ethyl red and quinoline blue, solubilized in nonionic micelles of β-D-octyl glucoside and Brij-35 were determined. The pK values were found to be markedly lower than the intrinsic pK values in water. This change was ascribed to different electrostatic image interactions of the dissociated and undissociated dye species at the micelle-water interface. Similar studies in several anionic micellar systems were carried out. The expected change in the apparent pK due to electrostatic potentials of the

micellar surface and the resultant change in the effective surface pH was pronounced and varied with the counterion concentration. This variation was found to be in excellent agreement with predictions from the Gouy-Chapman theory of the electrical double layer. The use of indicator dyes as probes for surface pH changes was investigated further in dodecyl sulfate systems containing a variety of counterions. Pronounced differences were observed. The specific effects of different counterions on the surface pH showed good correlation with similar effects observed on some published rate constants of the acid-catalyzed hydrolysis of methyl orthobenzoate in the same micellar systems.

The spectral changes of the aggregating dye, benzopurpurine 4B, in aqueous solutions of two polyethylene glycols and several Pluronic polyols were investigated and found to be similar. The data could be interpretated in terms of dye-polymer interactions including some cooperative nearest neighbor interactions. There was no need to invoke micelle formation in Pluronic polyols as suggested in the literature.

The pattern of solubilization of the fluorescent compound, 6-p-toluidino-2-naphthalene sulfonate, and an indicator dye, bromthymol blue, in solutions of several

sodium alkyl sulfates and bile salts were examined. In the case of the detergent type surfactants, the pattern of solubilization was found to be consistent with micelle formation which involves surfactant self-association with a high degree of cooperativity. In contrast, sodium cholate, sodium deoxycholate, and sodium chenodeoxycholate, showed a much lower degree of cooperativity. The interactions of these solubilizates with the bile salts appears to involve the formation of a preferential adduct between one solubilizate molecule and six to seven bile salt ions which seems to be relatively independent of the pattern of self-association of the bile salts.

The ^{19}F nuclear magnetic resonances of aqueous solutions of sodium perfluorooctanoate (SPFO), trifluprom azine hydrochloride, and trifluoperazine dihydrochloride were studied. The NMR chemical shifts of the micelle forming SPFO showed the expected sharp transition at the critical micellization concentration (CMC) region but the phenothiazine derivatives did not. On treating the NMR chemical shift data in an appropriate manner, it could be shown that the self-association in the case of the phenothiazines involves a stepwise open-ended association pattern without much cooperativity. This conclusion is consistent with

stacking interactions as expected from their molecular structures.

The mixing properties of fluorocarbon and hydrocarbon surfactant micelles were examined by electrical conductance and ^{19}F NMR measurements. The CMC data indicated that the mixing of SPFO micelles and those of three anionic hydrocarbon surfactants investigated was highly nonideal. The nonideality effects could be adequately described by the regular solution theory. In one case the nonideality was intense enough to cause a microscopic phase separation, i.e., the coexistence of two different kinds of micelles.

Approved Pasupati Mukerjee

Date September 30, 1980

To

My Parents

and

My Wife

ACKNOWLEDGEMENTS

I wish to express my sincere appreciation to:

Professor Pasupati Mukerjee, for his patience and guidance throughout my graduate career. Without his scientific insight this work would be impossible.

Professor George Zografi, for his encouragement, especially during the period when this dissertation was under preparation.

Dr. Gerald S. Brenner, for his understanding and allowing me to complete this work while in residence at Merck Sharp and Dohme Research Laboratories.

My wife, Grace, for her constant encouragement throughout my graduate career, which was essential for the completion of this work.

Special thanks are also to Dr. Karl J. Mysels for providing the conductivity cell and to Mr. James Blackbourn for his technical assistance.

Acknowledgement is also made to the Donors of the Petroleum Research Fund adminstered by the American Chemical Society and to the Public Health Services for partial support of this research.

TABLE OF CONTENTS

Page

Page

LIST OF FIGURE

Figure | Page

Figure | Page

Figure — Page

Figure | Page

LIST OF TABLES

1. INTRODUCTION

1.1. General Introduction

Amphiphilic molecules, containing distinct polar and nonpolar moieties, often exhibit surface activity in solutions and tend to adsorb at air-liquid or solid-liquid interfaces. They also form aggregates in aqueous as well as in some nonaqueous solutions. This class of compound has generally been referred as "surfactants".Solution properties of surfactants have been the subject of many investigations since the early development of detergents. The rapid increase in the applications of surfactants in many different areas has made this type of research of increasing interest in recent years.

Certain types of surfactant (e.g., long-chain detergent-like molecules) tend to form large aggregates containing thirty or more monomers in aqueous solutions above a certain concentration. These aggregates are called "micelles". The definition of micelle has recently been discussed in detail by Mukerjee and Mysels (1,2). Several reviews and monographs on micelle formation (3-5,12,64), micellar solubilization (6-8), and micellar catalysis (9,10,54) have been published. The basic and qualitative features of the currently accepted theory of micelle formation are largely based on the pioneering works of Hartley (11) and later elaborated by many other investigators. The forces

involved in the formation of micelles and the structure of micelle formed in aqueous solutions are, in many respects, similar to the formation and structure of biological lipid bilayer membranes (12). Micellar system has, therefore, been used as a model for bilayer membranes. Catalysis in micellar solution has been proposed as a model for enzymatic reactions (10,13). Several recent studies of photochemical reactions in micellar solutions have indicated that certain photoelectron transfer reactions, ordinarily not feasible in homogeneous bulk solutions, can be achieved in solubilized states. These findings suggest that micellar systems may be useful for conversion and storage of solar energy (14,15).

The solubilization of many normally insoluble substances by aqueous surfactant solutions is a well-known phenomenon. McBain (16,17) first suggested that the mechanism of solubilization in detergent solutions is due to the incorporation of water-insoluble substances into the colloidal, micellar aggregates. Many applications of micellar solubilization have been made in diversified areas. Processes such as the recovery of crude oil from porous rocks (24,206), the use of micelles as carriers for otherwise insoluble drugs (7,18), and organic synthesis via micellar catalysis (9,10,54) are only a few examples.

Although solution properties of surfactants have been studied extensively, many questions regarding the detailed

structure of aggregates formed by different types of surfactants, the effects of solubilized species upon the properties of micelles or surfactant aggregates in general, the location and orientation of solubilized species in surfactant aggregates, and the relationship between the structure of solubilized species and their solubility in micelles have not received unequivocal answers. In this report, some of the basic properties related to surfactants and their aggregates formed in aqueous solutions are examined: (i) the effects of charges on the solubilization of organic dyes in micelle-forming and nonmicelle-forming surfactants, (ii) the different patterns of self-association exhibited by surfactants of different structural types (i.e., flexible long chain surfactants, phenothiazines and salts of bile acids), and (iii) the mutual interactions of hydrocarbon and fluorocarbon long-chain-type surfactants in mixed micelles.

1.2. Aggregation Properties of Surfactants

Surfactants can be ionic, nonionic, or zwitterionic depending upon the polar groups on the molecule. In aqueous solutions, these molecules exhibit surface activity and tend to form aggregates via either self-association or mutual (mixed) association (5,25). The driving force for surfactant aggregation in aqueous solution comes mainly from the hydrophobic interactions of the nonpolar part of

the molecule (25,27). These forces are opposed by the repulsive interactions between polar groups of the surfactant molecules (25,26,58) and also the interactions between the polar groups and the nonpolar core of the micelles (27, 28). Under normal conditions, monomers and micelles are in rapid dynamic equilibrium. The exchange frequency of the monomer between the bulk solution and the aggregate is faster than 10^4 per second (29,55). As a result, only one nuclear magnetic resonance (NMR) signal is observed for each absorbing nucleus in a surfactant solution containing both monomer and aggregate. Because of the short-range characteristics of hydrophobic interactions, the molecular structure of the surfactant plays an important role both in the formation of the aggregate and the pattern of aggregation. Commonly observed surfactants can be classified into four different broad classes based on their structures (25): (I) flexible long-chain compounds, (II) compounds with rigid aromatic or heteroaromatic ring or fused ring structures, (III) alicyclic fused ring systems which are rigid but not planar, and (IV) macromolecules, such as proteins, enzymes, and some water soluble synthetic polymers.

1.2.1. Flexible Long Chain Surfactants

Compounds with a flexible, long hydrophobic chain and a polar head group are typical micelle-forming surfactants.

At low concentration in water, these surfactants exist mostly as monomers. As concentration increases to the CMC level, large numbers of the surfactant molecules aggregate spontaneously to form micelles with their polar groups exposed to water and the nonpolar, hydrophobic chains, forming a core. Micelles thus formed are roughly spherical in shape in many systems but can be asymmetric in others. When concentration is further increased above the CMC, almost all additional surfactants form micelles and the concentration of the monomer remains approximately the same. For many practical purposes, the monomer concentration can be assumed to be equal to the CMC and the concentration of the micellized surfactant can be calculated from the total surfactant concentration. The CMC of a surfactant decreases with increasing length of the hydrophobic chain. It is also generally lower for nonionic than for ionic surfactants of the same chain length. Micelles formed in water usually contain 30 or more monomers. Addition of salt increases the size of ionic micelles and reduces the CMC by reducing interionic repulsions between the head groups (26,30). Effects of the addition of salt on nonionic micelles are relatively small (31). At high concentrations of surfactant or added salt, spherical micelles sometimes grow and elongate to rod-like micelles (27). At even higher concentration lamellar micelles

and, finally, liquid crystal phases may also form and separate from the solution. Applications of micellar solutions in solubilization and catalysis are usually in the concentration range of isotropic solutions.

1.2.2. Surfactants of Rigid Aromatic, Heteroaromatic or Fused Ring Structures

Compounds of this class differ from the long chain surfactants by the absence of a polar or nonpolar end. They are roughly symmetrical with respect to their hydrophobicity on both sides of their planar or nearly planar structures. These molecules are thus capable of forming open ended stacking aggregates in a roughly linear array (25,32). Many dye molecules, e.g., cationic cyanine dyes and anionic azo dyes, are typical examples. (32,33). A large number of drug molecules, such as phenothiazine tranquilizers and structurally related compounds, are also likely to fall in this class (32,34,35,36,37). The ring structures of these compounds tend to be less hydrophobic in general than hydrocarbon chains of similar molecular weight. Their tendency towards association and the structures of the stacked aggregates are affected by their molecular geometry and the distribution of polar and nonpolar groups attached to the ring systems. Compounds of this class are also likely to exhibit rather different patterns of association from that of flexible chain surfactants. The cationic methylene blue dye, which is also an analog of phenothiazine,

was investigated in detail by Mukerjee and Ghosh (32,38,39, 40,41). Several different models of association were examined and compared with experimental results. The general conclusion was that the planar methylene blue shows a very different pattern of self-association from that of long chain surfactants. A continuous stepwise association with roughly similar association constant was indicated. Similar association behavior has also been suggested for many purine and pyridine bases of nucleosides (42). Such self-association phenomena are likely to be important in processes such as dyeing, drug binding and drug transport which are mainly controlled by the monomer activity and are thus affected by the self-association.

1.2.3. Surfactants of Alicyclic Fused Ring Structure

Bile acids, cholesterol, and many steroidal antibiotics, e.g., fusidic acid and helvolic acid, contain fused alicyclic ring systems, in which the polar groups are directed away from the backbone of the tetrahedral carbon atoms to one side or the other. In many cases, one side of the moleucle is more hydrophobic than the other. These compounds represent another class of surfactants. Aggregation of these surfactants, based on the effects of hydrophobic interactions, requires that the hydrophobic sides of the moleucle be put in contact with one another and the relatively polar side of the moleucle be exposed to water(25,43).

Due to the rigidity and nonplanar structure of these molecules, formations of dimers and small oligomers containing limited numbers of monomers have been proposed for bile acids and their salts (43-46). The detailed structures of the aggregates formed by this class of surfactants and their patterns of association are not entirely clear(44,46). This class of surfactants has many important biological actions have not been fully understood, the relationship between their surface activity, solubilization properties, and physiological functions have been explored qualitatively in several cases, e.g., in fate absorption (47,48), elemination of drug substances through the biliary route of excretion (49,50), and control of membrane structure by altering the output of cholesterol and phospholipids (49).

1.2.4. Macromolecules

Macromolecules, including naturally occurring and synthetic polymers, form another important class of self-associating solutes. Many proteins and enzymes with hydrophobic side groups are capable of forming aggregates. Their biological activities may be altered by either covering or uncovering the active functional groups during aggregation (51-53). In synthetic polysoaps, which are

polyelectrolytes with covalently attached long hydrophobic chains, the hydrophobic chains may form intramolecular clusters similar to micelles of flexible chain surfactants (56). The hydrophilic backbone of the polymer serves as the polar exterior. Hydrophilic homopolymers, e.g., polyethylene glycols, polyvinylpyrrolidone, and block copolymers, e.g., pluronic polyols, are commonly used as food and drug additives. Such polymers may exhibit strong surface activity at relatively low concentrations. However, they only show moderate solubilizing ability (19, 20,21). These solutes are seldom capable of forming large aggregates, such as micelles, because of the absence of large hydrophobic moieties in their polymeric segments.

1.3. Patterns of Surfactant Self-Association

Self-association of surfactants generally involves very complicated equilibria. A complete analysis of the modes of aggregation is difficult. Some limited simple patterns of association, however, have been found useful for approximate description of the behavior of many real systems. Several patterns of surfactant self-association have been investigated recently by Mukerjee and his coworkers (25,32,46,62). The aggregation equilibria in a nonionic associating surfactant system can be expressed by a scheme of stepwise association equilibria such as:

$$2b_1 \overset{k_2}{=} b_2 \qquad [1\text{-}1a]$$

$$b_1+b_2 \overset{k_3}{=} b_3 \qquad [1\text{-}1b]$$

$$b_1+b_{q-1} \overset{k_q}{=} b_q \ . \qquad [1\text{-}1c]$$

Here b_1 is the monomer, b_2, b_3, and b_q are the dimer, trimer and q-mer, respectively, and k_2, k_3, and k_q are the corresponding stepwise association constants.

The overall association constant, K_q, for the formation of b_q from b_1 in the equilibrium

$$qb_1 \overset{K_q}{=} b_q \qquad [1\text{-}2]$$

is represented by

$$K_q = \frac{(b_q)}{(b_1)^q} \qquad [1\text{-}3]$$

Here (b_q) and (b_1) are the activities of b_q and b_1, which may be replaced by the concentrations $[b_q]$ and $[b_1]$ in dilute solutions. K_q is a product of the stepwise association constants as shown in Equation 1-4,

$$K_q = \prod_{2}^{q} k_q \qquad [1\text{-}4]$$

The experimentally accessible total equivalent concentration of all species in solution, C, is given by

$$C = \sum_{q=1}^{q} q[b_q]. \qquad [1\text{-}5]$$

In this scheme, the absolute values of k_q and K_q reflect the tendency towards self-association. The higher these values, the more extensive is the association and the lower the concentration at which the association becomes important. Whether the products of the self-association are unique oligomers or multimers,or a distribution of oligomers or multimers depends on the relative variation of k_q or K_q with q (25,57,62).

In typical micelle-forming systems exhibiting aggregates containing many monomers, no appreciable amount of aggregation can be detected until the CMC region is reached. This is a result of positive cooperativity at the initial stages of self-association, in which k_q increases with q, followed by a decrease in k_q with q when q values are large. The results are that micelles of moderate q values are stable and further growth of the micelle is difficult. In many cases, a rather narrow size distribution of the micellar aggregates is observed at concentrations not too far above the CMC region (30,59,60,61). For such systems, monomer-micelle equilibria are usually approximated

by a single monomer-micelle equilibrium, assuming only monodispersed micelles are formed. For nonionic micelles, composed of n monomers, the equilibrium can be written as

$$nb_1 = b_n \qquad [1\text{-}6]$$

and the overall association constant, K_n, represented by

$$K_n = \frac{[b_n]}{[b_1]^n} \quad . \qquad [1\text{-}7]$$

In the case of ionic micelles, counterion interactions must be included. The association equilibrium for anionic surfactants with monovalent counterions, M^+, may be expressed as

$$mM^+ + nb_1^- = b_n^{-(n-m)} \qquad [1\text{-}8]$$

where m is the number of counterions bound to the micelle, $b_n^{-(n-m)}$. An overall association constant, $K_{n,m}$, is then given by

$$K_{n,m} = \frac{[b_n^{-(n-m)}]}{[M^+]^m \ [b_1]^{-n}}. \qquad [1\text{-}9]$$

The total equivalent surfactant concentration, Equation 1-5,can be represented for nonionic and ionic micelles, respectively, by

$$C = [b_1]+n[b_n] \qquad [1\text{-}10a]$$

$$C = [b_1^-] + n[b_n^{-(n-m)}] \qquad [1\text{-}10b]$$

C can also be expressed in terms of the monomer concentration as

$$C = [b_1] + nK_n[b_1]^n \qquad [1\text{-}11a]$$

$$C = [b_1^-] + nK_{n,m}[M^+]^m[b_1^-]^n \qquad [1\text{-}11b]$$

It is, thus, possible to calculate the equivalent surfactant concentration C, at any given monomer concentration by Equation 1-11, if the numbers n and m and the overall association constant, K_n or $K_{n,m}$, are known. As will be discussed later, the monomer and calculated micellized surfactant concentrations as a function of equivalent surfactant concentration simulate many observed solution properties of micelle-forming systems.

Systems showing continuous self-association, in which all the stepwise association constants, k_q, are roughly of the same magnitude, exhibit an important pattern of surfactant association (25,62). In these systems, a one-parameter model, assuming the same stepwise association constant for all oligomers and multimers, i.e., $k_2=k_3=k_4=\ldots=k_q=k$, can be employed to describe the monomer-aggregate equilibria. For an ideal nonionic or ionic system in which k_q is unaffected by surfactant concentration, the following equations can be written:

$$c = [b_1](1+2k[b_1]+3k^2[b_1]^2+....qk^{q-1}[b_1]^{q-1} \qquad [1\text{-}12]$$

thus

$$C = \frac{[b_1]}{(1-k[b_1])^2} \qquad [1\text{-}13]$$

when $k[b_1] < 1$.

Since the stepwise association constants are equal, there is no cooperativity involved in this pattern of aggregation. It has been shown that association of this kind leads to a wide distribution of sizes, the most probable distribution of sizes (25,62). The average degree of aggregation increases slowly with the total surfactant concentration and may be very low even when large fraction of the molecules is associated (25,62,63).

1.4. Critical Micellization Concentration (CMC) of Surfactants

Any solution property that reflects the concentration of monomers, the aggregates, or any unequally weighted combination of the two will show changes when aggregation begins. In micelle-forming systems, solution properties change relatively abruptly over a small range of concentration when the CMC region is reached. The CMC value is often determined from the intercept of two straight lines, extrapolated from curves measuring some solution property

above and below the CMC region. Since CMC represents a narrow range of concentration rather than a unique concentration, the value of CMC may be somewhat different for different methods of determination. In a typical micelle-forming system, CMC values obtained by different methods usually agree, however, within a few percent (65). Techniques for CMC determinations and CMC values for commonly observed surfactants have been reviewed and compiled by Mukerjee and Mysels (65).

One of the characteristic features of micelle formation, as mentioned before (cf.1.3), is the strong cooperativity at the initial stages of aggregation. When micelles first become detectable at the CMC region, they may already have a large aggregation number although virtually all the surfactant is in the monomeric form. For many practical purposes, the CMC value serves adequately as the concentration where micelle formation begins and above which any added surfactants form micelles so that the monomer concentration remains approximately unchanged. Processes such as solubilization or catalysis, which depend on the formation of micelles, occur only when the surfactant concentration reaches the CMC value of the specific system. Any phenomenon which depends on the activity of the monomer, on the other hand, will be limited by the formation of micelles at CMC.

It has been shown (25) that the appearance of a CMC

region can be demonstrated by plotting the calculated monomer or micellized surfactant concentration, based on Equation 1-10 and 1-11 with proper choices of the values of n and K_n, as a function of the equivalent surfactant concentration. A fairly sharp change in composition around the CMC region can be obtained with a value of n as low as 20. The sharpness of the CMC region increases as n increases. Varying the value of K_n merely shifts the concentration scales and does not affect the shape of the curves. However, the operational approach to the determination of CMC from plots of solution properties against concentration can lead to misleading results at times. For example it has been demonstrated recently (25) from several model calculations that apparent CMC values can be obtained in systems exhibiting only dimerization or a continuous self-association with low degrees of aggregation. In these systems, the monomer concentration changes continuously below and above the apparent CMC region. The apparent CMC value, therefore, has only a limited significance. Erroneous estimations of monomer or aggregate concentration may result if a simple micelle model is forced on these systems. Several attempts have been made to define CMC values theoretically (165,66,68,69). Phillips (66) and Chung and Hielweil (68) suggest that the CMC is the concentration at which $d^3Q/dC^3=0$ where Q is an ideal colligative property

of the solution. Hall (69) suggests a similar definition in terms of the chemical potential of the monomer. These definitions are of little practical use. CMC values are determined in an operational manner (1967). However, the natures of the transition involved in the CMC region of bonafide micellar systems can be demonstrated by treating experimental data in an appropriate manner. This approach was originally developed by Hartley (11) and later used by Mysels et al. (67) for conductance data. In this method, the rate of change of a suitable solution property with concentration, dQ/dC, is plotted as a function of the surfactant concentration. dQ/dC may be approximated by the ratio $(Q_1-Q_2)/(C_1-C_2)$ or $\Delta Q/\Delta C$, where Q_1 and Q_2 are measured at consecutive concentrations C_1 and C_2. This procedure reduces the subjective character of graphical differentiation. It also gives a severe test of experimental accuracy of Q. Differential curves of this kind not only show clearly the transition at the CMC region but also provide information about the pattern of surfactant aggregation when compared with calculated curves of different models of aggregations.

A solution property, Q, which is the sum of suitably weighted contributions from all species in the solution may be expressed by an equation, such as 1-14, for an ideal nonionic system:

$$Q=A_1[b_1]+2A_2[b_2]+3A_3[b_3]+....+qA_q[b_q] \qquad [1\text{-}14]$$

Here $A_1, A_2, ..A_q$ are the proportionality factors for the monomeric, dimeric, and q-meric surfactants, respectively. Equation 1-14 should apply to measurements of spectral properties of surfactant solution, e.g., UV, visible, or nuclear magnetic resonance absorption. Equation 1-14 can also be written in terms of the monomer concentration as

$$Q=A_1[b_1]+2A_2K_2[b_2]^2+3A_3K_3[b_3]^3+..+qA_qK_q[b_q]^q. \qquad [1\text{-}15]$$

Colligative properties, such as osmotic pressures, are more conveniently expressed in terms of the molar concentrations of the various species:

$$Q=A_1[b_1]+A_2K_2[b_1]^2+A_3K_3[b_1]^3+...+A_qK_q[b_1]^q. \qquad [1\text{-}15a]$$

The total surfactant concentration, C, can be written as

$$C=[b_1]+2K_2[b_1]^2+3K_3[b_1]^3+..+qK_q[b_1]^q. \qquad [1\text{-}16]$$

The first derivatives of Equation 1-15 or 1-15a are thus given by:

$$\frac{dQ}{dC}=\frac{A_1+2^2A_2K_2[b_1]+3^2A_3K_3[b_1]^2+..+q^2A_qK_q[b_1]^{q-1}}{1+2^2K_2[b_1]+3^2K_3[b_1]^2+..+q^2K_q[b_1]^{q-1}} \qquad [1\text{-}17]$$

and

$$\frac{dQ}{dC}=\frac{A_1+2A_2K_2[b_1]^2+3A_3K_3[b_1]^3+..+qA_qK_q[b_1]^q}{1+2^2K_2[b_1]^2+3^2K_3[b_1]^3+...+q^2K_q[b_1]^{q-1}}. \qquad [1\text{-}17a]$$

In a micellar system, if only monomers and monidispersed micelles are considered, Equation 1-17 simplifies to

$$\frac{dQ}{dC} = \frac{A_1 + A_n n^2 K_n [b_1]^{n-1}}{1 + n^2 K_n [b_1]^{n-1}} \quad . \qquad [1\text{-}18]$$

It is thus possible to calculate dQ/dC from $[b_1]$ if A_1,A_n,n and K_n are known; then the total concentration, C, can be calculated by Equation 1-11a. The parameter A_1 may be determined at low concentrations where monomers are the predominant species and $dQ/dC \rightarrow A_1$ as $C \rightarrow 0$. At high surfactant concentrations, $dQ/dC \rightarrow A_n$ as $C \rightarrow \infty$. Thus A_n can be estimated from a suitable extrapolation. In the case of a solution property described by Equation 1-15a, extrapolation to infinite surfactant concentration leads to the value of A_n/n.

To demonstrate the use of this approach the ratio of A_1/A_n is assumed to be unity. By eliminating A_1 from Equation 1-18, Equation 1-18a is obtained, i.e.,

$$\frac{1}{A_n}\frac{dQ}{dC} = \frac{J + n^2 K_n [b_1]^{n-1}}{1 + n^2 K_n [b_1]^{n-1}} \quad . \qquad [1\text{-}18]$$

Figure 1.1 shows the normalized differential curves expressed as $(1/A_n)(dQ/dC)$ versus C, calculated from Equation 1-18a assuming K_n to be unity and different values of n.

Several important features of these plots are noteworthy.

Figure 1.1. The plots of normalized gradient of solution property versus the concentration of surfactant calculated by Equation 1-18a with K_n= 1 and different values of n (the broken line has a value of $K_n=10^{20}$) and also the model of stepwise association,S, as discussed in the text.

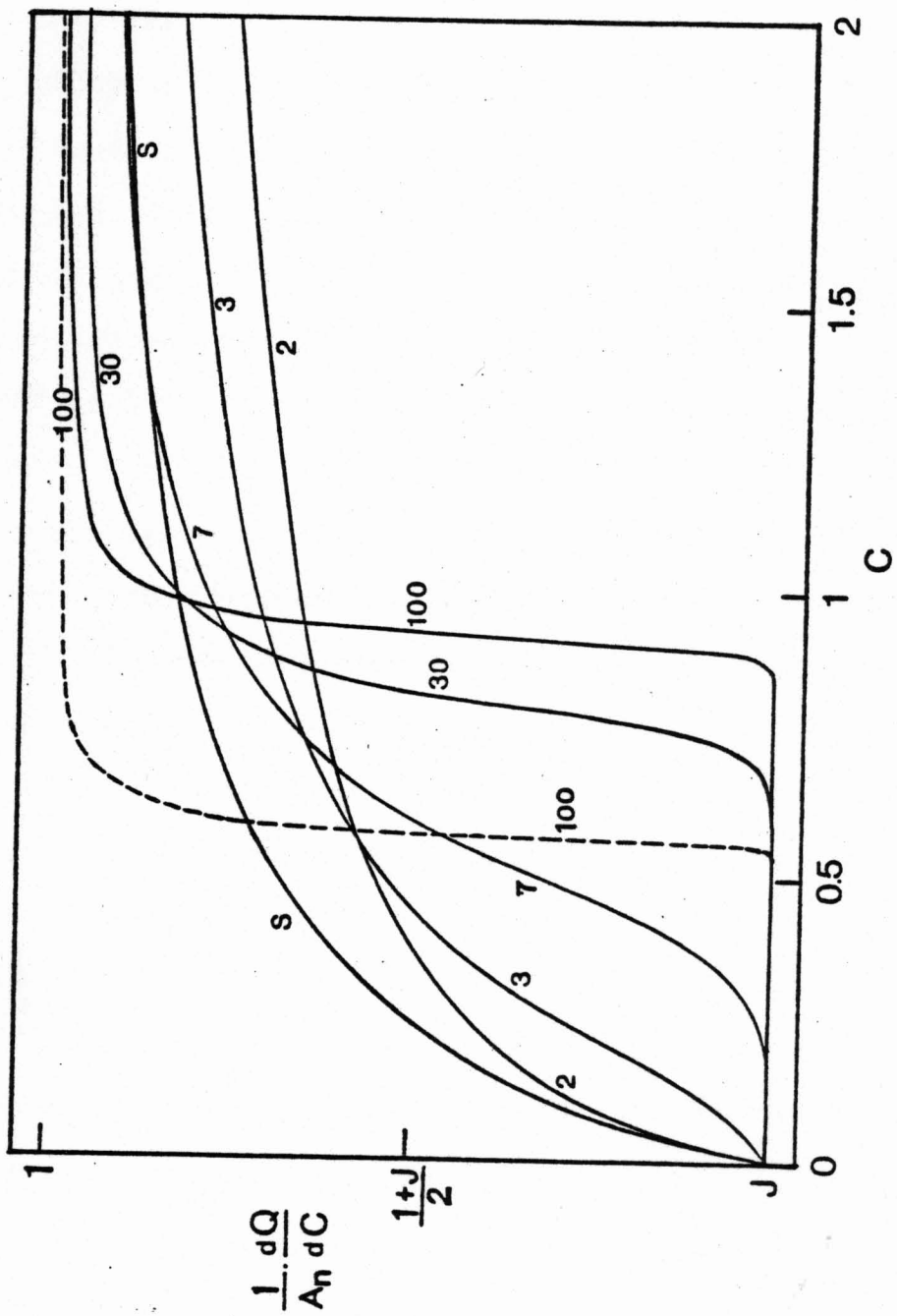
1
$\frac{1+J}{2}$
J
$\frac{1}{A_n}\frac{dQ}{dC}$
0
0.5
1
1.5
2
C
100
30
7
3
2
S

Every curve with n greater than two exhibits one inflection point. The transition becomes sharper as n increases. When the value of n is high, the gradient remains approximately constant until the transition region is reached and then changes rapidly in the transition region before leveling off to another roughly constant value. The transition occurs at the CMC region. Increasing the association constant, K_n, merely shifts the curve to a lower concentration without changing its shape. This is demonstrated by curves of n=100 and $K_n=10^{20}$ or 1 in Figure 1.1.These curves indicate that even for n=3, a slight cooperativity of self-association is implied in the association process. Thus, the formation of large monodispersed aggregates or multimers with a narrow size distribution must involve a considerable cooperativity of self-association, especially in the growing process of the aggregates. In the case of n=2, the self-association, of course, does not involve any such cooperativity. To underscore the essential difference between the cooperative self-association process and one without any cooperativity, Figure 1.1 also includes the calculated curve for the case of continuous stepwise association in which all the association constants are assumed to be unity and the proportional factors are assumed to be equal for all the aggregated species, i.e., $A_2=A_3=A_4=....=A_n$. This curve does not show any inflection even though the average degree of aggregation increases continuously. A system such as this may contain a

very large multimer,without a transition region.

The curves in Figure 1.1 are very similar in shape to the calculated curves of $d(C-b_1)/dC$,i.e.,the rate of change in the concentration of the aggregates with the total concentration of the surfactant. The only difference in this case is that the value of J equals zero. The curves in Figure 1.1 are thus of general significance and do not depend on the specific nature of the solution property being investigated. Treatment of data in the differential form illustrated in here should distinguish between different patterns of aggregation of surfactant systems. The analysis of some data on phenothiazine derivatives and salts of bile acids will be presented later.

1.5. Microenvironment of Micelles

On of the characteristic features of micelles is their ability to dissolve hydrophobic, water insoluble, organic molecules of various structures. This solubilizing ability led to the early proposal of liquid-like nature of the micellar core (5,11). The micellar core has been the subject of many investigations because of its importance in solubilization. Heat capacities (89) and compressibilities (90-92) of micelles have been found to be similar to those of liquid hydrocarbons. The fluidity of the micellar

interior has been studied by several different spectroscopic techniques. Fluorescent polarization (93-95) and electron spin resonance (ESR) (70,96-98) of solubilized probe molecules as well as direct measurements of proton (99-103) and C^{13} NMR (104) relaxation times of micellized long chain type surfactants have provided supporting evidence for the liquid-like nature of the micellar core, although some ordering of the hydrocarbon chains in the micellar core has also been suggested (95,100).

A liquid-like micellar core suggests the presence of only very limited amounts of water in the interior of the micelle because of the low solubility of water in hydrocarbons. There is still some controversy in the literature regarding the hydration of the hydrophobic micellar core. ^{19}F NMR studies on partially fluorinated ω-CF_3 surfactants suggest that the fluorocarbon group of a long chain surfactant is partially wet, based on the implicit assumption that the fluorocarbon group randomly samples the hydrophobic core (105). On the other hand, proton NMR chemical shifts and relaxation time studies indicate that water does not penetrate into the interior of alkylphenolpolyoxyethylene and alkylpolyoxyethylene micelles (101). Some doubt has been raised regarding the conclusions drawn from ^{19}F NMR data in that the ^{19}F NMR chemical shift data permit an alternative explanation based on the pronounced non-ideality of interaction between fluorocarbon and hydrocarbon surfactants

(109,110). Other evidence, such as the rate of hydrolysis of alkylsulfate micelles involving water attack on the α-carbon atom (111) and spin lattice relaxation times of methylene protons in micellized surfactants (100), have indicated that the first one or two carbon atoms from the polar head-group at the micellar surface are "wet" by water.

The micelle-water interface, containing polar head-groups, constitutes another important region for solubilization. In ionic micelles, this region is the inner part of the electrical double layer-the Stern layer. This ionic interface is rough, as would be expected from the dimension of the head-group and thermal fluctuations of monomers (112, 113). Large numbers of counterions, attracted by the head-groups, neutralize part of the electrical charges at the micellar surface and also create a high local electrolyte concentration in this region. In addition to the electrical charges, the proximity of the nonpolar micellar core also produces substantial effects on the local dielectric properties at the micelle-water interface. It has been shown that the effective dielectric constant at both ionic and nonionic micellar surfaces are much less than that of water (114, 115, 121). Alterations of physical and chemical properties of a solubilizate located in this region are, therefore, not unexpected.

In the outer part of electrical double layer, the diffused double layer, ionic species are distributed

according to their charge, valency, and concentration roughly in accordance with the Gouy-Chapman theory(80,116). A very important variable here is the double layer thickness.

The polar head-group of nonionic micelles can be glucose, polyoxyethylene, phosphine oxide, as also many other types of nonionic hydrophilic moieties. Among them, surfactants with polyoxyethylene head-groups are most often studied because of their practical importance. The structures of polyoxyethylene chains of such micelles have been investigated recently by NMR relaxation techniques (103,122). Some changes of the relaxation times of poloxyethylene protons at different temperatures have been found. These changes are consistent with a model describing the ethoxyl chains as a tightly coiled, tangled structure with water molecules entrapped among the chains at low temperatures and an extended configuration at higher temperatures. Some optical rotatary dispersion data suggested that the glucose head-groups of β-D-octyl glucoside micelles are not in a very different environment from that of the head-group in the monomeric form (123). This micelle may be regarded as a nonpolar micellar core surrounded by a layer of concentrated glucose solution , which provides a relatively simple system for studying the interfacial phenomena at nonionic micellar surface.

1.6. Solubilization in Surfactant Solutions

Surfactants have been used in many different situations to enhance the solubility of organic compounds (6-8). It is well known that the enhancement of solubility is related to the self-association of surfactants. In micelle-forming systems, little or no solubility increase is observed until the CMC is reached. Once micelles form the increase in solubility is almost directly proportional to the concentration of micellized surfactants over a large range. This phenomenon has, in fact, been used for CMC determinations (65). Like micelle formation, solubilization is also a dynamic process. A solute molecule (solubilizate) can get in and out of a micelle (solubilizer) at a rate of more than 10^4 times per second (70,95). The life-time of a solubilizate in a micelle is,however, long enough for its reorientation or diffusion to different locations within the micelle. Depending upon the polarity and charge distribution in the solubilizate molecule,it may be preferentially distributed at a certain location in the micelle. Nonpolar ,lipophilic compounds are likely to be incorporated into the hydrophobic core of the micelle. Amphipathic molecules may orient their hydrophilic part to the exterior of the micelle while the hydrophobic part remains in the core. Ions carrying opposite charge to the surfactant are likely to be taken into the

Stern layer of bound counterions. In systems of nonionic surfactants such as Brij and Tween, incorporation of the solubilizate can also occur in the polyoxyethylene sheath of the micelle (71,72).

Several recent studies on solubilization of aromatic compounds in different micellar systems have indicated that neutral or slightly polar molecules, such as benzene and naphthalene, are solubilized primarily at the surface of the micelle (73,74). This has been ascribed to a combination of two factors (73,74),namely the slight interfacial activity exhibited by molecules like benzene at an oil-water interface and the large surface to volume ratio of the micelle. It has also been shown that nonionic molecules with moderately polar functional groups, e.g., carbonyl, are also solubilized near the surface of the micelle (75,76). The micellar core-water interface situated between a nonpolar hydrocarbon medium and a polar aqueous medium is an important region for organic solubilizates with even a slight polarity.

The free energy change of solubilization, ΔG, includes at least three major contributing factors, i.e.,

$$\Delta G = \Delta G_h + \Delta G_c + \Delta G_i ,$$

where ΔG_h is the free energy change of transferring the nonpolar part of the solubilizate from the bulk solvent to the micelle. ΔG_c is the free energy of Columbic interaction

between the micellar ionic head-groups and the charges carried by the solubilizate and ΔG_i is the free energy change due to the self-potential of the charges carried by the solubilizate approaching the micellar core-water interface from the bulk solution (28,73). The change of self-potential at micellar surface can be approximated by an image interaction of a charge situated at the proximity of an interface dividing two different dielectric media. For a unit charge, e, situated in a medium of dielectric constant D_w at a distance r from a planar interface dividing another medium of dielectric constant D_m, the electrostatic energy, W, due to image interaction can be expressed as

$$W = \frac{(D_w - D_m) \cdot e^2}{(D_w + D_m) \cdot 4D_w r} \quad .$$

Since the dielectric constant of the aqueous solvent is higher than the dielectric constant of the nonpolar micellar core, the change of free energy due to self-potential for a charged solubilizate is alway opposing the solubilization.

The interaction of a solubilizate with micelle can be described either in terms of an association equilibrium or a two-phase partition. For example, the interaction of one solubilizate, D, with a micelle can be written as

$$D + b_n = Db_n \quad . \qquad [1\text{-}21]$$

and the equilibrium constant, K_e, can be expressed in terms of the concentrations of the solubilized species, $[Db_n]$, and

the free solute ,$[D_a]$, by the following equation:

$$K_e = \frac{[Db_n]}{[D_a]\ [b_n]} \quad . \qquad [1\text{-}22]$$

This approach has many difficulties, particularly if several solubilizate species are incoperated in one micelle.

The partition model, on the other hand, assumes a distribution of solubilizate between the bulk solution and the micellar sub-phase in analogy to a partition equilibrium between two immiscible phases. A partition coefficient,K_p,is related to the stoichiometric concentrations of solubilizates in the micellar phase,$[D_s]$, and the bulk solvent,$[D_a]$, by the following equation:

$$K_p = \frac{[D_s]\ \Phi_a}{[D_a]\ \Phi_m} \quad , \qquad [1\text{-}23]$$

where Φ_a and Φ_m are the volume fractions of the bulk solvent and the micelles. These parameters can be calculated from the partial molar volume of the micellized surfactant, $\bar{V}$, expressed in liter/mole, by the relationship

$$\Phi_m = (C - CMC)\bar{V} \qquad [1\text{-}24]$$

$$\Phi_a = 1 - \Phi_m \quad . \qquad [1\text{-}25]$$

At low micellar concentration, Φ_a approaches unity and Equation 1-23, after combination with Equation 1-24, becomes

$$K_p\bar{V} = \frac{[D_s]}{[D_a]\ (C - CMC)}. \qquad [1\text{-}26]$$

This approach usually ignores the effect of solubilizate on the CMC. If one assumes that the micelles are monodispersed and that the concentration of solubilizate is negligible compared to the concentration of micellized surfactant, Equation 1-26 can be rewritten for micelle of aggregation number n as

$$K_p\bar{V}\ n = \frac{[D_s]}{[D_a]\ [b_n]}. \qquad [1\text{-}26a]$$

Under these conditions the two approaches become identical, as indicated by the similarity between Equations 1-26a and 1-22. Although the partition model does not involve assumptions of monodispersed micelles, it is valid only at low concentrations of solubilizate, unless the effect of the solubilizate on the CMC is explicitly taken into consideration and the non-ideality effects are accounted for.

The association model of solubilization has been used in kinetic studies of micellar catalyzed reactions (10). In a study of naphthalene solubilization, Mukerjee and Cardinal applied the association model and models of aggregation to investigate the self-association patterns of sodium cholate (cf. 1.4) (46). The partition model has been used in the

study of dissociation constants of solubilized indicator dyes(80). Similar approaches will also be used in the present studies for analyzing the pattern of solubilization of bile salts and the dissociation constants of micellar solubilized indicator dyes.

2. EXPERIMENTAL

2.1. Materials

β-D-Octyl glucoside was synthesized according to the following procedure. Glucose (Matheson & Coleman) on acetylation followed by bromination (125) yielded aceto-bromoglucose. After three recrystallizations the material exhibited a melting point of 90.5 - 91.5°C. Following Noller's method (126), acetobromoglucose was then reacted with octanol in dry ether in the presence of silver oxide to give β-tetraacetyl octyl glucoside. This intermediate melted at 63 -64°C after two recrystallizations from absolute methanol. Octanol (Eastman Kodak) was purified by fractional distillation twice under reduced pressure; only the middle one-third protion was collected. β-D-Octyl glucoside was obtained after deacetylation of β-tetraacetyl octyl glucoside in sodium methylate solution. This crude product was repeatedly recrystallized by adding petroleum ether to a dry acetone solution and then washed with petroleum ether to remove any residual octanol. The final product was a white and crystalline solid melted at 63.5 - 65°C. Its purity was further checked by surface tensions of appropriate aqueous solutions which were consistent with reported values (127) and did not show a minimum in the CMC region.

Brij 35 (polyoxyethylene lauryl ether)(Fisher Scien-

tific Co.) was purified by shaking an aqueous solution with neutral decolorising carbon (Fisher, Norit A) and then passed through an aluminum oxide column (M. Woelm, W-200, basic) to remove any peroxide that might have been generated through the degradation of the polyoxyethylene groups. A white amorphous powder was obtained after freeze-drying the aqueous eluant. Surface tensions of purified Brij 35 in water did not show any minimum in the CMC region.

Two samples of sodium dodecyl sulfate were used. One was a gift from Dr. K.J. Mysels, and the other was supplied by BDH Labs. Both samples were purified by alternate recrystallization from water at 0°C and washing with ether until no impurity could be detected by surface tension measurements (128,129). Sodium myristyl sulfate (Schwarz/Mann), sodium decyl sulfate (Schwarz/Mann), sodium octyl sulfate (Schwarz/Mann), lauric acid (Applied Science) and perfluoro-n-octanoic acid (PCR Inc.) were all used as received.

Triflupromazine hydrochloride samples were kindly supplied by Dr. G. Zografi and Squibb & Sons. The material from Squibb & Sons was recrystallized three times from isopropyl alcohol before use. It gave results which were identical with the sample received from Dr. Zografi. Trifluoperazine dihydrochloride, supplied by Smith Kline & French Labs, was recrystallized once from isopropyl alcohol.

Chenodeoxycholic acid (Canada Packers Ltd.) was a kind gift from Dr. A. Hofmann. Cholic acid (Nu Chek), Deoxycholic acid (Nu Chek), and chenodeoxycholic acid (Nu Chek) were all purified by foam fractionation of their aqueous solutions of sodium salts at concentrations below the apparent CMC's. The acids were recovered by precipitation with 0.1 N hydrochloric acid and repeatedly washed with distilled water before drying. The purities were checked by thin layer chromatography (130) and titration with NaOH in ethanol-water (4:1) solutions. The foam part gave evidence of a considerable number of impurities on the TLC plate. It was found that all three of the bile acids recovered by acid precipitation from aqueous solutions contained water of hydration even after extensive drying in a desiccator over P_2O_5 for several days. The water content in each acid was determined by Karl-Fischer titration (Sargent-Welch) (131). The NaOH-titration results were in satisfactory agreement with water contents determined by Karl-Fischer titration (within about 0.2%). Residual isomeric bile acids were less than 0.1% in cholic acid and less than 0.3% in deoxycholic acid and chenodeoxycholic acid, as estimated by TLC using more than 100 mcg of samples. Sodium taurodeoxycholate was the best purity material obtained from Calbiochem (lot 510160) and was used without further purification.

Potassium 2-p-toluidinylnaphthalene-6-sulfonate

(Sigma Chemical Co.) was purified twice by recrystallization from water (132) and kept in a desiccator at 0°C. Ethyl red (Eastman Kodak), quinoline blue (K & K Laboratory), benzopurpurine 4B (Eastman Kodak), bromthymol blue (Eastman Kodak), and quinine sulfate (Merck) were used as received. Trifluoroacetic acid (Aldrich) and d_6-deuterated benzene (Aldrich) were spectroscopic grades.

Methyl ammonium chloride (Aldrich), dimethylammonium chloride (Aldrich), trimethylammonium chloride (Aldrich), tetramethylammonium chloride (Aldrich), tetraethylammonium bromide (Aldrich), tetra-n-propylammonium bromide (Eastman Kodak), and tetra-n-butylammonium bromide (Eastman Kodak) were dried before use.

All organic solvents were distilled at least once before use. Inorganic salts were of reagent grade.

2.2. Apparatus

Ultra-violet and visible spectra were obtained using a Cary Spectrophotometer, Model 14. The Cary Spectrophotometer Model 16 was used for measurements at single wavelengths. Uncorrected fluorescence spectra were obtained on a Perkin-Elmer MPF-4 Fluorescence Spectrometer. All of the three instruments were fitted with thermo-stated cell compartments connected to a circulating water bath in order to maintain the temperature constant within $\pm$0.1°C. The temperature of sample solutions in each cell compartment

was checked by a thermistor probe with the aid of an electrometer (Fenwal Electronics and Keithley Electrometer Model 610B).Unless otherwise indicated, all spectral measurements were made at 25.0 ± 0.1°C.

^{19}F NMR spectra were obtained on a Bruker HX90E NMR Spectrometer, modified by Dr. Craig Bradley and Mr. Jim Blackbourn. A Nicolet 1080 Data System was used in signal averaging and data manipulations.

Conductance measurements were carried out in a doughnut-type dilution cell equipped with a magnetic stirrer (133), placed in an oil bath at 25°C (controlled within ±0.015°C). A Beckman Model RC-18A conductivity bridge, capable of capacitance balancing, was used for resistance measurements. The average precision of the measurements was about 0.03%.

Interfacial tensions were measured by the Wilhelmy plate method with a platinum plate on a tensiometer equipped with a precision balance of capacity up to 500 mg.

pH measurements were made with either a PHM 64 Research pH Meter (Radiometer) equipped with a combined glass and calomel reference electrode (Radiometer, type GK 2301C) or with a Beckman Zeromatic II pH meter equipped with a Sargent combined electrode (Cat. #S-30072-15).

2.3. Experimental Methods

2.3.1. Solution Preparation

Double distilled water prepared from alkaline permangnate solution in an all glass apparatus was used in the preparations of aqueous solutions.

Surfactant or dye solutions of different concentrations were prepared by appropriate dilutions of stock solution by volume with a Hamilton syringe or by weight. Density corrections were applied whenever appropriate. A pyrex pycnometer with a capacity of 2 ml was used for density determinations. Hamilton syringes were calibrated with distilled water at room temperature before usage. The precision of volume delivered from a syringe was usually better than 0.1% in the 0.5 to 2 ml range.

Aqueous solutions of quinoline blue and ethyl red were somewhat unstable. They tended to fade after a few days of storage, especially in solutions at neutral or alkaline pH's. It was found that in the presence of anionic surfactants, these dyes were stable over a period of weeks without any significant reduction in absorbance. In order to minimize the decomposition of these dyes during measurements, solutions were prepared by mixing aliquots of a dye-surfactant solution and a buffer solution immediately before spectral measurements. This procedure was found to be satisfactory for obtaining reliable and precise measurements of absorbance.

Benzopurpurine 4B, bromthymol blue, and bromphenol blue soltuions were stable throughout the experimental

period. All dye stock solutions were stored in the dark and protected from light during handling.

Trifluprομazine HCl and trifluoperazine 2HCl were also unstable in aqueous solutions. They were sensitive to light and air oxidation (134). Freshly prepared stock solutions of these two compounds were diluted directly in 5 mm NMR tubes before measurement.

Solutions of the sodium salts of lauric acid, perfluoro-n-octanoic acid, cholic acid, deoxycholic acid, and chenodeoxycholic acid were prepared by titration of the acids to a pH above 8 with freshly prepared NaOH solution to keep the fraction of unionized acids to low values.

2.3.2. Determination of The Indicator Ratios of Indicator Dyes in Surfactant Solutions

The cationic cyanine dyes, ethyl red and quinoline blue, carrying ++ and + charges are of the

$$DH^{++} = D^{+} + H^{+}$$

type, in which D^{+} has a strong absorption band in the visible region and DH^{++} only absorbs in the UV range. The anionic triphenylmethane dye, bromthymol blue, carrying -- and - charges, has the dissociation equilibrium

$$Y^{-} = B^{=} + H^{+},$$

in which Y^{-} is the yellow form and $B^{=}$ is the blue form. The spectra of D^{+}, Y^{-} and $B^{=}$ in solutions of different surfactant or polymer concentrations were measured at sufficiently high pH so that only one form of the acid-base

pair was predominant. All dye species exhibited bathochromic shifts in surfactant solutions above the CMC or in hydrophilic polymer solutions of moderate concentrations. Since only one isobestic point was observed for each dye species in the presence of various surfactant concentrations, an indicator ratio, R, was defined for each dye at any surfactant concentration by

$$R = \frac{[DH_s^{++}] + [DH_a^{++}]}{[D_s^{+}] + [D_a^{+}]} = \frac{[D_t]}{[D_s^{+}] + [D_f^{+}]} - 1 \quad [2\text{-}1a]$$

or

$$R = \frac{[Y_s^{-}] + [Y_a^{-}]}{[B_s^{=}] + [B_a^{=}]} = \frac{[D_t]}{[B_s^{=}] + [B_a^{=}]} - 1 \quad [2\text{-}1b]$$

where $[DH^{++}]$, $[D^{+}]$, $[Y^{-}]$ and $[B^{=}]$ are the concentrations of the corresponding dye species, $[D_t]$ is the total dye concentration, and the subscripts "s" and "a" indicate the solubilized (or bound) and free dye, respectively.

The total concentration of the solubilized (bound) and the free D^{+} form of ethyl red or $B^{=}$ form of bromthymol blue were determined from the absorbance at the isosbestic wavelength using the following equations:

$$[D_s^{+}] + [D_a^{+}] = \frac{A_{iso}}{\varepsilon_{iso} \cdot L} \quad [2\text{-}2]$$

$$[B_s^{=}] + [B_a^{=}] = \frac{A_{iso}}{\varepsilon_{iso} \cdot L} \qquad [2\text{-}2a]$$

where "L" is the path length of light, and A_{iso} and ε_{iso} are the absorbance and molar absorptivity at the isosbestic wavelength, respectively. The approximate isosbestic region of each dye-surfactant or dye-polymer system was first determined from solutions containing the same amount of dye and different concentrations of the surfactant or polymer on a recording spectrophotometer, Cary-14. More precise values of isosbestic wavelengths and molar absorptivity were then obtained by absorbance measurements on the Cary-16 Spectrophotometer. The precision of the isosbestic point in most cases was better than $\pm$0.5 nm. Sodium phosphate and acetate buffers were used for pH control. The concentrations of dye solutions were in the range of 1.0 - 3.0x 10^{-5}M.

The apparent dissociation constant, K_{app}, in dye-surfactant or dye-polymer solutions could be calculated from the measured solution pH and R values by

$$K_{app} = \frac{[H^+]}{R} \; . \qquad [2\text{-}3]$$

Similarly, the intrinsic dissociation constant, K_a, of an indicator dye in bulk solution was determined from the indicator ratio, R_a, (e.g., $R_a=[DH_a^{++}]/[D_a^{+}]$), in solutions

buffered at different pH's without the presence of surfactant or polymer, i.e.

$$K_a = \frac{[H^+]}{R_a} \qquad [2\text{-}4]$$

The molar absorptivities of the visible spectra of quinoline blue exhibited strong concentration dependence above 5×10^{-6}M. It was, therefore, not possible to study the acid-base equilibrium of this dye by the same method used for other dyes. To overcome this difficulty, experiments were designed to take advantage of the lower pK value of quinoline blue in the micelle-solubilized state. Solutions were, therefore, maintained at acidic pH in which the equilibrium shifted to the DH^{++} form and the absorbance due to the D_a^+ form was negligible at a total dye concentration of $1 - 2 \times 10^{-5}$M. The concentration of the solubilized D^+ form, $[D_s^+]$, could be determined directly from the absorbance of the spectrum obtained in the visible region.

2.3.3. Dissociation Constants of Cationic Indicator Dyes in Anionic Alkylsulfate Micellar Solutions

Based on the apparent partition coefficients of the cationic cyanine dyes in non-ionic micellar systems, it was expected that the anionic micelle would incorporate the cationic dyes almost completely at concentrations above the CMC, as was reported for a similar dye, pinacy-

anol (135). This simplified the determination of the dissociation constants for solubilized dyes, since the concentration of the solubilized D_s^+ form could be determined directly from the absorbance at the wavelength of maximum absorption. The pH of the solutions was controlled by sodium acetate or sodium phosphate buffers. For all the anionic surfactants studied, sodium ion was used as the main counter-ion, other than H^+, unless otherwise stated. The ionic strength was varied by either adding sodium chloride to the buffer solutions or by simply adjusting the buffer concentration in the case of sodium acetate. The concentration of the dye was maintained in the range of $1.0 - 2.0 \times 10^{-5}$M.

2.3.4. Measurements of Spectral Changes of Aggregating Dye in Solutions of Hydrophilic Polymers

Benzopurpurine 4B was used for this study. Solutions of benzopurpurine 4B containing different concentrations of polymers were prepared by weight by dilution of a stock solution containing dye and polymer with another dye solution of the same dye concentration. Visible spectra of the dye solutions containing different amounts of polymers were recorded on a Cary - 14 spectrophotometer and the

absorbances at single wavelength were measured on a Cary-16 spectrophotometer.

2.3.5. ^{19}F NMR Measurement of Fluorophenothiazine Derivatives and Sodium Perfluoro-n-octanoate

^{19}F NMR spectra were obtained on a Bruker HX 90E Spectrometer at 84.67 MHz in the Fourier Transform (FT) mode. Typical settings of the FT parameters were a spectral width of 5000 Hz and an acquisition time of 2 to 15 minutes, resulting in an accuracy in the chemical shift determination of better than $\pm$0.007 ppm. The lock signal was obtained from an external standard solution of 2.5% (v/v) trifluoroacetic acid in deuterated d_6-benzene sealed in a 1 mm capillary inside the 5 mm tube with the sample. The chemical shifts were measured from the singlet of trifluoroacetic acid and reported as positive values for upfield and negative values for downfield shifts. Susceptibility corrections were estimated to be small and were not applied. The temperature in the probe was maintained at 33$\pm$2°C.

2.3.6. Conductivity Measurements of Surfactant Solutions

Conductivity measurements were made in the presence of 0.001 N sodium hydroxide, in some cases, added to supress any hydrolysis. The conductance was corrected for the contribution of sodium hydroxide. The effect of the presence of sodium hydroxide on the CMC values through the common-ion effect (8,136) may be considered negligible for comparative purposes.

The cell constant of the doughnut-type dilution cell was determined with standard potassium chloride solutions and rechecked between experiments. No substantial variation (less than 0.0025%) was observed. A cell constant of 5.304± 0.0013 cm^{-1} was used for all the conductivity calculations.

2.3.7. Fluorescent Measurements of Solutions of Alkylsulfates and Salts of Bile Acids

Potassium 2-p-toluidinylnaphthylene-6-sulfonate (TNS) was used as the fluorescent probe. Fluorescence measurements were made on a Perkin-Elmer Fluorescence Spectrophotometer, MPF-4. Both emission and excitation slits were set at 7 nm. The uncorrected emission spectra were obtained by excitation at 370 nm. Fluorescence intensities were measured at the wavelength of apparent emission maximum (429 nm and 456.5 nm for bile acids and sodium alkylsulfates, respectively). The mixtures of TNS and surfactant were pre-equilibrated to 25 ± 0.1°C in a water bath before being transferred to the cell holder which was also thermally controlled to the same temperature. The concentration of TNS was about 2.74×10^{-5}M.

The emission spectra of TNS obtained from different surfactant solutions were corrected by Parker's method (137). A solution of 12 mcg./ml. quinine sulfate in 0.1 N H_2SO_4 was used as a reference. Its emission spectrum was obtained under the same conditions as used in measurements of TNS-surfactant solutions. The apparent intensity of the quinine

sulfate reference was then compared to a true emission spectrum of 10 ppm quinine sulfate in 0.1 N H_2SO_4(138). The ratio of true intensity to the observed intensity of quinine sulfate at any particular wavelength was calculated and used as a correction factor. The observed fluorescent intensities from TNS-surfactant solutions were then multiplied by the corresponding correction factors at each wavelength to obtain the correct emission spectrum. The wavelength of maximum emission was then located from the corrected spectrum. Figure 2.1 shows the observed emission spectrum of quinine sulfate in 0.1 H_2SO_4. The true emission spectrum of quinine sulfate used as a standard for the spectral corrections is also illustrated in Figure 2.1. Table 2.1 summarizes the correction factors normalized to the value at 450 nm.

Figure 2.1. The uncorrected emission spectrum (solid line) of a 12 mcg./ml. quinine sulfate in 0.1N sulfuric acid solution obtained from a Perkin-Elmer MPF-4 fluorometer at an excitation wavelength of 370 nm and a slit width of 7 nm for both emission and excitation. Dashed line shows the true emission spectrum of a 10 ppm quinine sulfate in 0.1 N sulfuric acid solution reported in Perkin-Elmer Technical Memo No. 95, November 2, 1971.

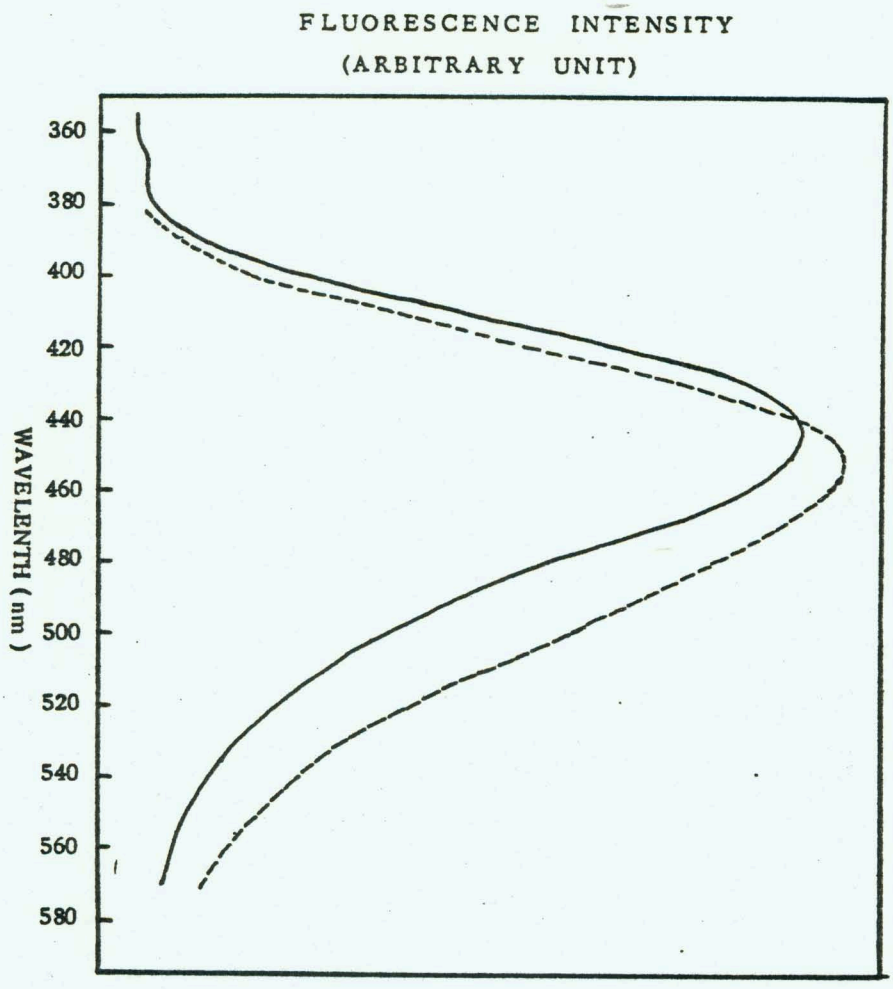
FLUORESCENCE INTENSITY
(ARBITRARY UNIT)
WAVELENTH (nm)
360
380
400
420
440
460
480
500
520
540
560
580

Table 2.1. Correction Factors For Emission Spectrum of TNS

Exicitation Wavelength :370 nm

Exicitation Slit Width: 7 nm

Emission Slit Width: 7 nm

Wavelength (nm)	Normalized Correction Factor*
380	0.338
390	0.643
400	0.643
410	0.715
420	0.769
430	0.847
435	0.889
440	0.930
445	0.963
450	1.000
460	1.068
470	1.190
475	1.242
480	1.242
490	1.472
500	1.600
510	1.747
520	1.824
530	1.945
540	2.024
550	2.085
560	2.186
570	2.232
600	2.517

*Normalized correction factors were obtained by the following equations:

$$\text{Correction Factor} = \frac{\text{true intensity}}{\text{observed intensity}}$$

$$\text{Normalized Correction Factor} = \frac{\text{correction factor}}{\text{correction factor at 450 nm}}$$

3. SOLUBILIZATION OF INDICATOR DYES IN MICELLAR SOLUTIONS

3.1. Review of Literature

dyes have often been used for probing the properties and microenvironments of micelles (79,80,88,112). Indicator dyes solubilized in ionic micelles provide information regarding the hydrogen ion concentration and the electrostatic potential at micellar surface. They also serve as model for studying solubilization and ionization behavior of organic ions at interfaces (79,80,88,268). The ionization constant of a weak acid or base group situated at a charged interface often differs from the value in the bulk solution (262). Hartley and Roe (263) and Davies and Rideal (264) suggested that the apparent dissociation constant of weak acid or base at a charged interface, K_{app}, is related to the surface potential and the dissociation constant in the bulk solution, K_a, by the following equation:

$$pK_{app} = pK_a - e\,\Psi_s/2.303\ kT\ , \qquad [3\text{-}1]$$

where Ψ_s is the surface potential including sign, e is the electronic charge, k is the Boltzman constant, and T is the absolute temperature. Shifts of dissocaition constants of indicator dyes upon solubilization in micelles have been reported in many surfactant systems. Mukerjee and Banerjee (80) inves-

tigated the dissociation equilibria of several anionic triphenylmethyl sulfonate dyes in cationic micelles. When the data were examined in terms of Equation 3-1, it became apparent that the dissociation constants at the surface, K_s, (the value at zero potential) were different from the bulk value; therefore, the pK_{app} differed from pK_a both because of the electrostatic potential at a charged interface as well as the nature of the microenvironment at the interface. Later Mukerjee and Desai found that the pK values of the same type of dyes solubilized in nonionic β-D-octyl glucoside or Brij 35 micelles were higher than the pK values in the bulk solutions (73,267). The change in pK upon solubilization was shown to correlate roughly with the pK_a value of the triphenylmethyl sulfonate dyes. Similar changes in pK of dyes solubilized in other nonionic micelles have been reported recently by Funasaki (88) and Fernandez and Fromherz (79).

Fernandez and Fromherz (79) studied the dissociation equilibria of two fluorescent coumarin dyes substituted with a long hydrocarbon side chain, one exhibiting a dissociation of the type $A = B^- + H^+$, the other $A^+ = B + H^+$. These authors reported that the changes of pK values of these dyes upon solubilization in Triton X-100 nonionic micelles were equal in magnitude but opposite in sign. By assuming that the solubilized dyes were in equilibrium with protons in the aqueous solution at the micellar surface,

they concluded that the pK change upon micellar solubilization is primarily due to the local medium effect at the micellar surface. Also by comparing the dissociation constants of the dyes in the Triton X-100 micellar system with those measured in dioxane-water mixtures, after appropriate corrections for the change of proton activity in the mixed solvent systems, these authors concluded that the solubilized coumarin dyes were experiencing a dielectric constant equivlent to 32 in a macroscopic system. This estimate is in fair agreement with the estimated effective dielectric constant at micellar interfaces reported by Mukerjee and coworkers (114,115,265). Based on the spectral changes of a solvent sensitive inter-ionic charge-transfer system, Mukerjee and Ray (114) found the effective dielectric constant in the Stern layer of dodecyl pyridinium iodide micelles to be about 36. The value obtained for Brij 35 was very similar (114). Triton X-100 is expected to be similar to Brij 35 in this regard.

Mukerjee and Desai (266) suggested that at least three factors need to be considered in examining the nature of the effective polarity at the micelle-water interface: (a) the proximity of a low-dielectric region, (b) dielectric saturation in the electric field present in ionic micelles, and (c) the presence of high local concentration of ions in the Stern layer of ionic micelles. Factor (c) was shown to be relatively unimportant for the short-range interactions

of ion-pairs in the Stern layer. The proximity of a low dielectric region is likely to be important in the solubilization of organic ions and also in the ionization of surface functional groups (73). Mukerjee and Desai (73,267) explained the changes of pK values upon micellar solubilization in terms of electrostatic image interactions of charges at interfaces (cf. Chapter 1). For triphenylmethyl sulfonate dyes, both the acid and the conjugated base carry permanent charges in the dissociation reaction, $Y^{-} = B^{=} + H^{+}$. Since the dissociation of a proton creates an additional charge on the dye molecule, the dissociation reaction is made unfavorable at the micelle-water interface and an increase in pK is observed. This explanation predicts an opposite effect on the pK for dyes which have equilibrium of the type $DH^{++} = D^{+} + H^{+}$, which are the subject of present study.

Image interaction has been successfully applied to explain surface tensions of electrolyte solutions by Onsager (271). It has also been suggested that the hydrated layers in proteins which are unavailable to the diffusible electrolytes may be a result of image interaction (269). Image forces are also believed to play crucial roles in the transport of ions across membranes (270). The importance of image interaction in the formation of ionic micelles has been discussed by Stigter (28) and Mukerjee (73).

3.2. Scope and Aims

In biological systems, the presence of an electrical charge on an organic molecule often plays a major role in determining its biological activity. For example, many drug molecules are acidic or basic in nature. Their biological activity sometimes depend on the degree of ionization or the amount of charge carried by the molecule. The binding or adsorption of a charged organic molecule to a non-polar binding site on a membrane or a protein, for example, may also be affected by the ionic nature of the molecule. Solubilization of indicator dyes in micellar system provides a simple model for examining interactions,such as mentioned above, occurring at an interface.

The physical and chemical properties of a molecule solubilized in a micelle are affected by the microenvironment of the loci. It has been shown that molecules that are even slightly polar tend to be preferentially solubilized at the micelle-water interface (74). For the polar dyes in the present study, it may be assumed that the dye, itself, and the polar dissociable groups, in particular, are located in the interfacial region. In other words, these groups are accessible to water and the aqueous ionic species such as hydrated protons.

As an extension of previous studies on solubilized anionic triphenylmethyl sulfonate dyes in cationic and non-

ionic micelles, the present study covers two cationic cyanine dyes also carrying permanent charges, solubilized in nonionic micelles of β-D-octyl glucoside and Brij 35, and anionic alkyl sulfate micelles. In the case of nonionic micelles, the changes in acid-base equilibrium of indicator dyes were studied. The effect of ionic strength and counter-ion binding on the dissociation constants of solubilized dyes in anionic micelles were examined. The data have been analyzed in terms of the micellar surface potential according to the electrical double layer theory. It is also the purpose of the present study to gain some insight into the role of charges in the solubilization of organic molecules in micellar systems and to provide a better understanding of the mechanism of the catalysis of solubilized species.

3.3. Results and Discussion

Figure 3.1 shows the structures of the two cyanine dyes used in the present study. In both cases, the singly charged dye exhibits strong absorption in the visible region. The addition of a proton removes the resonance condition responsible for the visible absorption band (275,276).

Most cyanine dyes tend to self-associate in aqueous solutions by forming a stacking type of aggregate (275-278). Such aggregates are more readily formed by the singly charged dyes than the doubly charged ones for two reasons. The

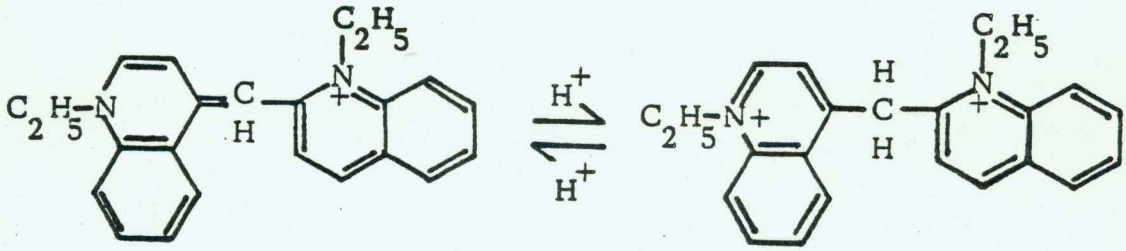

Ethyl Red

(1, 1' -diethyl-2, 4' -cyanine)

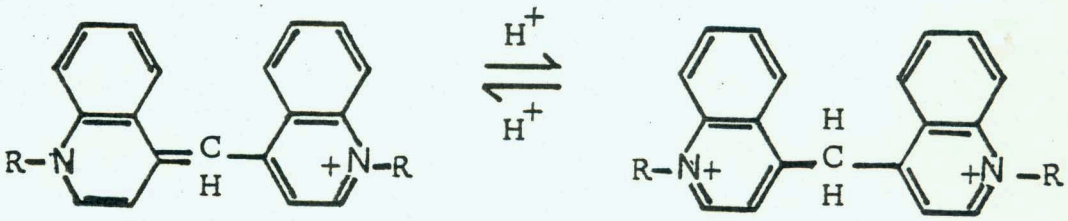

R = $CH_2CH_2CH(CH_3)_2$

Quinoline Blue

(1, 1' -diisoheptyl-4, 4' -cyanine)

Figure 3.1. Molecular structures and dissociation equilibria of ethyl red and quinoline blue.

Charge repulsion between aggregated ions is lower and there is much more restricted rotation around the central carbon atom (277) in the dye molecule.

The visible spectrum of quinoline blue, shown in Figure 3.2, exhibits a strong concentration dependence, indicating self-association of the dye in solution(275). Ethyl red, on the other hand, does not show any significant change in its visible spectra in the concentration range of $1x10^{-5}$ to $5x10^{-5}$ M. The spectrum of ethyl red, as illustrated in Figure 3.3,is consistent with the spectrum reported by Feldman,et al. (275). The spectra of quinoline blue are similar to the spectra of 1,1'-diethyl-4,4'-cyanine, a molecule analogous to quinoline blue (275).

A pK value of 6.25 was obtained for ethyl red from the data in Figure 3.4 which compares well with the value of 6.24 reported by Feldman, et al. From the data in Figure 3.5, a pK value of 7.95 was obtained for quinoline blue at a concentration of $1x10^{-6}$M. This value is consistent with the reported pK value of 7.83 for the related dye, 1,1'-diethyl-4,4'-cyanine, at a concentration of $2.5x10^{-6}$M (275). Feldman, et al. have found that the apparent pK value of 1,1'-diethyl-4,4'-cyanine determined from the visible spectra increases by approximately 0.5 units when the concentration is increased from $2.5x10^{-6}$ M to $2.5x10^{-5}$ M. The addition of 0.25 N potassium chloride also increases the pK value by approximately the same magnitude.

Figure 3.2. Visible spectra of quinoline blue in 0.05N sodium hydroxide solutions. The concentrations of quinoline blue were (1) $5x10^{-5}M$, (2) $3x10^{-5}M$, (3) $1x10^{-5}M$, (4) $8x10^{-5}M$, (5) $4x10^{-6}M$.

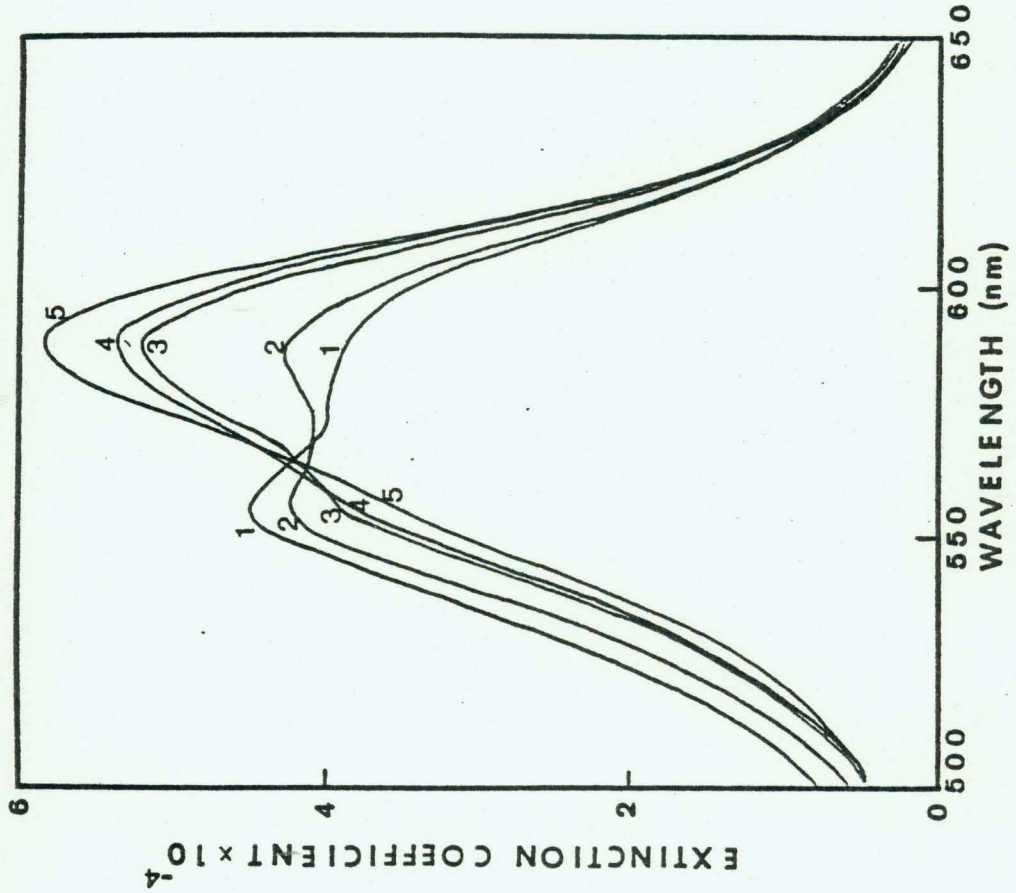
EXTINCTION COEFFICIENT × 10⁻⁴
0
2
4
6
500
550
600
650
WAVELENGTH (nm)
1
2
3
4
5
1
2
3
4
5

Figure 3.3. Visible spectra of ethyl red in 0.01N sodium hydroxide solution (1), and 1.3% (2), 1.8% (3), 2.7% (4) β-D-octyl glucoside.

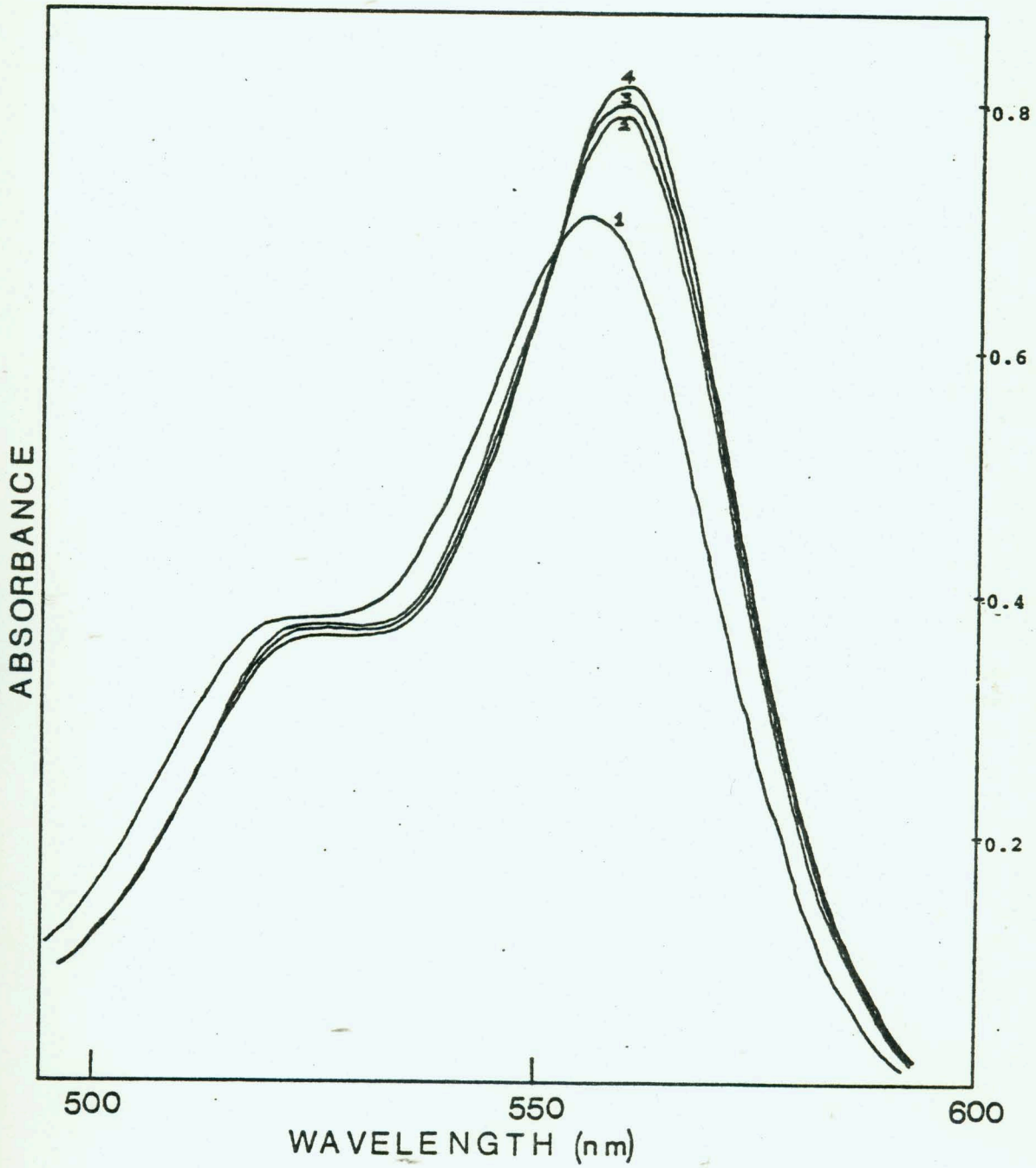
4
3
2
1
0.8
0.6
0.4
0.2
ABSORBANCE
500
550
600
WAVELENGTH (nm)

Figure 3.4. Plots of log($[D^+]/[DH^{++}]$) versus pH of ethyl red in buffer solutions (O), with 0.015M sodium dodecyl sulfate (●), and with 3% β-D-octyl glucoside (■). The concentration of ethyl red was 2.5×10^{-5}M. Straight lines have unit slope.

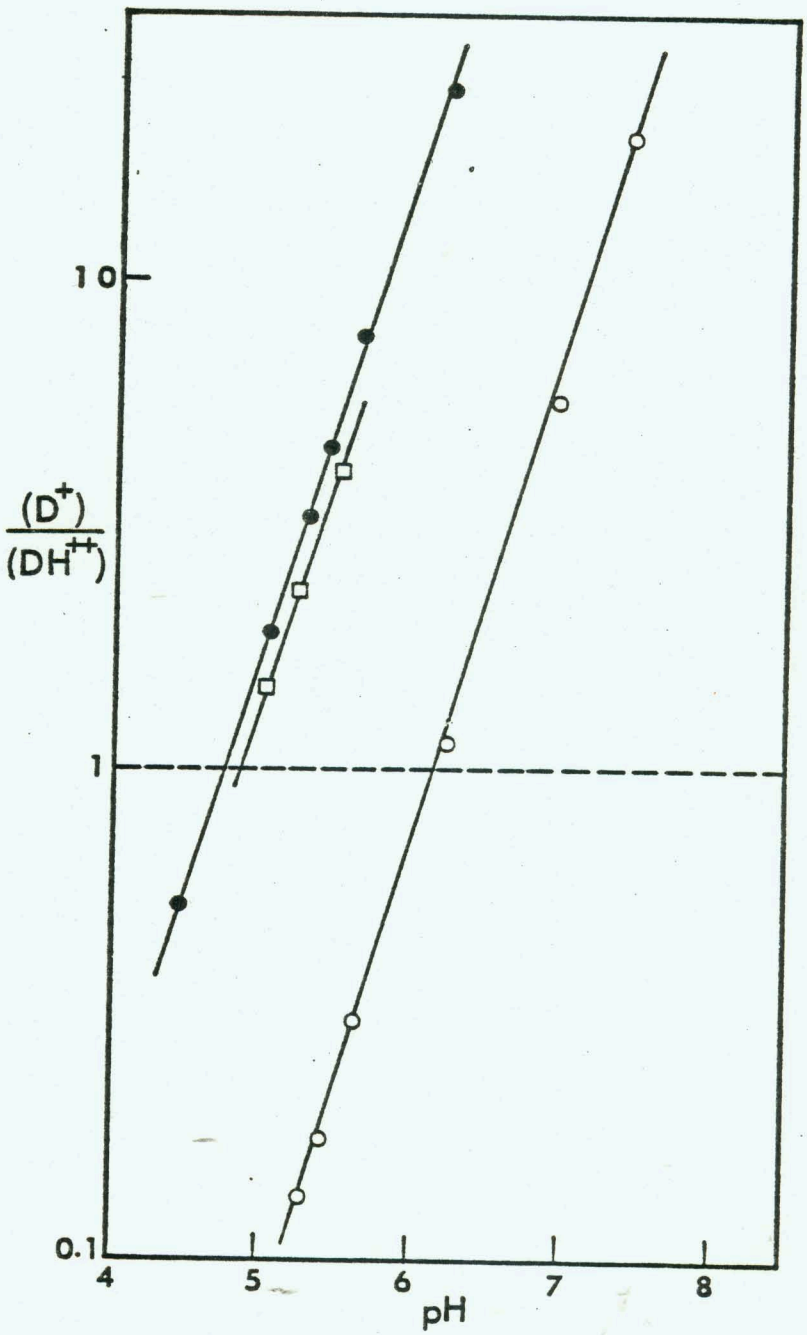
10
1
0.1
$\frac{(D^+)}{(DH^{++})}$
4
5
6
7
8
pH

Figure 3.5. Plots of log([D^+]/[DH^+]) versus pH for quinoline blue in buffer solutions with (□) and without (O) 3% β-D-octyl glucoside. The concentration of quinoline blue was $1x10^{-6}$M. Straight lines have unit slope.

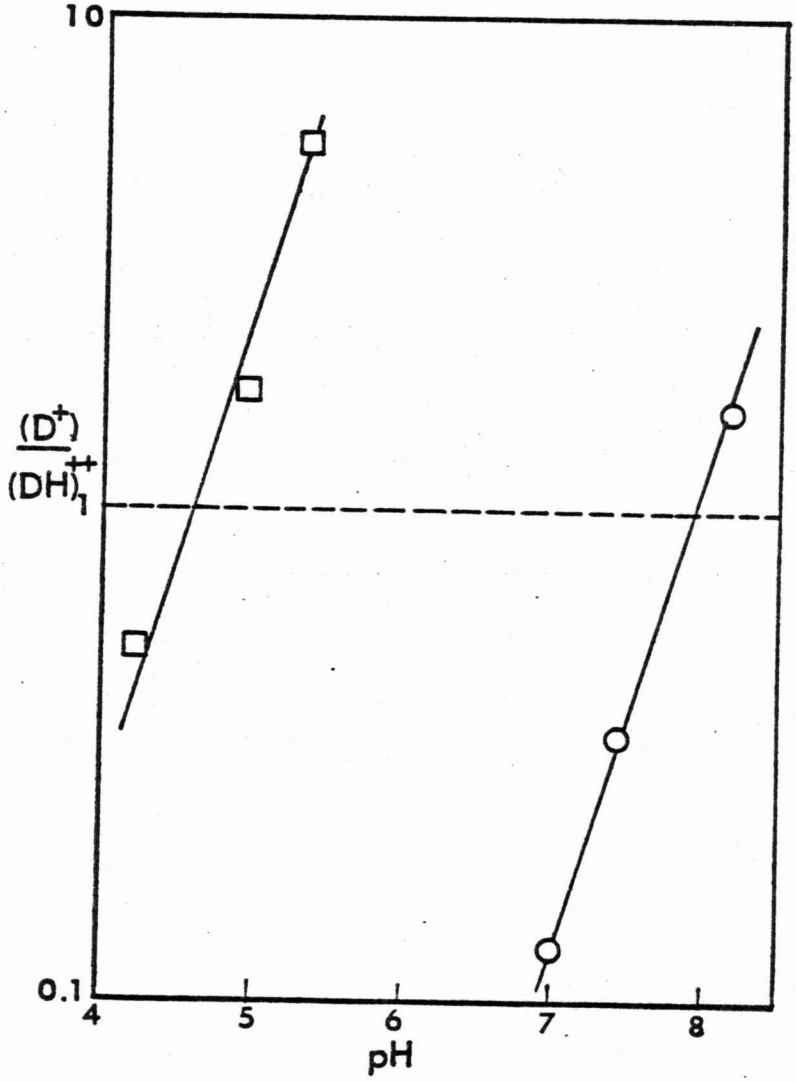
10
0.1
$\frac{(D^+)}{(DH)_1^{++}}$
4
5
6
7
8
pH

In order to minimize the effects of self-association of quinoline blue , the concentration of the singly charged form of quinoline blue was kept as low as possible by maintaining the solution pH at least 2 units below the pK (see also discussion in Section 2.3.2).

3.3.1. Solubilization in Nonionic Micelles

The solubilization behavior of the dye acid and its conjugate base was interpreted using a partition model (cf. Section 1.6). An isosbestic wavelength was observed in the solutions of both dyes in the singly charged form containing varying concentrations of either β-D-octyl glucoside or Brij 35. Figure 3.4 illustrats the spectral changes of ethyl red in the presence of different concentration of β-D-octyl glucoside micelles. At the isosbestic wavelength the solubilized and the free dyes have equal molecular absorptivity.

As shown in Figure 3.6, the indicator ratio of ethyl red in octyl glucoside solutions determined according to Equation 2-1, changes only slightly with increasing concentration until the CMC is reached. A CMC value of 0.7% was obtained from Figure 3.6 for β-D-octyl glucoside. The value is in good agreement with the CMC value reported in the literature (65). The indicator ratios of ethyl red determined in pH 5.01 sodium acetate and the pH 5.19 sodium phosphate buffer yielded the same CMC value.

Figure 3.6. Plots of R_a/R versus the concentration of β-D-octyl glucoside for ethyl red in pH 5.01, sodium acetate, and pH 5.19, sodium phosphate buffer solutions; (O) sodium acetate buffer, (□) sodium phosphate buffer.

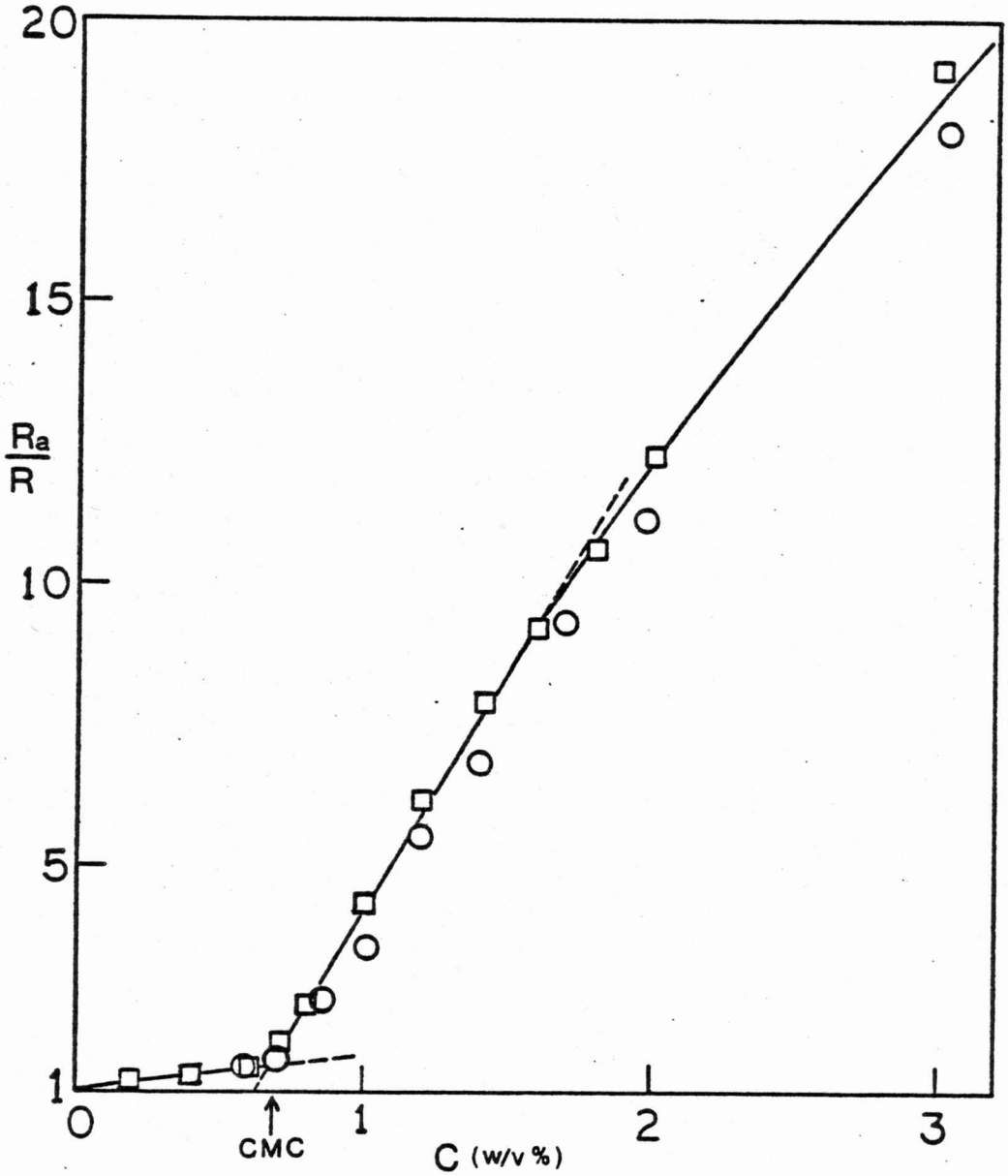
20
15
10
5
1
Ra
R
0
1
2
3
CMC
C (w/v %)

In order to analyze the solubilization data, the equations of Mukerjee and Banerjee (80) can be transformed into the following forms for cationic dyes:

$$\frac{(R/R_a) - 1}{\Phi_m / \Phi_a} = K_D \frac{R_s}{R_a} - K_D \frac{R}{R_a} \qquad [3\text{-}2]$$

where

$$K_D = ([D_s^+]\ \Phi_a)/([D_a^+]\ \Phi_m) \qquad [3\text{-}3]$$

and

$$R_s = [DH_s^{++}]/[D_s^+]. \qquad [3\text{-}4]$$

All the other symbols have been defined previously (cf. Sections 1.6 and 2.3.2). We define the number Y, obtainable directly from experiment as

$$Y = \frac{(R/R_a) - 1}{\Phi_m / \Phi_a}$$

Equation 3-2 then becomes

$$Y = K_D \frac{R_s}{R_a} - K_D \frac{R}{R_a} \qquad [3\text{-}2a]$$

By plotting Y versus R, according to Equation 3-2a, the R_s value is obtained at Y = 0. Equation 3-2a shows that the indicator ratio, R in surfactant solution is affected by the value of K_D and the value of R_s. In the case of the two cationic dyes investigated here, there were severe experimental problems in determining accurate values of R_s, the

quantity of primary interest, because of low K_D values.Thus, whereas, the experimental R values at high surfactant concentrations were fairly close to the R_s value,(i.e., the limit of R value in the case of anionic triphenylmethyl sulfonate dyes (267)), the R values at the highest surfactant concentration accessible to us in this study were far from the limiting R_s values. Further, for the cationic dyes, it was found that the change in pK on solubilization was very high, substantially higher than the change observed for the anionic dyes. As a result, very low values of R_s were obtained. Additional problems arose from the need to maintain low dye concentration to reduce self-association effects and from the sensitivity of the cationic dyes to light and some solution components such as chloride ion.

Figure 3.7 shows plots of the Y function versus R for ethyl red in solutions of β-D-octyl glucoside in three buffers of different pH values. A micellar density of 1.1 gm./ml. was used for the calculation of Φ_m (142). Because of slight change in R in dilute solutions, the value of R at CMC was used to calculate Y instead of R_a. This makes no difference in the estimate of R_s and only a small difference in the estimate of K_D. The plots are linear indicating a consistency of the data with the two-state partition model. Figure 3.8 also shows the plots of Y versus R for ethyl red solubilized in Brij 35 solutions. In order to minimize the uncertainty of the estimates, a nonlinear

Figure 3.7. Plots of the Y functions versus the indicator ratio, R, for ethyl red in β-D-octyl glucoside solutions of pH 5.01 (□), 5.19 (○), and 5.58 (△).

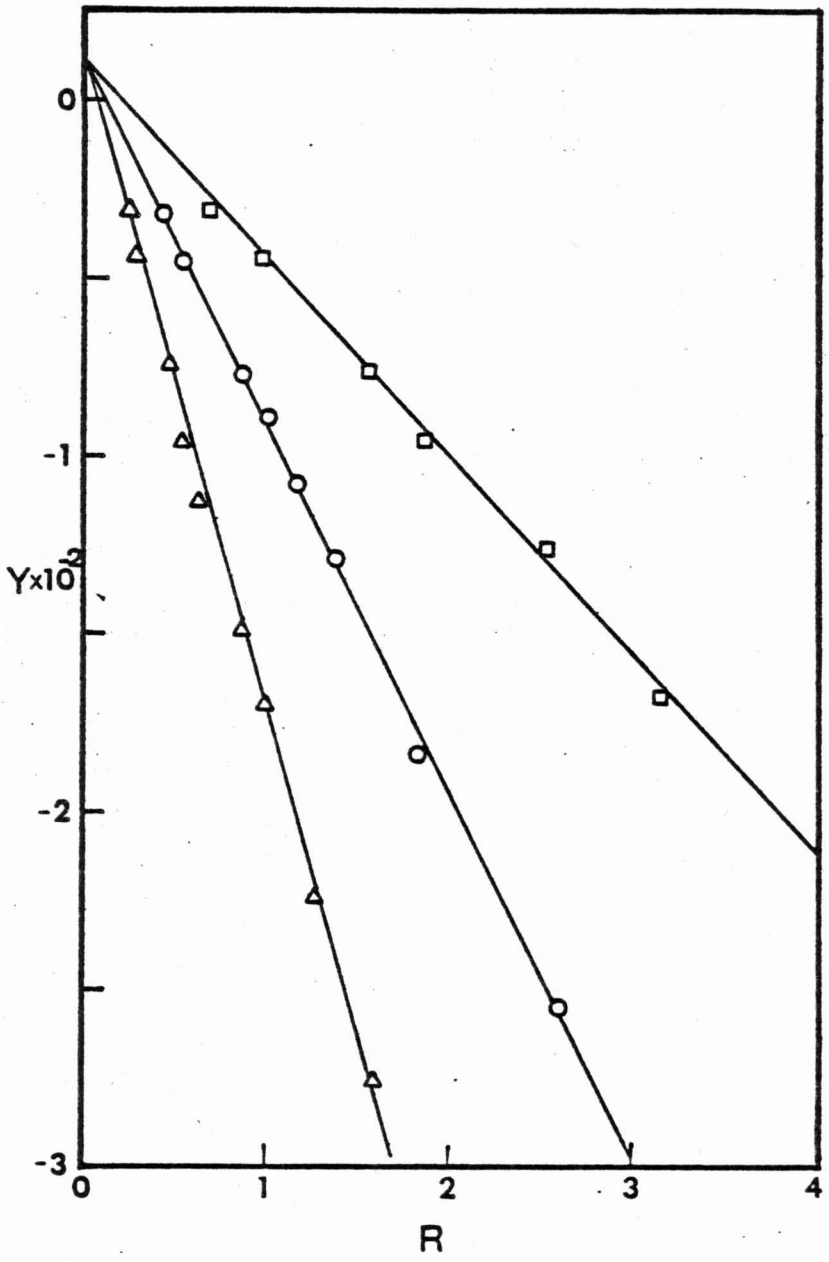
0
-1
-2
-3
Y×10
0
1
2
3
4
R

Figure 3.8. Plots of the Y function versus R of ethyl red in Brij 35 solutions of pH 5.01 (O) and pH 5.64 (□).

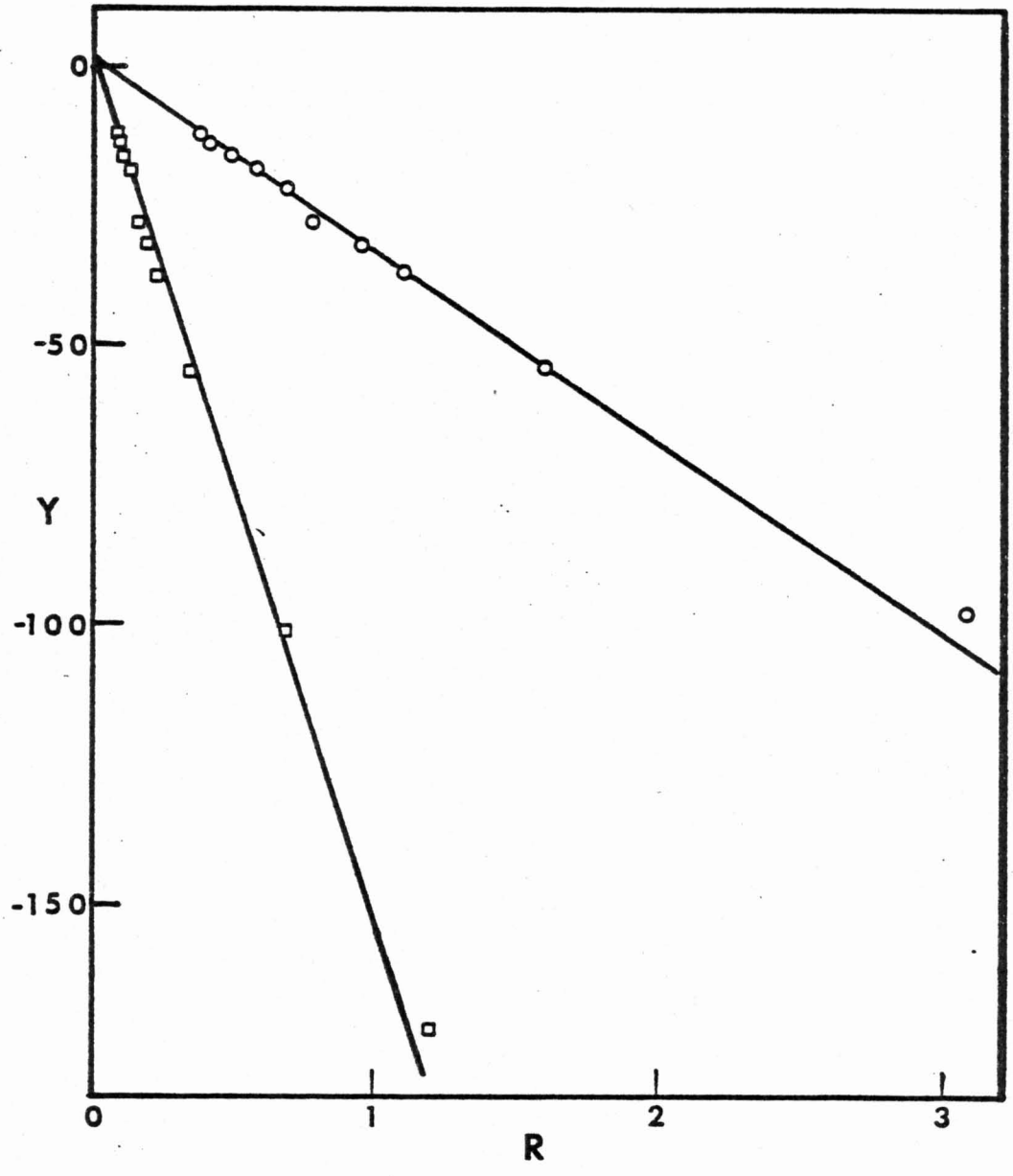
0
-50
-100
-150
Y
0
1
2
3
R

regression method (284) was used to determine R_s and K_D simultaneously from a best fit of the experimental values R and Φ_m/Φ_a in the following equation:

$$R = \frac{R_a + K_D R_s (\Phi_m/\Phi_a)}{1 + K_D (\Phi_m/\Phi_a)} \quad [3\text{-}5]$$

Equation 3-5 is obtained by rearranging Equation 3-2. Table 3.1 summarizes the indicator ratios of ethyl red obtained in β-D-octyl glucoside and Brij 35 micelles at different pH values. The standard errors in R_s and K_D and the range of pK_a- pK_s values are also given. The statistical data obtained from nonlinear regression analysis are reported in appendix 1.

From Table 3.1, it can be seen that the pK_s values of ethyl red solubilized in β-D-octyl glucoside or Brij 35 micelles are lower than the pK value in the bulk solution by very substantial amounts. The results are consistent with the image interactions of the charged species at the interface. The change in pK in Brij 35 appears to be greater than that in β-D-octyl glucoside. This is similar to that observed for the anionic dyes (73, 267). The larger effect observed in Brij 35 can be ascribed to the presence of a high polyoxyethylene concentration at the micelle surface arising from the head groups. It was found experimentally that the indicator ratio of ethyl red decreases with the concentration of the polymer, see Table 3.2. The indicator ratio of

Table 3.1. Indicator Ratios and Dissociation Constants of Ethyl Red in Nonionic Surfactant Solutions

Surfactant	pH	R_a	R_{CMC}	$R_s \pm$ Std Error	$K_D \pm$ Std Error	$pK_a - pK_s$ lower limit	$pK_a - pK_s$ best fit	$pK_a - pK_s$ upper limit	mean $pK_a - pK_s$
β-D-octyl glucoside	5.01	16.25	11.40	0.232±0.066	1014±40	1.74	1.84	1.99	
	5.19	11.27	7.50	0.201±0.030	1367±36	1.69	1.75	1.82	1.77
	5.58	4.66	3.05	0.088±0.055	1000±110	1.51	1.72	2.15	
Brij 35	5.01	16.25	----	0.049±0.057	584±147	2.18	2.52	∞	
	5.64	4.03	----	0.029±0.011	822±80	2.00	2.14	2.35	2.33

Table 3.2. Indicator Ratio of Ethyl Red in pH 5.38 PEG 1540 Solutions

W/V % PEG	R	pK_{app}
0	7.37	6.25
5	2.38	5.76
10	1.36	5.51
15	1.06	5.41
18.2	1.02	5.39

ethyl red does not show any significant change in aqueous glucose solution up to a 5M concentration. Therefore, in the case of β-D-octyl glucoside, the observed changes in pK are likely to be due primarily to image interactions caused by proximity of the micellar core with its low dielectric constant, whereas the head-groups play a minor role. For quinoline blue, the change in indicator ratio on solubilization was even more severe than in the case of ethyl red. Solutions of very low pH comparing to pK of 7.95 and more dilute dye concentration have to be used to avoid the effects of self-association of the dye. Figures 3.9 and 3.10 show the variation of R in β-D-octyl glucoside and Brij 35 solutions. Reliable estimates of R_s value could not be determined. Table 3.3 shows that the K_D values which are reliable are 5200 times higher as compared to ethyl red. This can be ascribed to the greater hydrophobic character of quinoline blue. The change in pK could not be estimated accurately but was greater than 3.5 for β-D-octyl glucoside and 3.7 for Brij 35. Thus, the effect of microenvironment at the micelle-water interface is very pronounced in this case. The results are again consistent with a stronger image interaction for the DH^{++} form as compared to the D^{+} form. This result also agrees with the observation previously made by Mukerjee and Desai (73,267) in the solubilization of anionic triphenylmethyl sulfonate dyes in the same micellar systems. They found a rough correlation between the change in pK on

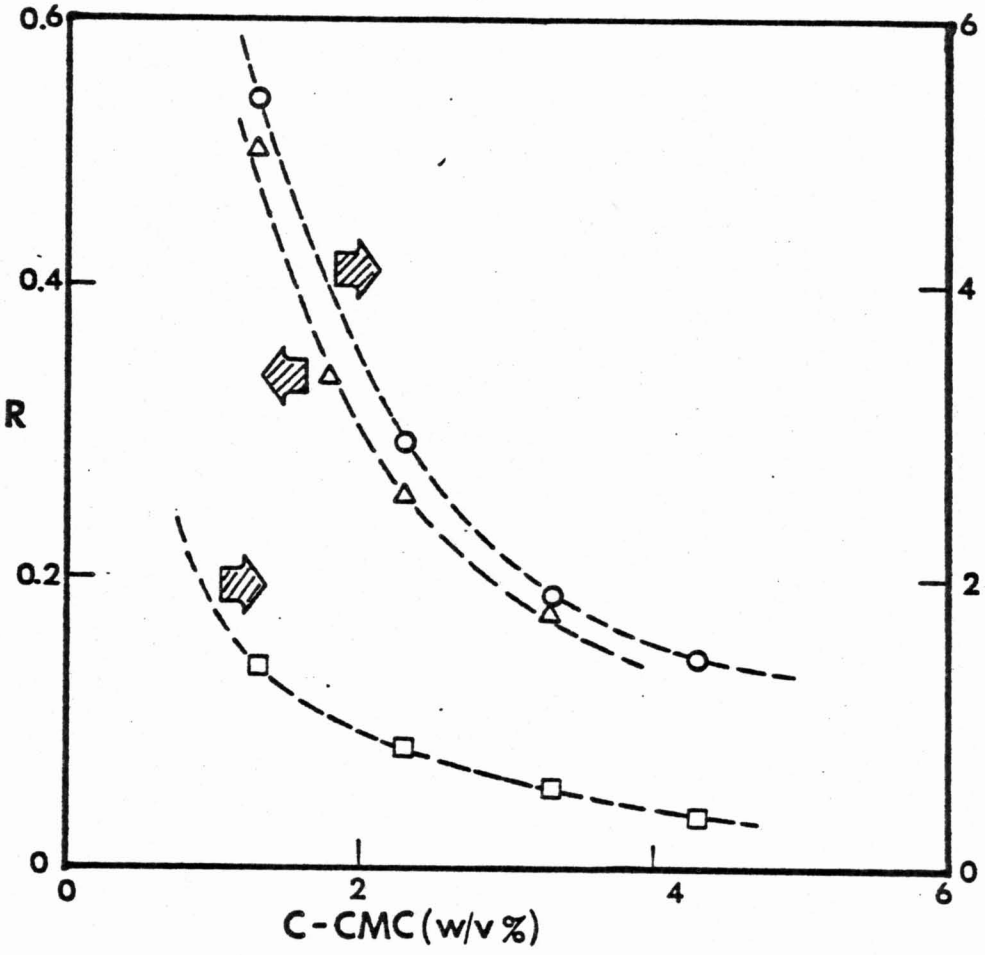

Figure 3.9. Plots of R versus C-CMC for quinoline blue in β-D-octyl glucoside solutions of pH 4.22 (O), 4.94 (□), and 5.34 (Δ).

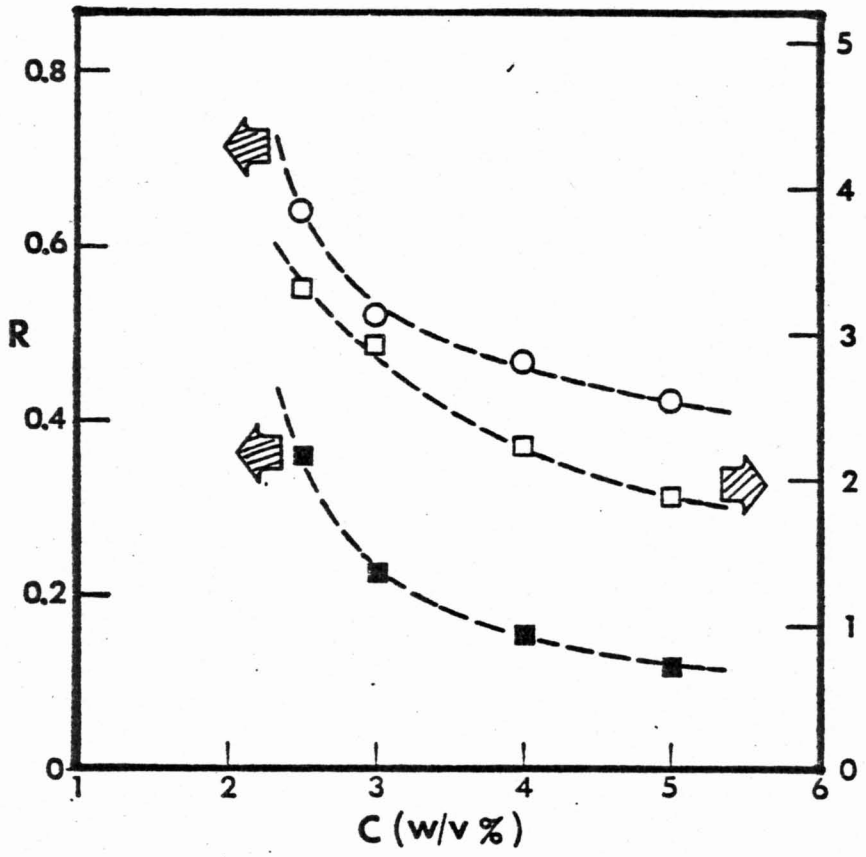

Figure 3.10. Plots of R versus C for quinoline blue in Brij 35 solutions of pH 5.34 (■), 4.95 (O), and 4.22 (□).

Table 3.3. Indicator Ratios and Dissociation Constants of Quinoline Blue in Nonionic Surfactant Solutions

Surfactant	$R_s/R_a \pm$ 95% conf.limit	K_D	pK_s	$pK_a - pK_s$
β-D-octyl glucoside	$0 \pm 3.0 \times 10^{-4}$	78000	<4.45	>3.5
Brij 35	$4 \times 10^{-6} \pm 2.2 \times 10^{-4}$	72500	<4.25	>3.7

solubilization with the pK_a of the dye itself. The magnitude of pK change becomes greater as pK_a increases.

The good fit of the experimental results to Equation 3-5 suggests the solubilization process can be satisfactorily described by a two-state model. The applicability of this model is also substantiated by the linearity and the unit slope of the log ($[D^+]/[DH^{++}]$) versus pH plots shown in Figure 3.4 for ethyl red and Figure 3.5 for quinoline blue solubilized in β-D-octyl glucoside micelles.

3.3.2. Solubilization in Anionic Micelles

The electrostatic potential at the surface of several cationic micellar systems have been examined by Mukerjee and Banerjee using anionic triphenylmethyl sulfonate indicator dyes (80). A corresponding study on an anionic micellar system has not been performed partly because of the limited availability of suitable ++ ⇌ + type cationic dyes. In the present study, ethyl red and quinoline blue have been used to probe the surface potentials of anionic alkyl sulfate micelles.

The dissociation constant of an indicator dye solubilized in ionic micelles is affected not only by the self-potential, as discussed in the nonionic micelles,but also the local hydrogen ion concentration in the vicinity of the ionizable functional group of the dye. Figure 3.11 shows the indicator ratio of ethyl red solubilized in sodium dodecyl sulfate solution of different concentrations of the

Figure 3.11. Plots of the indicator ratio,R, versus the concentration of sodium dodecyl sulfate for ethyl red at pH 4.4, 0.01N sodium acetate buffer solutions.

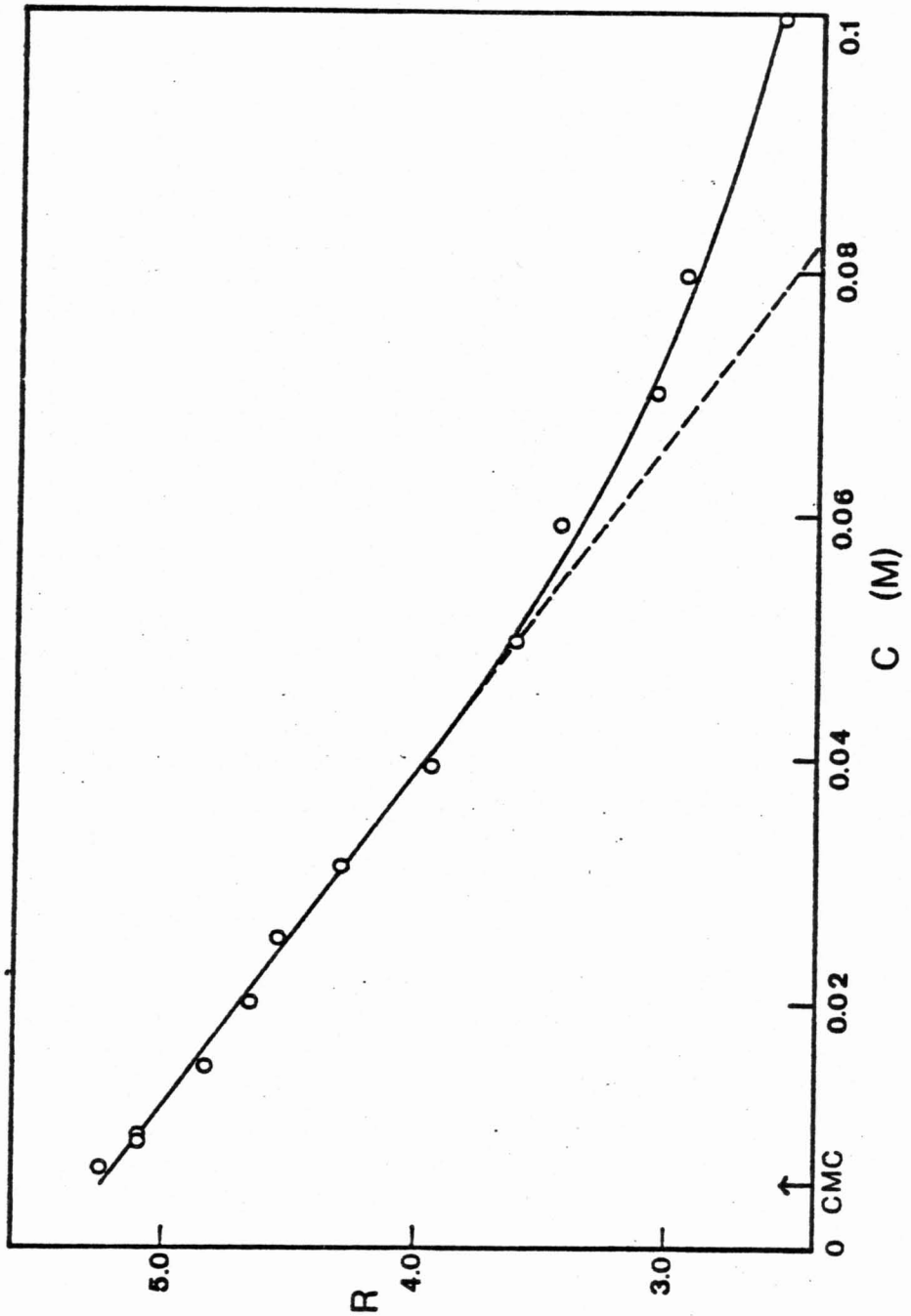
5.0
4.0
3.0
R
0 CMC
0.02
0.04
0.06
0.08
0.1
C (M)

surfactant. The R value decreases as the concentration of the surfactant is increased. This change can be ascribed entirely to the changes in hydrogen ion concentration at the micellar surface because these cationic dyes are essentially completely solubilized (80,135).

The measured indicator ratio, R, defined as $[DH^{++}]/[D^{+}]$, can be expressed as

$$\log R = pK_{app} - pH_a \ , \qquad [3\text{-}6]$$

where pH_a is the pH in the bulk solution. The corrected form of Equation 3-1 can be written as

$$pK_{app} = pK_s - e\,\Psi_s/2.303\ kT \ . \qquad [3\text{-}7]$$

Because the surface potential varies with the counter-ion concentration, the indicator ratio is expected to vary with the amount of electrolyte, or more specifically the counter-ion in the solution. To examine the effects of counter-ion, it is necessary to use R_{CMC}, the value of R at infinitive dilution of the micelle, to remove effects due to inter-micellar interactions. The R_{CMC} is obtained by extrapolation of the R values at higher surfactant concentrations to the CMC. Figures 3.11 and 3.12 show how R changes with counter-ion and micellar concentration. In the case of sodium dodecyl sulfate, when the logarithm of R_{CMC} is plotted against the logarithm of sodium ion concentration at the CMC, as shown in Figure 3.13, straight lines are obtained. It is well known that the surface potential of micelles at the CMC decreases as the counter-ion concentration increases (8,30).

Figure 3.12. Plots of the indicator ratio, R, versus the concentration of micellized sodium decyl sulfate for quinoline blue in pH 5.6 solutions of ionic strength 0.01N (O), 0.05N (△), 0.10N (□), and 0.50N (●).

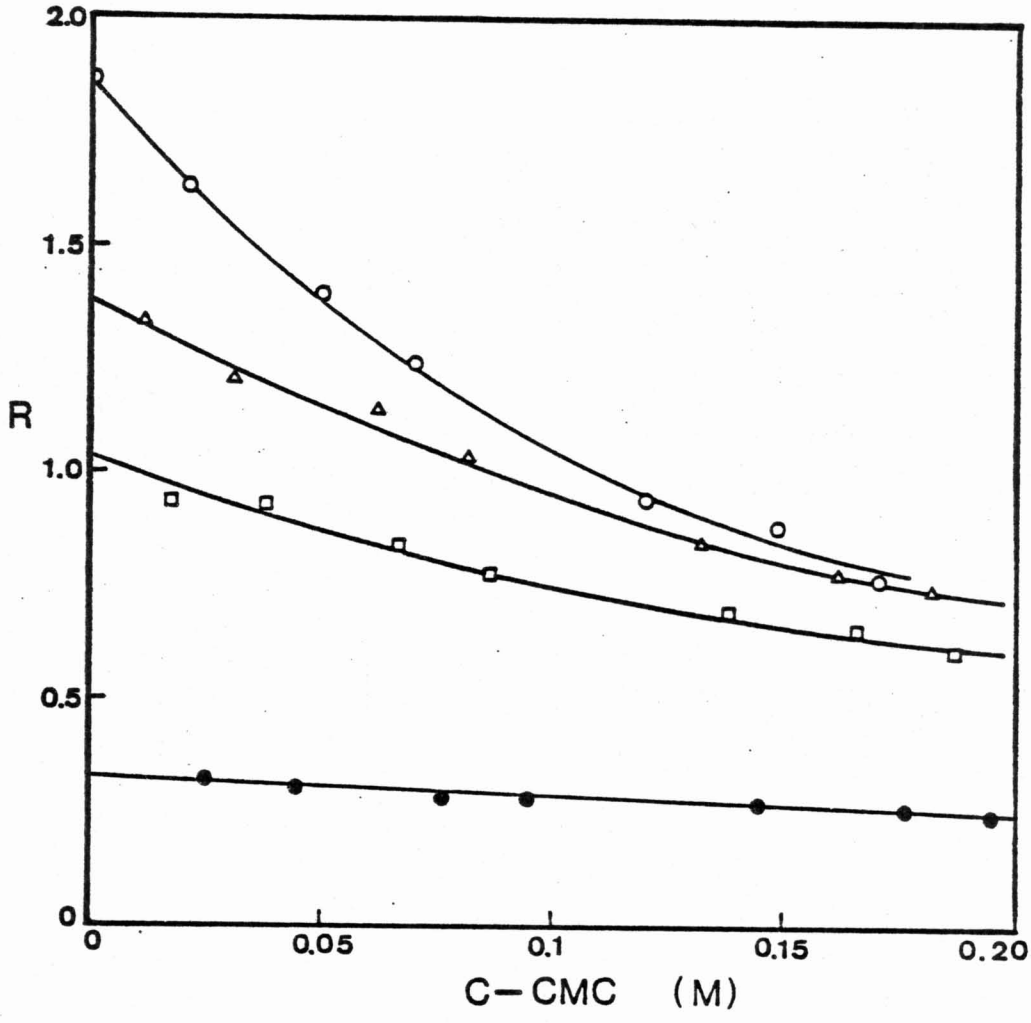
2.0
1.5
1.0
0.5
0
R
0
0.05
0.1
0.15
0.20
C—CMC (M)

Figure 3.13. Plots of R_{CMC} versus the logarithm of sodium ion concentration at the CMC of sodium dodecyl sulfate solutions for quinoline blue at pH 5.6 (O) and ethyl red at pH 4.4 (●). The straight lines have a slope of -0.76. The R_{CMC} values at high salt concentrations were corrected for slight changes in pH.

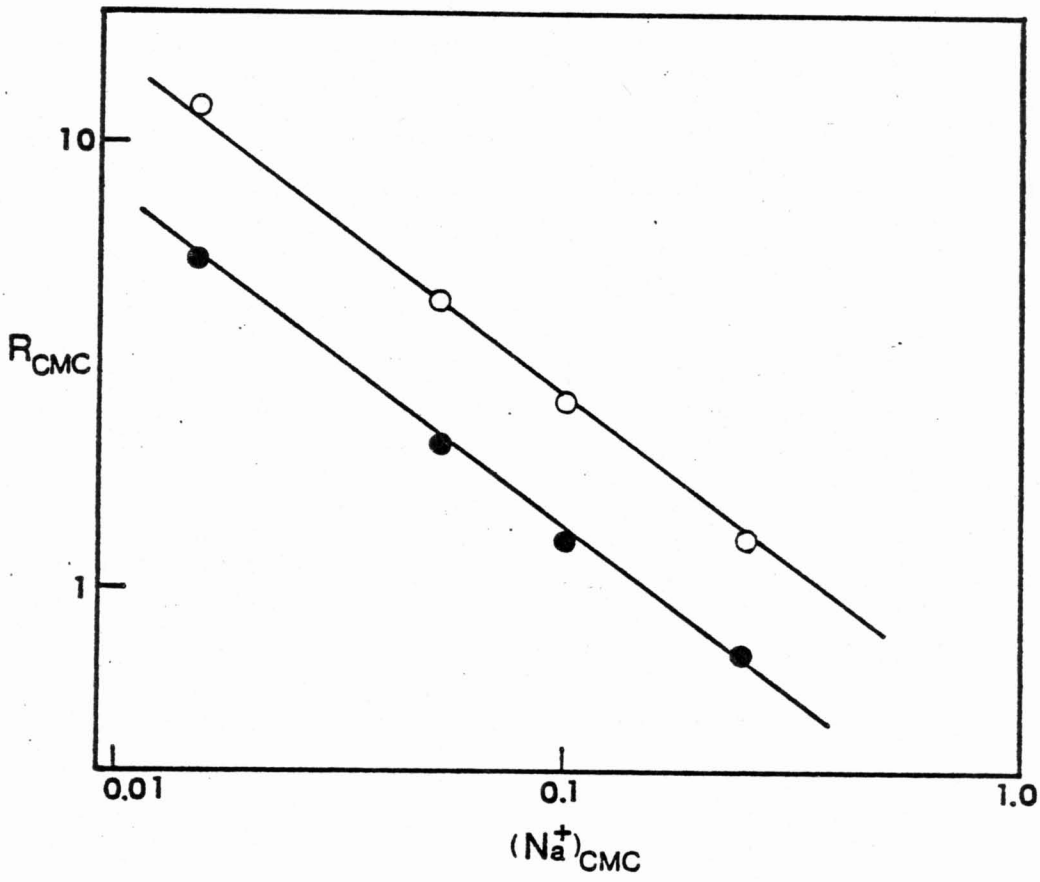
10
1
R_{CMC}
0.01
0.1
1.0
$(Na^+)_{CMC}$

The linear relationship seen in Figure 3.13 can be understood on this basis in terms of Equation 3-7.

Huisman calculated the surface potential of a series of sodium alkyl sulfate micelles at different electrolyte concentrations (8,30). Figure 3.14 shows the surface potential data in the reduced form, i.e., expressed as $e\psi_c/kT$, of sodium dodecyl sulfate at the CMC obtained from solutions containing different amounts of sodium ions (30). A linear relationship is observed. The line has a slope of 1.75. This linear relationship is consistent with the linear plots in Figure 3.13. Both dyes give identical slope of -0.76, the slope expected from the data in Figure 3.14, i.e., -1.75/2.303. Since the potential calculated by Huisman used the Gouy-Chapman theory, the present data show a remarkable consistency with this theory in so far as the ionic strength dependence of the potential is concern.

If the surface potential at the CMC calculated from the Gouy-Chapman theory (30) is used, the dissociation constant of the dye in the solubilized state, pK_s, can be obtained from Equation 3-7 using the R_{CMC} value or Equation 3-1a using the pK_{app} value. The calculated pK_s values for ethyl red and quinoline blue in sodium dodecyl sulfate micelles are reported in Table 3.4. A mean pK_s value of 2.42 and 3.90 are obtained for ethyl red and quinoline blue, respectively. The pK_s values of ethyl red and quinoline blue obtained from the anionic alkyl sulfate micelles and the nonionic micelles

Figure 3.14. Plots of $-e\Psi_c/kT$ versus the logarithm of sodium ion concentration at the CMC of sodium dodecyl sulfate. The straight line has a slope of -1.75. Data are taken from reference (30).

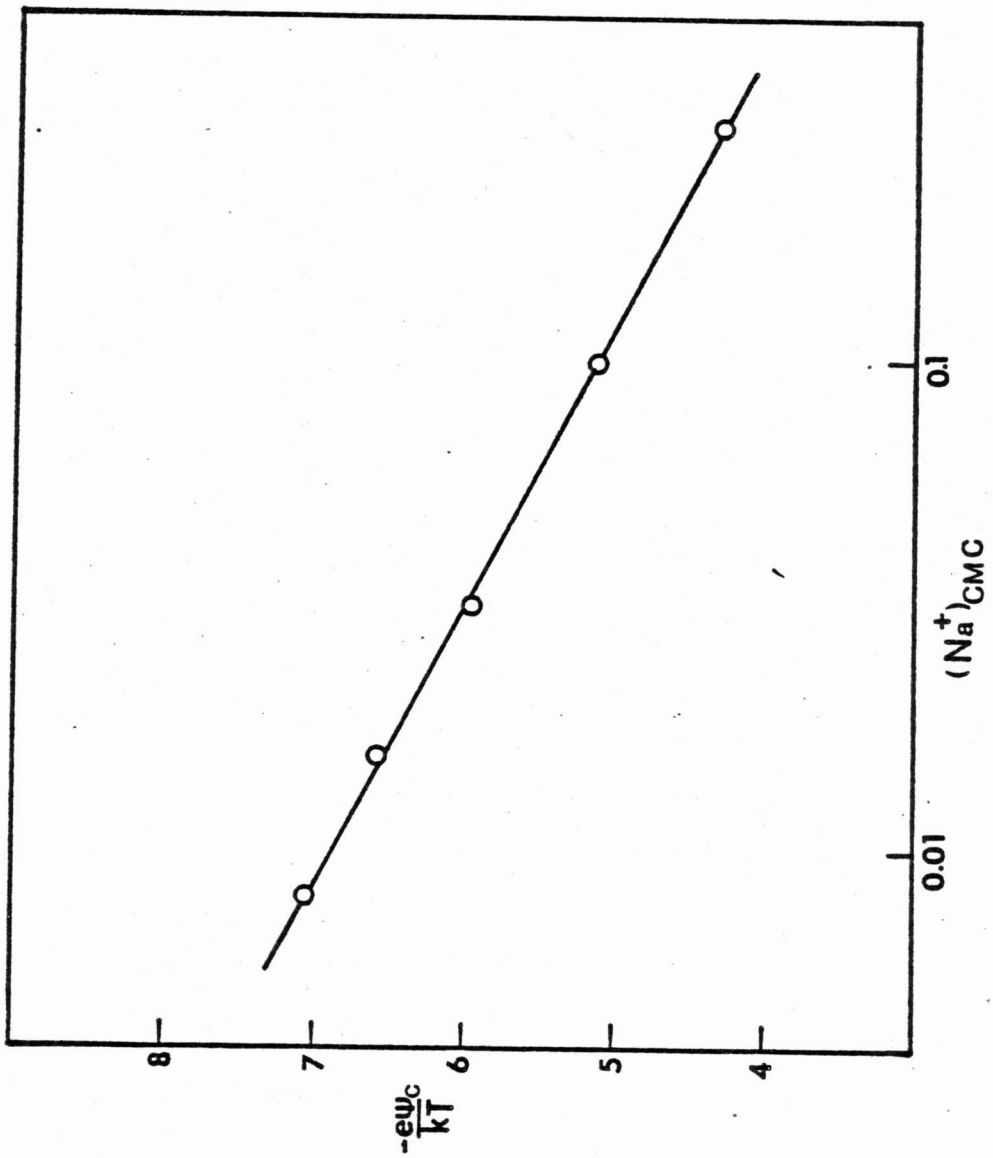
8
7
6
5
4
$-\frac{e\psi_c}{kT}$
0.01
0.1
$(Na^+)_{CMC}$

Table 3.4. Dissociation Constants of Ethyl Red and Quinoline Blue Solubilized in Sodium Dodecyl Sulfate Micelles

Dye	$[Na^+]_{CMC}$	$-e\,\Psi_c/2.303\,kT$	pK_s	mean pK_s
Ethyl Red	0.015	2.84	2.41	2.42
	0.052	2.44	2.40	
	0.102	2.23	2.41	
	0.251	1.92	2.45	
Quinoline Blue	0.015	2.84	3.92	3.90
	0.052	2.44	3.90	
	0.102	2.23	3.86	
	0.251	1.92	3.90	

are summarized in Table 3.5. In the case of ethyl red, the pK_s values in the nonionic micelles are considerably higher than the pK_s values in the anionic micellar systems. A similar difference is seen in quinoline blue, although the magnitude is somewhat lower.

Since the dye carrying opposite charges to the micellar surface, it is likely that the charged portion of the dye molecule is solubilized at the Stern layer of the anionic micelle. Theoretically, the Stern layer is a region where a strong electric field exists due to the high surface potential and the rapid drop of the potential within a relatively short distance. It is known that the dissociation constant of weak acid under a strong electric field increases as a result of the Wien effect (279,280). The dissociation of indicator dyes at the Stern layer may also be subjected to such an effect. The low pK_s values of both dyes in the anionic micelles indicate that the dissociation constant at the ionic micellar surface is increased as compared to the nonionic systems. Such an effect is also indicated in the dependence of pK_s values on the chain length of the alkyl sulfate micelles. The pK_s values of both dyes show a consistent increase , although small, from dodecyl sulfate to octyl sulfate micelles (see Table 3.5). It has been shown by Huisman (30) that the Gouy-Chapman potential at alkyl sulfate micellar surface decreases from dodecyl to octyl sulfate. The decrease in surface potential is

Table 3.5. Summary of pK_s Values of Ethyl Red and Quinoline Blue Solubilized in Nonionic and Anionic Micelles

Surfactant	pK_s	
	Ethyl Red	Quinoline Blue
β -D-octyl glucoside	4.48	<4.45
Brij 35	3.92	<4.25
Sodium dodecyl sulfate	2.42	3.90
Sodium decyl sulfate	2.53	4.00
Sodium octyl sulfate	----	4.20

expected to reduce the electric field and lessen the Wien effect. The present data, therefore, suggest that the dissociation of dyes in ionic micelles is not only affected by the local hydrogen ion concentration and the changing in self-potential but is also subjected to the effect of an electric field at the micellar surface due to the high potential.

The observed effect of surfactant concentration on the indicator ratio can be interpreted in terms of an increase in the ionic strength of the inter-micellar fluid (80). Such an increase in ionic strength is due to the negative adsorption of co-ions from the micellar surface. The effective ionic strength, I, in a solution of micellar concentration C_m can be approximated by Equation 3.8 (80),

$$I = I_{CMC} + A\ C_m \quad , \qquad [3\text{-}8]$$

where I_{CMC} is the ionic strength at the CMC, C_m is the equivalent concentration of micellized surfactant, and A is the negative adsorption expressed as the number of equivalence of co-ion excluded per equivalent of micellized surfactant. Since the buffer anions act as co-ions, their increase in concentration in the inter-micellar fluid is by the factor of I/I_{CMC}. The increase in the ionic strength causes a decrease of the surface potential. This decrease can be obtained from the observed effect of counter-ion on the surface potential, i.e., by the factor of $(I/I_{CMC})^{0.76}$. By combining these two factors, the total effect of negative

adsorption to the indicator R is then expressed by the following equation:

$$\frac{R}{R_{CMC}} = (1 + A\, C_m/I_{CMC})^{1.76} . \qquad [3\text{-}9]$$

Equation 3-9 can be rewritten as a power series:

$$\frac{R}{R_{CMC}} = 1 + 1.76\, \frac{AC_m}{I_{CMC}} + \frac{0.76 \times 1.76\, A^2 C_m^2}{2!\, I_{CMC}^2} + \ldots \qquad [3\text{-}9a]$$

Since A is usually small, the third and higher terms can be neglected. The negative adsorption, A, can, therefore, be determined directly from the initial slope of R versus C_m plots, such as the ones shown in Figures 3.11 and 3.12. The negative adsorption from sodium dodecyl sulfate micelles as determined by this method using two indicator dyes, ethyl red and quinoline blue at pH 4.4 and 5.6, respectively, are reported in Table 3.6. These data show excellent mutual consistency. The data can also be compared with the theoretical estimates obtained from the cauculated data based on the Gouy-Chapman theory reported by Huisman (30). The agreement is by and large fairly good. The data determined at low ionic strengths are relatively less precise because of the rapid change in R near the CMC.

3.3.3. Relation of Micellar Catalysis to Indicator Dye Ratio

Chemical reactions in aqueous solutions are often accelerated or inhibited by the presence of micelles. Such rate effects are related to the nature of solubilization by

Table 3.6. Negative Adsorption of Sodium Dodecyl Sulfate Determined by Dye solubilization Method

Ionic Strength At CMC	Negative Adsorption		
	Quinoline Blue At pH 5.6	Ethyl Red At pH 4.4	Theoretical Value (30)
0.015	0.102	0.100	0.128
0.052	0.097	0.101	0.135
0.102	0.136	0.140	0.148
0.251	0.173	0.181	0.197

micelles and local concentration of ionic reactants at the micelle-water interface.

Many studies on micellar catalysis of ester hydrolysis have been reported (10,281-283). Such hydrolytic reactions are catalyzed by hydrogen ion. It is, therefore, expected that anionic micelles, such as sodium dodecyl sulfate, will cause a rate acceleration because of the higher local hydrogen ion concentration at the micelle-water interface.

Dunlap and Cordes (283) conducted a systematic study on the hydrolysis of methyl orthobenzoate in 0.01M sodium dodecyl sulfate solutions containing different types of 1:1 electrolytes of different concentrations. The second-order rate constants obtained in these salt solutions were found to decrease monotonically with the concentration of the added electrolyte. Different curves were obtained for different electrolytes. These observations suggested that both the counter-ion concentrations and the nature of the counter-ion are important in catalysis. Since the indicator ratio, R, reflects the local hydrogen ion concentration, the R value of ethyl red at different concentrations of several different electrolytes in sodium dodecyl sulfate solutions were measured. All the electrolytes chosen were used by Dunlap and Cordes in their studies (283).Figure 3.15 shows that the R values decrease monotonically with salt concentration. It is also found that at the same salt concentration the R values differ when the counter-ion is different.

Figure 3.15. Plots of the indicator ratio, R, versus the concentration of added salt for ethyl red in solutions of pH 4.4, 0.01N sodium acetate buffer and 0.01M sodium dodecyl sulfate. The counter-ions are (△) Li^+ , (○) Na^+, (□) Cs^+, (■) Rb^+ at 43°C, and (▼) K^+ at 43°C .

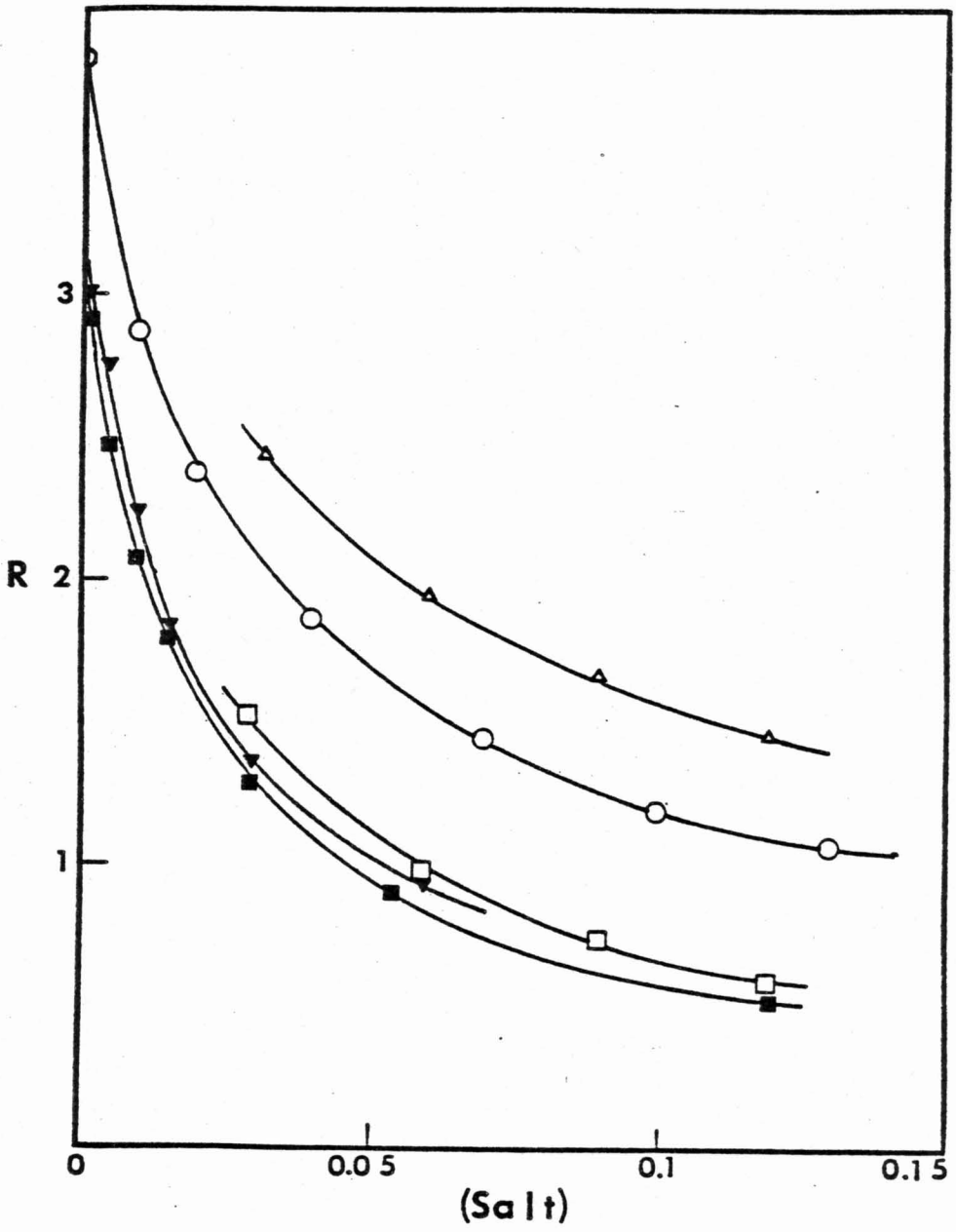
R
3
2
1
0
0.05
0.1
0.15
(Salt)

If these changes in R values, both with concentration and the nature of the counter-ion, can be ascribed to changes in the local hydrogen ion concentration at the micellar surface, then the changes in the R values should parallel the changes in the second-order rate constants of hydrolysis of methyl orthobenzoate. In other works, the assumption of the effective local hydrogen ion concentration at the micellar interfaces as an imprtant variable in micellar catalysis can be tested by comparing the kinetic data of Dunlap and Cordes with the present equilibrium data.

In Figure 3.16 the logarithm of second-order rate constant is plotted against the logarithm of the R value. The correlation in the case of sodium and lithium ions are excellent, as shown by the data falling on a line of unit slope. For the other counter-ions, the correlation is not quite as good over the entire concentration range. At high concentrations, however, many of these counter-ions approach the slope of unity in the log k_2 versus log R plots. Thus, the extremely complex specific counter-ion effects do seem to be somewhat different for the indicator dyes as compared to the catalytic reactions. Nevertheless, the correlations of the equilibrium R values with the kinetic data indicate that the easily determined indicator R ratio might provide an approach towards predicting or correlating catalytic effects at interfaces.

Figure 3.16. Plots of the second-order reaction rate constants, k_2, for the hydrolysis of methyl orthobenzoate in 0.01M sodium dodecyl sulfate solutions containing different amounts of added salt versus the indicator ratio of ethyl red obtained under the conditions described in Figure 3.15. The broken line has unit slope. The rate constants were taken from reference (283). The counter-ions are: (●) Na^+, (▲) Li^+, (⬢) Cs^+, (○) NH_4^+, (□) $CH_3NH_3^+$, (△) $(CH_3)_2NH_2^+$, (⬡) $(CH_3)_3NH^+$.

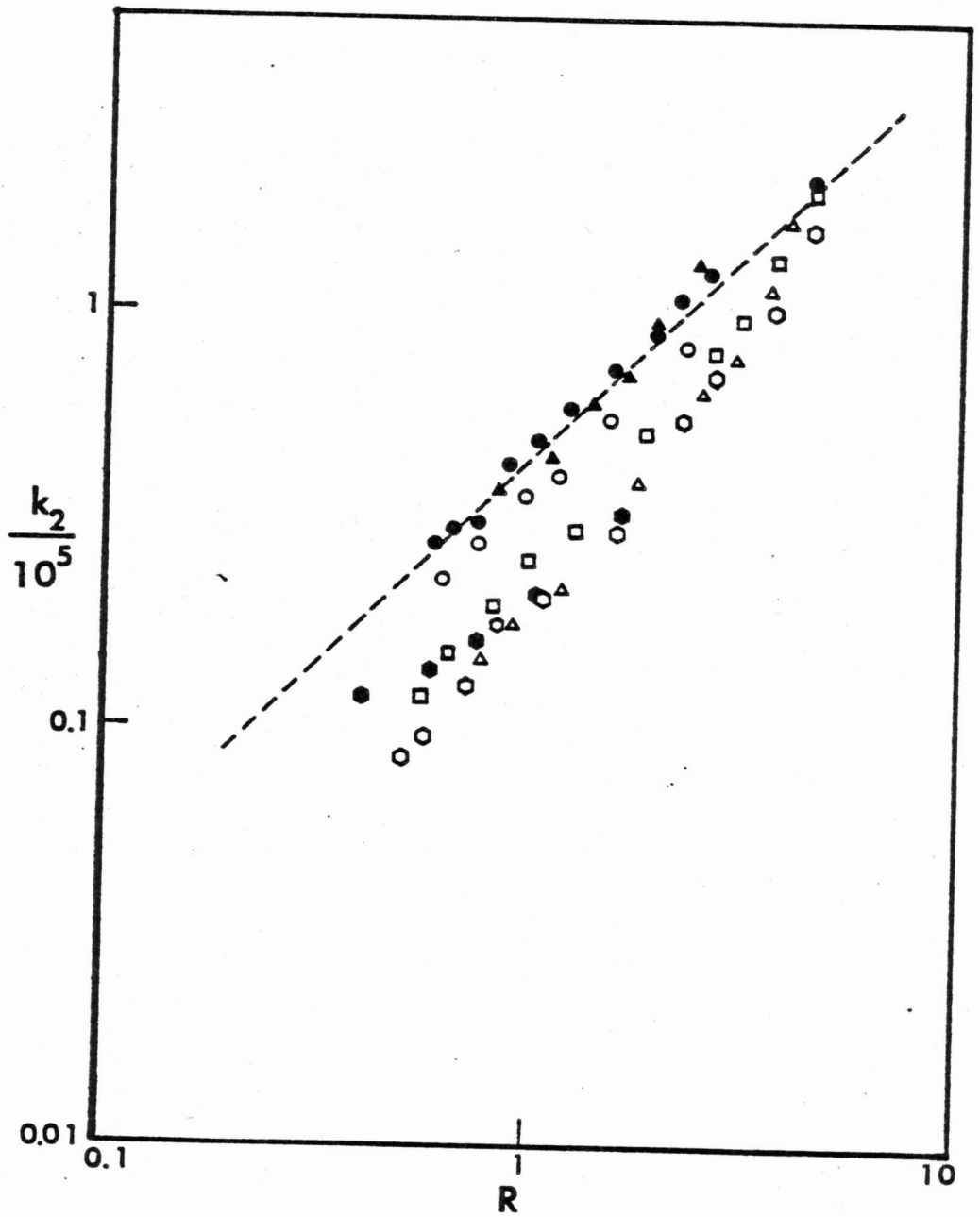
1
0.1
0.01
$\frac{k_2}{10^5}$
0.1
1
10
R

3.4. Conclusion

The dissociation constants of two cationic dyes, ethyl red and quinoline blue, solubilized in nonionic micelles of β-D-octyl glucoside and Brij 35 were found to be significantly lower than the intrinsic pK values obtained in bulk solution. These changes in pK value can be explained by the electrostatic image interactions of the charges carried by the dye molecule at the micelle-water interface. The effect of counter-ion concentration and inter-micellar interaction on surface potentials can also be studied by using these indicator dyes. The results obtained are in good agreement with previous studies and theoretical values.

The use of indicator dyes as probes for monitoring the effective local hydrogen ion concentration even in complex systems such as micellar solution containing different counter-ions was investigated by comparing some kinetic data from the literature with R values. The kinetic data relate to the hydrolysis rate constants of methyl orthobenzoate in 0.01M sodium dodecyl sulfate containing various amounts of added electrolytes of different types. The R values determined in such solutions show fair correlation with the kinetic data.

4. DEAGGREGATION OF AGGREGATED DYE BY POLYETHYLENE GLYCOLS AND PLURONIC POLYOLS AND THE SIGNIFICANCE OF APPARENT CRITICAL MICELLIZATION CONCENTRATION

4.1. Background

Polyethylene glycol (PEG) and many of its adducts have been studied extensively (178,200). Pluronic polyols are block copolymers of propylene oxide and ethylene oxide. Many of their properties in aqueous solutions have also been investigated (178). These polymers are highly surface active in aqueous solutions (178,218,222). Several papers (207-209, 222) have claimed that Pluronic polyols show micelle formation in the manner of detergents in aqueous solutions and exhibit a critical micellization concentration (CMC). Many of these CMC values have been obtained from measurements of spectral chages produced on iodine and the dye benzopurpurine 4B upon solubilization by the polymer (207-209). There are, however, serious disagreements in the published CMC values, which vary by a factor of ten or more, even when obtained by the same method. Light scattering (210,211) and ultracentrifugation (212) studies have indicated an aggregation number between one and two for several Pluronic polyols which are clearly inconsistent with micelle formation.

In some cases, microscopic phase separation can occur in solutions of block copolymers having polymeric constituents of substantially different solubility in the solvent

used (213-217). The less soluble part of the polymer usually forms the core of a microspherical particle which is surrounded by a layer of the more soluble polymer segments. Such microscopic phase separation has been interpreted as analogous to micelle formation of detergent solutions (213,216, 217). Many of the thermodynamic properties of aqueous polypropylene oxide and polyethylene oxide solutions have been studied (219-221). The results of these studies indicate that the polymers of ethylene oxide and propylene oxide do not form micelles in aqueous solutions (219,220). The solution properties of polyethylene oxide and polypropylene oxide are generally similar to each other. It is unlikely that their block copolymers, such as Pluronic polyols, form micelles or exhibit microscopic phase separation in aqueous solutions under normal conditions.

Polyethylene oxides have been known to solubilize many different organic molecules in aqueous solutions (21,22). The mechanism of solubilization and the interactions of multifunctional organic compounds with hydrophilic polymers in aqueous solution are of a complex nature and not fully understood (19-22,225). It has been suggested that hydrophobic interactions may be the main driving force for solubilizing nonpolar compounds in PEG solutions (21,223). Hydrogen bonding has also been proposed by some investigators to explain the solubilization of some phenolic compounds (224, 225). In a study on the solubilization of para-hydroxybenzoic

acid in PEG solutions of different molecular weights, Mukerjee and Johnson have concluded that multiple-site interactions are involved in the solubilization process(23).

In order to investigate the anomalies in the reported CMC values of Pluronic polyols and the solubilization properties of the polyethylene oxide type of polymers, the effect of several Pluronic polyols and PEG's of different molecular weights on the spectral properties of the dye benzopurpurine 4B has been studied.

4.2. Results and Discussion

Table 4.1 shows the composition and molecular weight of the Pluronic polyols used in the present study. The hydrophobicity of these polymers varies with the ratio of propylene oxide to ethylene oxide. As a result, the solubility of Pluronic polyols not only depends on the molecular weight but also varies considerably with the propylene oxide content. The solubilities of Pluronic F108, F68, and P75 in water are greater than 10% at room temperature. Pluronic L62, with the highest propylene oxide content, has a solubility of approximately 5% at room temperature, even though it has the lowest molecular weight among the polymers studied. It was noticed that the solubilities of Pluronic L62 and P75 increase with a decrease in temperature. This unusual temperature effect on solubility was not investigated.

Figure 4.1 shows qualitatively the effects of aggrega-

Table 4.1. Composition and Molecular Weight of Pluronic polyols

$$HO-(CH_2CH_2O)_r-(\underset{\underset{CH_3}{|}}{CHCH_2O})_s-(CH_2CH_2O)_t-H$$

Type	Molecular Weight	W/W % Ethylene oxide
L62	2500	20 to 30
P75	4160	50 to 60
F68	8000	80 to 90
F108	15550	80 to 90

Figure 4.1. Absorption spectra of 5.04×10^{-5}M benzopurpurine 4B in different solvents and in aqueous solutions containing different additives, 1) water; 2) 0.1N sodium chloride solution; 3) methanol; 4) 0.1N sodium chloride and 5% Pluronic F68; 5) 5% Pluronic F68 solution.

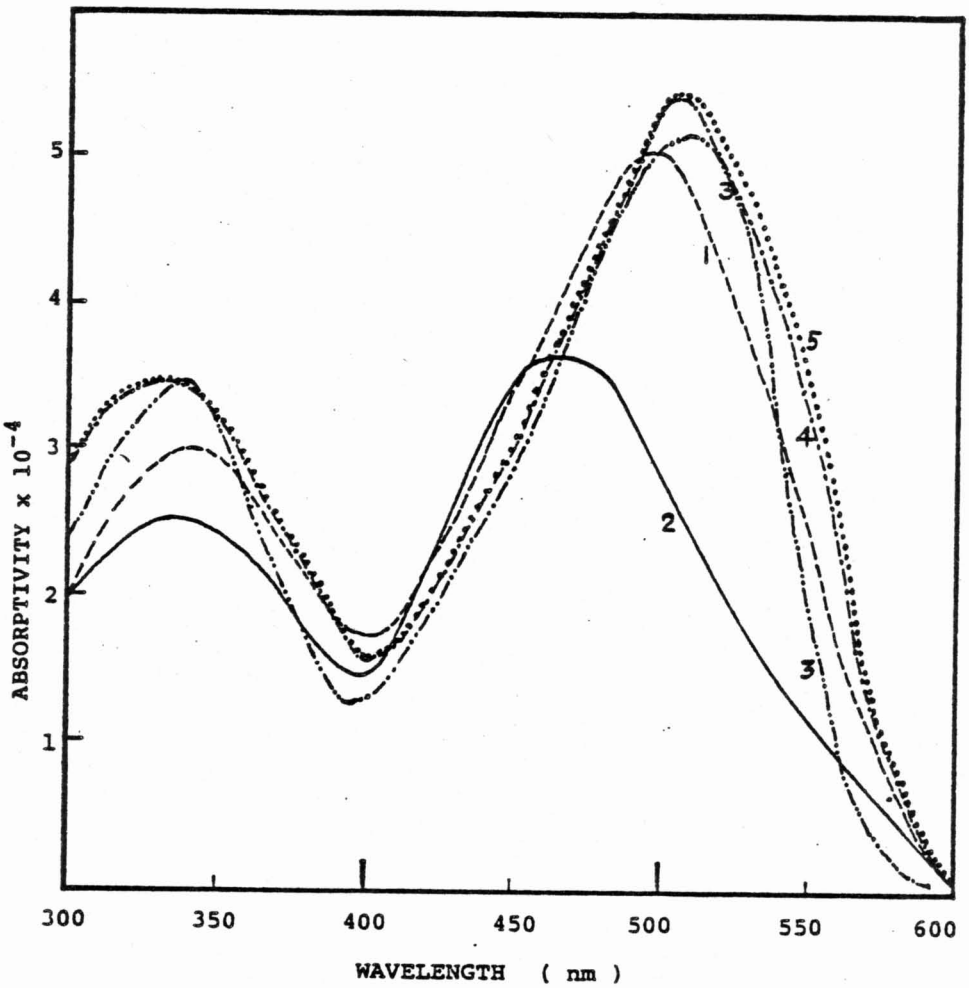
ABSORPTIVITY x 10^{-4}
5
4
3
2
1
300
350
400
450
500
550
600
WAVELENGTH (nm)
1
2
3
4
5

tion and polymer solubilization on the spectra of benzopurpurine 4B. The molecular structure of benzopurpurine 4B is shown in Figure 4.2. It has been reported that this dye is capable of forming stacking type aggregates in aqueous solutions (226-233). Its visible spectrum in water, like most aggregating azo dyes, shows very little concentration dependence (33,226). The absorptivity of benzopurpurine 4B at 500 nm, the band maximum, increases only by about 1% when the concentration changes from $2x10^{-5}$ to $6.36x10^{-6}$M (226). Upon the addition of 5% Pluronic P75, the band maximum shifts to a longer wavelength and the intensity increases. Similar spectral changes have also been observed in other Pluronic polyols and PEG solutions. The spectral characteristics of the dye in the polymer solutions are qualitatively similar to those obtained in methanol solution, in which the dyes are primarily in the monomeric form. Light scattering (232), conductivity (227-229), and diffusivity measurements (230,231) of benzopurpurine 4B solutions have indicated that the degree of aggregation of this dye increases drastically upon the addition of electrolyte to the aqueous solution. As a result, the spectrum exhibits an appreciable blue shift and reduction in intensity, as indicated in Figure 4.1. The band maximum, around 500 nm, in water shifts to a shorter wavelength in 0.1N sodium chloride solution and the intensity is reduced considerably. These effects are characteristic of an increase of the degree of aggregation

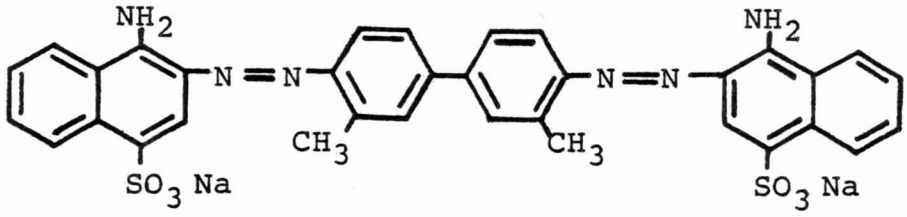

Figure 4.2. Molecular structure of benzopurpurine 4B

(226). The addition of 5% Pluronic P75 completely reverses this effect and the spectrum becomes similar to that obtained in a solution containing the same amount of polymer without added salt, suggesting deaggregation of the dye by the polymer. The effect of polymer concentration on the absorbance of the dye at 540 nm, the wavelength at which the maximum absorbance change occurrs, is shown in Figure 4.3, plotted as the absorbance change versus the logarithm of polymer concentration. From such curves, the CMC values of Pluronic polyols have been obtained by locating a concentration at which the rise in differential absorbance takes place (207-209). For example, a CMC value for Pluronic L62 may be located at about 0.002% from Figure 4.3. It is clear that the effects exhibited by PEG 6,000 and 20,000 are very similar to those of the Pluronics. If the same method is used,the data indicate micelle formation of both PEG 6,000 and 20,000 at about 0.01%. Other properties of PEG, however, do not indicate micelle formation in PEG solutions.

Figure 4.4 shows differential absorption data at two different dye concentrations in solutions of Pluronic F68. The curves are similar in shape, but the magnitude of the differential absorbance is higher at the higher dye concentration. If apparent CMC values are determined, from the curves where the slope changes rapidly, different CMC values are obtained at the two different dye concentrations. Both

Figure 4.3. Differential absorbance at 540 nm of a 5.04×10^{-5}M benzopurpurine 4B solution as a function of additive concentration, 1) PEG 6,000, 2) PEG 20,000; 3) Pluronic F68; 4) Pluronic L62; 5) Pluronic F108; 6) Brij 35.

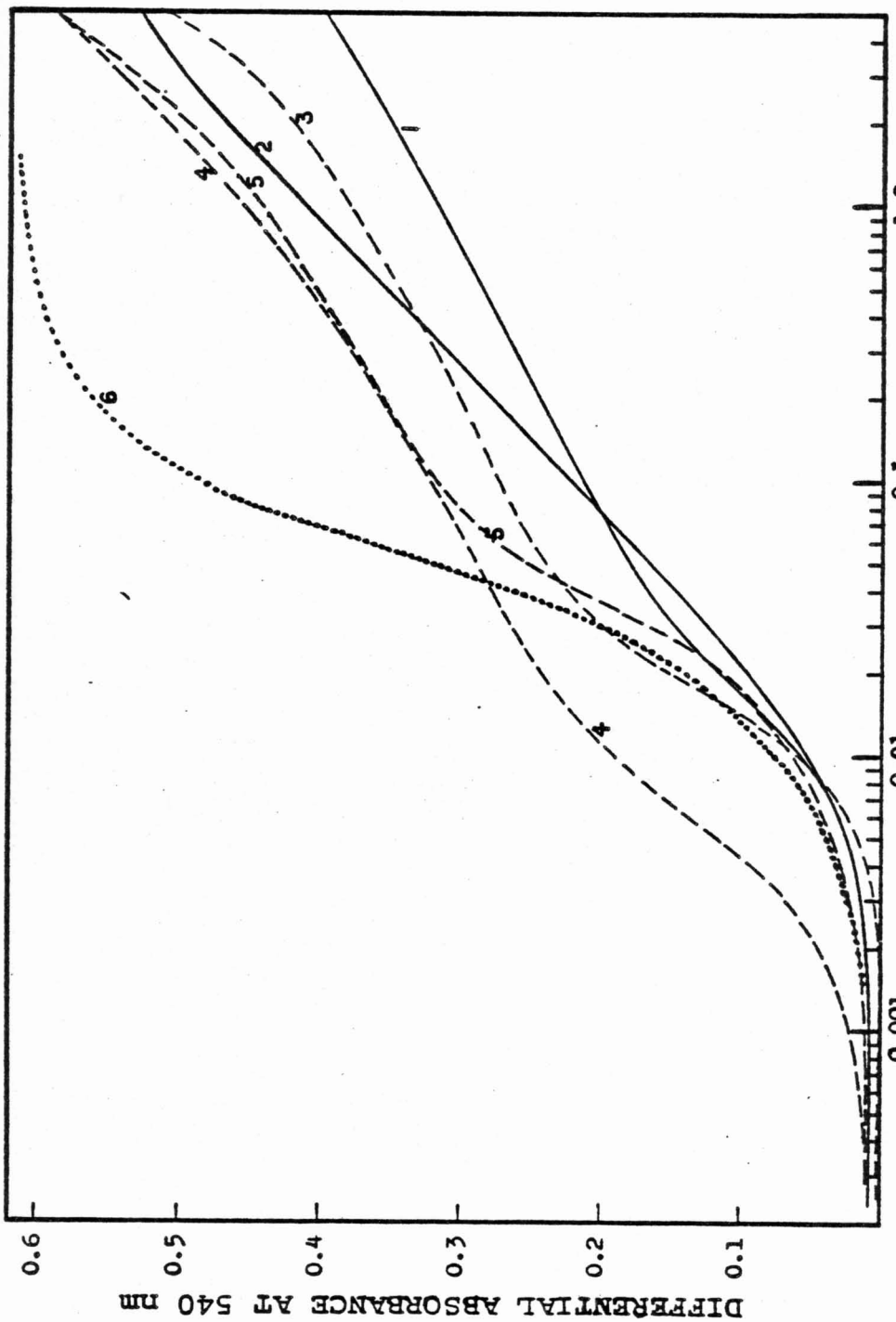
DIFFERENTIAL ABSORBANCE AT 540 nm
0.6
0.5
0.4
0.3
0.2
0.1
0.001
0.01
0.1
1.0
(W/V) % CONCENTRATION
1
2
3
4
5
6

Figure 4.4 Differential absorbance at 540 nm of 5.04×10^{-5}M (O) and 1.57×10^{-4}M (●) benzopurpurine 4B in Pluronic F68 solutions.

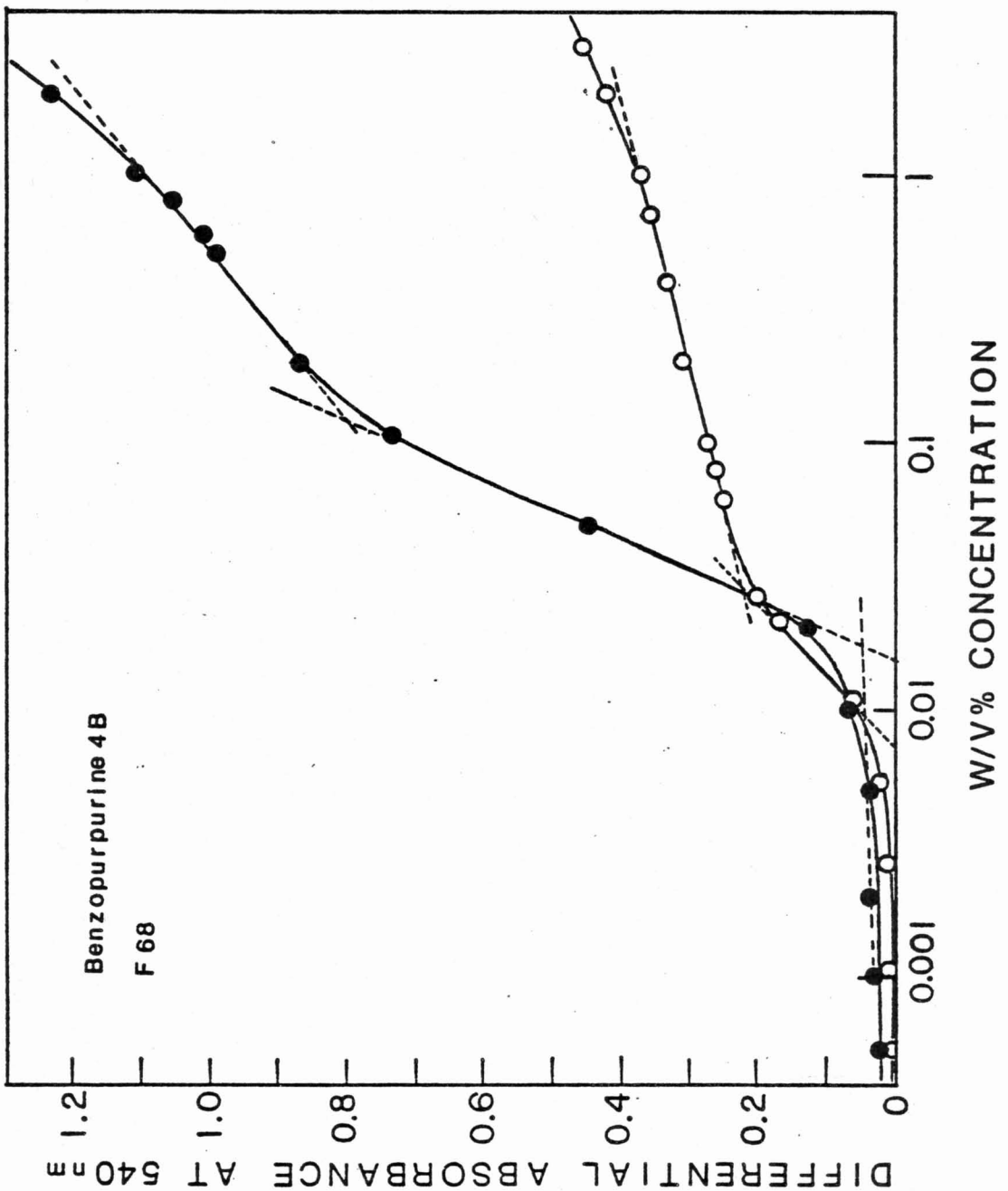
Benzopurpurine 4B
F 68
DIFFERENTIAL ABSORBANCE AT 540mμ
1.2
1.0
0.8
0.6
0.4
0.2
0
0.001
0.01
0.1
W/V% CONCENTRATION

the initial rise and the leveling off of the differential absorbance occur at a somewhat higher polymer concentration. These changes, again, are consistent with the deaggregation of the dye in the polymer solutions.

When the data in Figure 4.3 are plotted against the concentration of the polymer on a linear scale, as shown in Figure 4.5, the curves are all characterized by a rapid initial rise in absorbance produced at low concentrations of the polymer followed by a gentle leveling off; curves typical of adsorption or binding equilibria. The relative effectiveness of the polymers in causing deaggregation of benzopurpurine 4B is consistent with the hydrophobicity of the polymer. Thus, Pluronic L62, the most effective deaggregating agent in Figure 4.3, is also the one with the highest propylene oxide content. A pronounced difference is also observed between PEG 6,000 and 20,000 in the effectiveness of deaggregation. Such a difference suggests that a multiple site interaction with the polymer is involved in the solubilization (binding) of the dye, because, if the effect of the polymer end groups were negligible and the solubilization (binding) sites were independent of one another, the effectiveness of deaggregation would be a function of only the weight by volume concentration of the polymer and not be the molecular weight. This result is consistent with the conclusion derived previously by Mukerjee and Johnson (23) on the

Figure 4.5. Differential absorbance at 540 nm of 5.04×10^{-5}M benzopurpurine 4B in polymer solutions plotted against the concentration of the polymer on a linear scale, 1) PEG 6,000; 2) PEG 20,000; 3) Pluronic F68; 4) Pluronic L62; 5) Pluronic F108.

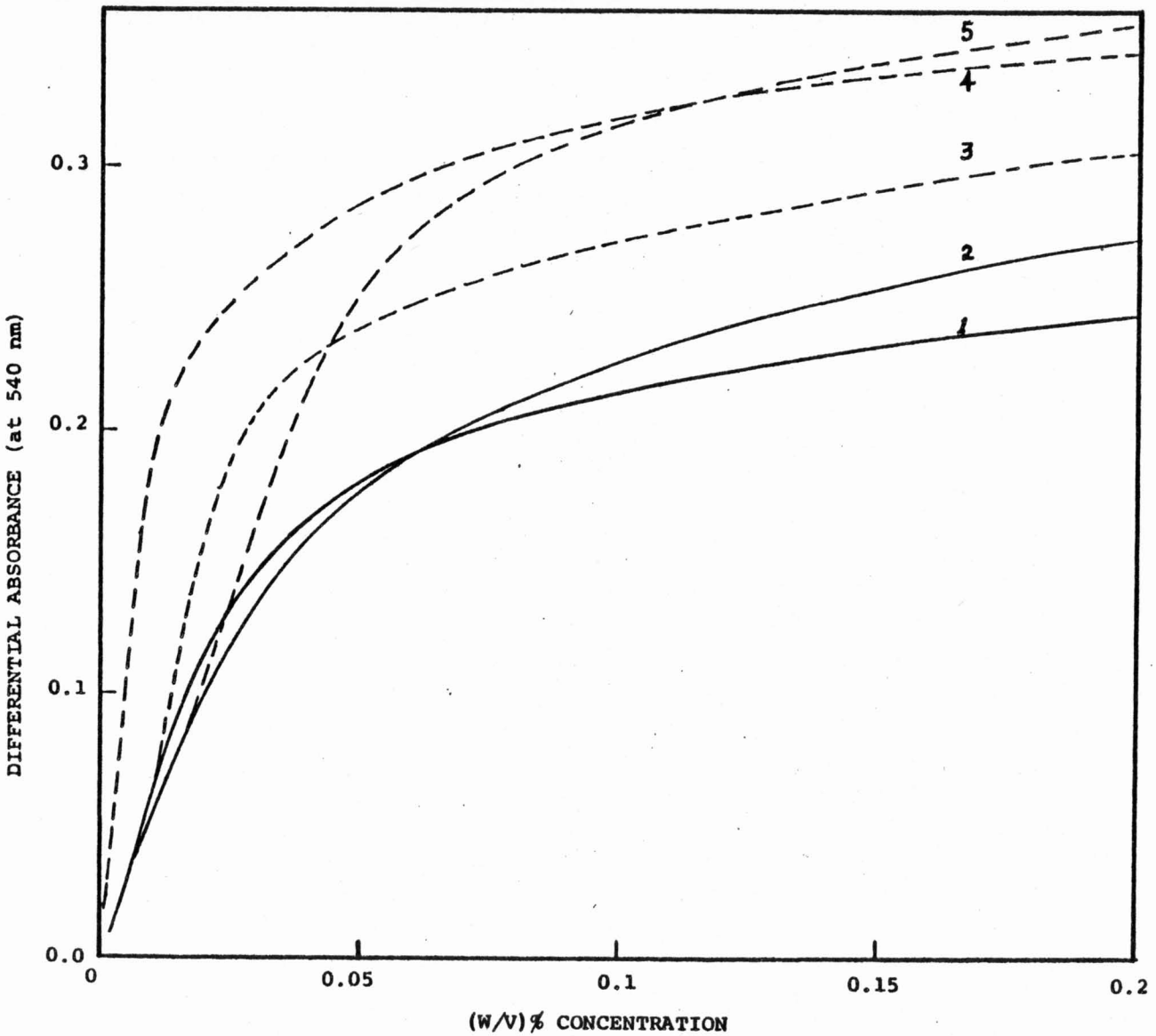
5
4
3
2
1
0.3
0.2
0.1
0.0
0
0.05
0.1
0.15
0.2
DIFFERENTIAL ABSORBANCE (at 540 nm)
(W/V)% CONCENTRATION

multiple-site interactions of solubilizing para-hydroxybenzoic acid in PEG solutions.

For comparison with the hydrophilic polymers, the effect of a well-known micelle forming surfactant, Brij 35, which is a laurylether of $OH(CH_2CH_2O)_{23}H$, is shown in Figure 4.3. The solubilization of the dye occurs, presumably, mainly in the hydrocarbon part of the micelle. The shape of the curve is simpler than that of the others, containing one inflection point, indicating the nature of solubilization in real micelles. For the polymers, the initial rapid rise is followed by a slower increase in absorption which, in turn, is followed by a more rapid increase. This complex shape of the curve suggests a cooperative interaction between the bound dye molecules when the concentration of the polymer is low, i.e., the dye to polymer ratio is high.

A quantitative interpretation of the spectral change in Figure 4.3 is difficult because of the number of equilibria involved. However, a qualitative or semi-quantitative analysis of the spectral changes may be made by applying appropriate polymer binding models. Cooperative binding of small molecules to linear macromolecules has often been analyzed by a one dimensional Ising lattice model (272-274). This model assumes a linear polymer as an array of lattice points, each point corresponding to one binding site. The length of this array is infinite. Binding of one small

molecule to a site whose nearest neighbors are unoccupied is considered as one type of binding process with a constant K_o, while binding to a site with either of the nearest neighbor sites occupied represents another type of binding with a constant K. In other words, only the nearest neighbor interaction of the bound dyes is considered. A cooperativity parameter, σ, is defined as

$$\sigma = K_o / K \ . \qquad [4\text{-}1]$$

The binding process is positively cooperative when $\sigma < 1$ and negatively cooperative (anticooperative) when $\sigma > 1$. The fraction of occupied binding sites (or degree of saturation), θ, which is usually observable experimentally, is expressed as

$$\theta = C_b / g\, C_p \qquad [4\text{-}2]$$

and

$$\theta = \frac{1}{2}\left[1 - \frac{(1 - S)}{\sqrt{(1 - S)^2 + 4 \sigma S}} \right] \qquad [4\text{-}3]$$

where $S = KC_f$ and C_b and C_f are the concentrations of the bound and free dye, respectively. C_p is the total polymer concentration and g is the number of binding sites per polymer molecule. It can be shown that when $K_o = K$, $\sigma = 1$, the binding process is non-cooperative and Equation 4-3 reduces to the Langmuir binding isotherm, i.e.,

$$\theta = \frac{K\, C_f}{1 + K\, C_f} \ . \qquad [4\text{-}4]$$

By combining Equation 4-2 and 4-3 and eliminating θ, an equation relating the fraction of the dye bound to the polymer, r, and the concentration of the polymer, C_p, is obtained.

$$\frac{g\,C_p}{C_o} = \frac{2\,r}{1 - \dfrac{1 - S_o\,(1 - r)}{\sqrt{[1-S_o(1-r)]^2+4\,\sigma\,S_o(1-r)}}} \qquad [4\text{-}5]$$

here $S_o=KC_o$, C_o being the sum of C_f and C_b.
The term $S_o(1-r)$ is equal to S in Equation 4-3. If S_o and σ are known, the concentration of polymer at any value of r can be calculated. Figures 4.6 and 4.7 show the curves of r versus log (gC_p/C_o) calculated by Equation 4-5 using different values of S_o and σ . The curves of $S_o=2$, as shown in Figure 4.6, vary in shape according to the value of σ . For σ smaller than unity, i.e., cooperative binding, the curve becomes biphasic; a relatively rapid rise of r is observed at low polymer concentrations followed by a gradual and slow increase in r as the concentration of the polymer is further increased. All curves share a common intersection at r=0.5 and $gC_p/C_o=1$ at which the following conditions are fulfilled:

$$1 - S_o(1-r) = 0$$

and $$r = (gC_p/C_o)/2$$

Such an intersection can be regarded as the transition point of the binding isotherm. It only exists when S_o is greater

Figure 4.6. Binding isotherm calculated using Equation 4-5 with $S_o=2$ and different values of σ, as indicated in the graph.

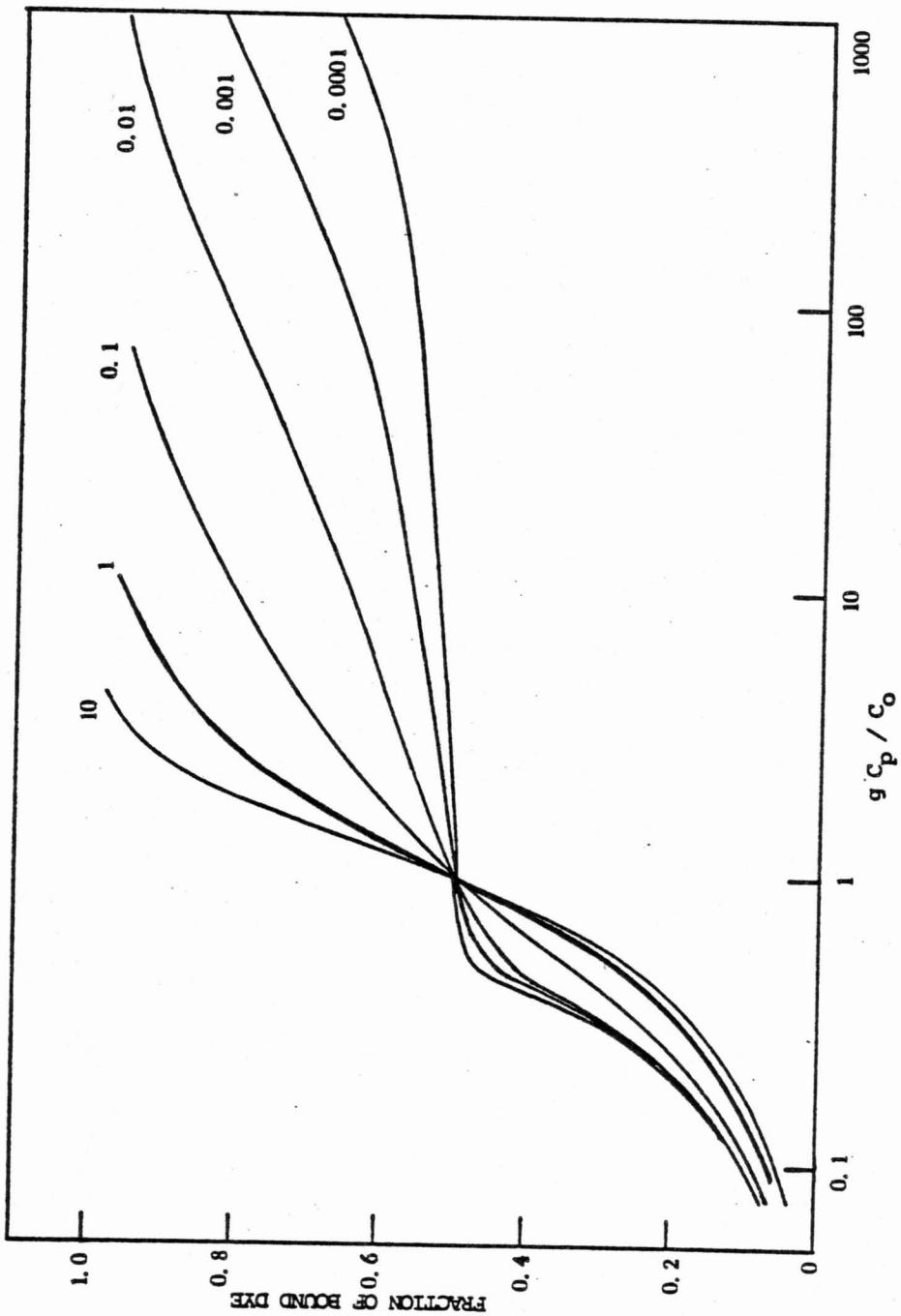
FRACTION OF BOUND DYE
1.0
0.8
0.6
0.4
0.2
0
0.1
1
10
100
1000
g C_p / C_o
10
1
0.1
0.01
0.001
0.0001

Figure 4.7. Binding isotherms calculated using Equation 4-5 with S_o=1, except as indicated, and different values of σ .

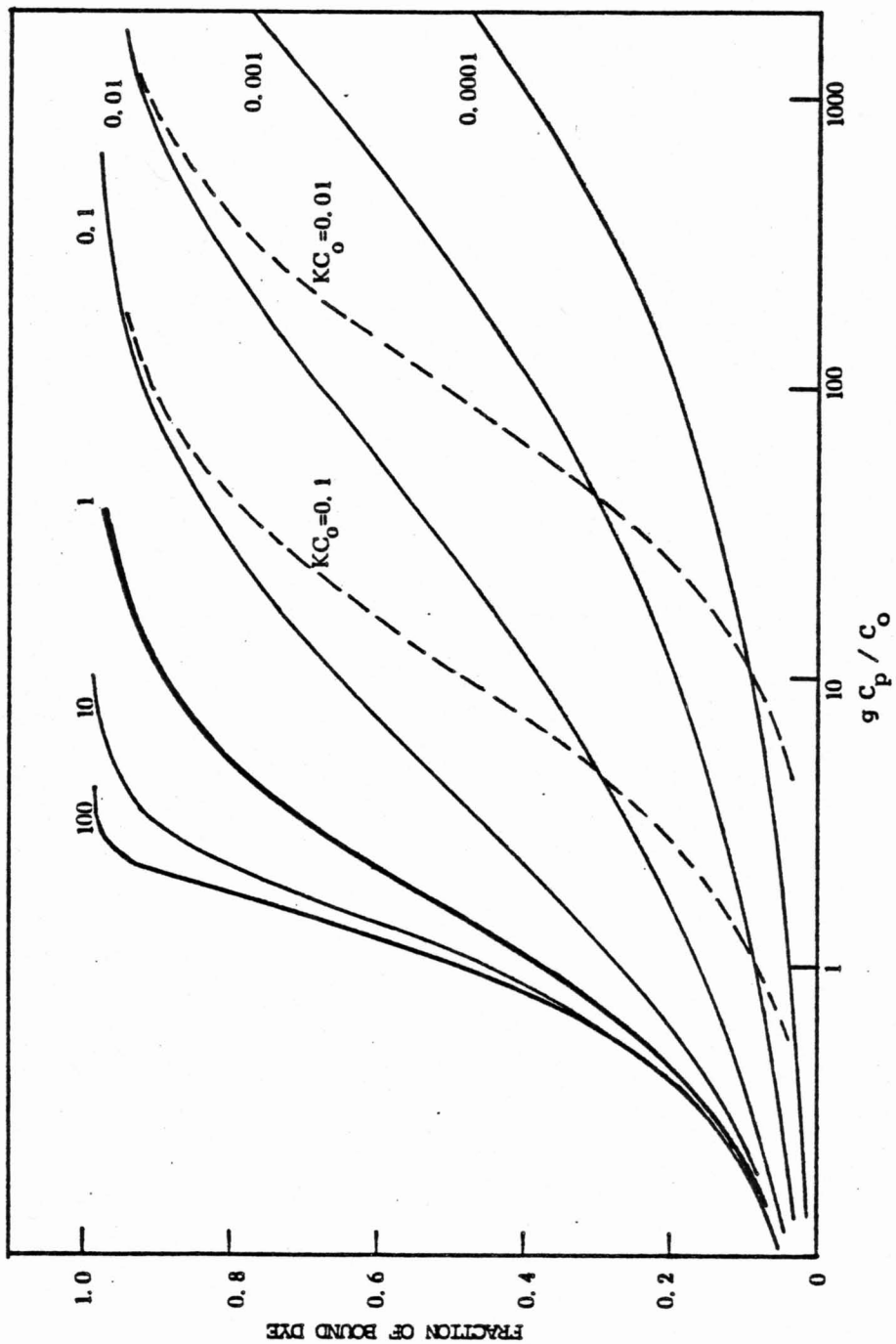
FRACTION OF BOUND DYE
1.0
0.8
0.6
0.4
0.2
0
1
10
100
1000
g C_p / C_o
0.1
0.01
0.001
0.0001
KC_o=0.1
KC_o=0.01
1
10
100

than unity. When S_o equals unity, the curves share a common intersection at r=0 and C_p=0. Typical curves of S_o equal to and smaller than unity are shown in Figure 4.7. In Figure 4.6, the initial rapid rise of r can be ascribed to a strong co-operative binding of the dye to the polymer and the bound dyes are predominantly aggregated. As the concentration of the polymer is increased, the bound dyes begin to deaggregate by redistributing to other binding sites. As the degree of cooperativity increases, i.e., σ is smaller, the value of r approaches the value at the transition point more rapidly and, correspondingly, further increase in r is slower.

Since the visible spectrum of benzopurpurine 4B changes very little with concentration in water, it may be assumed that the spectrum of this dye in the bound state is also unaffected by the degree of aggregation in the bound state. On can, therefore, assume that the dye exhibits two spectral states, one in the bulk solution and the other in the polymer bound state. The observed absorbance, A of the dye at any polymer concentration may be described by the following equation:

$$A = L\ (E_b C_b + E_f C_f) \qquad [4\text{-}6]$$

where L is the path length of the light and E_b and E_f are the absorptivities of the bound and free dye, respectively. In the absence of polymer the absorbance can be expressed as

$$A_o = L(E_f C_o) \qquad [4\text{-}7]$$

By subtracting Equation 4-7 from Equation 4-6, the following equation is obtained,

$$A - A_o = L\ (E_b - E_f)\ C_b \qquad [4\text{-}8]$$

Equation 4-8 can be written in terms of the fraction of bound dye, r, as

$$A - A_o = (A_\infty - A_o)\ r \qquad [4\text{-}9]$$

where $A_\infty = L\ E_b C_o$. The differential absorption is therefore, directly proportional to the fraction of bound dye. The data of Pluronic L62 is replotted in Figure 4.8, in which the fraction of bound dye is calculated by using a maximum differential absorbance, $A_\infty - A_o$, of 0.5. The curve in Figure 4.8 is calculated based on Equation 4.5 using an S_o value of 1.6 and σ value of 0.01. The data are represented very well by the calculated curve based on the Ising lattice model, suggesting that the binding of the dye is a cooperative process and the dye is aggregated in the polymer bound state when the dye to polymer ratio is high. It should be mentioned that the present model neglects the self-assocaition of the dye in the bulk solution completely. Such self-association effect can be included in the model with a proper description of the interaction between the dye molecules in the bulk solution. Inclusion of such interactions will produce some quantitative changes in the binding parameters. The qualitative profile of the binding behavior will remain unchanged.

The differential absorbance versus polymer concentration

Figure 4.8. Fraction of bound dye in 5.04×10^{-5}M benzopurpurine 4B solutions containing Pluronic L62, calculated by Equation 4-9 by assuming $A_{\infty}=0.5$, plotted against the logarithm of the polymer concentration (O). The solid curve is the binding isotherm calculated using Equation 4-5 with an S_o value of 1.6, σ of 0.01, and g of 5.

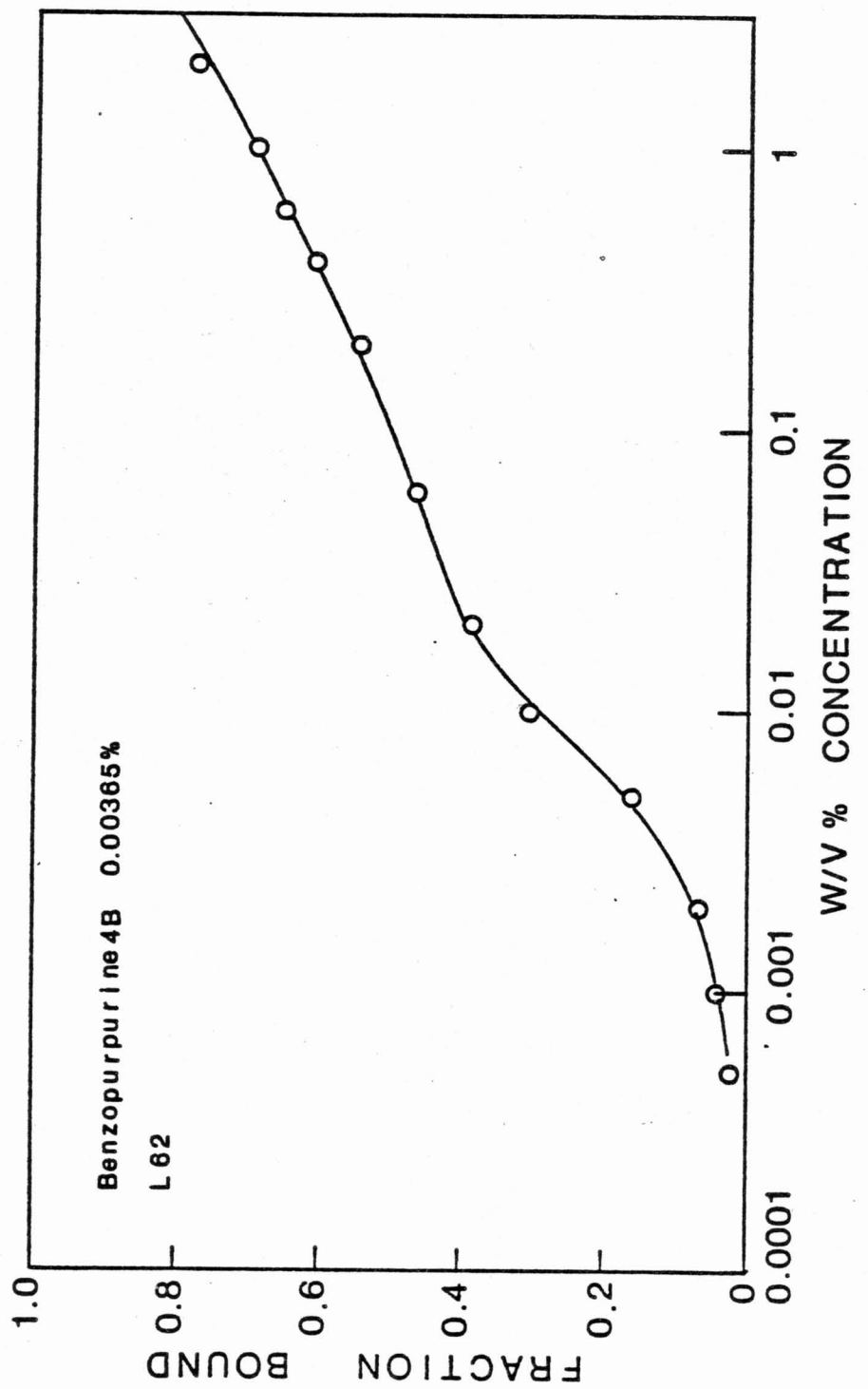
Benzopurpurine4B 0.00365%
L82
FRACTION BOUND
1.0
0.8
0.6
0.4
0.2
0
0.0001
0.001
0.01
0.1
1
W/V % CONCENTRATION

curves for all the polymers examined, including Pluronic polyols and PEG's, can be described by the cooperative Ising binding model. Quantitative comparison between the experimental data and the model is difficult because of the nature of the self-association of the dye is not known. Nevertheless, the present data indicate that the spectral change of benzopurpurine 4B in the polymer solutions can be ascribed to binding and deaggregation of the dye by the polymer without invoking micelle formation or self-association of the polymers.

4.3. Conclusion

The spectral changes of benzopurpurine 4B in aqueous solutions of polyethylene glycols of different molecular weights and some Pluronic polyols of different compositions have been investigated. The effects of PEG and Pluronic polyols on the spectrum of the dye are very similar in nature. There is no compelling evidence of micelle formation in these polymers, although an apparent critical micellization concentration can always be obtained from extrapolation of two linear regions on the plot of spectral changes versus the logarithm of polymer concentration. The complex pattern of interactions of benzopurpurine 4B with PEG and Pluronic polyols indicates that dye-dye interactions between bound dye molecules are important in some cases. A significant dependence of the deaggregation process on the molecular weight

of the PEG has been observed, suggesting a multiple-site interaction in the binding process.

5. SOLUBILIZATION OF A FLUORESCENT DYE AND AN INDICATOR DYE IN SOLUTIONS OF BILE SALTS

5.1. Review of Literature

Bile salts are physiological surfactants.They play important roles in the solubilization and absorption of fats (47,48,238), formation and dissolution of gallstones (234), and removal of toxic substances via the biliary route of excretion (49,50). These physiological and pharmacological activities are believed to be closely related to the self-association of the bile salts and their mutual aggregation with other amphiphates. The commonly observed bile salts in higher vertebrates are derivatives of C_{24} saturated carboxylic acids containing a cyclopentenophenanthrene steroidal nucleus. Most of the physiologically active bile salts have either two or three hydroxy groups on one side of the nucleus. These molecules are, therefore, hydrophobic on one side and hydrophilic on the other. Such a characteristic structure has led to the early postulation that bile salts form cylindrical aggregates in aqueous solutions by closely packing the hydrophobic backs of the molecules and exposing the hydrophilic sides to water (43,44). It has been suggested that large aggregates of bile salts form by association of the

primary, cylindrical aggregates via hydrogen bonding (43, 44). Some investigators have suggested that the formation of small bile salt aggregates also involves hydrogen bonding (235,247). There is, however, no compelling experimental evidence for hydrogen bonding in the aggregates of bile salts (236,237). In fact, dihydroxy bile salts tend to form aggregates at even lower concentrations than the trihydroxy salts. This tendency and also the ability of bile salts to solubilize nonpolar organic molecules of different sturctures suggest that hydrophobic interactions, rather than hydrogen bonding, are the prime forces for self-association of bile salts. In some cases, gel formation occurs in solutions of bile salts at either low pH or high concentrations of electrolytes (239-241). This phenomenon has been attributed to the formation of large helical aggregates of bile salts by hydrophobic interactions (239). A certain molecular geometry of the bile salt molecules is believed to play a crucial role in the formation of such aggregates (239-241). The detailed structure of aggregates and the mode of self-association of bile salts are not entirely clear.

Solubilization in solutions of bile salts has often been described as micellar solubilization using the model of flexible chain detergents (44, 242, 243). With this model, solubilization is expected to occur only at

concentrations above the critical micellization concentration (CMC) and increases with the amount of micelle present in the solution. Ekwall, et al., (244) and Fontell (245) investigated the pattern of solubilization of several different bile salts and concluded that the generally observed curves of the solubility of a solubilizate versus the concentration of bile salt could be divided into several discrete regions, the change from one region to another corresponding to a change in the size of the bile salt aggregates. Mukerjee and Cardinal (46), in contrast, showed that the solubilization curve of naphthalene in sodium cholate solutions exhibits a continuous and gradual increase over the whole concentration region. Further analysis of the solubilization data indicated that sodium cholate and possibly also other bile salts exhibit a pattern of solubilization different from that of the flexible chain detergents (25,46,62). A complex pattern of mutual association between the solubilizate and bile salt aggregates, including dimers and one or more higher oligomer, has been suggested (46). Because of the rigid, inflexible nature of bile salt molecules, solubilization in bile salts is likely to be affected by the molecular sturcture of the solubilizate. More recent data on the solubilization of p-xylene and other aromatic compounds in bile salts suggest that bile salts form certain

preferential adducts with the solubilizates, indicating a specificity of solubilization (246).

5.2. Scope and Aims

The dye, 6-toluidino-2-naphthalene solfonate (TNS) (see Figure 5.1 for sturcture) exhibits strong fluorescence in nonpolar or rigid media but shows very weak fluorescence in polar solvents such as water (248-250, 253). The development of the fluorescence of TNS in aqueous surfactant solutions occurs upon solubilization (83,85,86, 251, 252, 254,255). This dye and its analog, 2-N-arylamino-6-naphthalene-sulfonates (ANS) have been used for the determination of CMC's in several surfactant systems (83, 252, 255). The high sensitivity of the fluorescence technique permits the use of a very low concentration of the dye which minimizes pertubation that may be imposed on the equilibrium of surfactant self-association. Changes of the fluorescent spectrum of TNS upon solubilization also provide a measure of the local polarity in the surfactant aggregates. The indicator ratio of triphenylmethyl sulfonate dyes (cf. Chapter 3) is sensitive to minor changes in local hydrogen ion concentration. These dyes, carrying permanent charges with the same sign as the bile salts, represent another type of organic ions capable of solubilization in bile salts. A comparative study using the fluorescent dye, TNS, and an indicator dye, bromthymol blue,

BTB (see Figure 5.1 for structure), as probes for solubilization in the alkyl sulfates, sodium dodecyl sulfate, sodium decyl sulfate, and sodium octyl sulfate, and the bile salts, sodium cholate, sodium deoxycholate, and sodium chenodeoxycholate (see Figure 5.2 for structure), was conducted to further investigate the pattern of solubilization and the self-association of bile salts.

5.3. Results and Discussion

5.3.1. Solubilization of The Fluorescent Dye-TNS

The apparent emission spectra of TNS obtained in surfactant solutions generally exhibit a single broad peak. Figure 5.3 and Figure 5.4 show the typical apparent and corrected emission spectra of TNS obtained from solutions of two different types of surfactants. It was found that the spectrum of TNS was not significantly affected by the presence of inorganic salts used for maintaining ionic strength and pH in the solutions. Corrections on the emission spectra were made to obtaine the true spectral profile. No correction was made for the emission intensities. An arbitrary unit for the emission intensity was used in the spectra reported. The approximate maxima of emission bands of the corrected TNS spectra in different surfactant solutions are summarized in Table 5.1.

TNS exhibits a very weak fluorescence in water, but

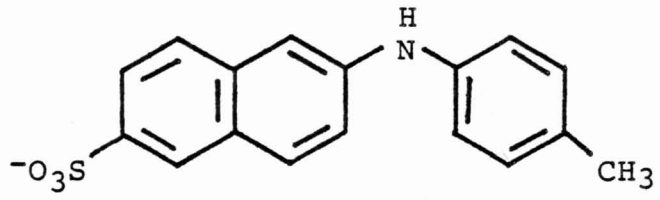

6-p-Toluidino-2-naphthalene Sulfonate

(TNS)

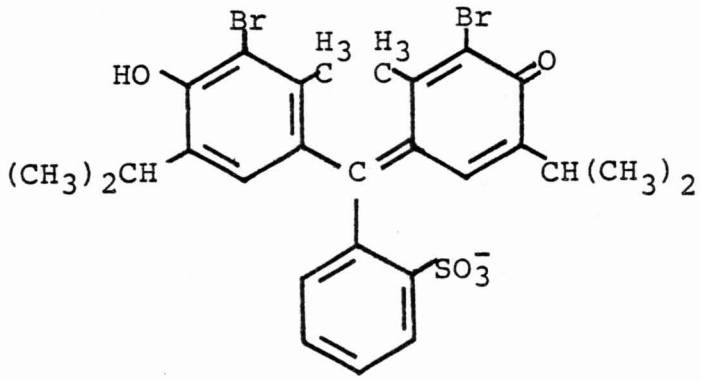

Bromthymol Blue

(BTB)

Figure 5.1. Molecular structures of 6-toluidino-2-naphthalene sulfonate (TNS) and bromthymol blue (BTB).

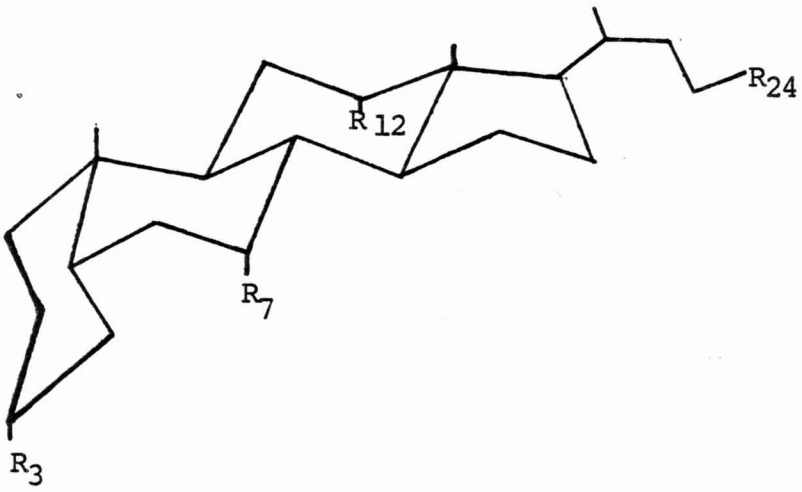

	R_3	R_7	R_{12}	R_{24}
Cholic Acid	OH	OH	OH	COOH
Deoxycholic Acid	OH	H	OH	COOH
Chenodeoxycholic Acid	OH	OH	H	COOH
Taurodeoxycholic Acid	OH	H	OH	$CONHCH_2CH_2SO_3H$

Figure 5.2. Molecular Structures of Bile Acids

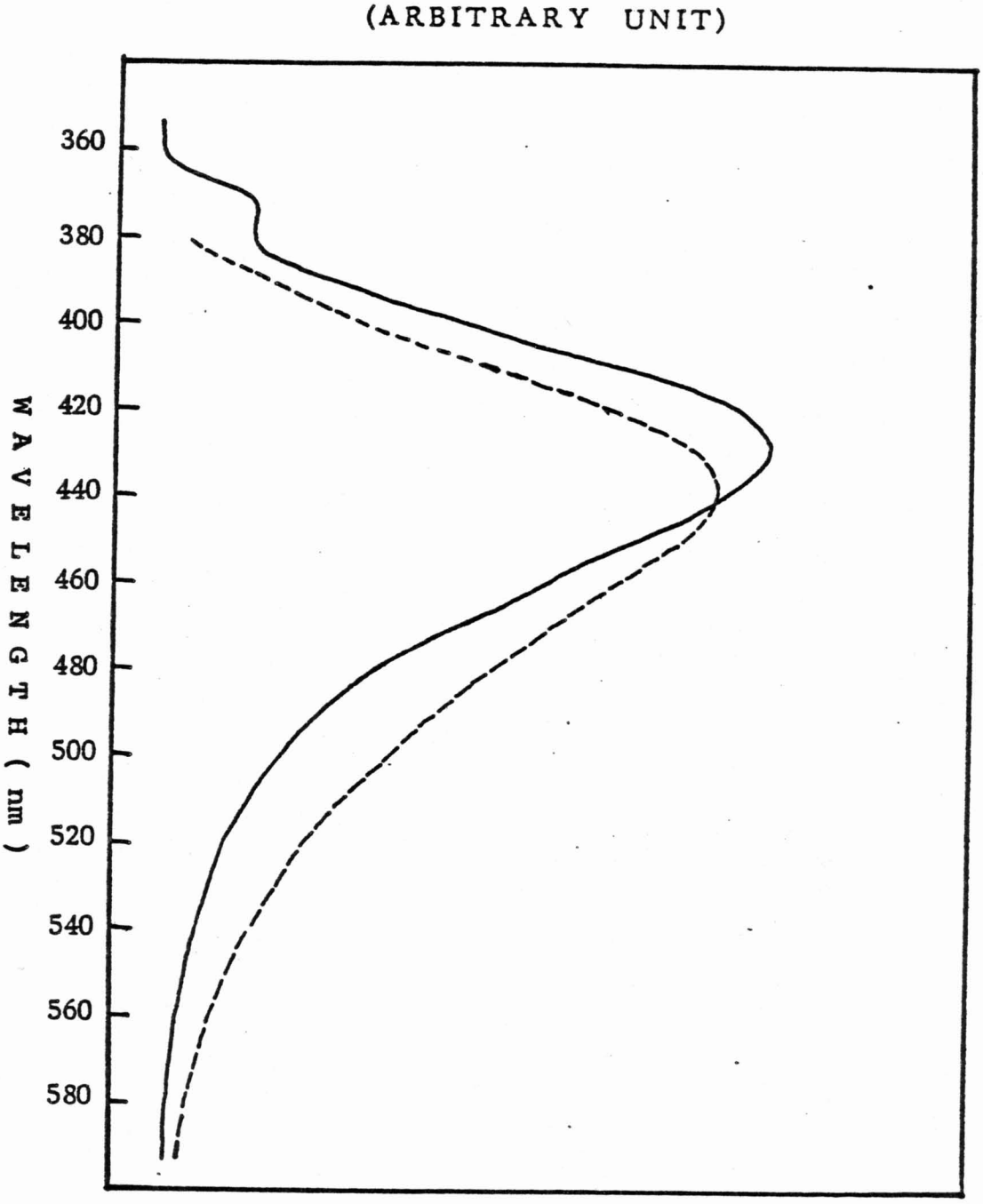

Figure 5.3. The apparent (—) and corrected (--) emission spectra of TNS in sodium cholate solution obtained at an excitation wavelength of 370 nm.

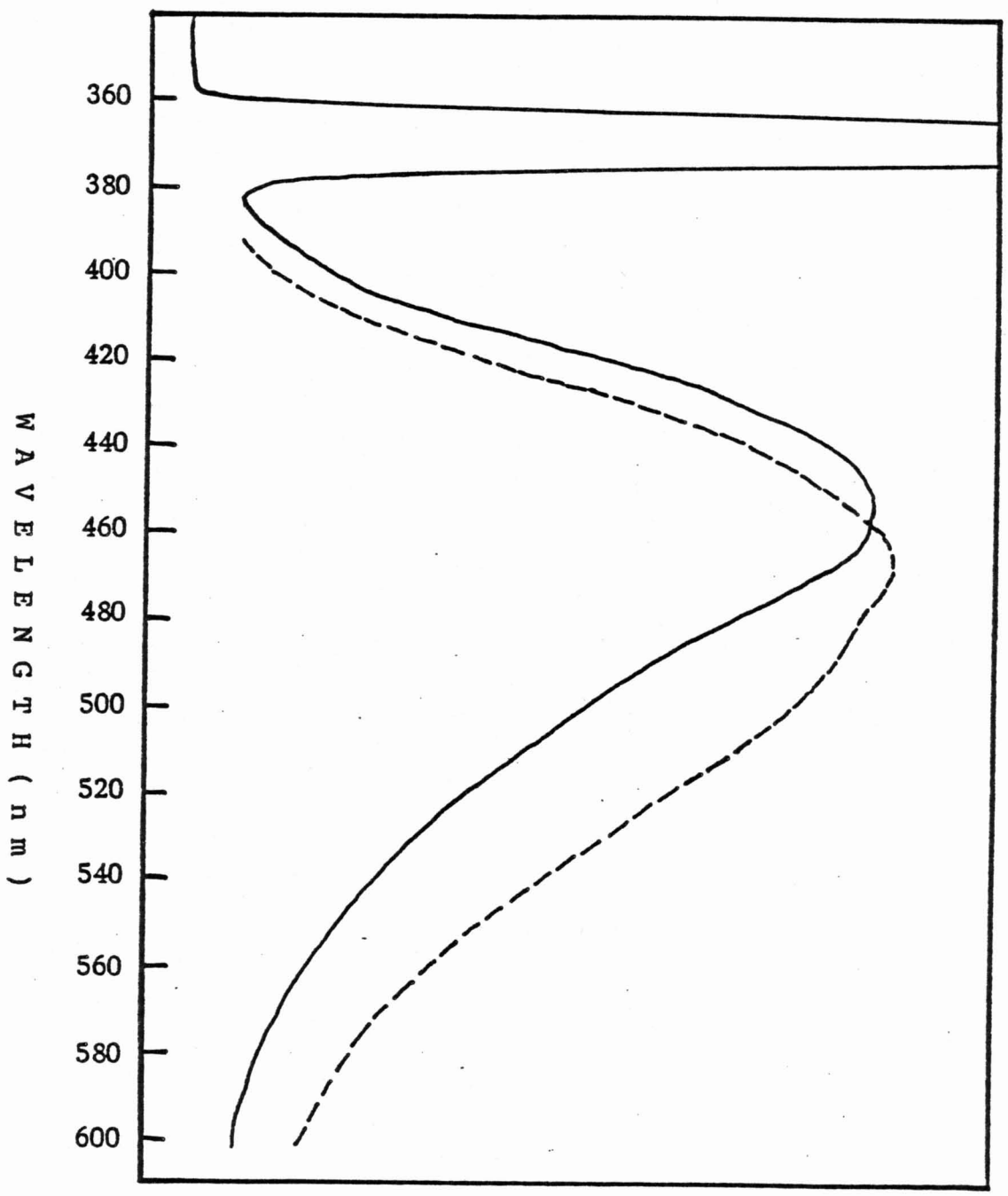

Figure 5.4. The apparent (—) and corrected (--) emission spectra of TNS in sodium dodecyl sulfate solution (0.0132M) obtained at an excitation wavelength of 370 nm.

Table 5.1. Fluorescence Band Maxima of TNS and Polarity Index Values of Surfactant Aggregates

Surfactant	Band Maximum (nm)	E_T
Sodium Octyl Sulfate	468	56.5
Sodium Decyl Sulfate	468	56.5
Sodium Dodecyl Sulfate	465	55.8
Sodium Cholate	435	46.1
Sodium Deoxycholate	438	46.5
Sodium Chenodeoxy-cholate	436	46.2

the fluorescence increases upon the addition of surfactant. Figure 5.5 shows the changes in fluorescent intensity of TNS as a function of alkyl sulfate concentration. In dilute solutions below the CMC only a slight increase in fluorescence in observed. The fluorescence shows a sharp increase in the CMC region. After the CMC, the fluorescence continues to increase rapidly with concentration and then gradually levels off at high surfactant concentrations. An apparent CMC value can be obtained, as shown in Figure 5.5 , by locating the intersection of two straight lines extrapolated from the concentrations below and above the CMC region. The CMC values obtained from Figure 5.5 for sodium dodecyl sulfate, sodium decyl sulfate and sodium octyl sulfate in water in this manner are 0.0075, 0.0315, and 0.118M, respectively. These values are approximately 5 to 10% lower than the best values reported in the literature (65). In all cases, a small but significant increase of fluorescence occurs in the premicellar region. This is especially pronounced in sodium octyl sulfate which has a high CMC and a wider transition range at the CMC. The pre-micellar interaction and the downward curvature at concentrations not too far above the CMC introduce some uncertainties in the determination of CMC by this method. Such uncertainties can, however, be reduced by proper treatment of the fluorescence data, as shown below.

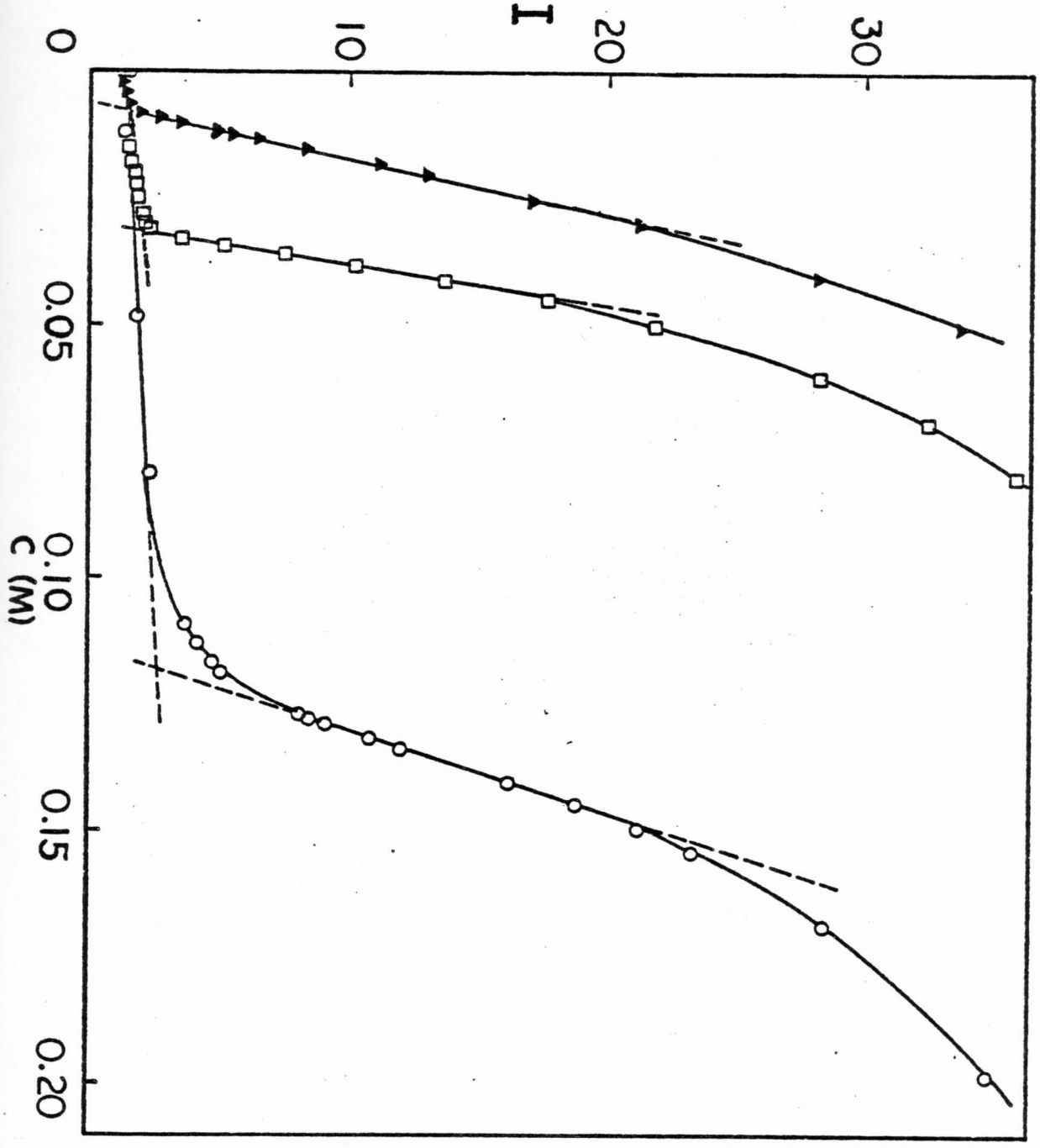

Figure 5.5. Fluorescent intensity of TNS in sodium dodecyl sulfate (▲), sodium decyl sulfate (□), and sodium octyl sulfate (O) solutions.

If the increase in fluorescence of TNS upon the addition of surfactant is due to the solubilization of the dye by the micelle and the solubilized dye exhibits one characteristic emission spectrum which differs from the spectrum in the bulk solution, the observed fluorescent intensity, I, at any given surfactant concentration, C ,can be expressed as

$$I = E_o[D_a] + E_n[D_s] \quad , \qquad [5\text{-}1]$$

where $[D_a]$ and $[D_s]$ are the concentrations of the dye in bulk solution and solubilized state, respectively. E_o and E_n are the corresponding emission constants. It can be shown that the ratio between the solubilized dye and the dye in the bulk solution, Q, is related to the fluorescent intensities by the following equation:

$$Q = \frac{[D_s]}{[D_a]} = \frac{I - I_o}{I_n - I} \quad , \qquad [5\text{-}2]$$

here $I_n = E_n[D_t]$ and $I_o = E_o[D_t]$, $[D_t]$ being the total concentration of the dye. If, at the low TNS concentration used, only one TNS molecule is assumed to be solubilized in a micelle, b_n, of aggregation number n following the equilibrium

$$D_a + b_n = Db_n \quad , \qquad [5\text{-}3]$$

an equilibrium constant, F_n, can be defined as

$$F_n = \frac{[Db_n]}{[D_a]\ [b_n]} \quad , \qquad [5\text{-}4]$$

in which $[Db_n]=[D_s]$ and $[b_n]$ is the concentration of the untagged micelles. After combining Equations 5-2 and 5-4, a simple equation describing the function Q is obtained, i.e.,

$$Q = F_n[b_n] \quad . \qquad [5\text{-}5]$$

When the concentration of the dye is negligible as compared to the concentration of the micelle, $[b_n]$ can be approximated by the total concentration of the micelle, C - CMC, and

$$Q = \frac{F_n}{n} (C - CMC) \quad . \qquad [5\text{-}5a]$$

In a simple micelle-forming system, Q is zero until the CMC is reached and the value of Q is then directly proportional to the concentration of micellized surfactants.

The values of I and I_o are experimentally determinable and the value of I_n can be obtained by an extrapolation method based on the following equation obtained by rearranging Equation 5-5a:

$$\frac{1}{I - I_o} = \frac{n}{F_n(I_n - I_o) (C - CMC)} + \frac{1}{I_n - I_o} \qquad [5\text{-}6]$$

Figure 5.6 shows plots of $(I - I_o)^{-1}$ versus $(C - CMC)^{-1}$ for TNS in the solutions of different alkyl sulfates. Straight lines are observed in these plots, suggesting that the solubilization of TNS in alkyl sulfates follows a two-state model and can be described by Equation 5-3. The extrapolated emission intensities at infinite surfactant concentrations

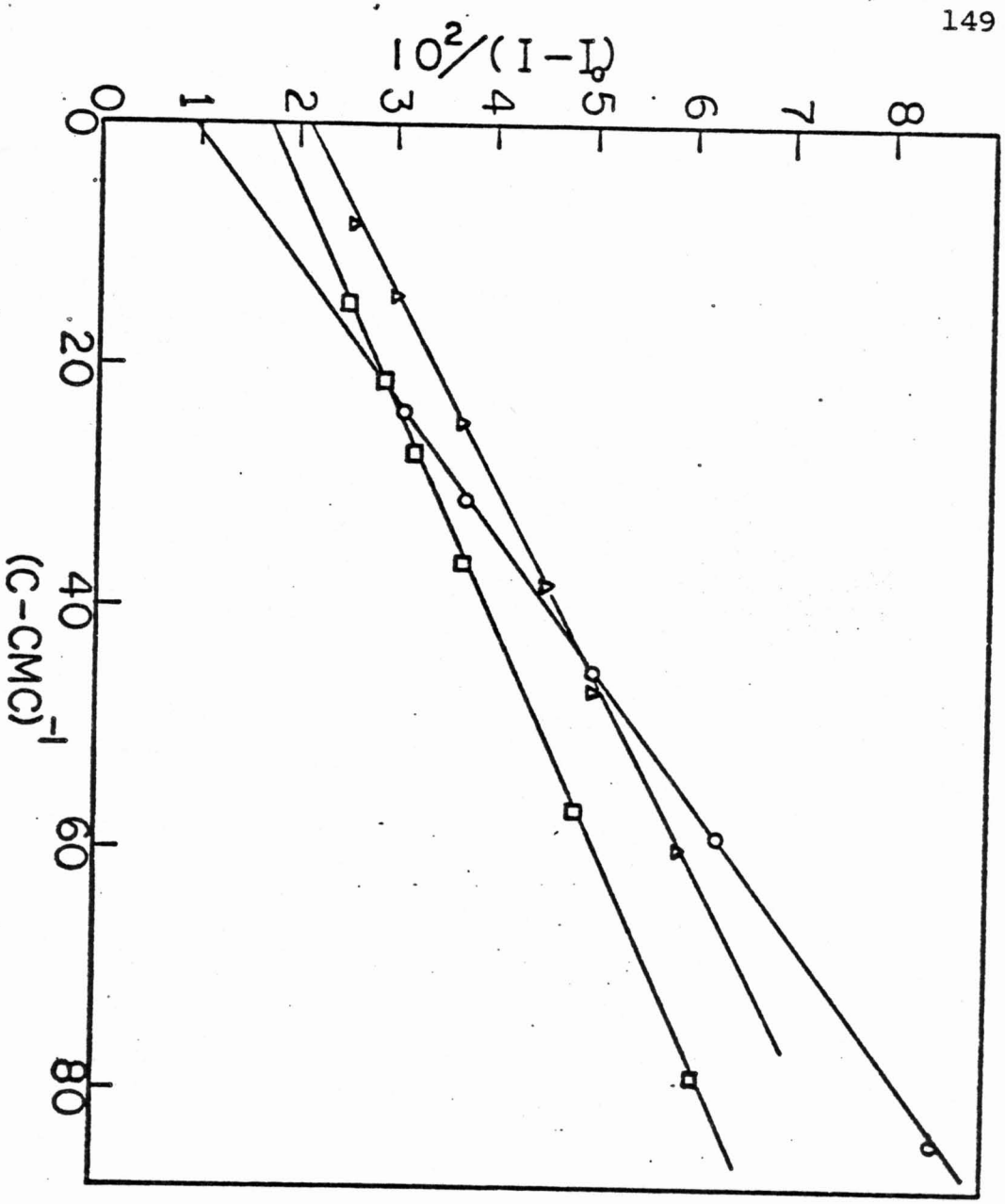

Figure 5.6. Plots of $1/(I - I_o)$ versus $1/(C-CMC)$ for TNS in sodium dodecyl sulfate (O), sodium decyl sulfate (□), and sodium octyl sulfate (△) solutions.

are reported in Table 5.2.

When the Q function is plotted against the surfactant concentration of sodium octyl sulfate, as shown in Figure 5.7, the transition region at the CMC becomes relatively narrower as compared to Figure 5.5. As expected from Equation 5-5a, the Q function increases linearly with the surfactant concentration above the CMC. The CMC values obtained from the Q versus C plots for sodium octyl sulfate, sodium decyl sulfate, and sodium dodecyl sulfate are, respectively, 0.130, 0.0328, and 0.0081M, in good agreement with literature data. Figure 5.8 shows the plot of Q versus the surfactant concentration of sodium dodecyl sulfate in the CMC region. Because of the sensitivity of the fluorescence method, the CMC region can be explored in some detail.

The data in Figures 5.7 and 5.8 indicate that the CMC region does not involve any discontinuity as predicted by the phase separation model. The sharpness of the change in Q around the CMC is related to the degree of cooperativity of the self-association process. This can be examined by constructing a curve of the first derivative of the Q versus C plot (cf. Section 1.4). Figure 5.9 shows such plots for sodium dodecyl sulfate, sodium decyl sulfate, and sodium octyl sulfate. The derivatives was approximated by the ratio of the finite differences between two adjacent data points, $\Delta Q/\Delta C$. This procedure removes any bias of graphical

Table 5.2. Extrapolated Fluorescent Intensities of 2.74×10^{-5} M TNS in The Solubilized State

Surfactant	I_n
Sodium Octyl Sulfate	46
Sodium Decyl Sulfate	57
Sodium Dodecyl Sulfate	107
Sodium Cholate	800
Sodium Deoxycholate	690
Sodium Chenodeoxycholate	730

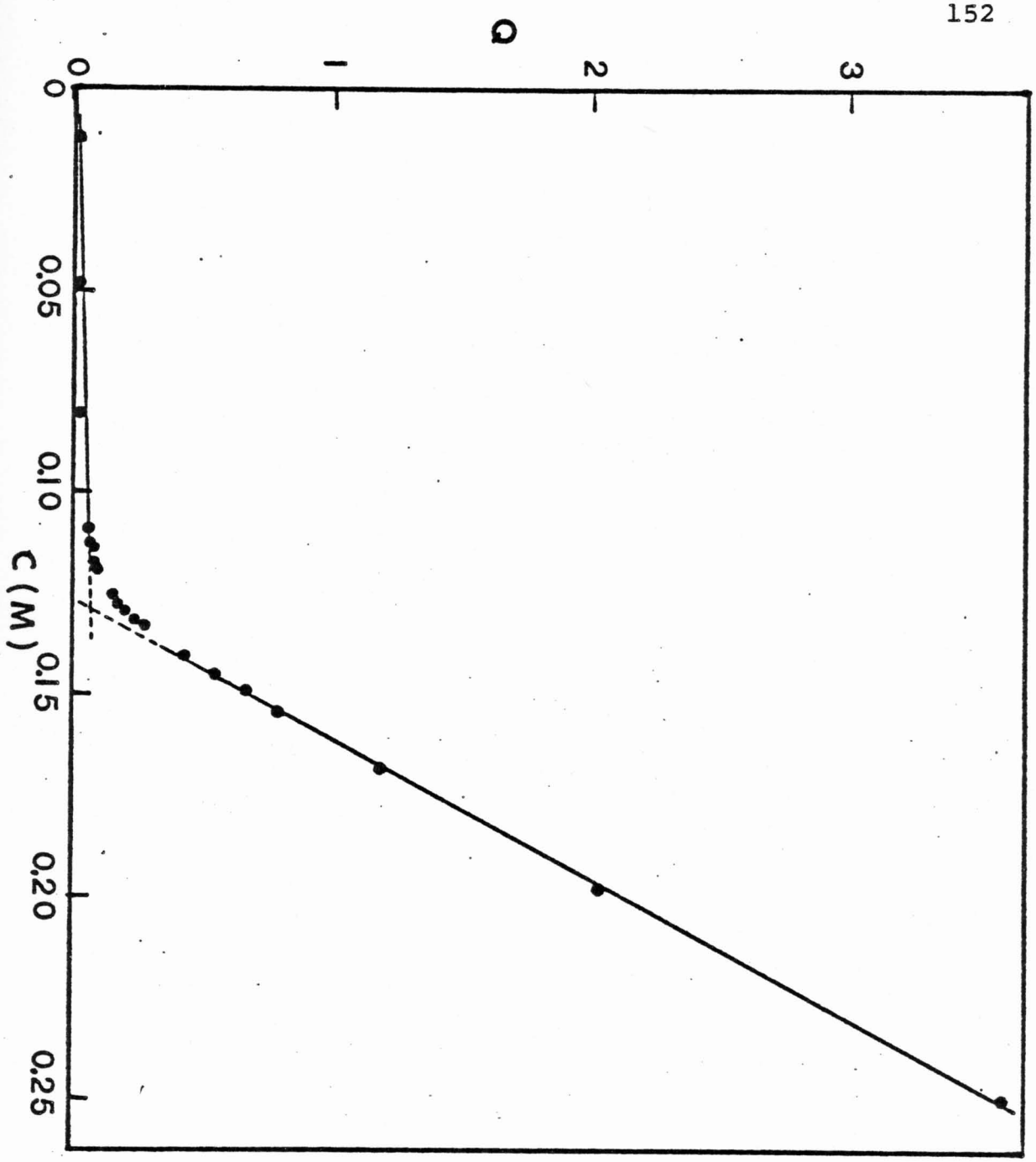

Figure 5.7. Plot of Q versus concentration of sodium octyl sulfate

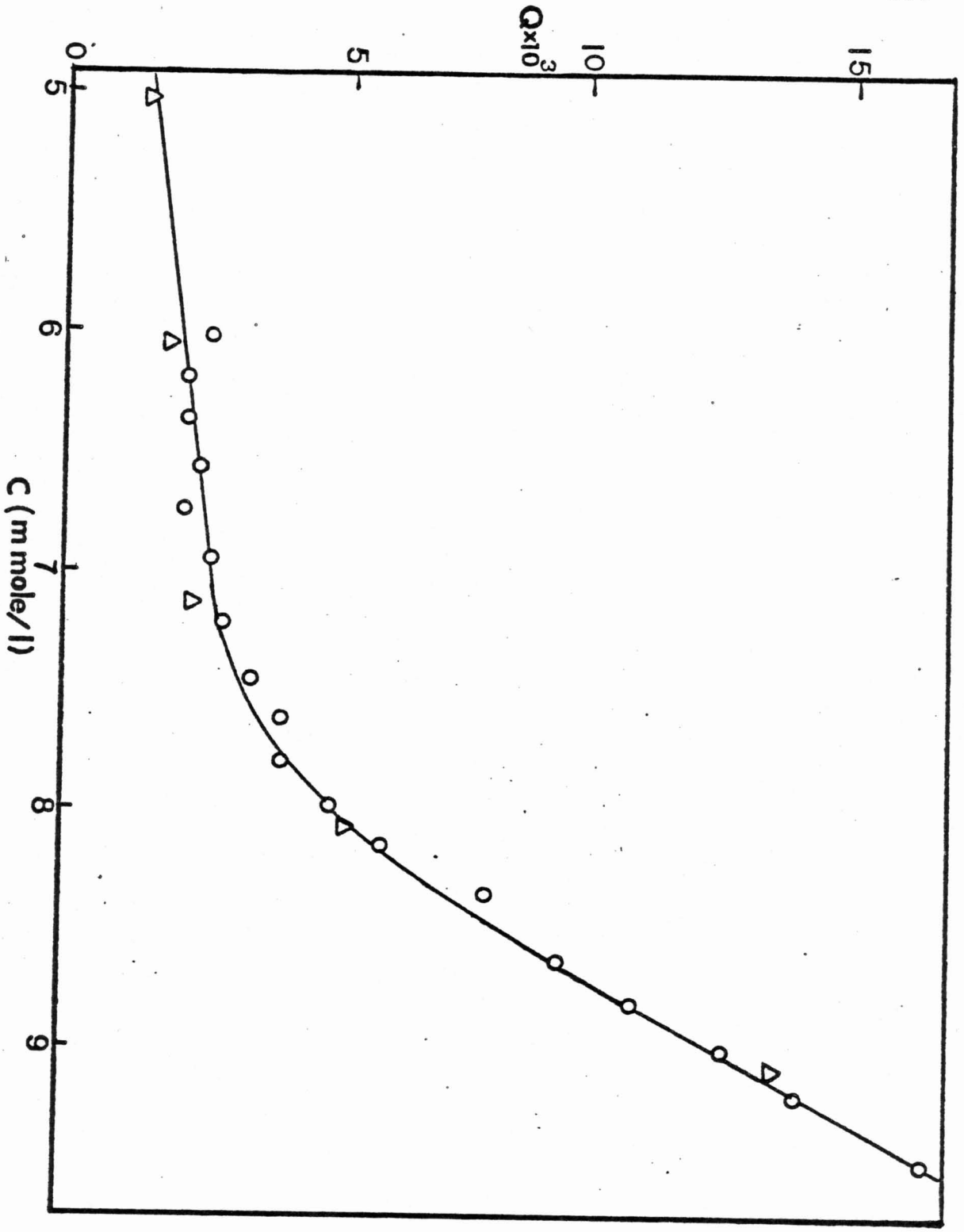

Figure 5.8. Plot of Q versus the concentration of sodium dodecyl sulfate at the CMC region.

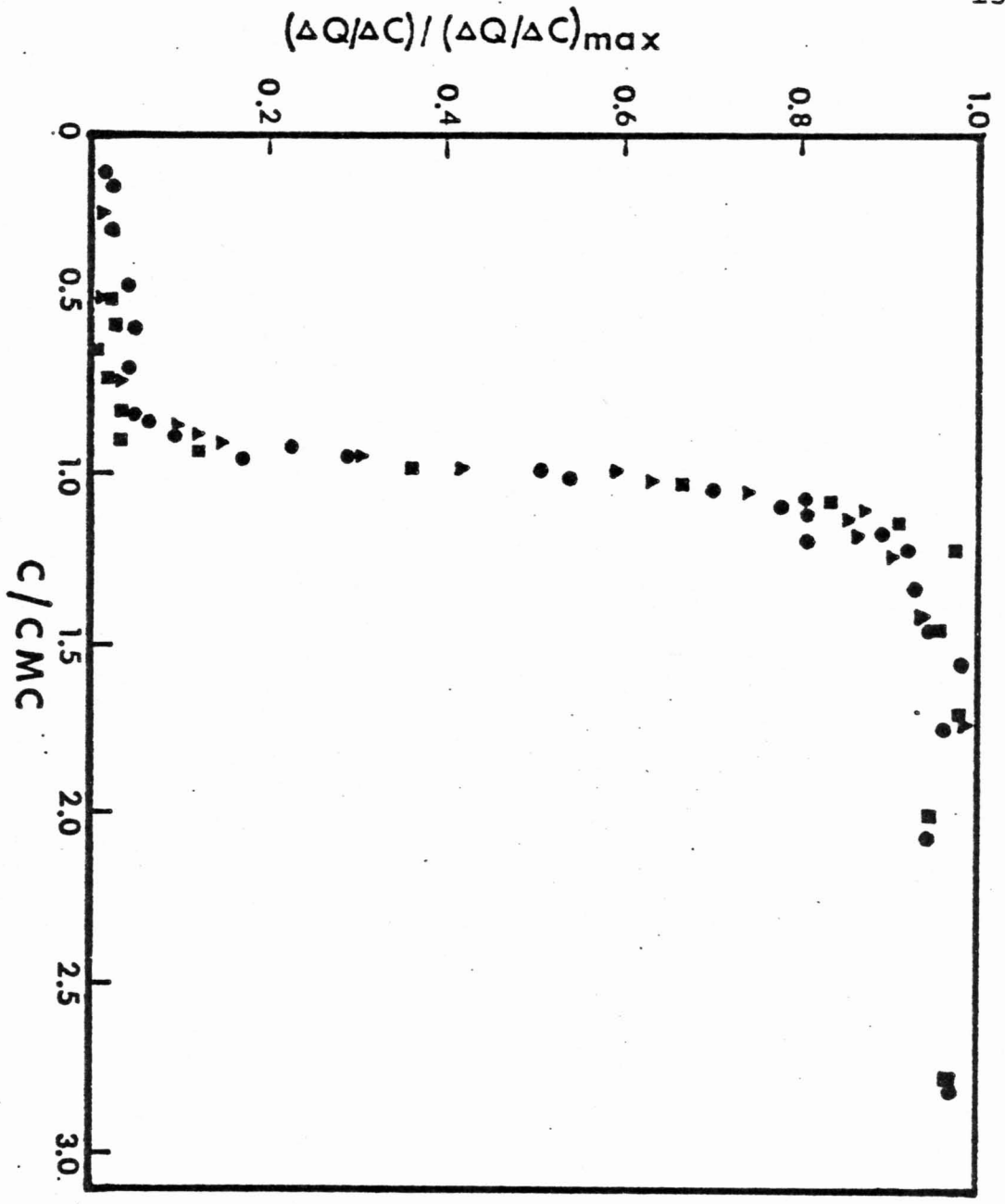

Figure 5.9. Plots of normalized differential function of Q versus the normalized mean surfactant concentration against the CMC for sodium dodecyl sulfate (O), sodium decyl sulfate (□), and sodium octyl sulfate (△).

differentiation and gives an exaggerated estimate of relative experimental precision. For comparing the three surfactants, the $\Delta Q/\Delta C$ values have been normalized by the maximum value at high concentrations. The mean concentration over which the $\Delta Q/\Delta C$ value is obtained has also been normalized by division with the CMC value of the surfactant. Figure 5.9 shows that the plot of $(\Delta Q/\Delta C)/(\Delta Q/\Delta C)_{max}$ against $\bar{C}$/CMC is nearly identical for all the alkyl sulfates. A range of values close to zero and a range of values close to unity are connected by a sharp transition in the expected CMC region. Below the CMC, a slight increase in Q is observed in all three surfactants, as shown in Figures 5.7 and 5.8 . This increase indicates that a weak interaction occurs between TNS and the surfactant monomer or premicellar aggregates. Such interactions, as well as the interactions responsible for micellar solubilization, are likely to be due to the hydrophobic nature of the dye molecule because it carries the same charge as the surfactant molecule.

In contrast to the micelle-forming surfactants, the plots of $(I - I_o)^{-1}$ versus C^{-1} for sodium cholate, as shown in Figure 5.10, exhibit considerable curvature even at concentrations well above the reported CMC regions (44). Similar curves are also observed in the sodium deoxycholate and sodium chenodeoxycholate systems. When the data obtained from solutions containing different amounts of salt are

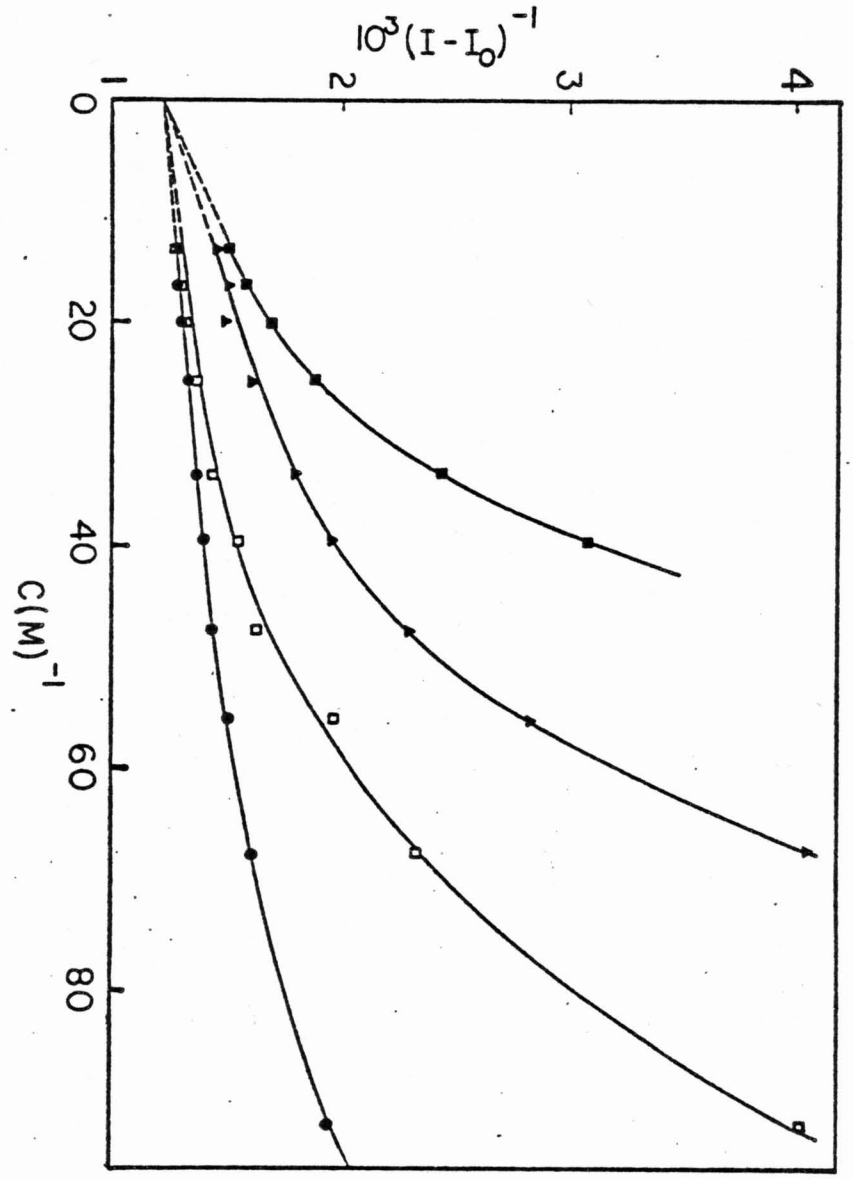

Figure. 5.10. Plots of $1/(I-I_o)$ versus $1/C$ for TNS in sodium cholate solutions containing different amounts of salt: no salt added (■), 0.05N sodium chloride (▲), 0.15N sodium chloride (□), and 0.45N sodium chloride (●).

extrapolated to infinite concentration of the surfactant, a common intercept at the $(I - I_o)^{-1}$ axis is obtained for a particular bile salt system, suggesting that the fluorescent intentisty is not affected by the presence of added salt. The I_n values obtained by extrapolations are included in Table 5.2.

As shown in Figure 5.11, the Q function of sodium cholate begins to increase at concentrations considerably below the reported CMC. A CMC value can not be obtained from such a plot because of the continuous curvature of the plot. Curves with a similar characteristic were also observed in the solubilization of naphthalene in sodium cholate solutions without added salt (46). The Q data show that the qualitative behavior is the same even at very high salt concentrations where large micelles are expected to form as suggested by the light scattering data (256-258). The difference in pattern of solubilization between the bile salt and the micelle-forming surfactant is further demonstrated in the differential plots, as shown in Figure 5.12, in which $\Delta Q/\Delta C$ is plotted against the mean concentration of the surfactant for sodium cholate and sodium decyl sulfate. The micelle-forming decyl sulfate has a CMC value similar to that of the reported value for sodium cholate under the present conditions. It can be seen from Figure 5.12 that sodium cholate does not show a sharp transition at the

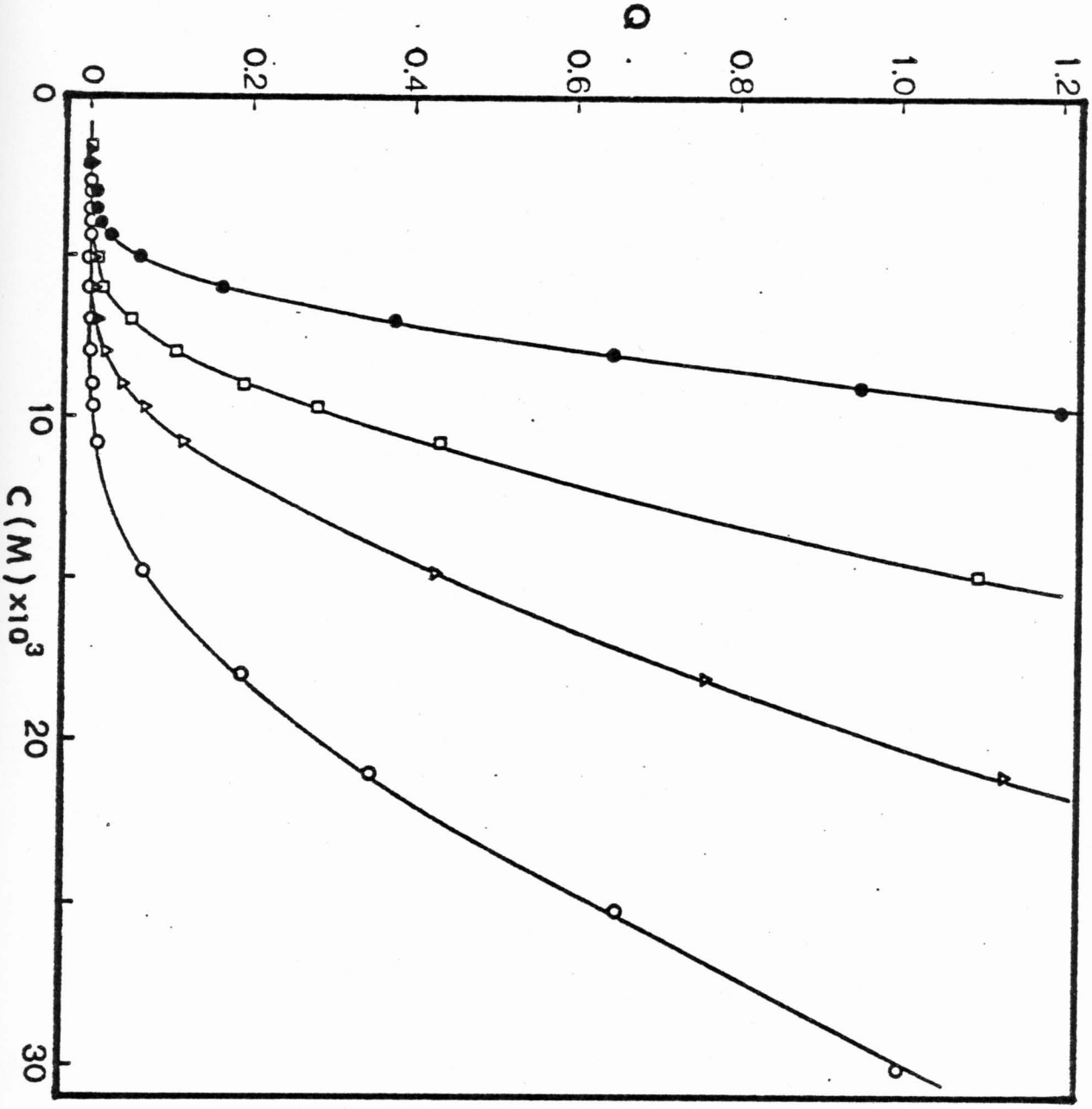

Figure 5.11 Plots of Q versus the concentration of sodium cholate in solutions containing no added salt (●), 0.05N (△), 0.15N (□), and 0.45N (O) sodium chloride.

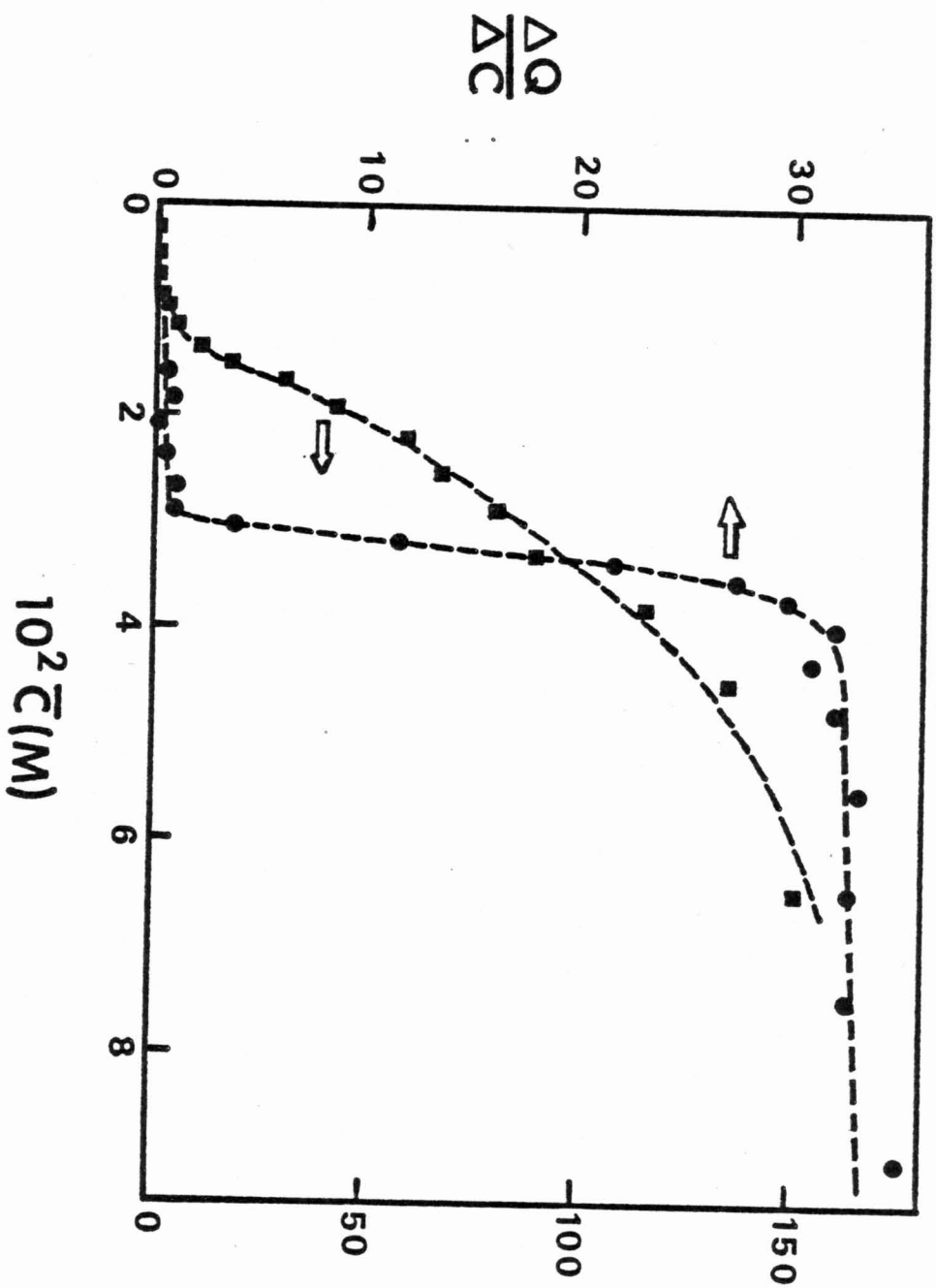

Figure 5.12. Plots of $\Delta Q/\Delta C$ versus the mean concentration of surfactant for sodium cholate (■) and sodium decyl sulfate (●).

reported CMC region. Instead, a gradual and continuous increase is observed.

Solubilization in a surfactant solution involving aggregates of multiple sizes may be described by a series of equilibria, as in Equation 5-7, to take into account all the aggregates and monomers, if necessary, i.e.,

$$D_a + b_q = Db_q \ , \qquad [5\text{-}7]$$

where Db_q and b_q are the surfactant aggregates containing q monomers with and without the solubilized dye, respectively. An equilibrium constant F_q can be defined as

$$F_q = \frac{[Db_q]}{[D_a]\ [b_q]} \ . \qquad [5\text{-}8]$$

Since the concentration of TNS is very low as compared to the total concentration of the surfactant, the probability of more than one dye being solubilized in each surfactant aggregate is small. Equilibria such as Equation 5-7 are, therefore, appropriate for describing the present system. If the emission constants of the fluorescent spectra of the dye associated with surfactants of different aggregation numbers are equal, the Q function obtained from a system consists of monomer, dimer, up to q-mer may be written as

$$Q = \sum_{q=1} F_q[b_q] \ . \qquad [5\text{-}9]$$

If, however, the emission constant, E_q, varies with the aggregation number q of the surfactant, then the Q function

should be expressed as

$$Q = \frac{\sum_{q=1} A_q F_q [b_q]}{1 + \sum_{q=1} (1 - A_q) F_q [b_q]} \quad , \qquad [5\text{-}10]$$

where

$$A_q = \frac{E_q - E_o}{E_\infty - E_o} \qquad [5\text{-}11]$$

and E_∞ is the emission constant obtained by extrapolation of the fluorescent intensity to infinite surfactant concentration, such as by the plot shown in Figure 5.10. The emission constant E_q is not readily determined experimentally. Presumably, its value lies between E_o and E_∞. The value of A_q, therefore, varies from zero to one. For smaller aggregates, A_q and also F_q are likely to be small. This is particularly true for the monomer. When the aggregates are large, A_q approaches unity and $(1 - A_q)$ approaches zero. Aggregates of moderate sizes are relatively more important in terms of $(1 - A_q)F_q[b_q]$. Since the total surfactant concentration is not very high in most of the systems studied, the concentrations of aggregates $[b_q]$ are relatively low. The denominator on the right hand-side-of Equation 5-10 may be approximated to unity and the Q function becomes

$$Q = \sum_{q=1} A_q F_q [b_q] \quad . \qquad [5\text{-}10a]$$

For nonionic surfactants or ionic surfactants containing high concentration of electrolyte, the concentration of

aggregate b_q can be expressed as $[b_q] = K_q[b_1]^q$. The first derivative of the logarithm of Q versus the logarithm of the equivalent surfactant concentration, C, can then be written as

$$\frac{d\ \ln Q}{d\ \ln C} = \frac{d\ \ln Q}{d \ln[b_1]} \cdot \frac{d\ \ln[b_1]}{d\ \ln C} = \frac{\bar{N}_{ns}}{\bar{N}_w} \qquad [5\text{-}11]$$

where

$$\bar{N}_{ns} = \frac{A_1F_1[b_1] + \sum_{q=2} qA_qF_qK_q[b_1]^q}{A_1F_1[b_1] + \sum_{q=2} A_qF_qK_q[b_1]^q} \qquad [5\text{-}12]$$

and

$$\bar{N}_w = \frac{[b_1] + \sum_{q=2} q^2K_q[b_1]^q}{[b_1] + \sum_{q=2} q\ K_q[b_1]^q} \qquad [5\text{-}13]$$

$\bar{N}_w$ is the weight-average aggregation number of the surfactant including the monomer. $\bar{N}_{ns}$ may be regarded as the number-average aggregation number of the surfactant weighted by solubilization of the probe molecule. The upper and lower limits of Equation 5-11 are both unity, i.e.,

$$\left(\frac{d\ \ln Q}{d\ \ln C}\right)_{c \to 0} \longrightarrow 1$$

$$\left(\frac{d\ \ln Q}{d\ \ln C}\right)_{c \to \infty} \longrightarrow 1$$

These limits are in agreement with experimental results as shown below.

For ionic surfactants, if counter-ion interaction is important, the concentration of aggregate b_q may be expressed as

$$[b_q] = K_q [b_1]^q [M]^p \quad , \qquad [5\text{-}14]$$

where [M] is the concentration of the unbound counter-ion and p is the number of bound counter-ion per aggregate b_q. The effect of the counter-ion term, according to Equations 5-14 adn 5-11, is to increase d lnQ/d lnC. Such an effect is relatively small for smaller aggregates because the degree of counter-ion binding is small. For large aggregates the effect of counter-ion becomes relatively more important. However, at high surfactant concentrations, when the amount of counter-ion is already sufficient to swamp the surface charges of surfactant aggregates, the effect of additional counter-ion on the surfactant aggregation and solubilization becomes relatively small.

For a micellar system, if monomers and micelles of uniform size are important, d lnQ/d lnC has a value of one below the CMC. As the concentration of the surfactant approches CMC, d lnQ/d lnC increases rapidly to a maximum at the CMC region and then decreases to unity again immediately above the CMC region. Figure 5.13 shows the plot of log Q versus log C for alkyl sulfates in water. Figure 5.14 shows the plot of $\Delta \log Q / \Delta \log C$ versus long $\bar{C}$ for sodium dodecyl sulfate in water, where $\bar{C}$ is the mean surfactant concentration of two adjacent data points. As would be expected from

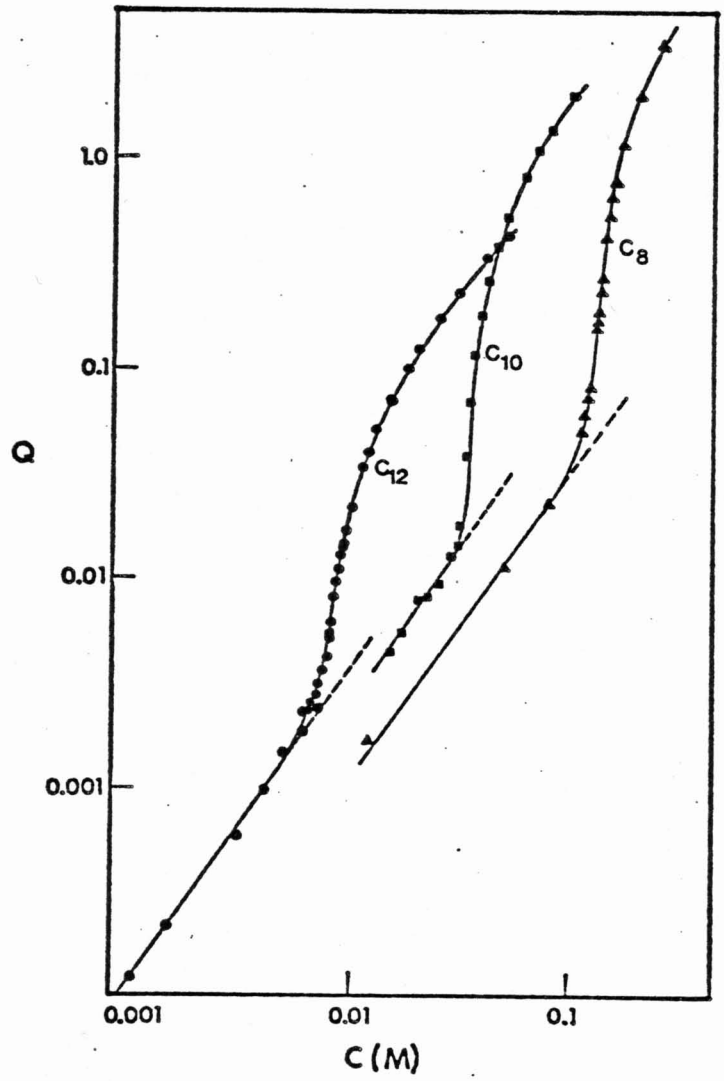

Figure 5.13. Plots of logarithm of Q versus the logarithm of surfactant concentration for sodium dodecyl sulfate (●), sodium decyl sulfate (■), and sodium octyl sulfate (▲). The straight lines have unit slope.

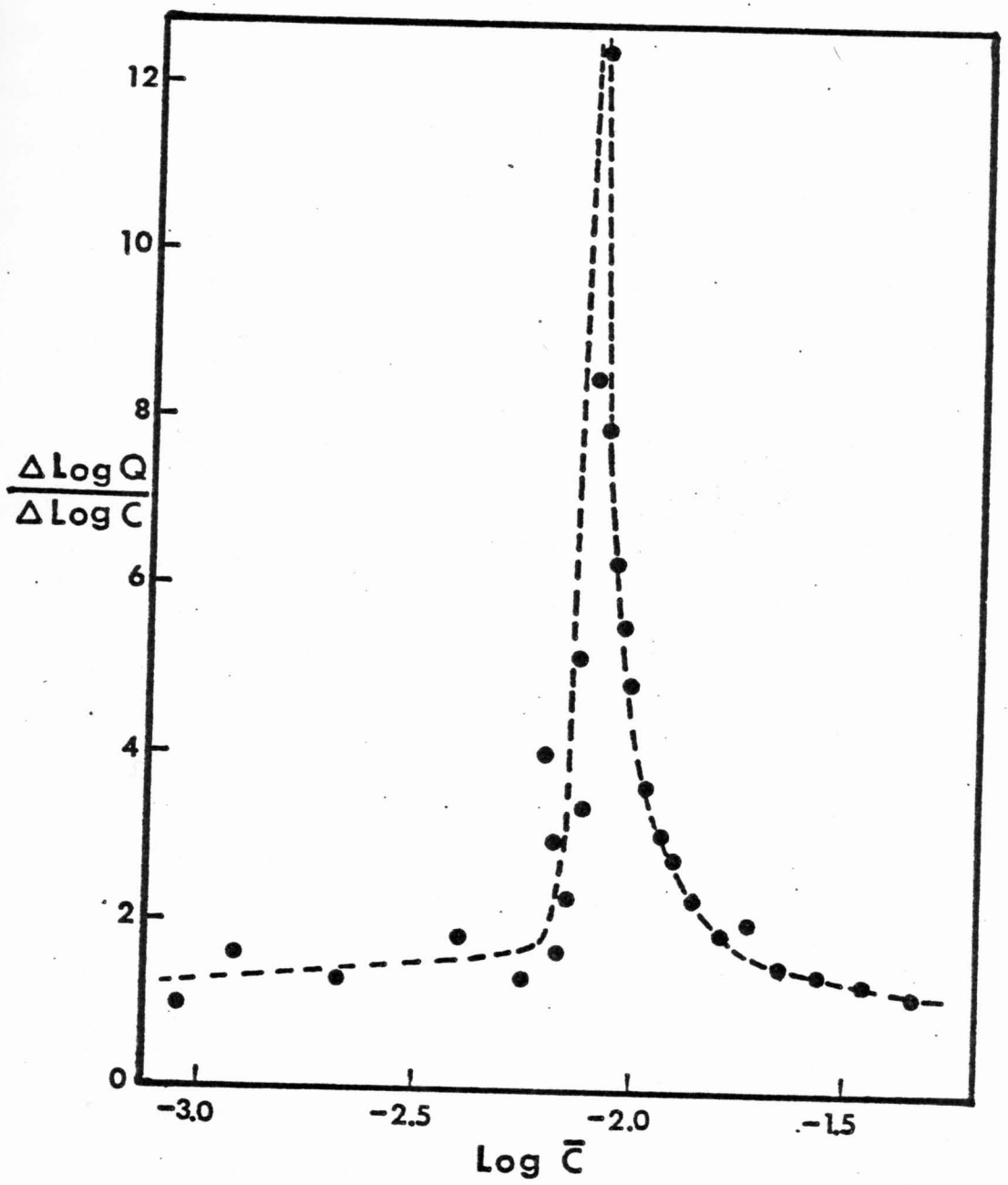

Figure 5.14. Plot of $\Delta \log Q / \Delta \log C$ versus $\log \bar{C}$ for sodium dodecyl sulfate in water, where $\bar{C}$ is the mean surfactant concentration.

Equation 5-11 for micelle formation with a high degree of cooperativity and large aggregation number of the micelle, $\Delta \log Q / \Delta \log C$ exhibits a sharp, narrow peak at the CMC region and a value of unity at concentrations both below and above the CMC. Because of the limited experimental data in the CMC region, the maximum value could not be determined. Nevertheless, the data in Figure 5.13 indicate a high slope at the CMC region for alkyl sulfates. The unit slope observed in very dilute solutions for all three alkyl sulfates suggests a 1:1 interaction between TNS and the surfactant. Correction for such interaction at the CMC region will increase the value of d logQ/d logC substantially.

Figures 5.15 to 5.17 show the plots of log Q versus log C for the bile salts. A similar profile has been observed for all three bile salts. In dilute solutions a unit slope has been obtained in the case of deoxycholate and chenodeoxycholate indicating a 1:1 interaction also occurs between TNS and these bile salts. For sodium cholate, where the concentrations in the dilute region are higher, the slopes are also somewhat higher indicating the possibility of dimers or lower oligomers interacting with TNS. Figure 5.18 shows the variation of $\Delta \log Q / \Delta \log C$ values with concentration of the bile salt, sodium cholate, containing different amounts of added salt. Figure 5.19 shows similar data for sodium deoxycholate and sodium chenodeoxycholate without

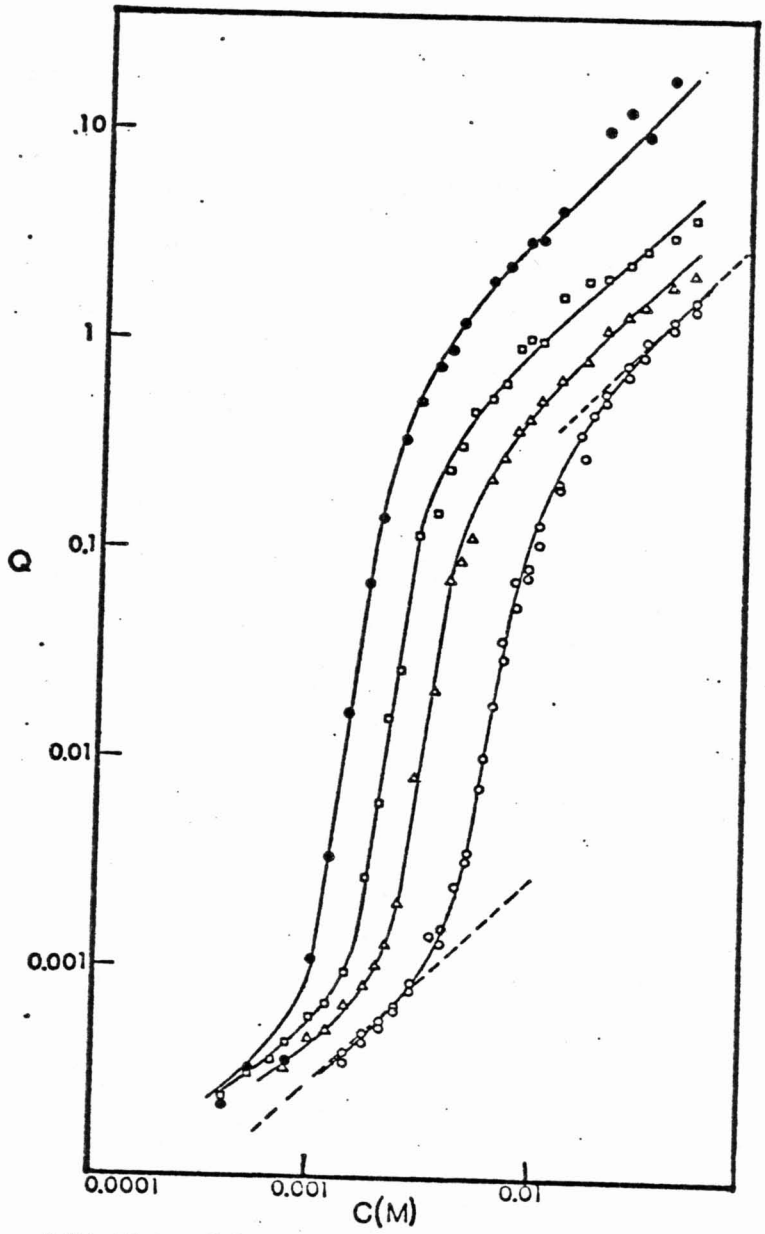

Figure 5.15. Plots of log Q versus log C of sodium deoxycholate solutions containing no added salt (O), 0.05N (△), 0.15N (□), and 0.45N (●) sodium chloride. The dashed lines have unit slope.

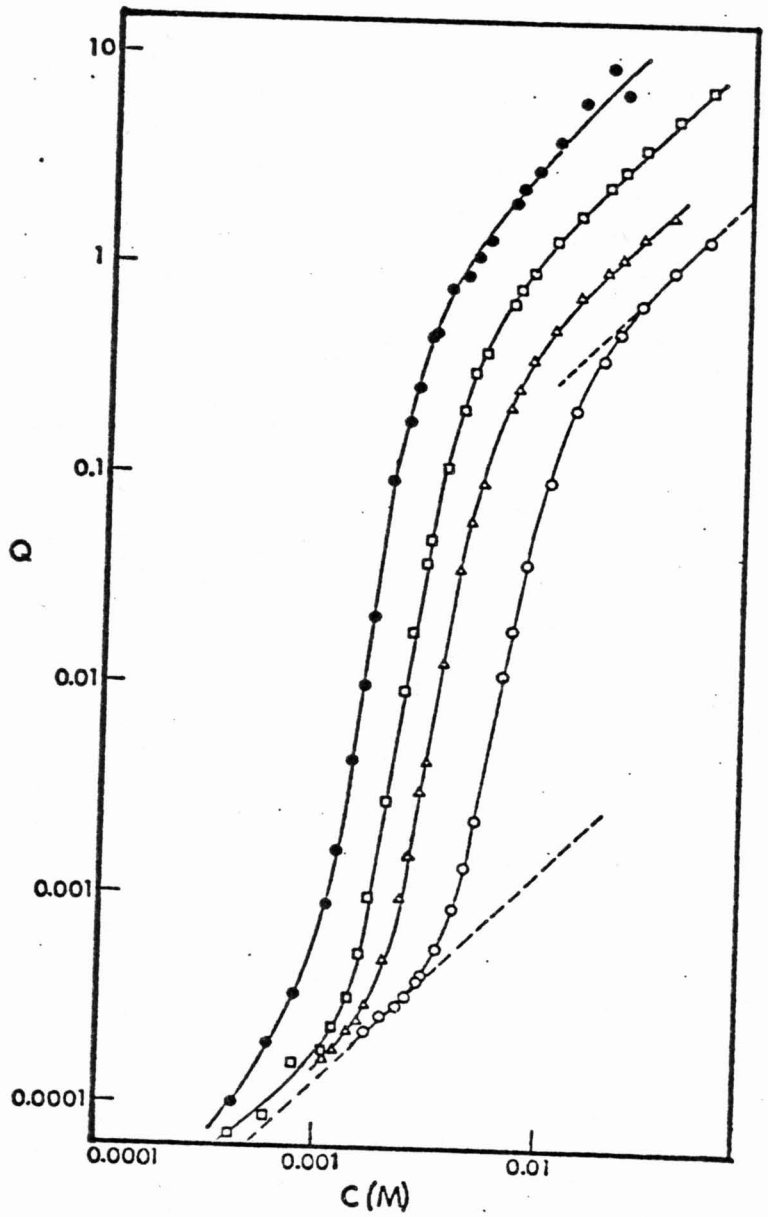

Figure 5.16. Plots of log Q versus log C of sodium chenodeoxycholate in solutions containing no added salt (O), 0.05N (Δ), 0.15N (□), and 0.45N (●) sodium chloride. The dashed lines have unit slope.

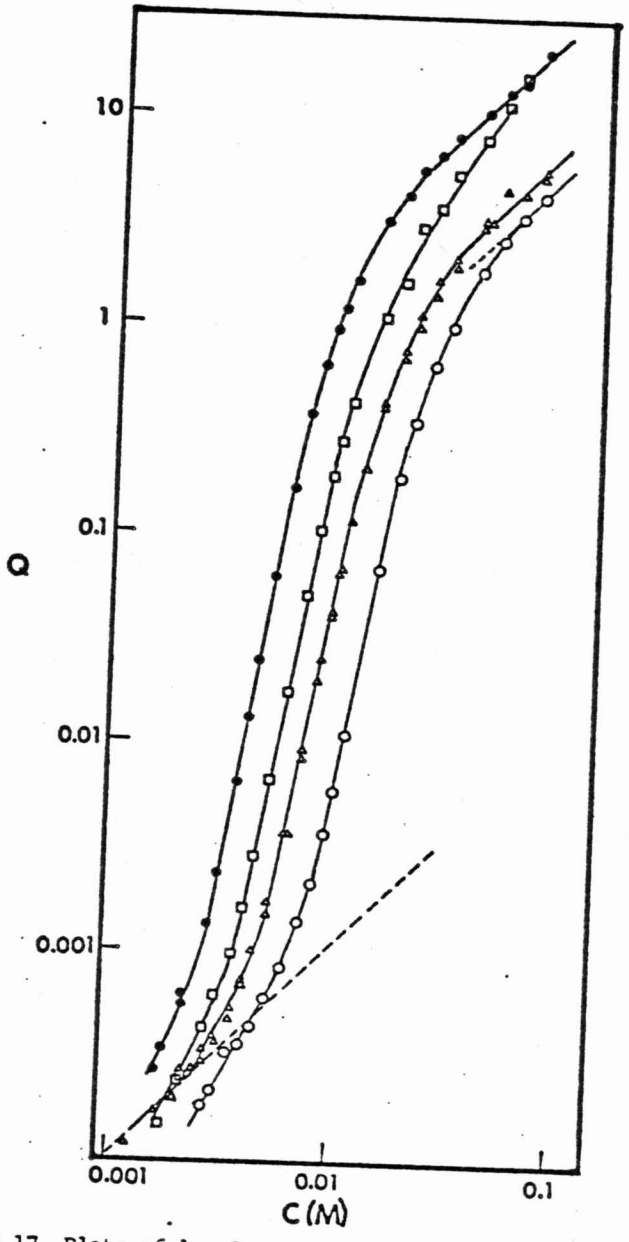

Figure 5.17. Plots of log Q versus log C of sodium cholate solutions containing no added salt (O), 0.05N (Δ), 0.15N (□), and 0.45N (●) sodium chloride. The dashed lines have unit slope.

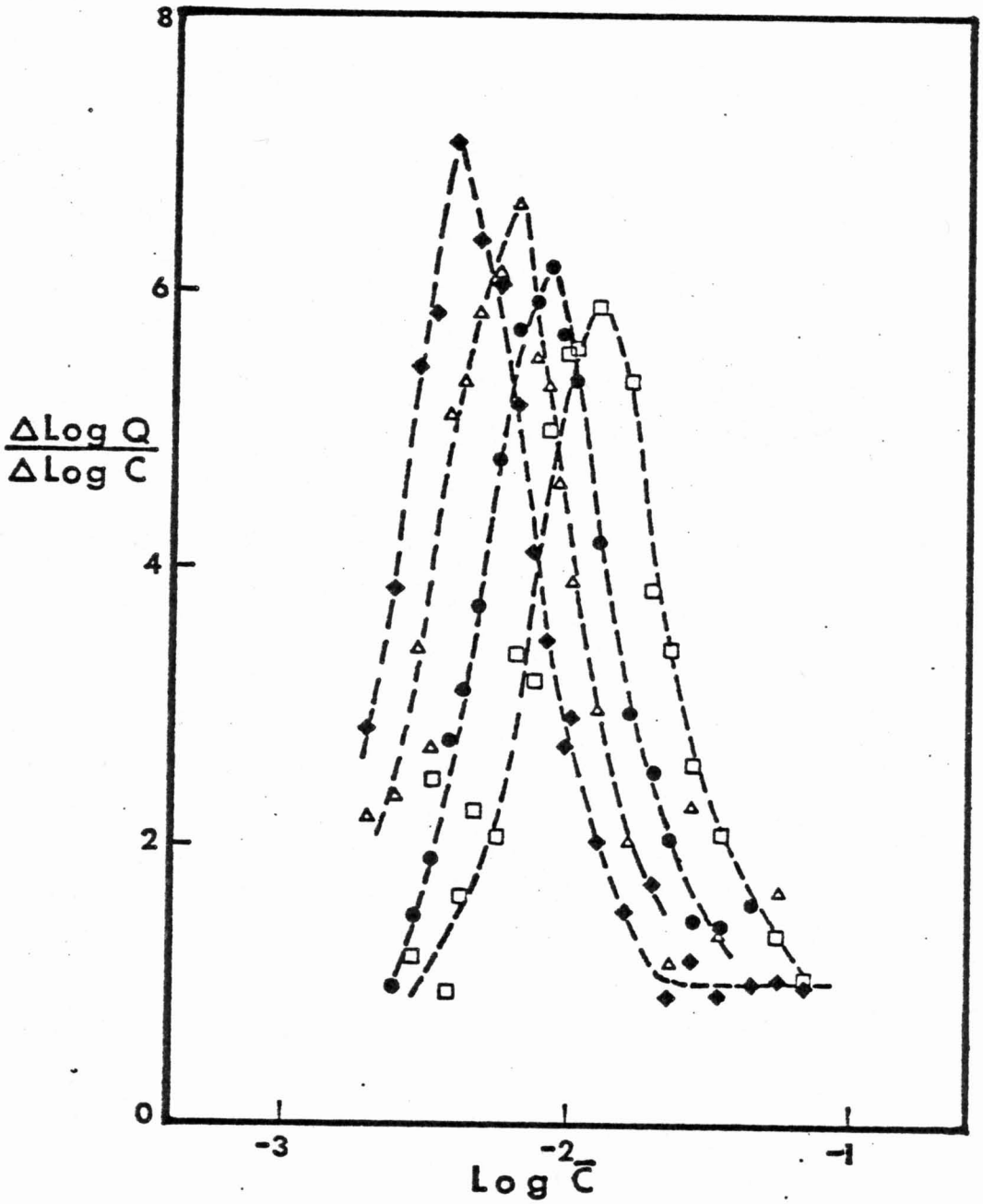

Figure 5.18. Plots of $\Delta \log Q / \Delta \log C$ versus $\log \bar{C}$ for sodium cholate without added salt (□), with 0.05N (●), 0.15N (△), and 0.45N (◆) sodium chloride.

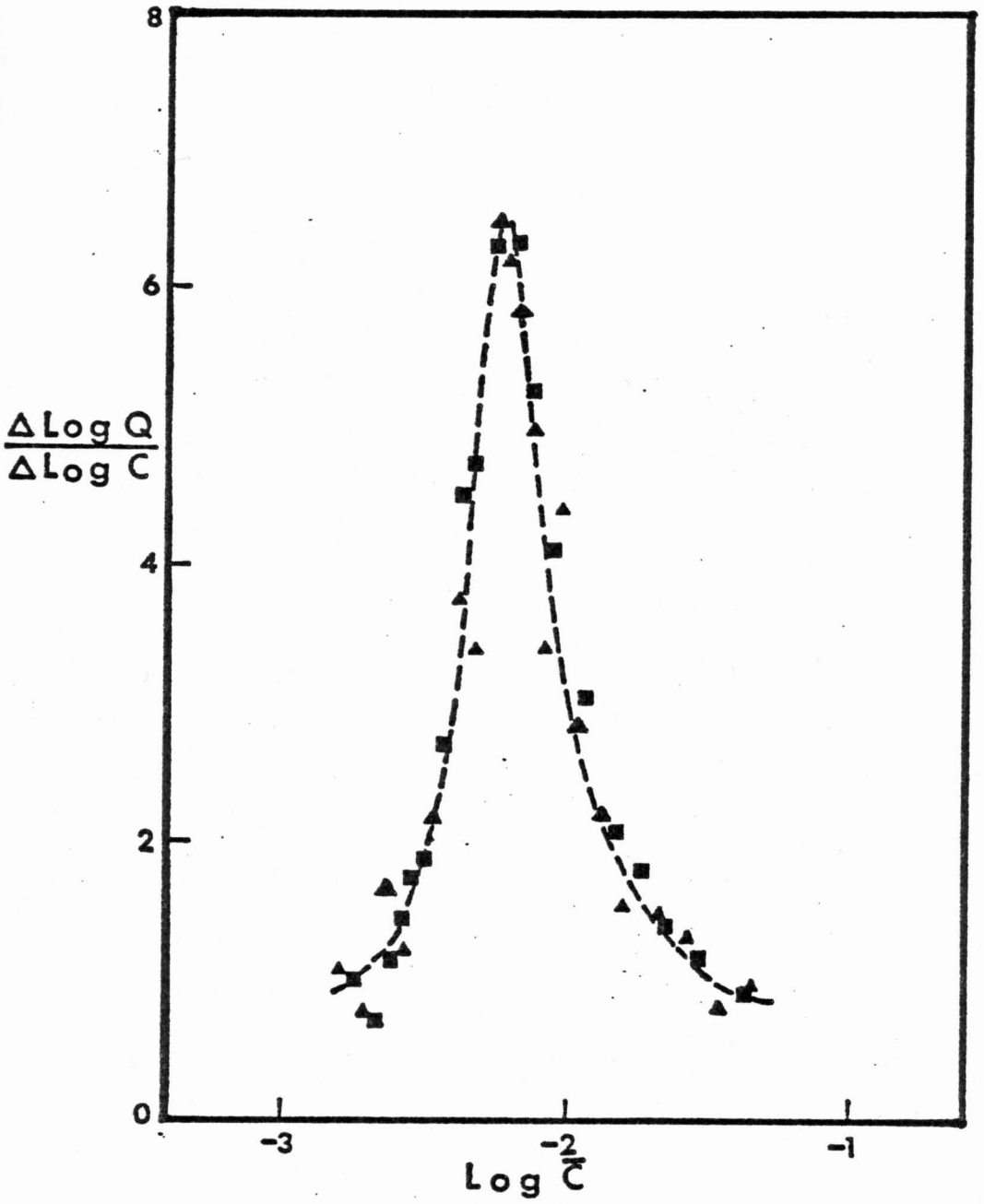

Figure 5.19. Plots of $\Delta \log Q / \Delta \log C$ versus $\log \bar{C}$ for sodium deoxycholate (▲) and sodium chenodeoxycholate (■) in water without added salt.

added salt. It shows the close similarity of the TNS solubilization in these two isomeric bile salts.

The plots of $\Delta \log Q / \Delta \log C$ versus $\log \bar{C}$ for all bile salts show a single peak as in the case of alkyl sulfates. The peaks for the bile salts are much broader, however, than those obtained with a micelle-forming surfactant, and the maximum value is between 6 and 7 in all cases. As shown in Figures 5.15 to 5.17, a mean slope of 6 to 7 is obtained in the log Q versus log C plot over a wide range of Q values, roughly over two to three orders of magnitude. If corrections are made for the very low intensities observed at low concentrations, which are due to the monomer-TNS adducts, these slopes do not change very much and continue to hold over a wide range of bile salt concentrations and Q values. Even the addition of large amounts of salt does not change the slope of the linear region in the log Q versus log C plots very much. As shown in Figures 5.15 to 5.18, the curve merely shifts to lower concentrations and the maximum slope increses slightly. The shift can be ascribed to the reduction of ionic repulsions between TNS and the bile salts at high salt concentrations.

Although the aggregation patterns of bile salts are not understood very well, it is known that the average degrees of aggregation vary over a very wide range with the added salt concentration and the type of bile salt (44,258). A

roughly constant slope of about 7 in relatively dilute solutions in all the bile salt solutions is thus an indication of a preferential adduct formation of TNS with about 7 bile salt anions. For such an adduct d lnQ/d ln[b_1] has a slope of 7, if other aggregates do not interact with TNS. The pattern of solubilization, at least in the initial stages, bears very little relation with the pattern of self-association. At high concentrations, as shown in Figures 5.15 to 5.17, the slope of log Q against log C decreases because d ln[b_1]/d lnC decreases as a result of self-assocaition of the bile salt.

The fluorescence data with TNS can also be used to estimate the effective polarity of the microenvironment of solubilized TNS. It is known that the fluorescent intensity and the band maximum of TNS emission spectrum are sensitive to the polarity and rigidity of the solvent system (249,250, 253). The fluorescent properties of this dye and other similar type of dyes, e.g., ANS, have been studied extensively by Kosower, et al. (249,250,259). These authors proposed that an intramolecular , excited-state charge-transfer reaction plays a key role in the solvent effect on the fluorescence of this type of dye. The charge-transfer reaction involves two distinct emitting species depending on the relative position of the two ring systems in the molecule. Consequently, the fluorescent intensity and band maximum of TNS increase with the decrease in polarity or increase in

rigidity of the solvent. As shown in Table 5.1, the fluorescent band maxima of TNS solubilized in different surfactant systems are all at a shorter wavelength than that of water. The band maximum in the flexible chain surfactants corresponds to a solvent polarity index value, $E_T(30)$ (260,261), of approximately 56 in all three alkyl sulfates. The $E_T(30)$ value of bile salts is approximately 46. This value is also the same in three different bile salts, indicating a similarity of packing which is also shown by the roughly constant slopes of d lnQ/d lnC curves discussed earlier. The value is also significantly lower than that of the flexible-chain surfactant. As indicated in Table 5.2, the extrapolated fluorescent intensities of TNS in bile salts are also considerably higher than those of the alkyl sulfate micelles. These results indicate that the microenvironment of TNS in the surfactant aggregates is less polar than water. The microenvironment in the bile salt aggregates seems to be more rigid and less polar than that in the flexible chain micelles. This is consistent with the expected structural differences of the aggregates.

5.3.2. Solubilization of Bromthymol Blue

The dissociation constant of indicator dyes often changes upon solubilization in micelles. Such a change has been ascribed to the proximity effect of the nonpolar micellar core and , in the case of ionic micelles, to the micellar surface charge (cf. Chapter 3). The pK value of an anionic dye is

usually higher in the micellar solubilized state than its intrinsic pK in the bulk solution (80). As a result, the indicator ratio of this kind of dye increases in the presence of nonionic or anionic micelles. Under the condition of very low dye to surfactant ratio, the solubilization process can be described by the following equilibria:

$$Y + b_q = Yb_q \text{ and } B + b_q = Bb_q ,$$

where Y and B represent the yellow and blue form of BTB. The corresponding equilibrium constants can be written as

$$F_{Yq} = \frac{[Yb_q]}{[Y_a][b_q]} \qquad F_{Bq} = \frac{[Bb_q]}{[B_a][b_q]} . \qquad [5\text{-}15]$$

Here $[Y_a]$ and $[B_a]$ represent concentrations of the dye in the bulk aqueous solution. Since the indicator ratio for the dye in the bulk solution, R_a, and in the surfactant solubilized state, R_s, are defined as

$$R_a = \frac{[Y_a]}{[B_a]} \quad \text{and} \quad R_{sq} = \frac{[Yb_q]}{[Bb_q]} ,$$

a ratio Q_r can be obtained for the solubilization of the yellow form of the dye, i.e.,

$$Q_r = \frac{(R/R_a - 1)}{(1 - R/R_s)} = F_{Yq}[b_q] \qquad [5\text{-}16]$$

A similar equation can be derived for the blue form of the dye. The values of R and R_a are directly determined experimentally. R_{sq} can be estimated by an extrapolation method as

discussed before (cf. 3.3.). Mukerjee and Banerjee (80) have reported that the apparent pK of bromophenol blue, an analog of BTB, increases from a value of 3.84 in the bulk solution to 5.67 upon solubilization in sodium dodecyl sulfate micelle. Such an increase in pK corresponds to an approximately 67 fold increase in the indicator ratio , i.e., R_a/R_{sq}=0.015. The pK value of BTB solubilized in the nonionic β-D-octyl glucoside micelle has been reported to be 1.3 units higher than that in the bulk solution (73). According to Equation 3-1a, if the pK value of BTB in β-D-octyl glucoside micelle is assumed to be the pK_s and the Gouy-Chapman potential of either sodium dodecyl sulfate or sodium decyl sulfate micelle is used, the apparent pK of BTB in these micelles would be 2 to 3 units higher than the pK value in the bulk solution. The ratio of R_a/R_{sq} should, therefore, be smaller than 0.01. Since R varies from R_a to R_{sq}, the ratio R/R_{sq} is small as compared to unity at low surfactant concentrations. Equation 5-16 can then be approximated by

$$Q'_r = (R/R_a - 1) = F_{Yq}[b_q] \quad . \qquad [5\text{-}17]$$

For a surfactant system involving multiple aggregates, Equation 5-17 can be expanded into the following form:

$$Q'_r = \sum_{q=1} F_{Yq}[b_q] \qquad [5\text{-}17a]$$

Equation 5-17a is smilar to Equation 5-1a,derived for the solubilization of TNS in surfactant solutions. For a micellar system, if only the monomer, b_1, and the micelle, b_n, are

important, Equation 5-17a takes the following form

$$Q'_r = F_{Y1}[b_1] + F_{Yn}[b_n] \qquad [5\text{-}18]$$

At concentrations below the CMC, only monomers exist. Equation 5-18 becomes

$$Q'_r = F_{Y1}C \; . \qquad [5\text{-}18a]$$

The monomer concentration is approximately constant above the CMC and Equation 5-18 can be written as

$$Q'_r = F_{Y1}(CMC) + F_{Yn}(C - CMC)/n$$

$$= (F_{Y1} - \frac{F_{Yn}}{n}) \cdot (CMC) + \frac{F_{Yn}}{n} C \qquad [5\text{-}18b]$$

A plot of Q'_r versus C is, therefore, expected to show two straight lines, one with a slope of F_{Y1} at concentrations below the CMC and the other F_{Yn}/n at concentrations above the CMC. At the CMC region, a transition occurs. This phenomenon is demonstrated in Figure 5.20, in which Q'_r is plotted against the concentration of the surfactant, sodium dodecyl sulfate, in solutions of pH 7.56 and an added sodium ion concentration of 0.0450N. Two linear regions are observed in this plot. The line at concentrations below the CMC has a slope of approximately zero, indicating that the interaction between BTB and the surfactant monomer is relatively unimportant. A slope of 3200 is obtained from the data at concentrations above the CMC. This slope measures F_{Yn}/n. Figure 5.21 shows a similar plot for BTB in sodium decyl sulfate solutions of pH 7.56 and 0.0423N added sodium

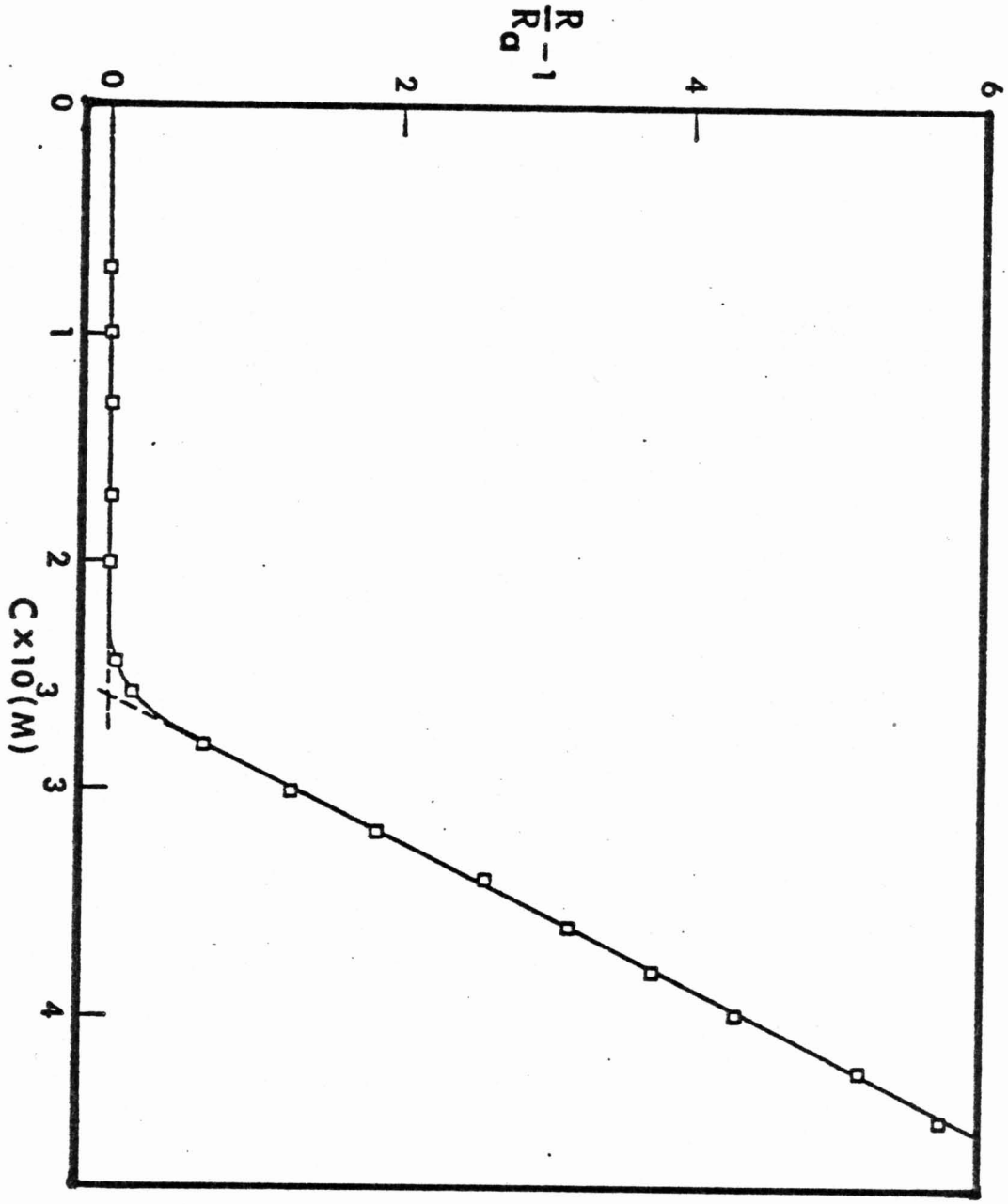

Figure 5.20. Plot of R/R_a-1 versus the concentration of sodium decyl sulfate in solutions of pH 7.56 and an added sodium ion of 0.0235N.

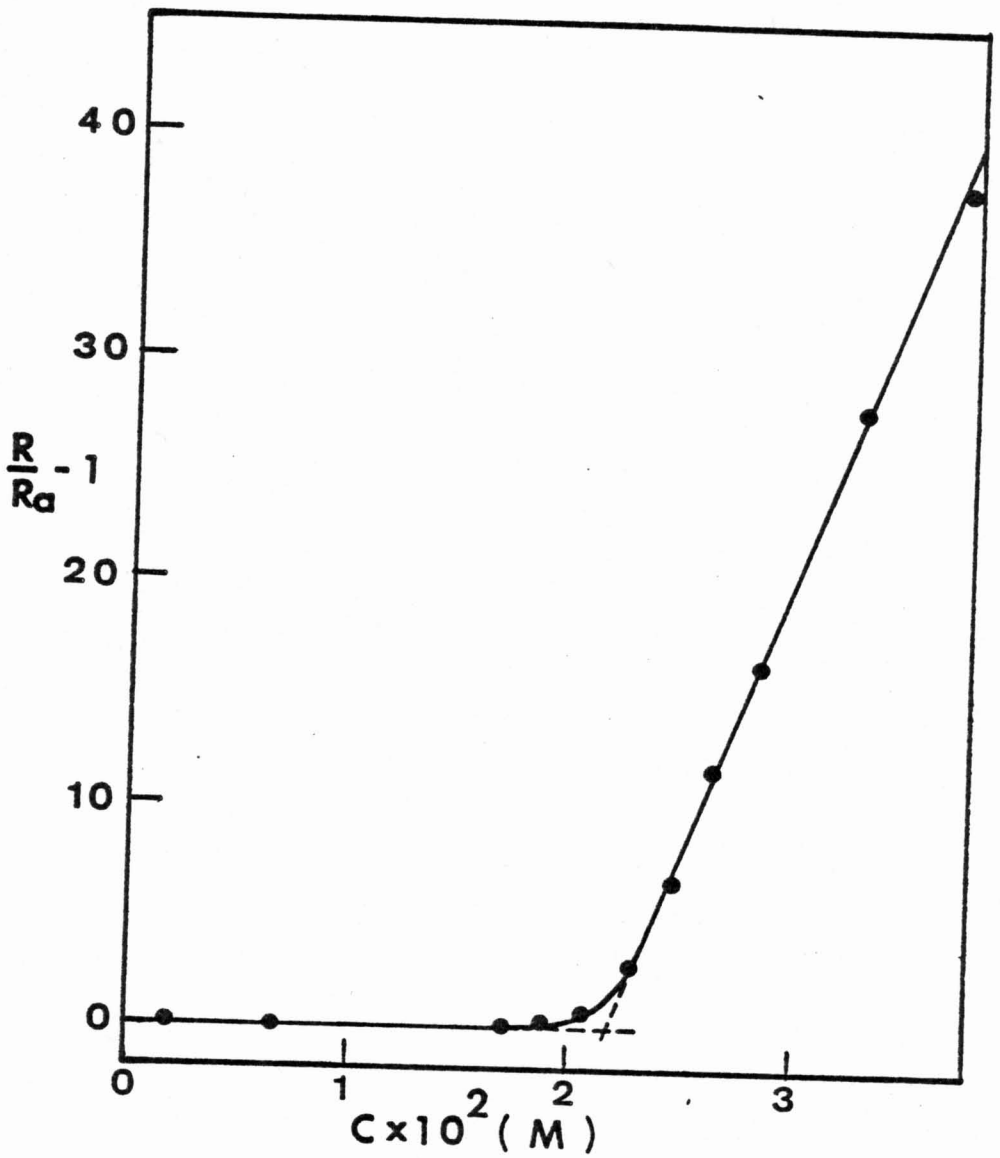

Figure 5.21. Plot of $R/R_a - 1$ versus the concentration of sodium decyl sulfate in solutions buffered to pH 7.56 and having an added sodium ion concentration of 0.0235N.

ion. The straight line above the CMC has a slope of 2400. It is expected that the surface potential of sodium dodecyl sulfate is higher than that of sodium decyl sulfate micelles in the buffer used (30). The higher surface potential, in the present case, should reduce the solubilization of the charged dyes. Nevertheless, the data indicate that BTB is solubilized more in sodium dodecyl sulfate than in the decyl sulfate micelles. The higher affinity of BTB towards the sodium dodecyl sulfate micelles is probably partly due to the larger sizes of these micelles.

The CMC values obtained from Figures 5.20 and 5.21 for sodium dodecyl sulfate and sodium decyl sulfate are 2.58×10^{-3} and 2.16×10^{-2}M, respectively. These values are in good agreement with the predicted CMC values, 2.3×10^{-3} and 2.2×10^{-2}M, obtained by interpolation of the literature CMC data to the corresponding sodium ion concentration at the CMC (65).

Figure 5.22 shows the plot of Q_r' versus the surfactant concentration of sodium taurodeoxycholate in solutions of pH 7.33 with an added sodium ion concentration of 0.061N. Unlike the alkyl sulfates, the Q_r' value of taurodeoxycholate increases nonlinearly with the surfactant concentration beginning at very dilute solutions. The data start to show downward curvature at a relatively low value of Q_r' in solutions of moderate surfactant concentration where the plots of sodium decyl and sodium dodecyl sulfates are linear.

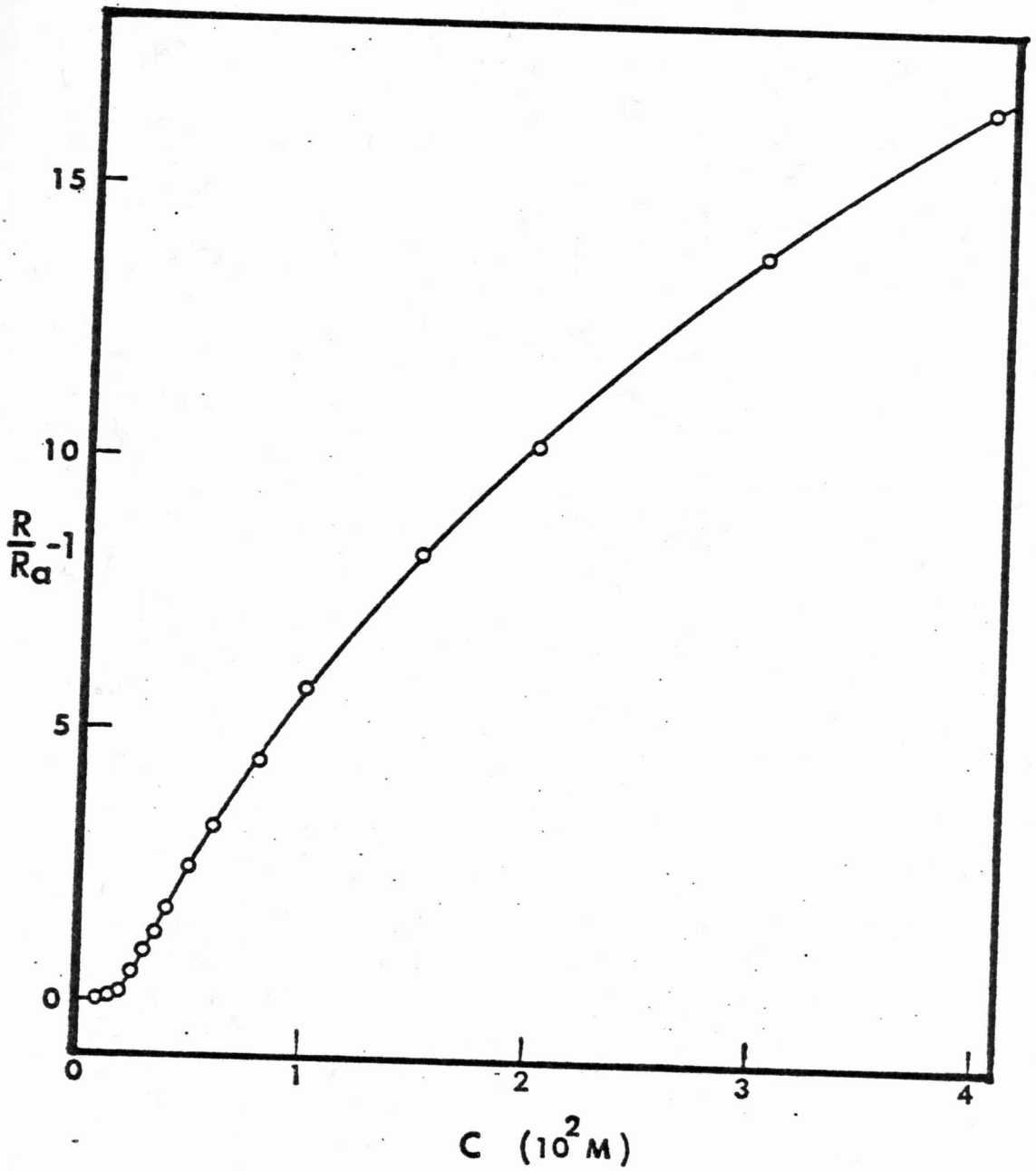

Figure 5.22. Plot of $R/R_a - 1$ versus the concentration of taurodeoxycholate in solutions of pH 7.33 and an added sodium ion concentration of 0.061N.

Because of the nonlinearity in the Q'_r versus C plot, an unbiased CMC value can not be obtained. As shown in Figure 5.23, the intersection of two straight lines drawn from the data points at low and at high concentrations varies considerably depending on the section of data being considered. The gradual change in Q'_r with the surfactant concentration ,on the other hand, suggests a low degree of cooperativity of solubilization in the sodium taurodeoxycholate system.

To further examine the pattern of solubilization, a plot of log Q'_r versus log C is constructed and shown in Figure 5.24. Unlike those of the TNS-bile salt systems, the solubilization curve of BTB in sodium taurodeoxycholate solutions exhibits an initial slope of approximately 6 and remains at the same slope for a wide concentration range. This indicates that BTB does not interact with sodium taurodeoxycholate aggregates smaller than hexamer. In other words, at least six taurodeoxycholate molecules are required to solubilize one BTB molecule. The extended linear region in the log Q'_r versus log C plot suggests that an adduct of one BTB with at least six taurodeoxycholate molecules is formed over a wide concentration range. For TNS the data suggested that seven molecules of bile salt were required for solubilizing one molecule of dye.

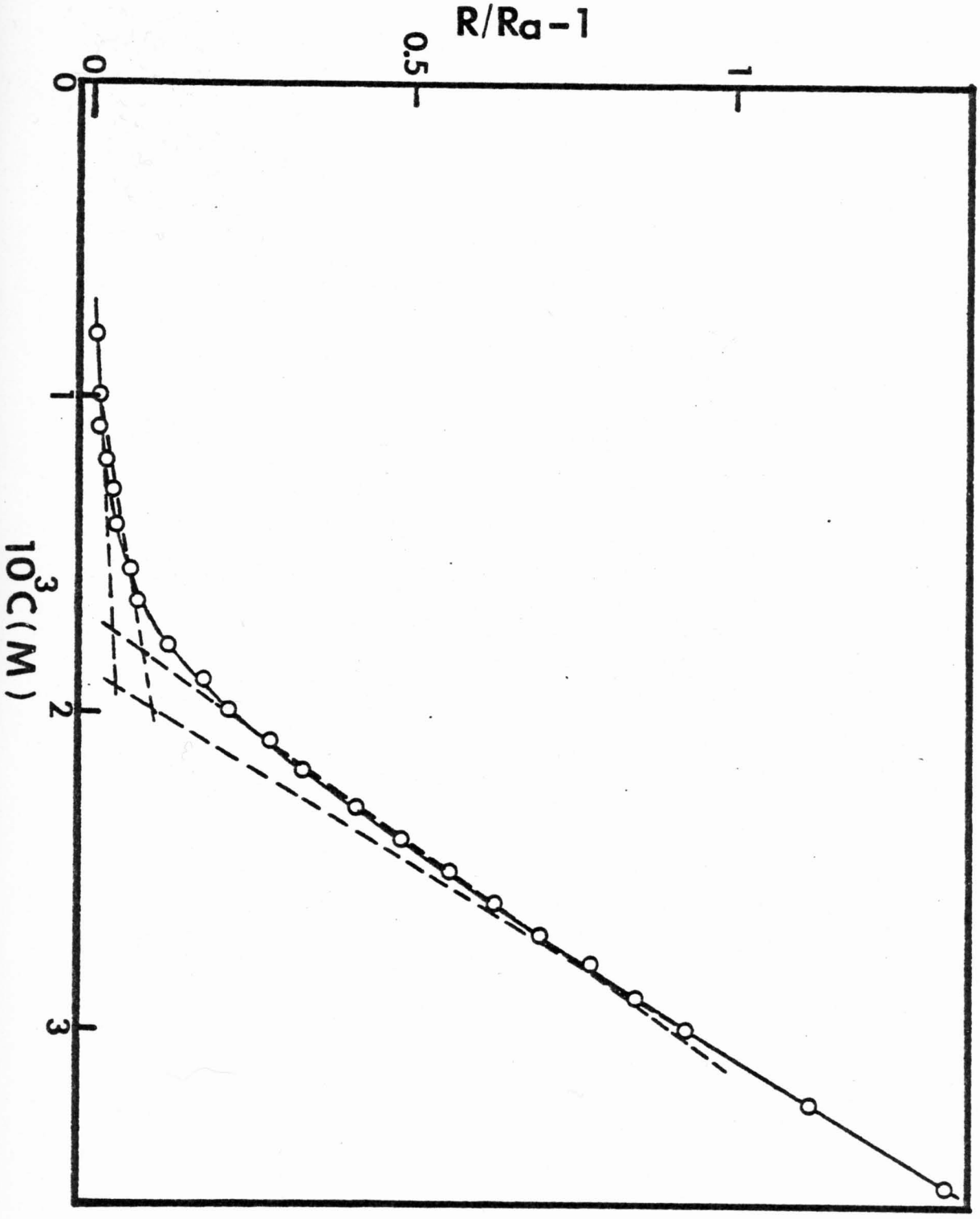

Figure 5.23. Plot of R/R_a-1 versus C for sodium taurodeoxycholate at low concentrations.

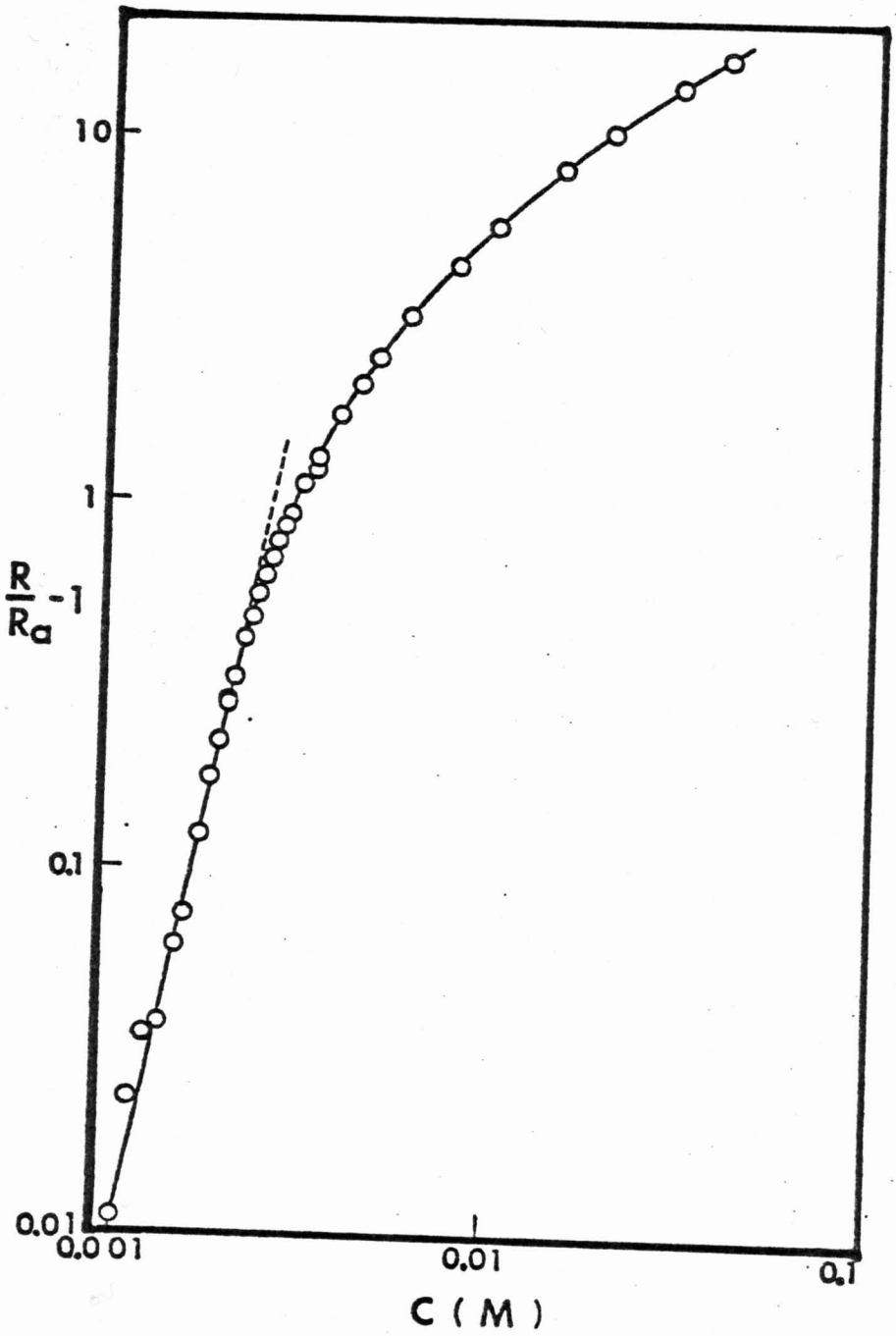

Figure 5.24. Plot of log (R/R_a-1) versus log C of sodium taurodeoxycholate system.

5.4. Conclusion

The development of the fluorescence of TNS upon solubilization has been used to compare the pattern of solubilization of bile salts and alkyl sulfates. In the case of sodium dodecyl sulfate, sodium decyl sulfate, and sodium octyl sulfate, the pattern of solubilization is consistent with a process of micelle formation with a high degree of cooperativity. The bile salts, including sodium cholate, sodium deoxycholate, and sodium chenodeoxy cholate, show a much lower degree of cooperativity than the flexible chain surfactants. The solubilization of TNS in bile salts appears to involve the formation of a mixed aggregates which seems to be relatively independent of the pattern of self-association exhibited by the bile salts. The fluorescent bands are sensitive to medium polarity. The polarity of the microenvironment of TNS solubilized in bile salts has been found to be different from that in alkyl sulfate micelles.

The indicator dye, bromthymol blue, has also been used as a probe for comparing the pattern of solubilization in the alky sulfate micelles and sodium taurodeoxycholate. As in the case of the fluorescent dye, the solubilization pattern of BTB in the micelle forming alkyl sulfates exhibits a high degree of cooperativity. The bile salts, on the other hand, shows a less cooperative solubilization pattern which involves the formation of a preferential adduct between

BTB and six bile salt ions at least in the dilute solutions.

6. FLUORINE NUCLEAR MAGNETIC RESONANCE STUDIES OF AGGREGATION PROPERTIES OF TRIFLUORO-PHENOTHIAZINE DERIVATIVES AND FLUOROCARBON SURFACTANT

6.1. NMR Studies of Surfactant Solutions

Nuclear magnetic resonance signals are sensitive to the environment of the nuclei involved. Changes in NMR spectra of surfactants upon aggregation provide information on the local environment in the aggregate as well as on the mode of association. Many studies of surfactant solutions by NMR technique have been reported (99,100,105-108,166-175) and an extensive review has also been published recently by Nakagawa and Tokiwa (122).

The reported NMR studies are mostly measurements of chemical shifts (99,100,105-108,166-172), spin-lattice, spin-spin or nuclear quadrupole relaxation (173-177) of suitable nuclei of the surfactant molecule, solvent molecule or solubilizate. Several papers have also appeared recently regarding the use of chemical shifts for the determination of CMC (105-108,171,172). The major requirement of this kind of measurement is that the chemical shifts of one or more nuclei of the surfactnat must change appreciably with the change in environment. Changes of chemical shifts on micelle formation are relatively small for proton and ^{13}C NMR, because of their low sensitivity to changes of solvent polarity

(179-182). As demonstrated by Muller and coworkers (105-108), the change of ^{19}F NMR chemical shift is large between monomeric and micellized surfactants. These authors also synthesized several partially fluorinated long chain surfactants and determined their CMC values from ^{19}F chemical shifts.

The chemical shift measured from a surfactant solution, δ, is generally assumed to be a weight average of the chemical shifts from the monomeric, δ_1, and the aggregated surfactant, δ_n, by the following relationship:

$$\delta = ([b_1]/C)\,\delta_1 + ([b_n]/C)\,\delta_n \qquad [6\text{-}1]$$

where C is the total equivalent surfactant concentration, $[b_1]$ and $[b_n]$ are the concentrations of the monomer and aggregate containing n surfactant molecules. The CMC is frequently determined from the δ versus C^{-1} curve by locating the intersection of two straight lines extrapolated from the low and high concentration regions (122,196). At concentrations below the CMC, the chemical shift is only due to the monomer. The value of δ_n can be obtained by extrapolating the δ versus C^{-1} plot to a zero value of C^{-1}. CMC values obtained by this method are generally in agreement with the results obtained by other methods for flexible chain surfactants.However, this method is not without some uncertainties, especially for systems exhibiting gradual changes in the CMC region. The main uncertainty arises from the inherent character of the reciprocal concentration scale, in which the data at high concentrations tend to be compressed

and low concentrations expanded. Deviation from the ideal micelle formation , such as pre-micellar association, can often be concealed in such a plot. It is also possible that this type of plot may lead to false CMC values in systems which do not show much cooperativity of self-association (1,25,62). For these reasons, the NMR data would need more careful analysis for CMC determinations. In the present study, ^{19}F chemical shift of trifluorophenothiazine derivatives and long chain fluorocarbon surfactant are examined. The changes in chemical shift as a function of surfactant concentration are analyzed in terms of different patterns of self-association.

6.2. Review of Literature on Aggregation of Phenothiazines

Many phenothiazine derivatives exhibit pharmacological activity in the central nervous system. Derivatives containing aminoalkyl groups attached to the phenothiazine ring nitrogen are major tranquilizers (183-185). These derivatives are also surface active and form aggregates in aqueous solutions (186.187.189,190,195). Surface tensions of several phenothiazine derivatives have been studied by Seeman and Bialy (37), Zografi and Munshi (189), and Kitler and Lamy (190). Triflupromazine and trifluperazine have been found to show surface tension depression comparable to that of the micelle forming surfactant, sodium dodecyl sulfate, in

the concentration range of 10^{-6} to 10^{-5}M in Ringer's buffer solution (37). Chloropromazine and promethazine are also fairly surface active. Monolayer formation of several of these compounds under different conditions have also been studied by Zografi and coworkers (189,191-194). Florence and Parfitt (171,197) reported the proton NMR chemical shifts of several phenothiazine derivatives at different concentrations. An upfield shift of the aminomethyl protons was observed when concentration of the phenothiazine derivatives was increased. The chemical shift data were interpreted according to Equation 6-1 with an a priori assumption that these compounds formed simple micelles. CMC values obtained from the plot of chemical shift versus reciprocal concentration were reported by these authors. Based on the magnitude and the direction of shift of the aminomethyl protons, they proposed that the phenothiazine derivatives associate in a manner of vertical stacking with the N-alkyl side chain alternating to the opposing sides (171). Light scattering study of the same derivatives, on the other hand, indicated a low degree of aggregation even at concentrations two or three times above the reported CMC (195).

The aggregation behavior of a phenothiazine dye, methylene blue, has been investigated in detail by Mukerjee and Ghosh (32,38-41). A pattern of continuous stepwise self-association with a stacking structure has been suggested by

these authors based on the isoextraction data and comparison with several theoretical models of self-association. A low degree of aggregation has been indicated because of the low cooperativity in the formation of such an aggregate (1,25, 62). It has also been demonstrated that an apparent CMC can be obtained for such a system when a solution property is plotted as a function of the concentration. Such a CMC value may not have much physical significance because of the absence of a strong cooperativity of aggregation.

6.3. Scope and Aims

The large change in ^{19}F NMR chemical shifts upon micelle formation provides a sensitive means of monitoring the self-association of fluorine containing surfactants. Triflupromazine and trifluoperazine are two of the major tranquilizers which exhibit strong surface activities in solution (188). Their aggregation properties are expected to be similar to other phenothiazine derivatives on structural grounds.Based on the aggregation behavior of methylene blue in aqueous solutions, a similar stacking interaction is also expected for these two trifluorophenothiazine derivatives. If this is the case, their pattern of self-association should be different from micelle formation of flexible chain surfactants. ^{19}F NMR studies on these two compounds have not been reported to date. For the purpose of comparison, a long chain fluorocarbon surfactant, sodium

perfluoro-n-octanoate (SPFO), has also been studied. The hydrochloride salts, triflupromazine hydrochloride (TEPO HCl) and trifluoperazine dihydrochloride (TFPE 2HCl) (see Figure 6.1 for structures) have been used in the study.

6.4. Results and Discussion

The ^{19}F NMR spectrum of a 0.1M SPFO solution is shown in Figure 6.2. All chemical shifts are upfield from the external standard, 2.5% trifluoroacetic acid in d_6-benzene. The measured chemical shifts are consistent with the reported values (108) with two well defined triplets at about 6 ppm and 41 ppm, corresponding to the ω-trifluoromethyl and the fluorine atoms on the C-2 carbon atom, respectively. In addition, a broad peak near 51 ppm from the C-7 fluorines and several unresolved peakes between 46 and 48 ppm due to the overlapping of the fluorine signals on carbons at C-3 to C-6 positions have also been observed. Among all the chemical shifts, the ω-fluorines exhibt maximum change upon micellization. Therefore, only the center signal of the triplet from the ω-fluorines has been used for data analyses. In the solutions of TFPO HCl and TFPE 2HCl, only one singlet down field from the external standard has been observed in each case.

Figure 6.3 shows the plots of chemical shifts as a function of the reciprocal concentration of SPFO in water and in 0.054N sodium chloride. Similar plots for TFPO HCl

Figure 6.1. Molecular structures of trifluprom azine hydrochloride and trifluoperazine dihydrochloride.

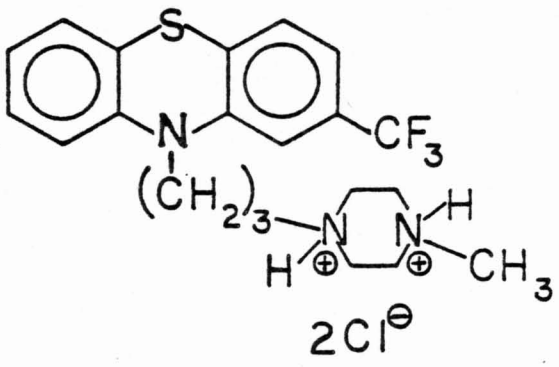

TRIFLUOPERAZINE·2HCl
(TFPE·2HCl)

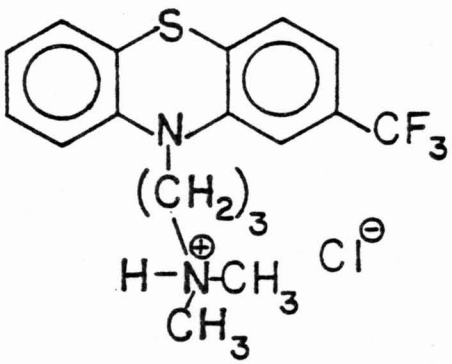

TRIFLUPROMAZINE·HCl
(TFPO·HCl)

Figure 6.2. ^{19}F NMR spectrum of a 0.1M sodium perfluoro-n-octanoate aqueous solution.

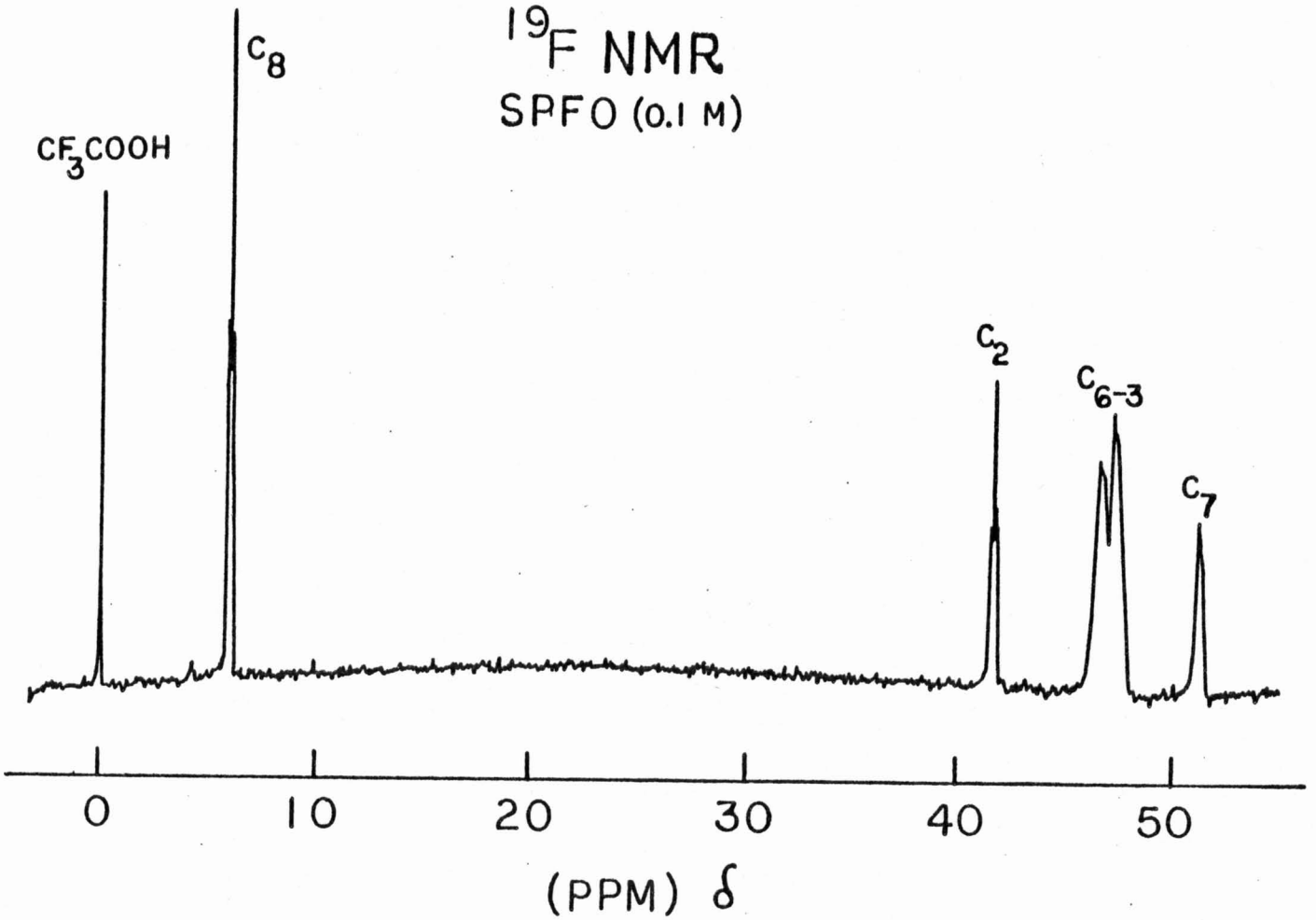
^{19}F NMR
SPFO (0.1 M)
CF_3COOH
C_8
C_2
C_{6-3}
C_7
0
10
20
30
40
50
(PPM) δ

Figure 6.3. Plots of chemical shift versus the reciprocal concentration of SPFO in water (O) and 0.0547N sodium chloride (□).

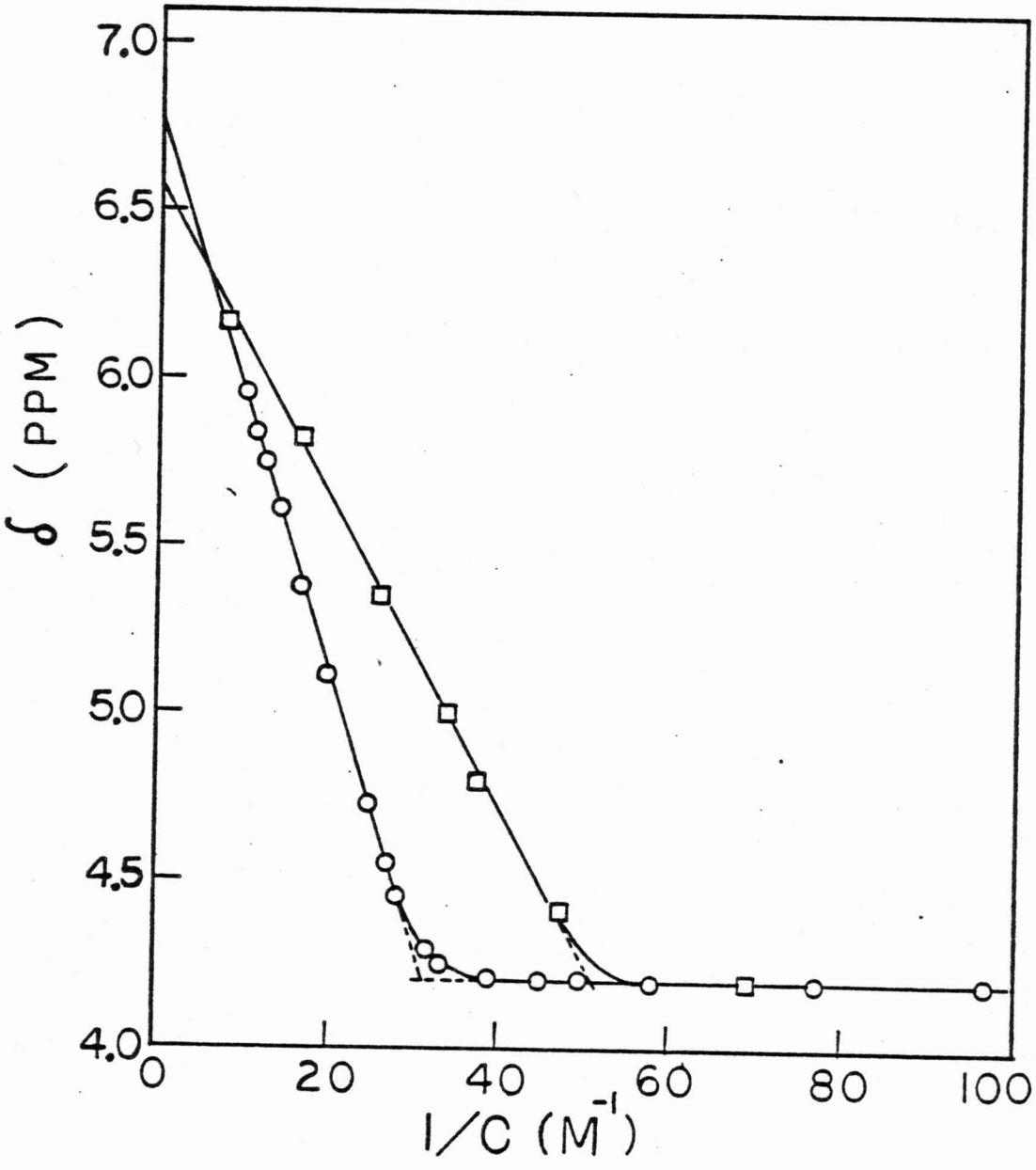
7.0
6.5
6.0
5.5
5.0
4.5
4.0
δ (PPM)
0
20
40
60
80
100
1/C (M⁻¹)

and TFPE 2HCl are shown in Figure 6.4. The CMC values of SPFO obtained from the reciprocal plots are reported in Table 6.1.

When two straight lines are extrapolated from the high and low concentration regions in the TFPO HCl and TFPE 2HCl curves, the intersections are at 0.0246 and 0.0125M for TFPO HCl in water and 0.05N sodium chloride solution, respectively,and 0.043M for TFPE 2HCl in water. These values are in good agreement with the reported CMC values of similar phenothiazine derivatives obtained by proton NMR measurements (171,197). However, a plot of the chemical shifts against the concentration of the surfactant, as shown in Figure 6.5, shows that a substantial change of chemical shift has already occurred at concentrations well below the "apparent CMC" obtained from the reciprocal plots. The difference between the micelle forming surfactant SPFO and the phenothiazine derivatives is apparent in Figure 6.5. There is no appreciable change in chemical shift in SPFO until the CMC is reached. A sharp change in chemical shift occurs in a relatively narrow concentration range corresponding to the CMC of SPFO. The lacking of such a change in TFPO HCl and TFPE 2HCl suggests that a different pattern of aggregation is involved in these phenothiazine derivatives.

Figure 6.4. Plots of chemical shift versus the reciprocal concentration of TFPO HCl in water (O), TFPO HCl in 0.05N sodium chloride solution (●), and TFPE 2HCl in water (■).

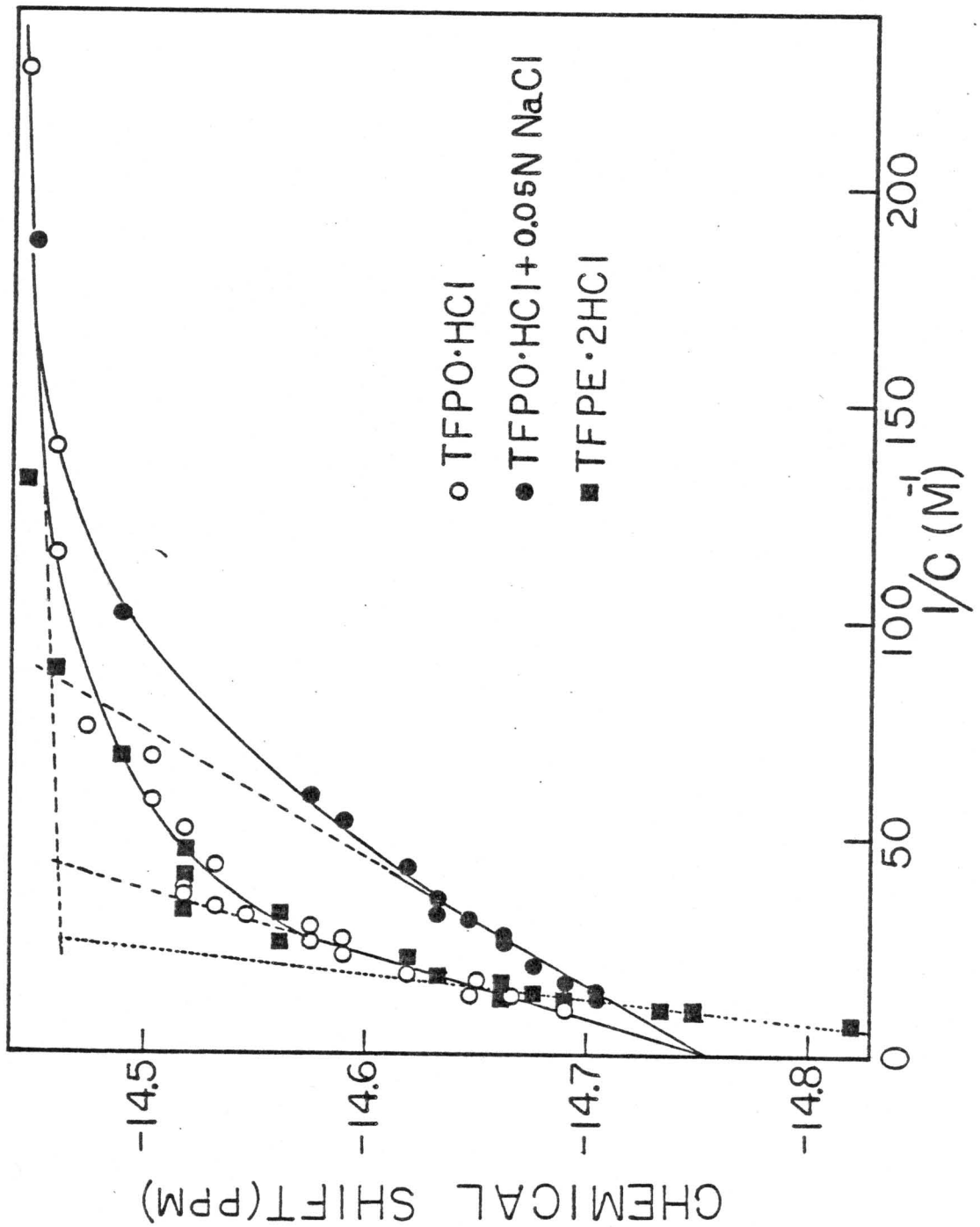
CHEMICAL SHIFT(PPM)
-14.5
-14.6
-14.7
-14.8
0
50
100
150
200
1/C (M⁻¹)
○ TFPO·HCl
● TFPO·HCl+0.05N NaCl
■ TFPE·2HCl

Table 6.1. CMC Values of Sodium Perfluoro-n-octanoate at 33°C (mole/liter)

Solvent	from δ vs C^{-1}	from $C\delta$ vs C
water	0.0322(0.031)*	0.0328
0.0152N NaCl	0.0272	0.0289
0.0310N NaCl	0.0236	0.0249
0.0547N NaCl	0.0194	0.0205

* From reference (108), CMC determined at 35°C.

Figure 6.5. Plots of chemical shift versus the concentration of SPFO in water (Δ), TFPO HCl in water (O), TFPO HCl in 0.05N sodium chloride solution (●), and TFPE 2HCl in water (■).

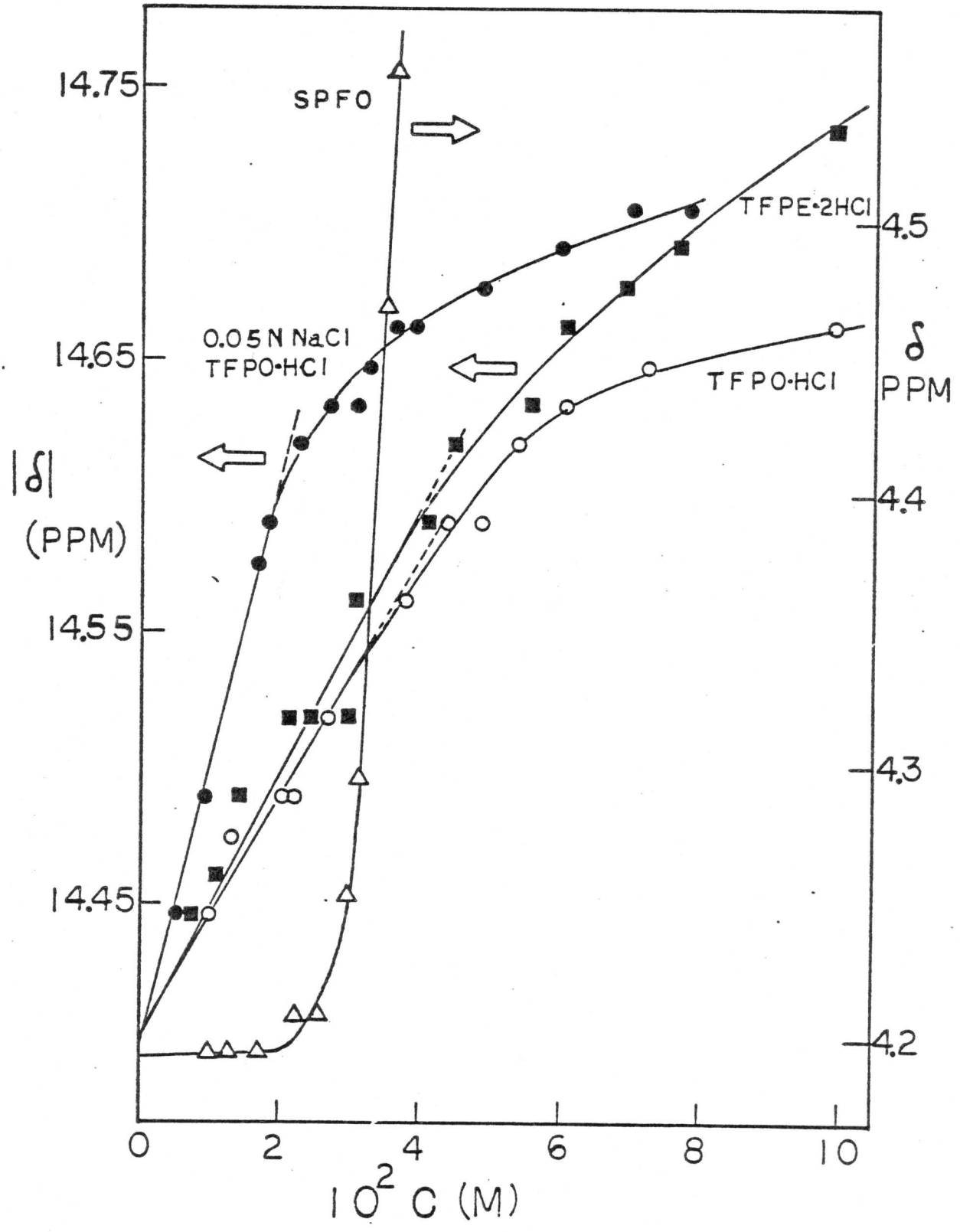
14.75
14.65
14.55
14.45
|δ| (PPM)
SPFO
TFPE·2HCl
0.05 N NaCl
TFPO·HCl
TFPO·HCl
4.5
4.4
4.3
4.2
δ PPM
0
2
4
6
8
10
10² C (M)

6.4.1. NMR Data Treatment

In order to eliminate the ambiguity of the reciprocal plot and to further examine the significance of the apparent CMC in the phenothiazine derivatives, Equation 6-1 is rearranged into the following form:

$$C\delta = (\delta_1 - \delta_n)[b_1] + \delta_n C \ . \qquad [6\text{-}1a]$$

For a system exhibiting simple micelle formation, when $C\delta$ is plotted against the total equivalent surfactant concentration, C, Equation 6-1a predicts two straight lines with slopes of δ_1 and δ_n intercepting at the CMC. Such properties are a consequence of the monomer concentration being equal to the total equivalent surfactant concentration below the CMC and becoming approximately constant above the CMC. The following information may be obtained from this type of plot: (i) deviation from linearity at concentrations below the expected CMC indicates the occurrence of an early aggregation, (ii) the constancy of chemical shift in the aggregated form, δ_n, can be examined from the linearity of the data at concentrations above the CMC, (iii) the sharpness of the transition at the CMC reflects the degree of aggregation and also the cooperativity of association.

The data obtained from SPFO in solutions of different salt concentrations are presented in Figure 6.6 as $C\delta$ versus C plot. The micelle forming property of SPFO is clearly indicated by the presence of two linear regions and

Figure 6.6. Plots of C δ versus the concentration of SPFO in water (●), 0.0152N sodium chloride (O), 0.0310N sodium chloride (△), and 0.0547N sodium chloride (□) solutions.

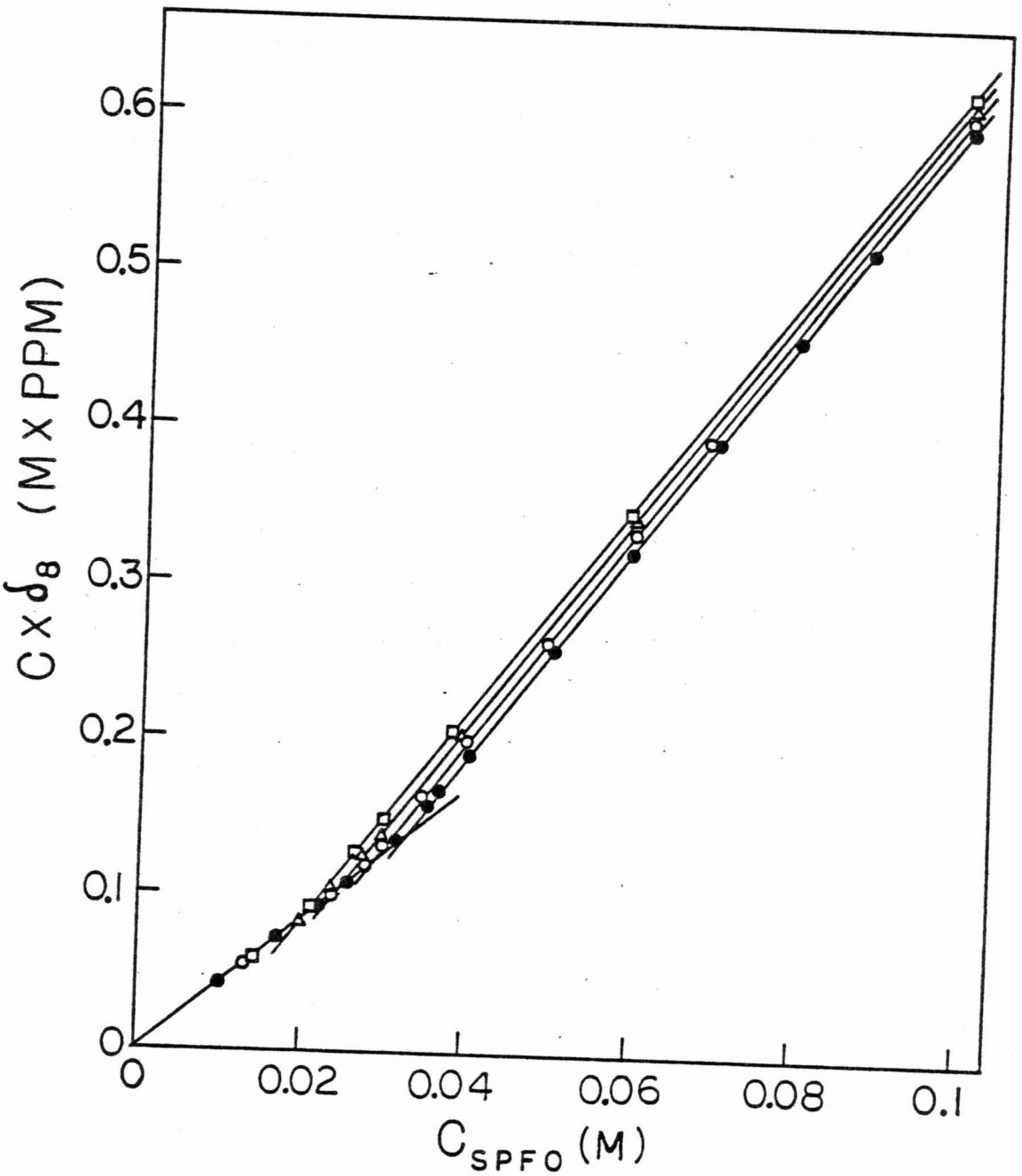
0.6
0.5
0.4
0.3
0.2
0.1
0
0
0.02
0.04
0.06
0.08
0.1
C x δ8 (M x PPM)
CSPFO (M)

a sharp transition at the CMC. Chemical shifts at concentrations below the CMC are not affected by the presence of salt. At concentrations above the CMC, parallel lines are obtained indicating that the chemical shift in the micellar state is constant within experimental error and also not affected by the presence of added salt. The CMC values obtained from Figure 6.6 by linear regression are reported in Table 6.1. A somewhat higher CMC,by 2 to 6%, has been observed in the C δ versus C plots than that obtained directly from the curves of δ versus C^{-1}. The logarithm of the CMC is linearly related to the logarithm of the total sodium ion concentration at the CMC, as shown in Figure 6.7. A slope of-0.56 is obtained from the straight line as compared to an estimated value of-0.53 from the CMC data reported for potassium perfluoro-n-octanoate (188).

The change of chemical shift in TFPO HCl is relatively small and no appreciable curvature is seen in the C δ versus C plot, see Figure 6.8. A plot of C($\delta - \delta_1$) versus C curve was then constructed to magnify any change in the chemical shift as a function of concentration, where δ is the chemical shift at concentration C and δ_1 the extrapolated chemical shift at zero concentration from Figure 6.5. The data show a continuous increase beginning from very low concentration. If straight lines are forced through the data points at low and high concentration regions, an apparent CMC can always

Figure 6.7. Plot of logarithm CMC versus logarithm of sodium ion concentration at the CMC of SPFO determined from Figure 6.6.

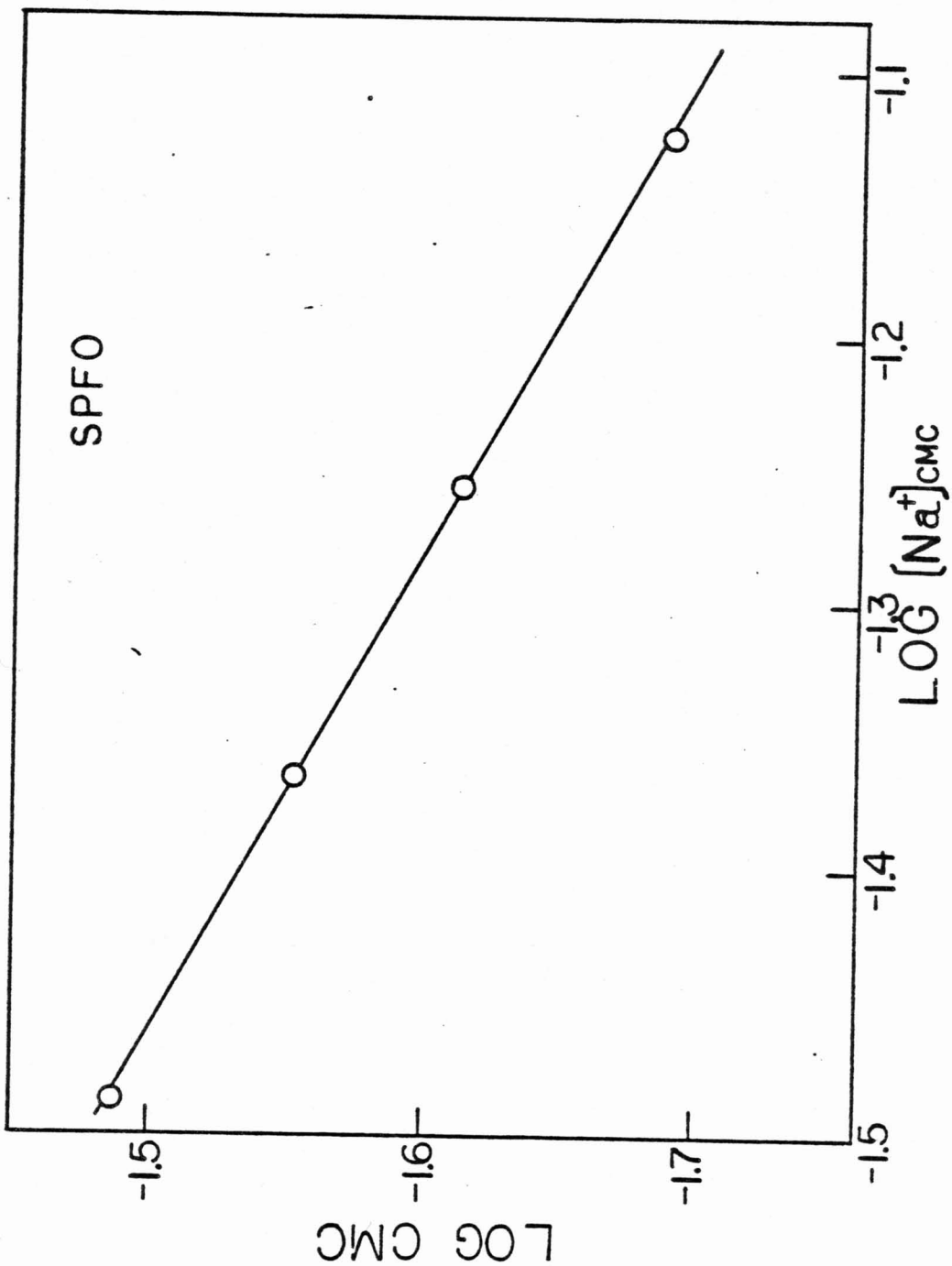
SPF0
LOG CMC
-1.5
-1.6
-1.7
-1.5
-1.4
-1.3
-1.2
-1.1
LOG [Na+]CMC

Figure 6.8. Plots of C δ versus the concentration of TFPO HCl in water (●) and C($\delta - \delta_1$) versus the concentration of TFPO HCl in water (O).

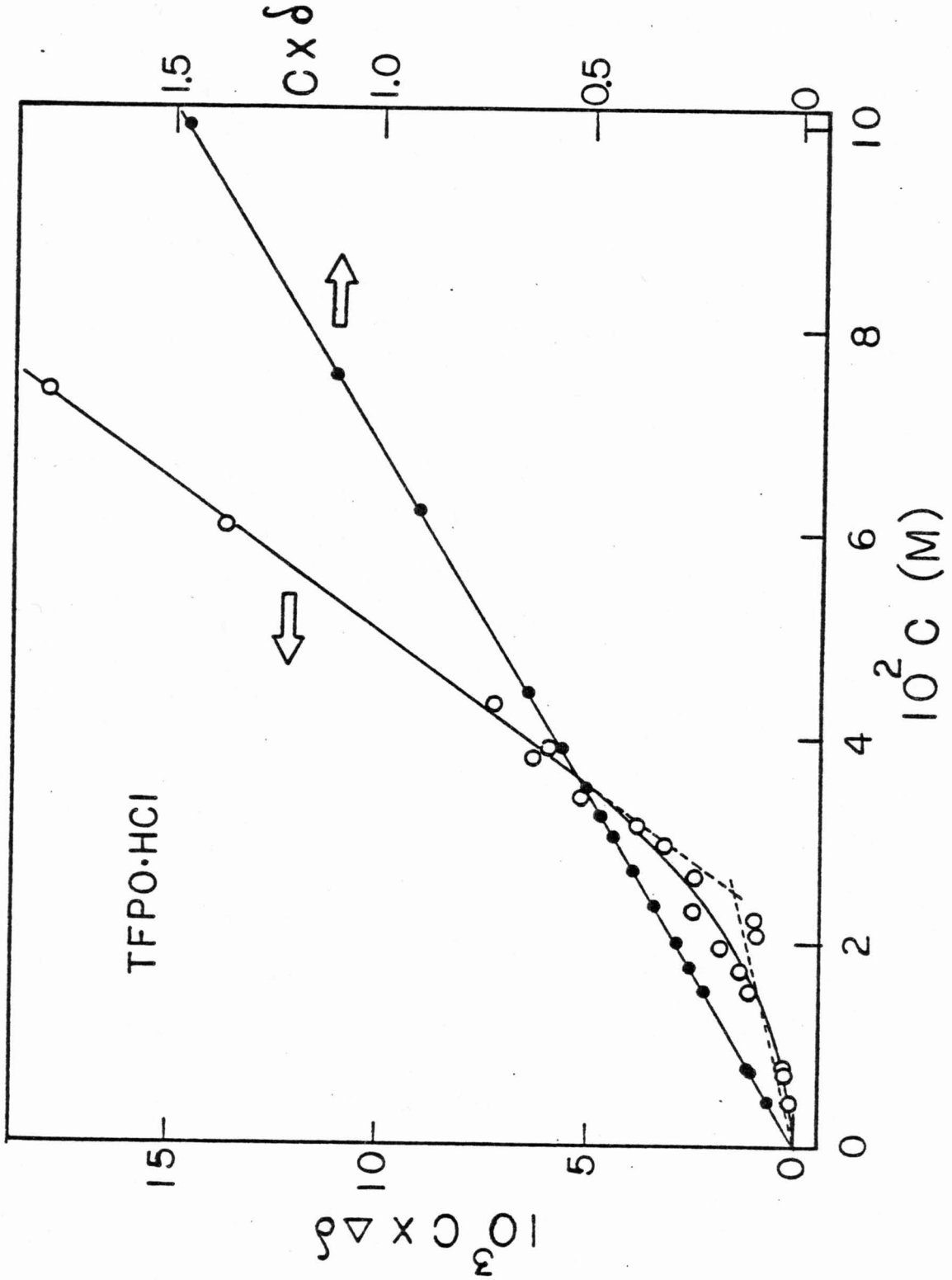
TFPO·HCl
$10^3 C \times \Delta\delta$
$C \times \delta$
$10^2 C$ (M)
0
5
10
15
0.5
1.0
1.5
2
4
6
8
10

be obtained even though it may not have much physical significance. Curves similar to the one showing in Figure 6.8 have been reported in the light scattering studies of several other phenothiazine derivatives in which the turbidity is plotted against the concentration of phenothiazine (195).

The pattern of surfactant self-association, as discussed in Chapter 1 (cf. Sections 1.3 and 1.4), can be qualitatively examined by constructing a differential curve, in which the gradient of a suitable solution property is plotted against the total surfactant concentration. The differential curves of the chemical shifts measured in SPFO and TFPO HCl are shown in Figure 6.9 as $d(C\delta)/dC$ versus C and $\Delta(C\delta)/\Delta C$ versus $\bar{C}$, respectively, where $\Delta(C\delta)$ and ΔC are the differences between two adjacent experimental points, and $\bar{C}$ the mean concentration of these two adjacent points. Only the data of TFPO HCl in 0.05N sodium chloride solutions are plotted in Figure 6.9, because of an enhanced aggregation is expected in the presence of salt. Nevertheless, the data of TFPO HCl are distinctively different from the micelle forming surfactant SPFO. The differential data of SPFO do not show significant change at concentrations below the CMC. A sharp increase occurs at the concentration range corresponding to the CMC and followed by a rapid levelling off to another approximately constant value. The middle point of the transition corresponds to the CMC observed from the $C\delta$

Figure 6.9. Differential plots of $d(C\delta)/dC$ versus the concentration of TFPO HCl in 0.05N sodium chloride solution (O) and $\Delta(C\delta)/\Delta C$ versus the mean concentration of SPFO in water (□).

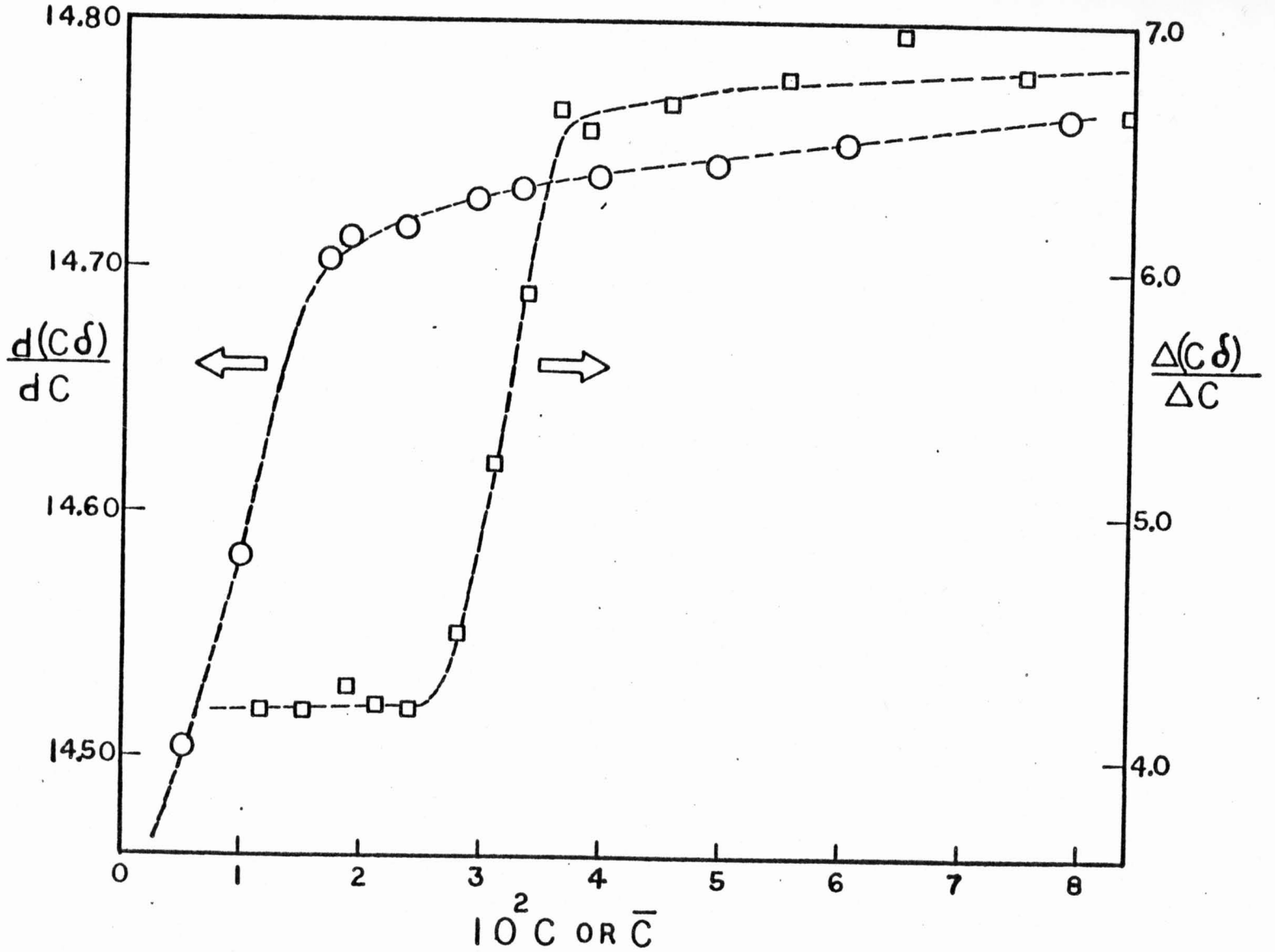
14.80
14.70
14.60
14.50
7.0
6.0
5.0
4.0
d(Cδ)/dC
Δ(Cδ)/ΔC
0
1
2
3
4
5
6
7
8
10² C OR C̄

versus C plot. TFPO HCl , on the other hand, does not show any transition at the apparent CMC observed previously. The $d(C\delta)/dC$ increases continuously from the lowest concentration up to and beyond the apparent CMC at 0.125M. The differential curve of TFPO HCl is qualitatively similar to the curve of either a continuous stepwise association without cooperativity or a dimer or trimer formation as shown in Figure 1.1.

For further analysis, an assumption of the same chemical shift for all the aggregated species from dimer up to n-mer is made and the concentration of the monomer at any concentration C is given by

$$[b_1] = C \left(\frac{\delta_n - \delta}{\delta_n - \delta_1} \right) . \qquad [6\text{-}2]$$

Figure 6.10 shows the concentrations of monomers of SPFO and TFPO HCl calculated from Equation 6-2. In systems exhibiting micelle formation, there is no significant aggregation below the CMC, and the slope of a plot of $[b_1]$ versus C is unity. Above the CMC, the monomer concentration changes very slightly or remains practically unchanged. The surfactant SPFO clearly shows the typical micelle forming behavior. In constrast, the monomer concentrations of TFPO HCl start to deviate from the line of unit slope at very low concentrations and continuously to increase appreciably beyond the apparent CMC region. The caluculated data at the

Figure 6.10. Plots of monomer concentration versus the total concentration of SPFO (□) and TFPO HCl (O) in water. The monomer concentrations were calculated from Equation 6-2 by using δ_l=4.195, δ_n=6.770 for SPFO and δ_l=14.400 , δ_n=14.760 for TFPO HCl.

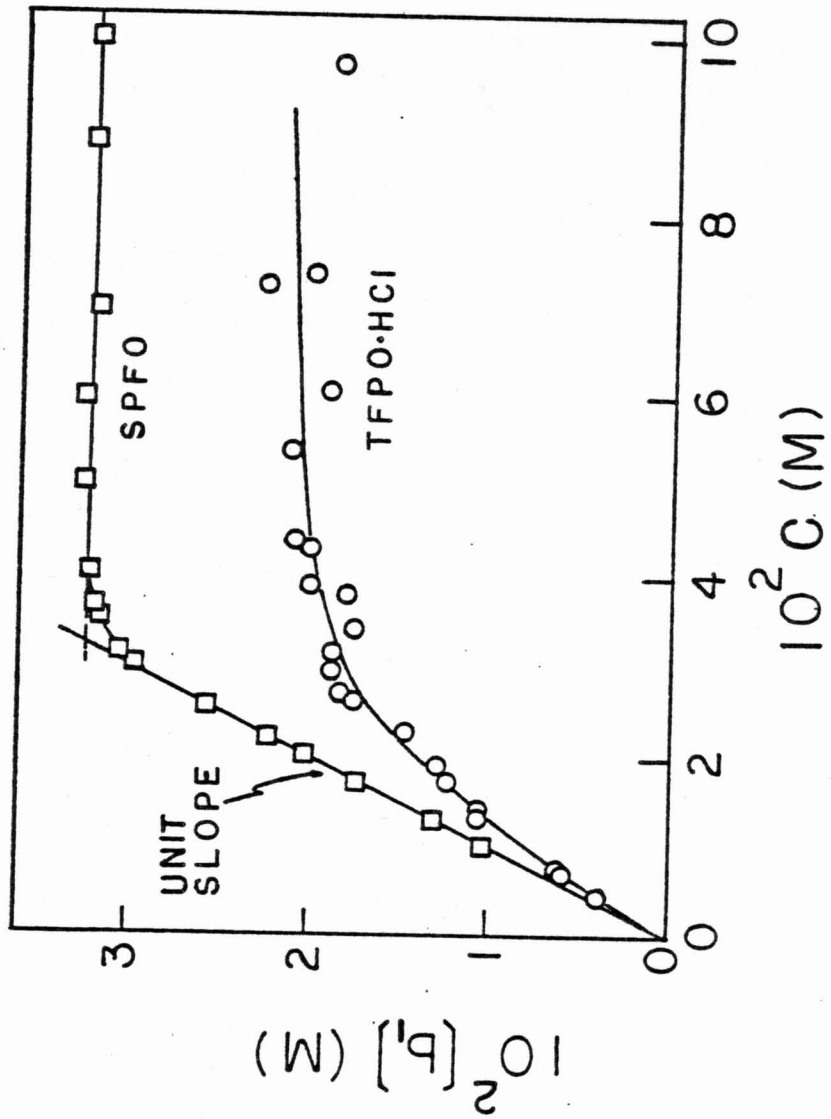
SPFO
TFPO·HCl
UNIT SLOPE
$10^2[b_1]$ (M)
10^2 C (M)
0
1
2
3
0
2
4
6
8
10

highest concentrations are not very reliable because of small differences between δ and δ_n in Equation 6-2. The fraction of surfactant present as monomer has also been calculated and is shown in Figure 6.11. The difference in the monomer fraction between TFPO HCl and SPFO is very pronounced at low concentrations. If a classical model of micelle formation, assuming no aggregation below the apparent CMC, is employed for the estimation of the monomer concentration of TFPO HCl, an error of 20 to 30% can easily be introduced. This monomer fraction is believed to have considerable importance to pharmacological activity and drug transport (201-203,25). It should, however, be noted that the chemical shifts of aggregated fluorophenothiazines may not remain constant as the degree of association changes. It is more likely that the chemical shift increases as the aggregation number increases, at least for the smaller aggregates, as the environment surrounding the trifluoromethyl group changes with the degree of aggregation. If this is the case, the true concentration of monomer at each surfactant concentration will be lower than that calculated by assuming a single value of chemical shift for the aggregated species in the dilute region.

The molecular structure of several phenothiazine tranquilizers have been shown by x-ray diffraction (199,204) to be of a nonplanar, butterfly-shaped configuration with a

Figure 6.11 Plots of monomer fraction versus the total concentration of SPFO (□) and TFPO HCl (○).

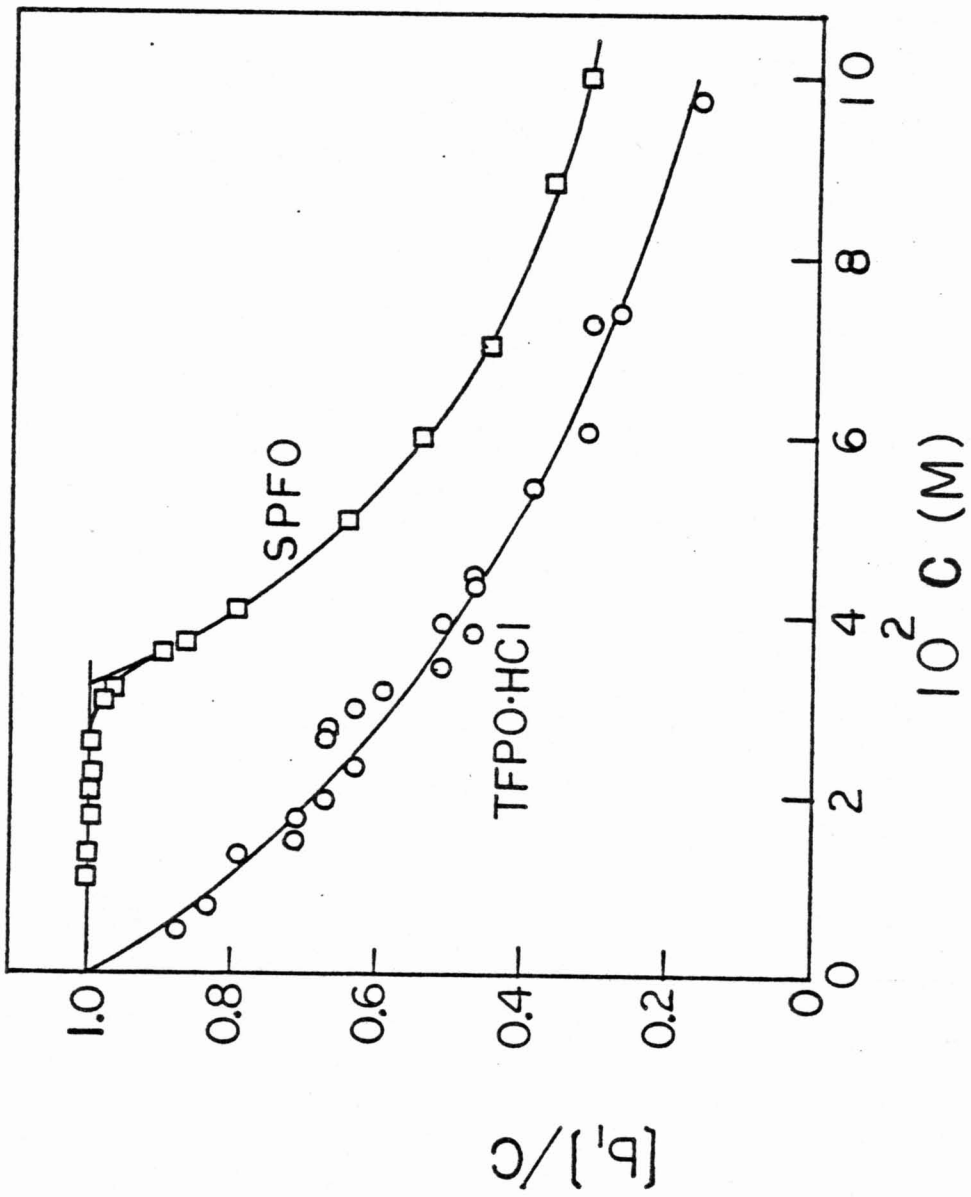
SPFO
TFPO·HCl
1.0
0.8
0.6
0.4
0.2
0
2
4
6
8
10
10^2 C (M)
$[b_i]/C$

dihedral angle of approximately 130° along the sulfur and nitrogen axis in the central ring. Theoretical calculations of similar compounds indicate that the bulky alkylamino side chain creats an energy barrier for the inversion of the central ring system (205). These molecules are, therefore, likely to retain their rigid configuration in solution. A stacking structure with back-to-face and alternating location of the polar amino or piperazine groups on opposite sides of the ring system,as suggested by Florence and Parfitt (171) and Mukerjee (57,62), is likely to be the mode of association. The NMR data presented are consistent with this type of aggregate.

6.5. Conclusion

Fluorine nuclear magnetic resonances of SPFO and two trifluorophenothiazine derivatives, TFPO HCl and TFPE 2HCl, have been studied. The chemical shifts of ^{19}F NMR of the micelle forming surfactant, SPFO, show evidence of a sharp transition at the critical micellization concentration region, as would be expected for a process with a high degree of cooperativity in self-association. TFPO HCl and TFPE 2HCl, on the other hand, do not show such sharp transition at the reported CMC regions. The data indicate that the self-association of these two drugs is not consistent with the typical cooperative aggregation of detergents. They

are more in agreement with a pattern of stacking interactions as suggested by their structures. The apparent CMC values from plots of the chemical shifts against the reciprocal concentration may not have any significance as regard to the nature of the aggregation in TFPO HCl and TFPE 2HCl. A plot of $d(C\delta)/dC$ versus C is suggested for testing the applicability of a micellar model and for the qualitative identification of the pattern of association, particularly with respect to cooperative processes.

7. MIXING PROPERTIES OF FLUOROCARBON AND HYDROCARBON SURFACTANTS

7.1. Background

Formation of mixed micelles may be regarded as a special case of solubilization in which the "solubilizates" are also surfactants and capable of forming micelles by themselves. Generally, hydrocarbon surfactants are miscible; they form mixed micelles of various compositions depending on the concentrations of the individual components in the solution. Since the micellar core of long chain surfactants is usually considered to be liquid-like (cf 1.6), the formation of mixed micelles of surfactants carrying similar polar head-groups but different hydrophobic chains may be treated in terms of the mixing of liquids consisting of the hydrophobic chains (140,141). It has been shown that the mixing of hydrocarbon moieties of homologous long chain surfactants is nearly ideal (140,142), and the CMC values of their binary mixtures fall within the range of the values of the individual pure components (139). CMC of mixture of ionic and nonionic polyoxyethylene type surfactants has been found to exhibit an apparent negative deviation from ideal mixing (142,143). This deviation is believed to be mainly due to the interactions between the hydrophilic polyoxyethylene chains and the ionic head groups of the surfactants (143).

Recently, Mukerjee and Mysels (109) pointed out that the well known, but often neglected, nonideal mixing behavior of hydrocarbon and fluorocarbon compounds may also exist in micellar systems. From available CMC data, they have found that, although the perfluoroalkyl surfactants are more hydrophobic than the hydrocarbon ones containing the same number of carbon atoms, partially fluorinated surfactants exhibit considerably higher CMC values than the hydrocarbon surfactants. By analyzing the available surface tension data and CMC values of sodium dodecyl sulfate and perfluoro-n-octanoic acid mixtures, they have also bound a strong mutual phobicity between these two types of surfactants in forming mixed micelles. An observation reported by Tiddy and Wheeler, who found the solubilization of octanol by ammonium perfluorooctanoate micelles is about four times less than that in sodium octanoate (144), is in accord with the expected non-ideality effects (109). Anacker et al. have also observed that the solubilizing power of ω-trifluorododecyltrimethylammonium bromide micelle for a hydrophobic dye, orange-OT, is only about one half of dodecyltrimethylammonium bromide (145). Interfacial tensions of partially fluorinated surfactants at heptane/water interface have been reported recently by Thoai (146). The lowering of the interfacial tension at low concentrations is greater for the partially fluorinated surfactants than their hydrocarbon homologues, but the limiting value of the interfacial tension,

in contrast to their low air/water interfacial tension (147, 148), is much higher. This fact is attributed to the hydrophobic and lipophobic nature of the fluorocarbon moiety which leads to a low packing density of the adsorbed surfactants at the oil-water interface and,therefore, to a high limiting value of the interfacial tension. The mutual phobicity between fluorocarbons and hydrocarbons has also been observed in contact angle measurements of fluorocarbon surfactant solutions on several non-fluorine containing low energy solids (149).

The aforementioned observations suggest that the non-ideality of interaction between hydrocarbon and fluorocarbon moieties may be widespread and may significantly affect the properties of (i) carbon-fluorine compounds in biological systems (150), (ii) fluorine-labeled molecules for probing the hydrophobic environments of proteins, enzymes, lipid membranes, or micellar systems (151-158),and (iii) surfactants at interfaces, such as in wetting, adsorption, or emulsification phenomena, when fluorocarbon-hydrocarbon interactions are involved (149,159).

Muller and his coworkers (105-108) used fluorine NMR chemical shifts to study the local environment of fluorine atoms in micelles of sodium perfluoro-n-octanoate and several ω-trifluoroalkyl surfactants. In order to characterize this environment, they developed a parameter, Z, defined

as

$$Z = \frac{\delta_m - \delta_w}{\delta_o - \delta_w}$$

where δ is the chemical shift and the subscripts m,o,and w indicate micelle, organic solvent, and water, respectively. If no water is present in the vicinity of the fluorocarbon group in the micelle, $\delta_m = \delta_o$ and Z = 1. In micelles of the ω-triflurinated surfactants, C_{10} and C_{12} carboxylates (105), C_{12} sodium sulfate (106), and a C_8 nonionic (107) system, they found the Z values close to 0.5 in each case indicating a semi-aqueous environment of the terminal CF_3 group. Based on the implicit assumption that this group randomly sampled the core of the micelle, they concluded that water molecules penetrated into the interior of the micelle (105). This conclusion is in opposition to all available evidence about the hydrophobic nature of the micellar core (cf 1.6). It is also important to note that the Z values of the terminal CF_3 group in micelles of perfluorosurfactants, i.e., 0.82 for C_4 carboxylic acid (109) and 0.84 for C_8 sodium carboxylate, are considerably higher than that of the partially fluorinated ω-trifluorosurfactants (108). This result suggests that the CF_3 terminal group of the partially fluorinated surfactants may be present at the micellar surface more often than expected from random mixing because of the mutual phobic nature of the fluoro and hydrocarbon moieties (109).

7.2. Scope and Aims

The mutual solubility between hydrocarbon and fluorocarbon compounds in binary mixtures has been investigated extensively, and summarized by Hildebrand, Prausnitz, and Scott (160). The regular solution theory (161-164) is useful for qualitative explanation of certain unusually large positive deviation from ideal mixing in liquids.

The only quantitative study on the mixing properties between long chain hydrocarbon and fluorocarbon surfactants was reported by Klevens and Raison (165) on the surface tension measurements of sodium dodecyl sulfate and perfluorooctanoic acid mixtures. This study was not focused on the nonideal mixing behavior of these two surfactants. Although they noted the peculiar character of their results, they did not provide any explanation. In addition, the sodium dodecyl sulfate sample investigated by them contained minor impurities which prevented precise determination of the CMC values from their surface tension data.

In the present studies, the mixing properties of a fully fluorinated surfactant, sodium perfluoro-n-octanoate (SPFO), with hydrocarbon surfactants, sodium dodecyl sulfate (SDS), sodium decyl sulfate (SDeS), and sodium laurate (SL), have been investigated by electrical conductivity and ^{19}F NMR chemical shift measurements. The measured CMC values of

mixed micelles are compared with theoretical values calculated from ideal mixing and complete demixing cases. The regular solution theory for nonideal mixtures is also applied to estimate the magnitude of the non-ideality of mixing between the fluorocarbon and hydrocarbon surfactants.

7.3. Results and Discussion

The CMC values of SPFO and mixtures of SPFO with SDS, SDeS, or SL in the presence of 0.001N sodium hydroxide or in water adjusted to pH about 8.6 by the addition of sodium hydroxide solution were obtained from plots of equivalent conductance against the square root of the concentration, in equivalent/liter, a procedure particularly useful for mixtures of ionic surfactants (139). Typical plots of the CMC determinations are shown in Figure 7.1 for SPFO and SDS mixtures. Values of the CMC obtained in this manner are listed in Table 7.1. Figures 7.2 and 7.3 show the CMC curves of the binary mixtures of SPFO with various mole fraction of hydrocarbon surfactants, SL, SDeS, and SDS.

7.3.1. Ideal Mixing

The interactions of hydrophobic chains in mixed micelles may be treated by solution theories of liquid mixtures (140, 141). For an ideal binary liquid mixture, the ratio of actual vapor pressure, P, to that of the saturated vapor pressure over the pure liquid, P_o, is equal to the mole fraction of

Figure 7.1. Equivalent conductance of SPFO and SDS mixtures; SDS only (▲), 0.5 mole fraction SDS (◐), 0.3 mole fraction SDS (■), 0.2 mole fraction SDS (O), 0.1 mole fraction SDS (●), 0.05 mole fraction SDS (□), SPFO only (△).

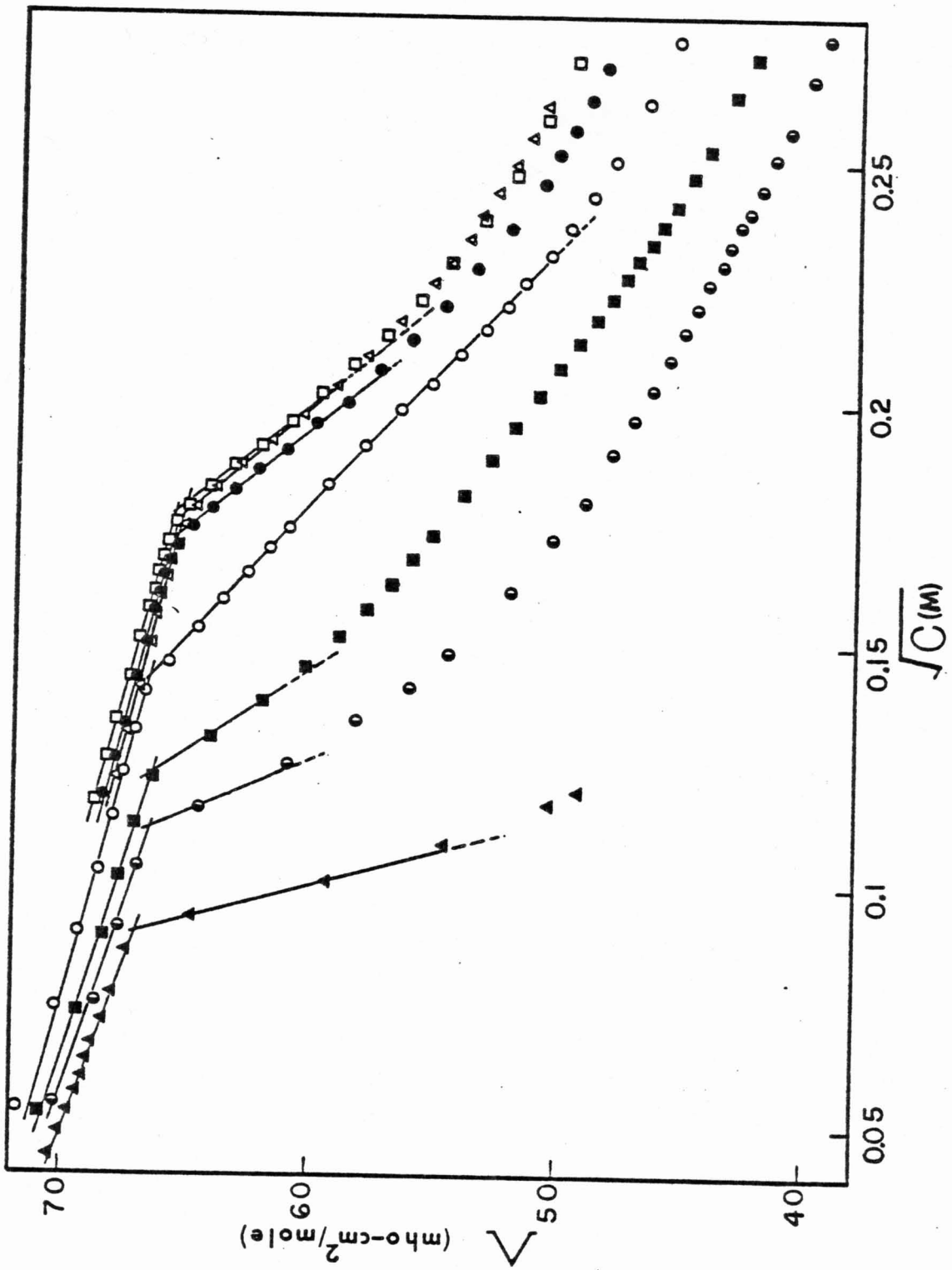
70
60
50
40
Λ (mho-cm²/mole)
0.05
0.1
0.15
0.2
0.25
√C (M)

Table 7.1. CMC values of mixed micelles of SPFO and hydrocarbon surfactants ($x10^3$ M)

mole fraction of SL	CMC[a]	mole fraction of SDeS	CMC[a]	mole fraction of SDS	CMC[b]
1.00	25.6	1.00	31.5	1.00	8.1
0.83	27.8	0.90	32.7	0.50	12.3
0.66	31.9	0.75	36.2	0.36	14.9
0.50	35.4	0.50	40.6	0.20	20.9
0.42	37.4	0.25	35.4	0.10	29.9
0.33	37.5	0	31.1	0.05	31.0
0.16	33.4			0	31.1
0	31.1				

[a] Solutions contained 0.001N sodium hydroxide.

[b] Solutions were adjusted to pH 8.4 with sodium hydroxide.

Figure 7.2. CMC data of mixtures of SPFO-SDeS (Δ) and SPFO-SL (O) at 25°C. Dashed lines show expected values on ideal mixing of the micelles. Curves 1,2,3, and 4 are the expected CMC values of complete demixing of micelles. Curves 2,3, and 4 calculated for K_i=1.645. Curve 1 calculated for K_i=1.56.

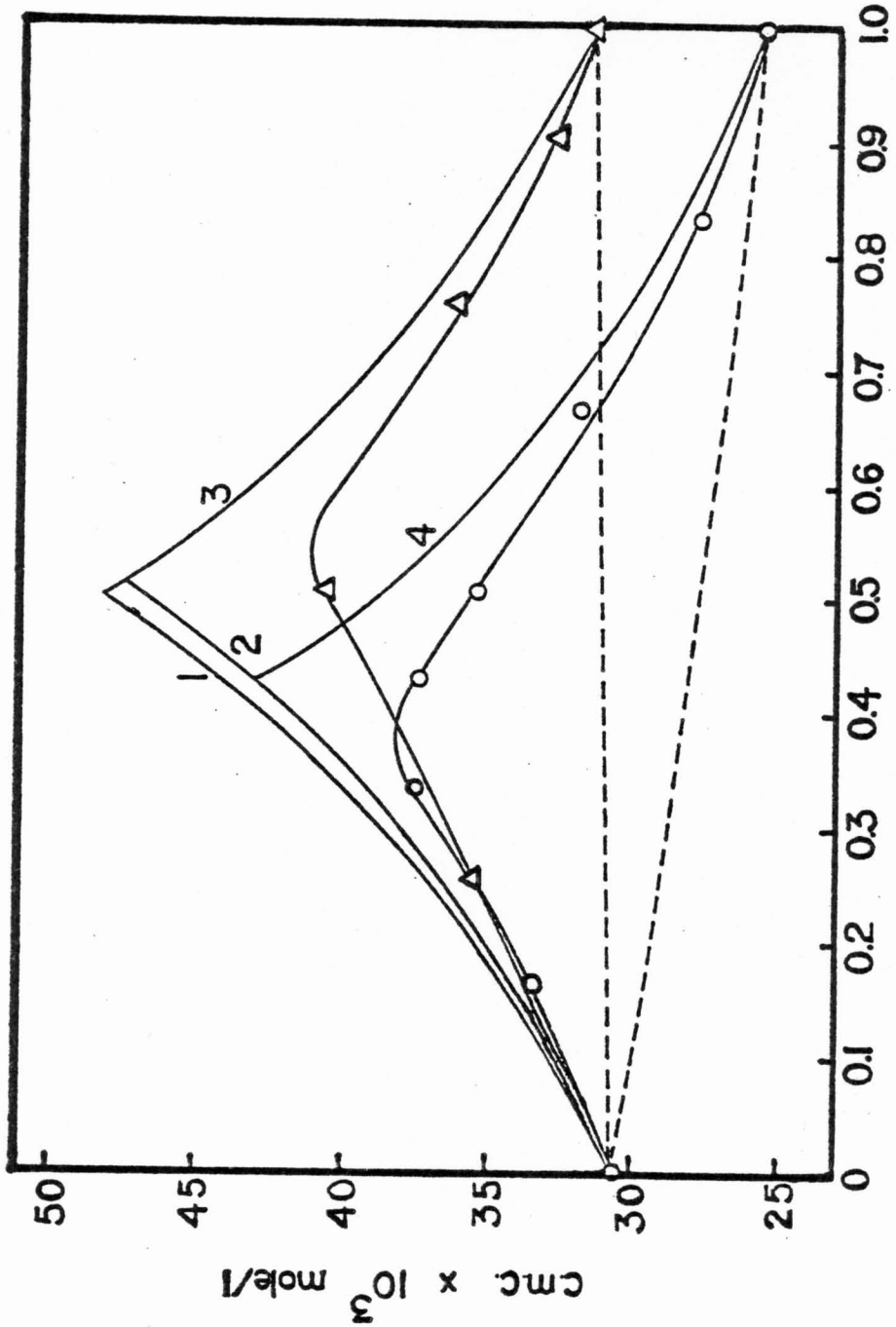
cmc x 10³ mole/l
50
45
40
35
30
25
0
0.1
0.2
0.3
0.4
0.5
0.6
0.7
0.8
0.9
1.0
Mole Fraction of Hydrocarbon Surfactant
1
2
3
4

Figure 7.3. Observed CMC values of mixtures of SPFO and SDS (O) at 25°C and calculated CMC values of ideal mixing (curve 1), complete demixing (curve 4), and nonideal mixing of micelles according to regular solution theory assuming $\omega/RT = 2.0$ (curve 2) and $\omega/RT = 3.0$ (curve 3). Dashed lines are expected micellar composition of ideal mixing (curve 5) and nonideal mixing of micelles according to regular solution theory, assuming $\omega/RT = 3.0$ (curve 6). Dotted lines show the corresponding compositions of monomer and micelle.

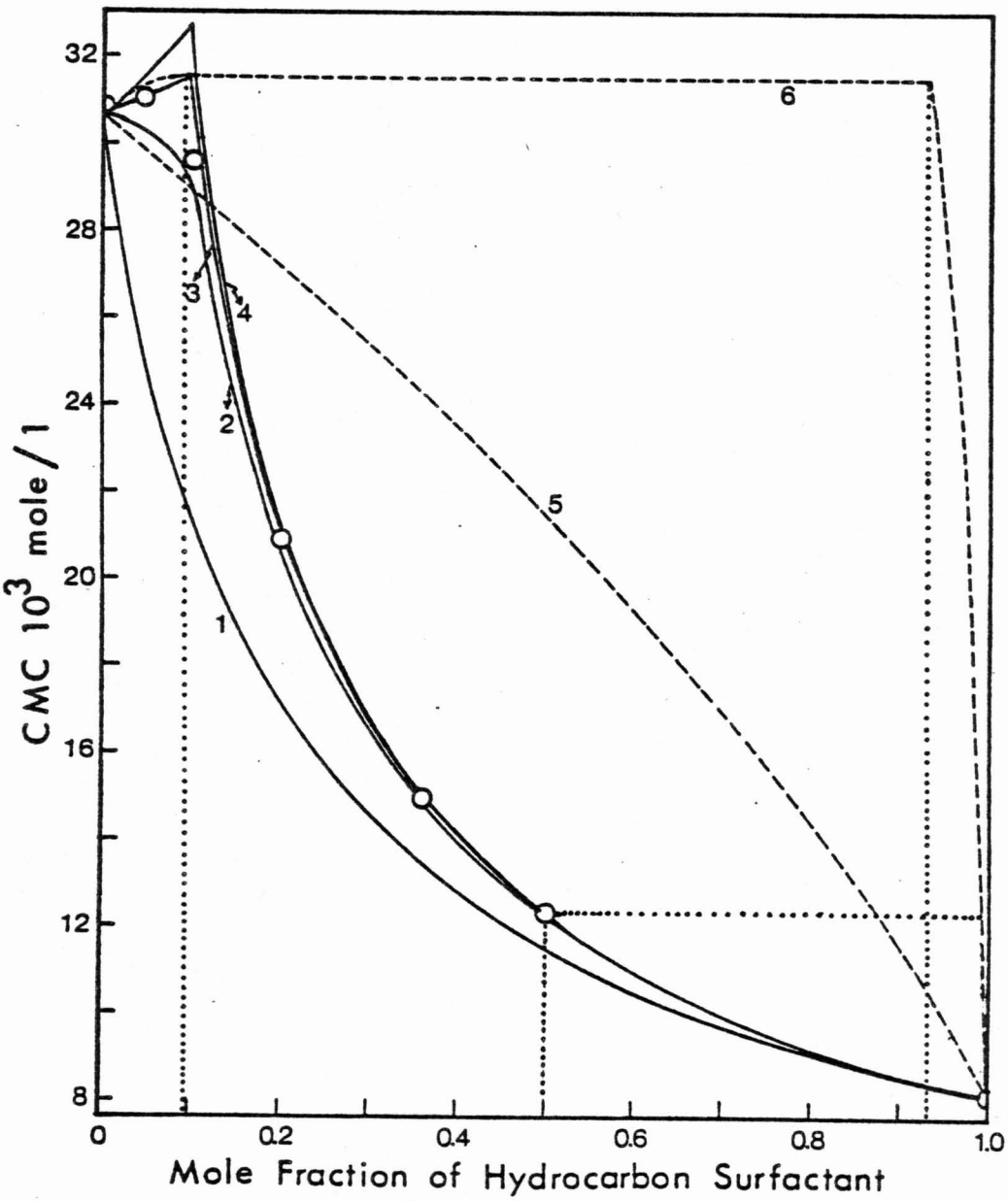
32
28
24
20
16
12
8
CMC 10^3 mole / l
0
0.2
0.4
0.6
0.8
1.0
Mole Fraction of Hydrocarbon Surfactant
1
2
3
4
5
6

the liquid in the mixture. By applying the same principle for the ideal mixing of surfactants, the ratio of the actual monomeric concentration of surfactant "i" at the CMC of a mixed system, C_{im}, to the concentration of the CMC of pure system, C_{ig}, (in the presence of the same counterion concentration) is equal to the mole fraction Y_i in the micelle:

$$\frac{C_{im}}{C_{ig}} = Y_i \quad . \qquad [7\text{-}1]$$

The observed CMC of the mixed system C_m is equal to the sum of the individual monomeric concentrations at this point and also equal to the total counter-ion concentration,g, (for 1:1 electrolytes). Thus, for a binary mixture of components 1 and 2,

$$C_m = C_{1m} + C_{2m} = g \quad . \qquad [7\text{-}2]$$

The mole fraction of component "i" in the monomeric form, X_i, is defined by

$$X_i = \frac{C_{im}}{C_m} \quad . \qquad [7\text{-}3]$$

The CMC of the ionic surfactant, C_{ig}, is related to the total counter-ion concentration by the well known empirical equation

$$C_{ig} = \frac{C_{ia}^{K_i}}{g^{(K_i-1)}} \quad . \qquad [7\text{-}4]$$

where K_i is a constant, whose value depends on the nature of

the surfactant and the counterion, C_{ia}, is the CMC of the surfactant in the absence of added salt. After combining Equations 7-1 to 7-4 and eliminating C_{ig}, the following Equation is obtained

$$Y_i = X_i \left(\frac{C_m}{C_{ia}}\right)^{K_i} \quad . \qquad [7\text{-}5]$$

Using this Equation for a binary mixture, and noting that $Y_1+Y_2=1$, and $X_1+X_2=1$, Equation 7-5 can be rewritten for X_1 as

$$X_1 = \frac{1 - \left(\frac{C_m}{C_{2a}}\right)^{K_2}}{\left(\frac{C_m}{C_{1a}}\right)^{K_1} \left(\frac{C_m}{C_{2a}}\right)^{K_2}} \qquad [7\text{-}6]$$

It is, therefore, possible to calculate X_1 for any value of C_m from C_{1a}, C_{2a}, K_i, and K_2 which are usually experimentally obtainable. The composition of the micelle, Y_1 and Y_2, can be calculated from Equation 7-5 using the value of X_1. For SDeS micelle, a K_i value of 1.645 has been reported (285). A K_i value of 1.56 has been obtained from the CMC's of SPFO determined by ^{19}F NMR chemical shifts as reported in Chapter 6.

The expected values of mixed CMC's on the ideal mixing of micelles, according to Equation 7-6 and assuming

K_i of 1.56 for SPFO, are shown in Figures 7.2 and 7.3. The micellar compositions of SDS-SPFO system, caluclated from Equation 7-5, are also included in Figure 7.3. It has been found that the values of C_m and Y_i are not sensitive to minor variations of K_i. A 10% change in K_i causes approximately a 2% variation in Y_i and C_m in the SDS-SPFO system. Smaller effects are expected for the SDeS-SPFO and SL-SPFO systems because of the similar CMC values for the pure components. The mixing of carboxylate and sulfate head groups has relatively little effect on the CMC. This is evident from the measured CMC of an equimolar mixture of SL and SDeS, for which a CMC of 0.0294 M was obtained as compared to the value of 0.0282 M calculated from ideal mixing with K_i of 1.645 for both SL and SDeS. On the other hand, substantial deviations of the CMC values from ideal mixing are observed in all systems where fluorocarbon and hydrocarbon chains are mixed. The observed nonidealities are consistent with a positive deviation from Raoult's law observed in binary mixtures of hydrocarbon-fluorocarbon systems (160,163,164). Such nonideality effects are likely to lead to high activity coefficients of the individaul chains in the mixed micelles and, consequently, to a lower stability of the mixed micelles. If the nonideality effects are sufficiently intense, two kinds of micelles may form as a result of

phase separation.

7.3.2. Demixing Case

To access the intensity of such nonideality of mixing, the experimental data are first examined in terms of complete demixing of the micelles. If the surfactants are nonionic, the CMC-mole fraction diagram is composed of two curves corresponding to each of the two components given by Equation 7-7,

$$C_m = \frac{C_{ia}}{X_i} \qquad [7\text{-}7]$$

For ionic surfactants, however, the counterion of one component affects the CMC of the other through common-ion effect (136). According to Equation 7-4, the CMC of a completely demixed ionic system is given by

$$C_m = \frac{C_{ia}}{(X_i)^{1/K_i}} \quad . \qquad [7\text{-}8]$$

Figures 7.2 and 7.3 show curves of CMC's for the demixed case calculated from Equation 7-8 by the use of the same K_i value, 1.645, for SDeS, SDS, and SL. The calculated CMC's are not sensitive to small variations of K_i. In the case of SPFO, K_i values of 1.56 and 1.645 were both used in Figure 7.2 and only the former value was used in Figure 7.3. Both Figures 7.2 and 7.3 show that the experimental CMC

data are not too far from the calculated case of complete demixing indicating that the nonideality of mixing is indeed severe in these cases.

7.3.3. Partially Miscible Micelles

The intensity of nonideality of mixing exhibited by the CMC data shown in Figure 7.2 and Figure 7.3 suggests the possilibity of demixing micelles, i.e., the presence of two kinds of micelles coexisting in the solution. To investigate this possibility the conductance data of SDS-SPFO system are analyzed. The data are shown in Figure 7.4 as differential conductance, $10^3 \Delta K/\Delta C = 10^3(K_2-K_1)/(C_2-C_1)$ where K_2 and K_1 are the specific conductances at two adjacent concnetrations, C_2 and C_1, respectively, plotted against the mean concentration $\bar{C}=(C_2+C_1)/2$. $\Delta K/\Delta C$ is thus an average value of dK/dC over the concentration range C_2-C_1. The differential curve, as mentioned previously, (cf. Chapter 6 and Section 1.4.), is capable of indicating the relatively abrupt change in solution composition at the CMC (139). Curves 1 and 7 of Figure 7.4 represent the data for individual surfactants, SDS and SPFO, respectively. The $\Delta K/\Delta C$ shows an abrupt drop in the CMC region and then attains a nearly constant value. The $\Delta K/\Delta C$ of SPFO-SDS mixtures (Curves 2,3, and 4), in contrast to the solution of single surfactants, changes its character and becomes biphasic; it shows two inflection points before leveling off at high concentrations. The first drop corresponds to

Figure 7.4. Differential conductance versus the mean concentration of surfactant for mixtures of SPFO and SDS in pH 8.4 solutions, curve 1: SDS only, curve 2: 0.5 mole fraction SDS, curve 3: 0.35 mole fraction SDS, curve 4: 0.20 mole fraction SDS, curve 5: 0.10 mole fraction SDS, curve 6: 0.05 mole fraction SDS, curve 7: SPFO only.

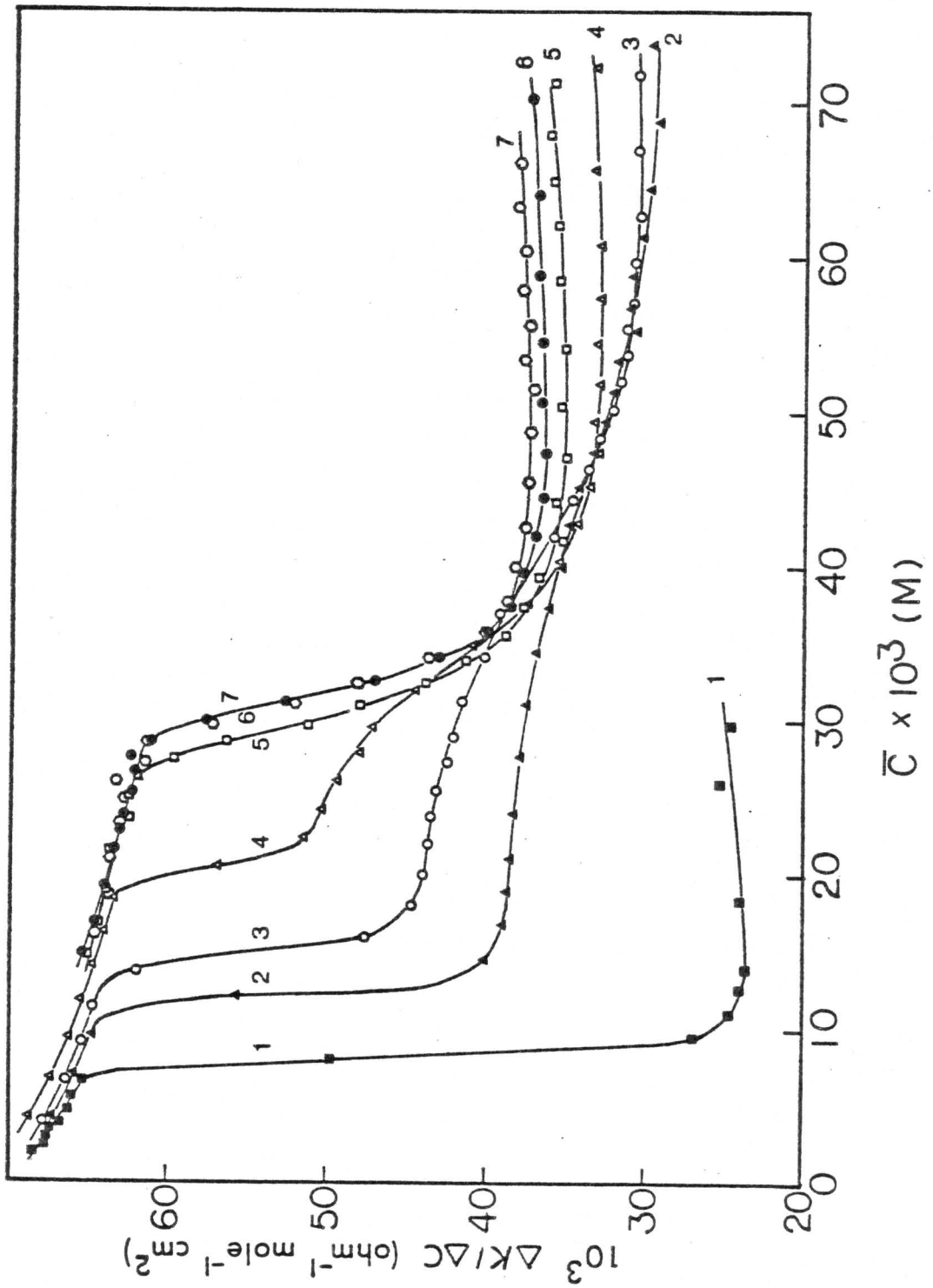
$10^3\ \Delta K/\Delta C$ (ohm^{-1} mole^{-1} cm^2)
$\bar{C} \times 10^3$ (M)
20
30
40
50
60
0
10
20
30
40
50
60
70
1
2
3
4
5
6
7
8

the onset of micelle formation i.e., the CMC. This biphasic character of conductance data is consistent with the explanation suggested by Mukerjee and Mysels for explaining some complex surface tension data of SDS and perfluoro-octanoic acid mixtures (109). They have proposed that the first micelles formed are composed primarily of the more hydrophobic SDS component. As the total concentration increases, the concentration of monomer as also the ratio of monomeric SPFO to SDS increase. At about the second inflection point, the activity of SPFO becomes sufficiently high to form micelles which are composed primarily of the SPFO component. At the highest concentrations, the two kinds of micelles coexist, one rich and the other poor in the fluorocarbon component.

The partial miscibility between SDS and SPFO is further substantiated by the ^{19}F NMR chemical shift data. The chimical shifts obtained from the mixture of SDS-SPFO are shown in Figure 7.5 as $\Delta(C\delta)/\Delta C=(C_2\delta_2-C_1\delta_1)/(C_2-C_1)$ plotted against the mean concentration of SPFO, where δ_i is the chemical shift of the terminal CF_3 group in SPFO. For the purposes of comparison, the differential conductance data are also included. The value of $\Delta(C\delta)/\Delta C$ shows only a slight increase at concentrations corresponding to the first drop of $\Delta K/\Delta C$, indicating that the first micelle formed has only a small amount of SPFO. As the total

Figure 7.5. Differential chemical shift, $\Delta(C\delta)/\Delta C$, plotted against the mean concentration of SPFO of the equal molar mixture of SDS-SPFO (O), SPFO only (□), and SPFO in 0.0152N sodium chloride solutions (Δ). Differential conductance of equal molar mixture of SDS-SPFO plotted against the mean concentration of SPFO (●).

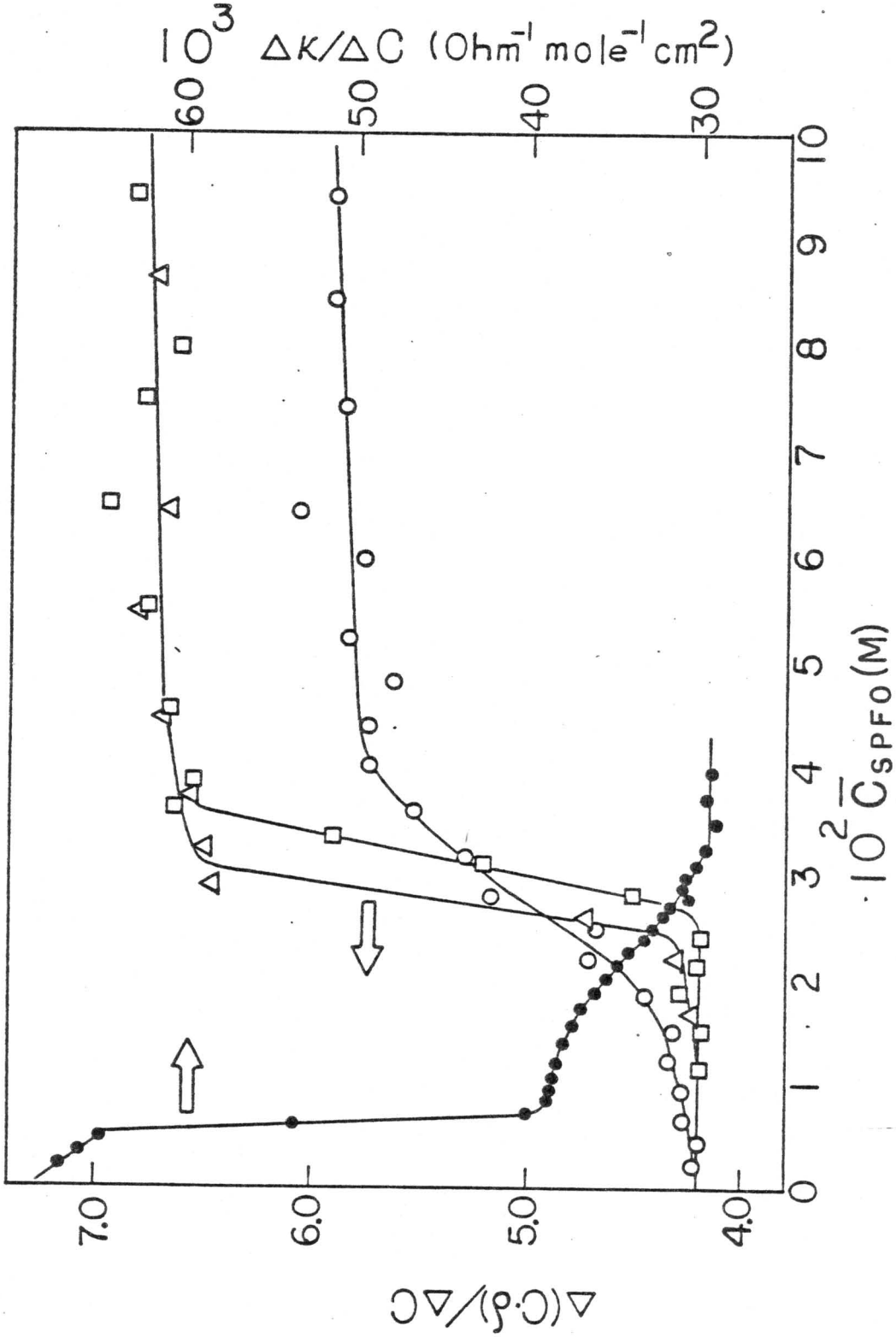
10^3 ΔK/ΔC (Ohm^{-1} mole^{-1} cm^2)
60
50
40
30
7.0
6.0
5.0
4.0
Δ(C.δ)/ΔC
0
1
2
3
4
5
6
7
8
9
10
$10^2 \bar{C}_{SPFO}$(M)

concentration increases, $\Delta(C\delta)/\Delta C$ shows little change before reaching the second inflection of $\Delta K/\Delta C$, suggesting that the micelles formed in this region do not change in composition very much. The rapid increase of $\Delta(C\delta)/\Delta C$, at about the second inflection point of $\Delta K/\Delta C$, followed by a leveling off to a constant value at higher concentrations is consistent with the formation of micelles composed mainly of SPFO. The limiting value of $\Delta(C\delta)/\Delta C$ is, however, significantly lower than that of the pure SPFO surfactant or in the presence of added salts. This result suggests that the micelles formed at high concentrations contain some SDS. The SDS content of these micelles appears to be low enough, however, to have only a minor effect on the second transition. As indicated by the $\Delta(C\delta)/\Delta C$ curves, the concentrations at the mid-point of the transition in the mixture is similar to the CMC of SPFO in the presence of added salt, the two systems having a comparable concentration of counterions at the CMC.

To explore further the nonideality effects and the possible "phase separation" in the micellar "phase", the theory of regular solutions for nonideal mixing of liquids is used. It is well known, that hydrocarbon fluorocarbon liquid mixtures are not described very well by this theory (160). Nevertheless, this theory using a single nonideality parameter is the simplest one to use and should account for the gross behavior of mixed micelles.

7.3.4. Regular Solutions

In a binary mixture, if the two components exhibit completely random mixing and satisfy all the conditions to form an ideal solution except that the interchange energy is not zero, the partial vapor pressure of component i over the mixture is related to the vapor pressure of the pure liquid by the relation (161)

$$\frac{P_i}{P_i^o} = Y_i \exp[(1-Y_i)^2(\omega/RT)] \qquad [7\text{-}9]$$

where ω is the interchange energy, and R and T are the gas constant and absolute temperature, respectively. The mutual solubility and conditions for phase separation, under this approximation, depend solely upon the value of ω/RT. When ω/RT equals 2, the system is in a critical mixing condition. For any value of $\omega/RT > 2$, two phases coexist in the system.

One can rewrite Equation 7-1 in analogy to Equation 7-9 for the binary mixtures of surfactants as

$$\frac{C_{im}}{C_{ig}} = Y_i \exp[(1-Y_i)^2(\omega/RT)]. \qquad (7\text{-}10]$$

By combing Equation 7-10 with Equations 7-2 to 7-4, one then obtains for component 1,

$$\ln\frac{Y_1}{X_1}+K_1 \ln C_{1a}+(1-Y_1)^2\frac{\omega}{RT} = K_1 \ln C_m \qquad [7\text{-}11]$$

and

$$\ln\frac{Y_1^u}{1-Y_1}+[u(1-Y_1)^2-Y^2]\frac{\omega}{RT}+\ln\frac{X_1^u}{1-X_1} = uK_1\ln\frac{C_{1a}}{C_{2a}} \qquad [7\text{-}12]$$

where $u=\frac{K_2}{K_1}$.

The formulas for component 2 are analogous.

The composition of the micelle in terms of Y_i values and the observed CMC, C_m, of a binary mixture can, therefore, be calculated by Equations 7-11 and 7-12. It has also been found that u can be assumed equal to unity in Equation 7-12 without introducing serious errors in either C_m or Y_i. A value of 1.645 has been used for both K_1 and K_2 in Equations 7-11 and 7-12 for the calculations of C_m and Y_i by using several different values of ω/RT for the SDeS-SPFO and SDS-SPFO systems as shown in Figures 7.3 and 7.6.

The observed CMC values of SPFO and SDS mixtures (Figure 7.3) are close to the calculated lines of nonideal mixing of micelles according to regualr solution theory using $\omega/RT=3.0$. As indicated by the micellar composition curve, Curve 6 of Figure 7.3, the first micelles formed in an equimolar mixture of SPFO with SDS contains very little

Figure 7.6. Observed CMC values of SPFO-SDeS mixtures at 25°C (O), and the expected CMC values (solid curves) and micellar compositions (dashed curves) calculated by Equation 7-11 and Equation 7-12, assuming $K_1=K_2=1.645$ and different values of ω/RT: curve 1 $\omega/RT=$ 1.7, curve 2 $\omega/RT=$ 2.0.

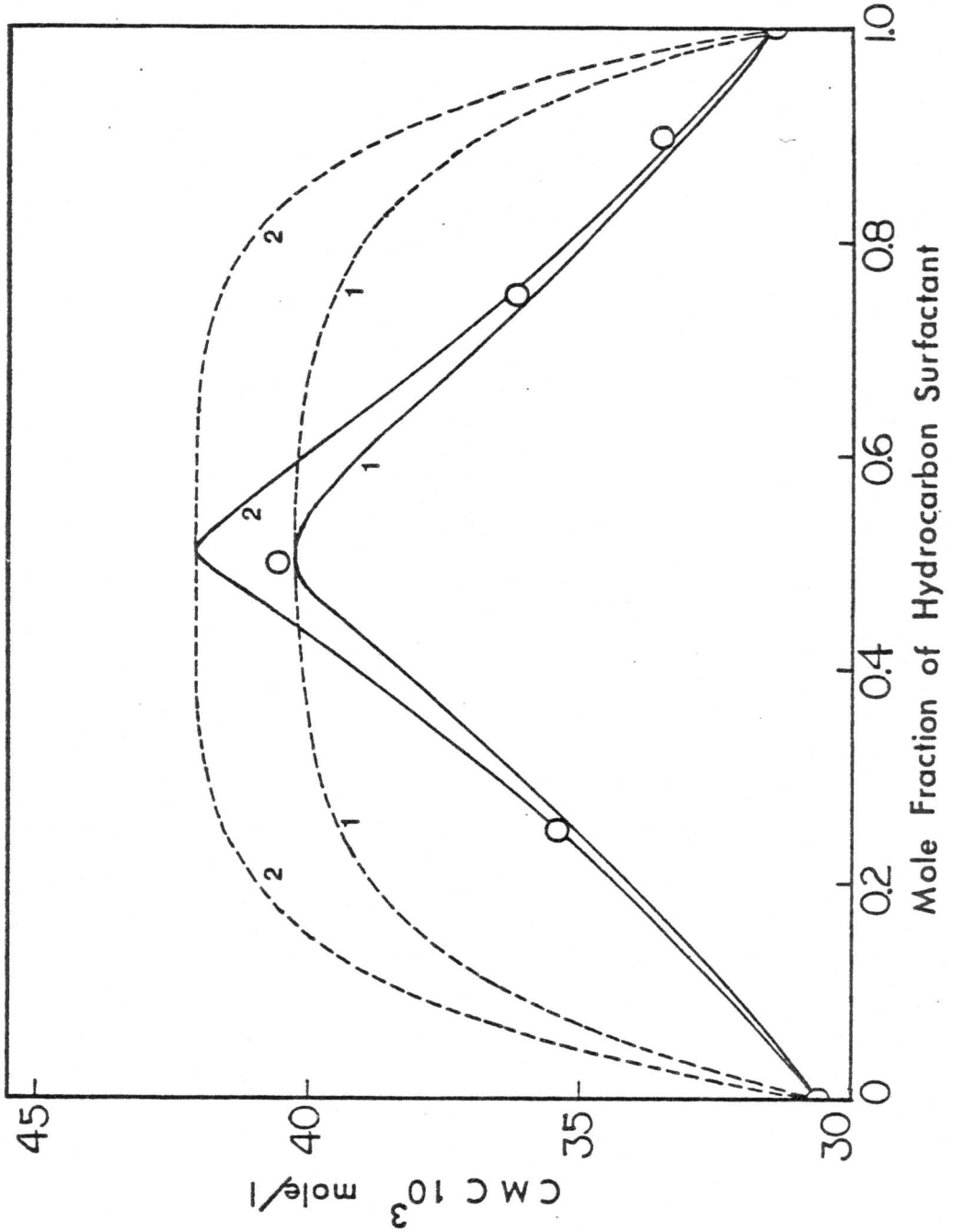
45
40
35
30
0
0.2
0.4
0.6
0.8
1.0
Mole Fraction of Hydrocarbon Surfactant
CMC 10³ mole/l
1
2
1
2
1
2

SPFO (as shown by the dotted lines). This is consistent with the previous observations based on the conductance and ^{19}F NMR chemical shift measurements at the concentration corresponding to the onset of the first micelles. As total concentration increases, the composition and concentrations of the monomers change gradually along the CMC curve towards the higher concentrations. The micellar composition shows only a slight change as the total concentration increases which is also consistent with the measured NMR chemical shift data of Figure 7.5. When the monomer concentration reaches the maximum value on the CMC curve, a new kind of micelle composed mainly of SPFO begins to form. The two different kinds of micelles, one rich in SPFO and the other in SDS, coexist in the solution. Further increases in the surfactant concentration will not change the composition or concentration of the monomers but will result in the formation of more micelles of the two different compositions. The two kinds of micelles, as indicated by the composition curve of Figure 7.3, contain less than 10% of the corresponding minor component. These results are in good agreement with the proviously drawn conclusion and explanations for the conductance and ^{19}F NMR data obtained from the SPFO and SDS mixtures.

The observed CMC values of SPFO-SDeS mixtures, on the

other hand, are slightly below the expected CMC line calculated by the regular solution model with an ω/RT value of 2.0, as shown in Figure 7.6, suggesting that the formation of two kinds of micelles ("phase separation") may not happen in these mixtures. The reported critical mixing temperature of perfluoro-n-heptane and n-heptane mixture is 50°C, and that for the perfluoro-n-heptane and isooctane mixture is about 25°C (160). It is possible that the cirtical mixing temperature for the SDeS and SPFO micelles may be below 25°C.

However, the micellar composition curve of SPFO-SDeS mixtures is not far from that calculated using $\omega/RT=1.7$, which is close to the point of phase separation. In view of the approximate nature of the treatment of micelles as a pseudo-phase, and the simplicity of the regular solution theory, the semi-quantitative agreement of the data with the theory is gratifying. For a more detailed analysis, it will be necessary to obtain information about the variation of micellar composition with concentration and to use more realistic mass-action models.

7.4. Conclusion

The severity of the nonideality of mixing between fluorocarbon and hydrocarbon surfactants is clearly indicated in the CMC's, the differential conductance and ^{19}F NMR

data of mixtures of SPFO with SL, SDeS, or SDS surfactants. The analysis of the experimental data and their comparison with a simple regular solution model also indicates that the partial miscibility between perfluorocarbon and hydrocarbon surfactant micelles is to be expected under certain circumstances. The present observations, along with some others on the anomalous behavior of partially fluorinated surfactants, suggest that effects due to this nonideality may be widespread and may significantly affect the properties of systems involving fluorocarbon-hydrocarbon interactions.

8. REFERENCES

1. K.J. Mysels and P. Mukerjee, in IUPAC, Commission on Colloid and Surface Chemistry, published in Pur and App. Chem.,51, 1083 (1979).

2. P. Mukerjee, in "Encyclopaedic Dictionary of Physics", Pergamon Press, New York.

3. P. Mukerjee, Ber. Bunsenges. Phys. Chem.,82,931(1978).

4. K.L. Mittal and P. Mukerjee, in "micellization, Solubilization, and Microemulsions", vol.1,Ed. by K.L. Mittal, Plenum Press, (1977).

5. P. Mukerjee, Advan. Colloid Interface Sci.,1,241(1967).

6. E.M.L. McBain and E. Hutchinson, "Solubilization and Related Phenomena", Academic Press, New York,(1955).

7. P.H. Elworthy, A.T. Florence, and C.B. Macfarlane, "Solubilization by Surface Active Agents and Its Applications in Chemistry and the Biological Sciences", Chapman & Hall, London, (1968).

8. K. Shinoda, T. Nakagawa, B. Tamanushi, and T. Isemura, "Colloidal Surfactants", Academic Press, New York(1963).

9. E. Cordes, Ed. "Reaction Kinetics in Micelles",Plenum Press, New York-London (1973).

10. J.H. Fendler and E.J. Fendler, "Catalysis in Micellar and Macromolecular Systems", Academic Press (1975).

11. G. Hartley, "Aqueous Solutions of Paraffin Chain Salts", Hermann, Paris (1936).

12. C. Tanford, "The Hydrophobic Effect", Wiley, New York (1973).

13. R.A. Moss and R.C. Nahas, in "Micellization, Solubilization, and Microemulsions", vol.2,Ed. by K.L. Mittal, Plenum Press (1977).

14. M. Grätzel, in "Micellization, Solubilization, and Microemulsions", Ed. by K.L. Mittal, vol.2,Plenum Press (1977).

15. A.J. Frank, in "Micellization, Solubilization, and Microemulsions", Ed. by K.J. Mittal, vol.2,Plenum Press (1977).

16. J.W. McBain, Trans. Faraday Soc.,9, 99 (1913).

17. J.W. McBain, in "Colloid Chemistry", Ed. by J. Alexander vol. 5, pp.102, Reihold Publishing Co.,New York (1944).

18. J. Swarbrick, J. Pharm. Sci.,54, 1229 (1965).

19. P. Molyneux and H.P. Frank, J. Amer. Chem. Soc.,85, 3169 (1961).

20. P. Molyneux and H.P. Frank, J. Amer. Chem. Soc.,85, 3175 (1961).

21. D.L. Wedderburn, in "Advances in Pharmaceutical Sciences" Ed. by M.S. Bean, A.M. Beckett, and J.E. Carless, vol.1, Academic Press, New York (1964).

22. G.M. Miyawaki, N.K. Patel, and H.B. Kostenbauder, J. Pharm. Assn.,Sci. Ed.,48, 315 (1958).

23. P. Mukerjee and E.R. Johnson, Unpublished results.

24. R.L. Healy and R.L. Reed, Soc. Pet. Eng.J.,14,491 (1974)

25. P. Mukerjee, J. Pharm. Sci.,63, 972 (1974).

26. D. Stigter and J.Th.G. Overbeek, Proc. Int. Cong. Surface Activity, 2nd, 1, 311 (1957).

27. P. Mukerjje, in "Micellization, Solubilization, and Microemulsions", Ed. by K.L. Mittal, vol.1,pp171, Plenum Press (1977).

28. D. Stigter, J. Phys. Chem.,78, 2480 (1974).

29. N. Muller, in "Reaction Kinetics in Micelles",Ed.by E. Cordes, pp.1, Plenum Press (1973).

30. F. Huisman, Proc. Kon. Ned. Akad. Wetensch.,Ser. B,67, 388,407,(1964).

31. P. Mukerjee, J. Phys. Chem.,69,4038 (1965).

32. P. Mukerjee and A.K. Ghosh. J. Amer. Chem. Soc.,92,6419, (1970).

33. D.G. Duff and C.H. Giles, in "Water, A Comprehensive Treatis", Ed. by F. Frank, vol. 4,pp.169,Plenum Press (1975).

34. G. Zografi, D.E. Auslander, and P.L. Lytell, J. Pharm. Sci., 53, 573 (1964).

35. M.A. Spirtes and P.S. Guth, Biochem.Pharmacol.,12, 37 (1963).

36. A.R. Freeman and M.S. Spirtes, Biochem. Pharmacol., 12, 47 (1963).

37. P.M. Seeman and H.S. Baily, Biochem. Pharmacol., 12, 1184 (1963).

38. A.K. Ghosh and P. Mukerjee, J.A.C.S.,92,6408 (1970).

39. P. Mukerjee and A.K. Ghosh, J.A.C.S., 92,6403 (1970).

40. A.K. Ghosh and P. Mukerjee, J.A.C.S., 92, 6413 (1970).

41. A.K. Ghosh, J.A.C.S., 92, 6415 (1970).

42. P.O. Ts'o, in "The molecular Association in Biology", Ed. by B. Pullman,pp.39, Academic Press (1968).

43. D.M. Small, Advan. Chem. Ser., 84, 31 (1968).

44. D.M. Small, in "The Physical Chemistry of Cholanic Acid" Chapter 8 of "The Bile Acids", Ed. by P.P. Nair and D. Kritchevsky, Plenum Press (1970).

45. K. Fontell, Colloid-Z.u.Z. Polymers,24, 253 (1971).

46. P. Mukerjee and J.R. Cardinal,J.Pharm.Sci.,65,882(1976).

47. H. Brockerhoff and R.G. Jensen, in "lipolypic Enzymes" Academic Press, New York (1974).

48. A.F. Hofman and B. Borgstrom,J.Clin.Invest.,43,247(1964).

49. R.J. Vonk, P. Jekel, and D.K.F. Miejer, Naunyn Schmie Deberg's Arch. Pharmacol.,290, 375 (1975).

50. G.E. Gibson and E.L. Forker, Gastroenterology,66,1046 (1974).

51. J.A. Reynolds and C. Tanford, J. Biological Chem.,245, 5161 (1970).

52. S. Lewin, "Displacement of Water and Its Control of Biochemical Reactions", Academic Press (1974).

53. G. Felsenfeld and H.T. Miles, Ann. Rev. Biochem.,36, Part II, pp.407 (1967).

54. K.L. Mitall, Ed.,"Micellization, Solubilization, and Microemulsions", vol. 2, Plenum Press (1977).

55. E.A.G. Aniansson and S.N. Wall, J. Phys. Chem.,78, 1024 (1974), and ib id.,79,857 (1975).

56. P. Becher, "Emulsions: Theory and Practice", 2nd Ed., Reinhold Publishing Co., (1965).

57. P. Mukerjee, J. Phys. Chem., 76, 565 (1972).

58. I. Reich, J. Phys. Chem.,60, 257 (1956).

59. E.W. Anacker and H.M. Ghose, J. Amer. Chem. Soc.,90, 3161 (1968).

60. E.W. Anacker and H.M. Ghose, J. Phys. Chem.,67, 1713 (1963).

61. J.M. Corkill and T. Walker, J. Colloid Interface Sci., 39, 621 (1972).

62. P. Mukerjee, in "Physical Chemistry: Enriching Topics From Colloid and Surface Science", Ed. by H. VanOlphen and K.J. Mysels, pp. 135,published by Theorex,La Jolla, California (1975).

63. P.J. Flory, "Principles of Polymer Chemistry", Cornell University Press, Ithaca, New York (1953).

64. L.R. Fisher and D.G. Oakenfull, Rev. Chem. Soc.,6,25 (1977).

65. P. Mukerjee and K.L. Mysels,"critical Micelle Concentrations of Aqueous Surfactant Systems",NSRDS-NBS 36 (1971), U.S. National Bureau of Standard.

66. J.N. Phillips, Trans. Faraday Soc.,51, 561 (1955).

67. K.J. Mysels and R.J. Otter, J. Colloid Sci.,16,462(1961).

68. H.S. Chung and I.J. Heilweil, J. Phys. Chem.,74,488 (1970).

69. D.G. Hall, J.C.S. Faraday Trans.II,68,668 (1972).

70. J. Oakes, Nature, 231, 38 (1971).

71. P. Mukerjee, J. Pharm. Sci.,60,1528 (1971).

72. P. Mukerjee, J. Pharm. Sci.,60,1531 (1971).

73. P. Mukerjee, J.R. Cardinal, and N.R. Desai, in "Micellization, Solubilization, and Microemulsions",vol.1, Ed. by K.L. Mitall, pp. 241 (1977), Plenum Press.

74. P. Mukerjee and J.R. Cardinal, J. Phys. Chem.,82,1620 (1978).

75. N.J. Turro, K.-C. Liu, and M.-F. Chow, Photochemistry and Photobiology, 26, 413 (1977).

76. P.R. Worsham, D.W. Eaker, and D.G. Whitten, J. Amer. Chem. Soc.,100, 7091 (1978).

77. R.J. Williams, J.N. Phillips, and K.J. Mysels, Trans. Faraday Soc.,51, 728 (1955).

78. H. Schott, J. Phys. Chem., 70, 2966 (1966).

79. M.S. Fernandez and P. Fromherz, J. Phys. Chem.,81, 1755 (1977).

80. P. Mukerjee and K. Banerjee, J. Phys. Chem.,68,3567 (1964).

81. N.J. Turro,M.W. Geiger, R.R. Hautala, and N.E. Schore, in "Micellization, Solubilization, and Microemulsions", Ed. By K.L. Mittal, vol. 1,pp75, Plenum Press (1977).

82. K. Kalyanasundaram and J.K. Thomas, J. Phys. Chem.,81, 2176 (1977).

83. H.-C. Chiang and A. Lukton, J. Phys. Chem.,79,1935 (1975).

84. R.C. Mast and L.V. Haynes, J. Colloid Interface Sci., 53, 35 (1975).

85. P. Horowitz, J. Colloid Interface Sci.,61, 197 (1977).

86. K.S. Birdi, T. Krag, and J. Klausen, J. Colloid Interface Sci.,62,562 (1977).

87. N,J, Turro and A. Yekta, J. Amer. Chem. Soc.,100,6951 (1978).

88. N. Funasaki, J. Colloid Interface Sci.,60,54(1977); ibid.,62, 336 (1977); ibid.,62,189 (1977).

89. E.D. Goddard, C.A.J. Hoeve, and G.C. Benson, J. Phys. Chem.,61, 593 (1957).

90. K. Shigehare, Bull. Chem. Soc.,Japan,38, 1700 (1965).

91. T.S. Brun, H. Høiland, and E. Vikingstad, J. Colloid Interface Sci.,63,89 (1978).

92. E. Vikingstad, A. Skauge, and H. Høiland,J. Colloid Interface Sci.,66, 240 (1978).

93. M. Gratzel and J.K. Thomas, J. Amer. Chem. Soc.,95, 6885 (1973).

94. M. Shinitzsky, A.C. Dianonx, C. Gitler, and G. Weber, Biochemistry, 10, 2106 (1971).

95. M. Almgren. F. Grieser, and J.K. Thomas, J. Amer. Chem. Soc.,101, 279 (1979).

96. C. Jolicoeur and H. Friedman, J. Solution Chem.,7,813 (1978).

97. J. Oakes, J. Chem. Soc.,Faraday Trans.II,68,1464(1972).

98. H. Yoshioka, J. Colloid Interface Sci.,66, 353 (1978).

99. J. Clifford and B.A. Pethica, Trans. Faraday Soc.,61, 182 (1965).

100. J. Clifford, Trans. Faraday Soc.,61, 1276 (1965).

101. F. Podo, A. Ray, and G. Nemethy, J. Amer. Chem. Soc., 95, 6164 (1973).

102. K.D. Lawson and T.J. Flautt. J. Phys. Chem.,69,3204 (1965).

103. C.J. Clemett, J. Chem. Soc.,(A),2251 (1970).

104. A.A. Ribeiro and E.A. Dennis, in "Colloid and Interface Science", Ed. by M. Kerker, vol.2,pp.325,Academic Press (1976).

105. N. Muller and R. Birkhahan, J. Phys. Chem.,71,957(1967); ibid.,72, 583 (1968).

106. N. Muller and T.W. Johnson, J. Phys. Chem.,73,2042(1969).

107. N. Muller and F.E. Platko, J. Phys. Chem.,75,547(1971).

108. N. Muller and H. Simsohn, J. Phys. Chem.,75,942(1971).

109. P. Mukerjee and K.J. Mysels, in "Colloidal Dispersions and Micellar Behavior", Ed. by K.J. Mittal, Amer. Chem. Soc. Symp. Ser.,No.9,239 (1975).

110. P. Mukerjee and A.Y.S. Yang, J. Phys. Chem.,80,1388 (1976).

111. J.L. Kurz, J. Phys. Chem.,66,2239 (1962).

112. D. Stigter and K.J. Mysels, J. Phys. Chem.,59,45(1955).

113. D. Stigter, J. Phys. Chem.,68,3603 (1964).

114. P. Mukerjee and A. Ray, J.Phys. Chem.,70,2144 (1966).

115. A. Ray and P. Mukerjee, J.Phys. Chem.,70,2138 (1966).

116. E.J.W. Verwey and J.TH.G. Overbeek,"Theory of the Stability of Lyophobic Colloids", Elsevier Publishing Company (1948).

117. F.H. Quina and H. Chaimovich, J. Phys. Chem.,83,1844 (1979).

118. N. Funasaki, J. Phys. Chem.,83, 1998 (1979).

119. N. Funasaki, J. Colloid Interface Sci.,64,461 (1978).

120. M. Almgren and R. Rydholm, J. Phys. Chem.,83,360(1979).

121. E.J.R. Sudholter and J.B.F.N. Engberts, J. Phys. Chem., 83, 1854 (1979).

122. T. Nakagawa and F. Tokiwa, in "Surface and Colloid Science", Ed. by E. Matijevic, vol.9,pp.69,John Wiley & Sons (1976).

123. P. Mukerjee, J. Perrin, and E. Witzke, J. Pharm. Sci., 59, 1513 (1970).

124. C. Wagner, Physik. Z.,25,474 (1924).

125. R.U. Lemieux, in "Methods in Carbohydrate Chemistry", Ed. by R.L. Whistler and M.L. Wolfrom, vol. II,pp.221, Academic Press (1963).

126. C.R. Noller and W.C. Rockwell, J. Amer. Chem. Soc.,60, 2076 (1938).

127. K.S. Shinoda, T. Yamanaks, and K. Kinoshita, J. Phys. Chem.,63,647 (1959).

128. P.H. Elworthy and K.J. Mysels.,J. Colloid Sci.,21,331 (1966).

129. K.J. Mysels and A.T. Florence, in "Clean Surface: Their Preparation and Characterization For Interfacial Studies" Ed. by G. Goldfinger, pp. 227, Marcel Dekker,Inc.,(1970).

130. T. Usui, J. Biochem.,54, 283 (1963).

131. K.A. Conners,"A Textbook of Pharmaceutical Analysis", 2nd Ed.,Wiley-Interscience (1975).

132. R.P. Cory, R.R. Becker, R. Rosenbluth, and I. Isenberg, J. Amer. Chem. Soc.,90, 1643 (1968).

133. K.J. Mysels, J. Phys. Chem.,65, 1081 (1961).

134. C. Bodea and I. Silberg, Advan. Heterocyclic Chem.,9, 321 (1968).

135. P. Mukerjee and K.J. Mysels, J. Amer. Chem. Soc.,77, 2937 (1955).

136. P. Mukerjee, K.J. Mysels, and P. Kapauan, J. Phys. Chem. 71, 4166 (1967).

137. C.A. Parker, "Photoluminescence of Solutions", Elsevier Publishing Co., Amsterdam,London,New York (1968).

138. T.J. Porror and R.E. Anacreon, Perkin-Elmer Co.,UV/ Fluorescnece Product Department, Technical Memo Number 95, November 2 (1971).

139. K.J. Mysels and R.J. Otter, J. Colloid Sci.,16,462(1961).

140. K.J. Mysels and R.J. Otter, J. Colloid Sci.,16,474(1961).

141. K.J. Mysels, J. Colloid Interface Sci.,66,331 (1978).

142. V.H. Lange and K.-H. Beck, Kolloid-Z. u. Z. Polymer, 251, 424 (1973).

143. N. Nishikido, J. Colloid Interface Sci.,60,242 (1977).

144. G.J.T. Tiddy and B.A. Wheeler, J. Colloid Interface Sci.,47, 59 (1974).

145. H.E. Gerry, P.T. Jacobs, and E.W. Anacker, J. Colloid Interface Sci.,62, 556 (1977).

146. N. Thoai, J. Colloid Interface Sci.,62, 222 (1977).

147. T. Kuwamura, M. Ohihima, and E. Kameyama, Nippon Kay. Kai.,3, 545 (1974).

148. L.A. Shifts, N.A. Safronova, P.A. Rebinder, and B.N. Maksimov, Akad. Nauk. SSSR, Proceedings Phys. Chem., Sect.,180, 369 (1968).

149. R.A. Pyter, Master Thesis, University of Wisconsin, Madison (1976).

150. "Carbon-Fluorine Compounds, Chemistry, Biochemistry, and Biological Activities", Ciba Foundation Symposium, Elsevier, New York (1972).

151. N.J.M. Birdsall, A.G. Lee, Y.K. Levine, and J.C. Metcalfe, Biochim. Biophys. Acta.,241, 693 (1971).

152. N. Muller and R. Mead, Jr., Biochemistry,12,3831(1973).

153. J. Johnson and N. Muller, Biochemistry,9, 1943(1970).

154. M. Smith and N. Muller, Biochemical and Biophysical Research Communications,62, 723 (1975).

155. E. Zeffren. Arch. Biochem. Biophys.,137, 219 (1970).

156. K.L. Gammon, S.H. Smallcombe, and J.H. Richard, J. Amer. Chem. Soc.,94,4673 (1972).

157. J.T. Gerig and R.A. Rimesman, J. Amer. Chem. Soc.,94, 7558 (1972).

158. B.D. Sykes, J. Amer. Chem. Soc.,91,949 (1969).

159. P. Garrett, J. Colloid. Interface Sci.,69,107 (1979).

160. J.H. Hildebrand, J.M. Prausnitz, and R.L. Scott, "Regular and Related Solutions",Van Nostrand Reinhold, New York (1970).

161. E.A. Guggenheim,"Thermodynamics", 5th Ed.,North-Holland Publishing Co.,(1967).

162. J.H. Hildebrand, J. Amer. Chem. Soc.,51,66 (1929).

163. J.B. Gilmour, J.O. Zwicker, J. Katz, and R.L. Scott, J. Phys. Chem.,71,3259 (1967).

164. R.L. Scott, J. Phys. Chem.,62, 136 (1958).

165. H.B. Klevens and M.J. Raison, J. Chimie,51,1 (1954).

166. J.C. Eriksson, A. Johansson, and L.O. Andersson, Acta Chem. Scand.,20,2301 (1966), and reference therein.

167. B.R. Donaldson and J.C.P. Schwarz, J. Chem. Soc.,Phys. Org. Section, 395 (1968).

168. P.A. Arrington, A. Clouse, D. Doddrell, R.E. Dunlop, and E.H. Cordes, J. Phys. Chem.,74, 665 (1970).

169. J.F. Yan and M.B. Palmer, J. Colloid Interface Sci., 30, 177 (1969).

170. F. Tokiwa and K. Tsujii, J. Phys. Chem.,75,3560(1971).

171. A.T. Florence and R.T. Parfitt, J. Phys. Chem.,75, 3554 (1971).

172. B.-O. Persson, T. Drakenberg, and B. Lindman, J. Phys. Chem.,80, 2124 (1976).

173. U. Henriksson and L. Ödberg, J. Colloid. Interface Sci. 46, 212 (1974).

174. A.A. Ribeiro and E.A. Dennis, Biochem.,14, 3746(1975).

175. H. Gustarsson and B. Lindman, J. Amer. Chem. Soc.,97, 3923 (1975).

176. I.D. Robb and R. Smith, J. Chem. Soc.,Faraday Trans., I, 70, 287 (1974).

177. I.D. Robb, J. Colloid Interface Sci.,37,521 (1971).

178. N. Schönfeldt, "Surface Active Ethylene Oxide Adducts", Pergamon Press, New York (1969).

179. T. Axenrod and G.A. Webb, Ed.,"NMR Spectroscopy of Nuclei Other Than Protons", Chapter 9, John Wiley & Sons New York (1974).

180. J.W. Emsley, J. Feeney, andL.H. Sutchiffe, "High Resolution Nuclear Magnetic Resonance Spectroscopy", vol. 2, Chapter 11, Pergamon Press (1966).

181. J.W. Emsley and L. Phillips, Molecular Physics,11, 437 (1966).

182. D.F. Evans, Proc. Chem. Soc.,115 (1958).

183. I.S. Forrest, C.J. Carr, and E. Usdin, Ed.,"phenothiazine and Structurally Related Drugs", Raven Press, Publishers, New York (1974).

184. A Burger, Ed. "Drugs Affecting the Central Nervous System", vol. 2, Marcel Dekker, Inc.,(1968).

185. M. Gordon, Ed.,"psychopharmacological Agents", vol.II, Academice Press (1967).

186. E.F. Domino, R.D. Hudson, and G. Zografi, in "Drugs Affecting The central Nervous Systems", Chapter 8, Ed. by A. Burger, Marcel Dekker, Inc.,(1968).

187. A.T. Florence, Adv. Colloid Interface Sci.,2,115(1968).

188. K. Shinoda, M. Hato, and T. Hayashi, J. Phys. Chem., 76, 909 (1972).

189. G. Zografi and M.V. Munshi, J. Pharm. Sci.,59,819(1970).

190. M.E. Kitler and P. Lamy, Pharmaceutica Acta Heluetial, 46, 483 (1971).

191. G. Zografi, D.F. Auslander, P.L. Lytell, J. Pharm. Sci., 53, 573 (1964).

192. G. Zografi and D.E. Auslander, J. Pharm. Sci.,54,1313 (1965).

193. R.M. Patel and G. Zografi, J. Pharm. Sci.,55,1345(1966).

194. G. Zografi and I. Zarenda, Biochemical Pharmacology,15, 591 (1966).

195. A. Attwood, A.T. Florence, and J.M.N. Gillan, J. Pharm. Sci.,63, 988 (1974).

196. J.M. Corkill, J.F. Goodman, T. Walker, and J. Wyer, Proc. Roy. Soc.,A,312, 243 (1969).

197. A.T. Florence and R.T. Parfitt, J. Pharm. Pharmacol., 22, Suppl. 1215 (1970).

198. L. Ravin and R. Warren, J. Pharm. Sci.,60,329 (1971).

199. M.C. Malmstrom and A.W. Cordes, J. Hetercycl. Chem., 10, 715 (1973).

200. M.J. Schick, Ed.,"nonionic Surfactants", Marcel Dekker, New York (1967).

201. A.T. Florence,in "Micellization, Solubilization, and Microemulsions", Ed. by K.L. Mittal, Plenum Press(1977).

202. K. Thoma and E. Vasters, Pharm. Ztg., 119,1430 (1974).

203. A. Felmeister and R. Schaubman, J. Pharm. Sci.,58,1232 (1969).

204. J.J.H. McDowell, in "phenothiazine and Structurally Related Drugs", Ed. by I.S. Forrest, C.J. Carr, and E. Usdin, Raven Press, New York (1974).

205. J.J. Kaufman and E. Kerman, in "Phenothiazine and Structurally Related Drugs", Ed. by I.S. Forrest, C.J. Carr, and E. Usdin, Raven Press, New York (1974).

206. J.C. Melrose and C.F. Brandner, J. Cand. Petrol. Technol. 13, 54 (1974).

207. S. Ross and J.P. Olivier, J. Phys. Chem.,63, 1671(1959).

208. I.S. Schmolka and A.J. Raymond, J. Amer. Oil Chem. Soc. 42, 1088 (1965).

209. W. Saski and S.G. Shah, J. Pharm. Sci.,54, 71 (1965).

210. A.M. Mankowich, J. Phys. Chem.,58, 1027 (1954).

211. J.M.G. Cowie and A.F. Sirianni, J. Amer. Oil Chem.Soc., 43, 572 (1966).

212. C.W. Dwiggins,Jr., R.J. Bolen, and H.N. Dunning, J. Phys. Chem.,64, 1175 (1960).

213. D.A. Allport and W.H. Janes, Ed."Block Copolymers", John Wiley & Sons, (1973).

214. G.E. Molau, Ed.,"Colloidal and Morphological Behavior of Block and Graft Copolymers", (1971).

215. T. Kotaka, T. Tanaka, M. Hattori, and H. Inagaki, Macromolecules,11, 138 (1978).

216. S.L. Aggarwal, Ed.,"Block Polymers".Plenum Press, New York, page 79, (1970).

217. T. Inoue, T. Soen, T. Hashimoto, and H. Kawai, J. Polymer Sci.,A-2,7, 1283 (1969).

218. J.E. Glass, J. Phys. Chem.,72, 4459 (1968).

219. G.N. Malcolm and J.S. Rowlinson, Trans. Faraday Soc., 53, 921 (1957).

220. P.H. Elworthy and A.T. Florence, Kolloid-Z. u. Z. Polymer, 208, 157 (1966).

221. B. Chew and A. Couper, Trans. Faraday Soc.,I,382(1973).

222. K.N. Prasad, T.T. Luong, A.T. Florence, J. Paris, C. Vaution, M. Seiller, and F. Puisieux, J. Colloid Interface Sci.,69, 225 (1979).

223. S.M. Blaug and S.S. Ahsan, J. Pharm. Sci.,50, 441(1961).

224. F. Shihah, J. Sprowls, and J. Nematollahi, J. Pharm. Sci.,60, 56 (1971).

225. A.D. Marcus, E. Weststein, and M. Ruderman, J. Amer. Pharm. ASsn.,17, 453 (1956).

226. S.E. Sheppard and A.L. Geddes, J. Amer. Chem.Soc.,66, 1995 (1944).

227. C. Robinson and J.L. Moilliet, Proc. Roy. Soc.,A143, 630 (1934).

228. C. Robinson and H.A.T. Mills, Proc. Roy. Soc.,A131, 576 and 596 (1931).

229. C. Robinson and H.E. Garrett, Trans. Faraday Soc.,35, 771 (1939).

230. C. Robinson, Proc. Roy. Soc.,A148, 681 (1935).

231. E. Valko, Trans. Faraday Soc.,31, 230 (1935).

232. P. Alexander and K.A. Stacy, Proc. Roy. Soc.,A212,274 (1952).

233. H.P. Frank, J. Colloid Sci.,12, 480 (1957).

234. R.G. Danzinger, A.F. Hofmann, L.J. Schoenfield, and J.L. Thistle, N. Engle. J. Med.,286, 1 (1972).

235. D.G. Oakenfull and L.R. Fisher, J. Phys. Chem.,81, 1838 (1977).

236. R Zana, J. Phys. Chem.,82, 2440 (1978).

237. M. Vandnere, R. Natarajan, and S. Lindenbaum, J. Phys. Chem.,84, 1900 (1980).

238. A.F. Hoffmann, Adv. Chem. Ser.,5, 53 (1968).

239. D.S. Blow and A. Rich, J. Amer. Chem. Soc.,82,3566(1960).

240. G. Sugihara, M. Tanaka, N. Nishikido, K. Isomura, and N. Yamanaka, Abstract, No. 167, Colloid and Surface Chemistry Division, Amer. Chem. Soc./Chem. Soc.,Japan, Chemical Congress Meeting, April 2, 1979, Honululu, Hawaii.

241. G. Sugihara, T. Ueda, S. Kaneshina, and M. Tanaka, Bull. Chem. Soc.,Japan,50, 604 (1977).

242. A.F. Hofmann and D.M. Small, Annu. Rev. Med.,18,333 (1967).

243. M.C. Carey and D.M. Small, Amer. J. Med.,49,590 (1970).

244. P. Ekwall, K. Fontell, and A. Sten, Proc. Int. Cong. Surf. Act., 2nd, 397 (1957).

245. K. Fontell, Kolloid-Z. u. Z. Polym.,244 246 (1971); ibid.,244, 253 (1971); ibid., 250, 333 (1972).

246. P. Mukerjee and N.A. Williams, unpublished results (1980).

247. L.R. Fisher and D.G. Oakenfull, J. Phys. Chem.,84, 937 (1980).

248. W.O. McClure and G.M. Edelman, Biochemistry,5,1908(1966).

249. E.M. Kosower and K. Tanizawa, Chem. Phys. Lett.,16,419 (1972).

250. E.M. Kosower, H. Dodiuk, K. Tanizawa, M. Ottolenghi, and N. Orbach, J. Amer. Chem. Soc.,97,2167 (1975).

251. C.J. Biaselle and D.B. Millar, Biophysical Chem.,3,355 (1975).

252. R.C. Mast and L.V. Haynes, J. Colloid Interface Sci., 53, 35 (1975).

253. C.J. Selisker and L. Brand, J. Amer. Chem. Soc.,93,5405 (1971).

254. K.S. Birdi, J. Phys. Chem.,81, 934 (1977).

255. K.S. Birdi, H.N. Singh, and S.U. Dalsager, J. Phys. Chem.,83, 2733 (1979).

256. J.P. Kratohvil and H.T. DelliColli, Can. J. Biochem., 46, 945 (1968).

257. L.B. Vittello, Ph.D. Thesis, Clarkson College of Technology, Potsdam, New York (1973).

258. Y. Chnag and J.R. Cardinal, J. Pharm. Sci.,67,174(1978).

259. R.P. Detoma, J.H. Easter, and L. Brand, J. Amer. Chem. Soc., 98, 5001 (1976).

260. Ch. Reichardt and K. Dimroth, Fortschr. Chem. Forsch., 11, 1 (1968).

261. Ch. Reichardt, Angew. Chem. Internat. Ed.,4,29 (1965).

262. T.W. Healy and L.R. White, Adv. Colloid Interface Sci., 9, 303 (1978).

263. G.S. Hartley and J.W. Roe, Trans. Faraday Soc.,36,101 (1940).

264. J.T. Davies and E.K. Rideal, "Interfacial Phenomena", Academic Press, New York (1961).

265. J.R. Cardinal and P. Mukerjee, J. Phys. Chem.,82,1614 (1978).

266. P. Mukerjee and N.R. Desai, Nature, 223, 1056 (1969).

267. P. Mukerjee and N.R. Desai, unpublished results (1971).

268. L.K.J. Tong and M.C. Glesmann, J. Amer. Chem. Soc.,79, 4305 (1957).

269. M.F. Perutz, Science, 201, 1187 (1978).

270. P. Läuger and B. Neumacke, in "Membranes", vol.2,pp. 1, Ed. by G. Eisenman, Marcel Dekker, Inc.,(1973).

271. L. Onsager and N.N.T. Samaras, J. Chem. Phys.,2,528 (1934).

272. G. Schwarz, Eur. J. Biochem.,12,442 (1970).

273. F.W. Schneider, C.C. Cronan, and S.K. Podder, J. Phys. Chem.,72, 4563 (1968).

274. N.S. Goel, Theoretical Biology,2, 213 (1972).

275. L.H. Feldman, A.H. Herz, and T.H. Regan, J. Phys. Chem., 72, 746 (1975).

276. G.S. Levinson, W.T. Simpson, and W. Curtis, J. Amer. Chem. Soc.,79, 4314 (1957).

277. R.E. Graves and P.I. Rose, J. Phys. Chem.,79,746(1975).

278. R. Steiger, R. Kitzing, R. Hagen, and H. Stoeckli-Evans, J. Photographic Sci.,22, 151 (1974).

279. L. Onsager, J. Chem. Phys.,2, 599 (1934).

280. A. Sanfeld, "Introduction to The Thermodynamics of Charged and Polarized Layers", Wiley-Interscience, New York (1968).

281. E.H. Cordes and R.B. Dunlap, Acct. Chem. Res.,2,329 (1969).

282. R.B. Dunlap and E.H. Cordes, J. Phys. Chem.,73, 361 (1969).

283. R.B. Dunlap and E.H. Cordes, J. Amer. Chem. Soc.,90, 4395 (1968).

284. A.J. Barr, J.H. Goodnight J.P. Sall,and J.T. Helwig, "A User's Guide to SAS, 76", Sas Institute Inc.,(1976)

285. K.J.Mysels and P. Kapauan, J. Colloid Sci.,481 (1961).

APPENDIX 1

NONLINEAR REGRESSION ANALYSIS OF SOLUBILIZATION DATA

The indicator ratios of ethyl red and quinoline blue solubilized in nonionic micelles (cf.3.3.1) were obtained by analyzing the experimental data based on Equation 3-5 by a nonlinear regression method. A "NLIN" subroutine of a SAS software system was used on an IBM 370 for this analysis. Equation 3-5 was transformed into the following formate in the computer program

$$R = (RA + A*RS*C)/(1 + A*C)$$

where RA = R_a, A = K_D, RS = R_s, and C = Φ_m/Φ_a.

The "NLIN" subroutine produces least-squares estimates by first performing a grid search within a specified boundary condition to determine the starting values for the coefficients RS and A. A modified Gauss-Newton iterative(284) method is then used to find the least-squares estimates until a pre-specified convergence criterion is fulfilled. The convergence criterion used was the difference between the last the current residual sum of squares less than 10^{-8}. No particular weight was imposed on any of the parameters. The computer program and out-put of the regression analysis are listed in the following pages.

Computer Program For Nonlinear Regression Analysis

PHDYE1.DATA

```
00010 DATA;
00020 INFILE AAA;
00030 INPUT RA C R;
00040 CARDS;
00050 TITLE PKA OF MICELLAR SOLUBILIZED DYE BY R VS. C;
00060 PROC PRINT;
00070 PROC NLIN BEST=10 METHOD=GAUSS;
00080 PARMS RS=0 TO 0.6 BY 0.002
00090 A=500 TO 2000 BY 10;
00100 BOUND RS =0 A =0;
00110 MODEL R=(RA+A*RS*C)/(1+A*C);
00120 DER.A=C*(RS-RA)/(1+A*C)**2;
00130 DER.RS=A*C/(1+A*C);
```

RESULTS OF ETHYL RED SOLUBILIZED IN OCTYL GLUCOSIDE MICELLES AT pH 5.01

NON-LINEAR LEAST SQUARES SUMMARY STATISTICS DEPENDENT VARIABLE R

SOURCE	DF	SUM OF SQUARES	MEAN SQUARE
REGRESSION	2	23.72308339	11.86154169
RESIDUAL	4	0.02104893	0.00526223
UNCORRECTED TOTAL	6	23.74413232	
(CORRECTED TOTAL)	5	4.39905616	

PARAMETER	ESTIMATE	ASYMPTOTIC STD. ERROR	ASYMPTOTIC 95% CONFIDENCE INTERVAL LOWER	UPPER
RS	0.23157476	0.06632917	0.04741794	0.41573157
A	1014.07165726	39.94495462	903.16818414	1124.97513038

ASYMPTOTIC CORRELATION MATRIX OF THE PARAMETERS

	RS	A
RS	1.000000	0.869486
A	0.869486	1.000000

RESULTS OF ETHYL RED SOLUBILIZED IN OCTYL GLUCOSIDE MICELLES AT pH 5.19

NON-LINEAR LEAST SQUARES SUMMARY STATISTICS DEPENDENT VARIABLE R

SOURCE	DF	SUM OF SQUARES	MEAN SQUARE
REGRESSION	2	15.69260418	7.84630209
RESIDUAL	6	0.01066594	0.00177766
UNCORRECTED TOTAL	8	15.70327012	
(CORRECTED TOTAL)	7	3.57200987	

PARAMETER	ESTIMATE	ASYMPTOTIC STD. ERROR	ASYMPTOTIC 95% CONFIDENCE INTERVAL LOWER	UPPER
RS	0.20080011	0.02981546	0.12784426	0.27375596
A	1367.79810816	36.05062584	1279.58534088	1456.01.87543

ASYMPTOTIC CORRELATION MATRIX OF THE PARAMETERS

	RS	A
RS	1.000000	0.835120
A	0.835120	1.000000

RESULTS OF ETHYL RED SOLUBILIZED IN OCTYL GLUCOSIDE MICELLES AT pH 5.58

NON-LINEAR LEAST SQUARES SUMMARY STATISTICS DEPENDENT VARIABLE R

SOURCE	DF	SUM OF SQUARES	MEAN SQUARE
REGRESSION	2	2.56588502	1.28294251
RESIDUAL	5	0.01726451	0.00345290
UNCORRECTED TOTAL	7	2.58314953	
(CORRECTED TOTAL)	6	0.37302826	

PARAMETER	ESTIMATE	ASYMPTOTIC STD. ERROR	ASYMPTOTIC 95% CONFIDENCE INTERVAL LOWER	UPPER
RS	0.08762292	0.05540789	-0.05480552	0.23005136
A	1000.18578200	110.39941812	716.39915636	1283.97240763

ASYMPTOTIC CORRELATION MATRIX OF THE PARAMETERS

	RS	A
RS	1.000000	0.894767
A	0.894767	1.000000

RESULTS OF ETHYL RED SOLUBILIZED IN BRIJ 35 MICELLES AT pH 5.01

NON-LINEAR LEAST SQUARES SUMMARY STATISTICS DEPENDENT VARIABLE R

SOURCE	DF	SUM OF SQUARES	MEAN SQUARE
REGRESSION	2	4.02021447	2.01010723
RESIDUAL	6	0.01283957	0.00213993
UNCORRECTED TOTAL	8	4.03305404	
(CORRECTED TOTAL)	7	0.45577652	

PARAMETER	ESTIMATE	ASYMPTOTIC STD. ERROR	ASYMPTOTIC 95% CONFIDENCE INTERVAL LOWER	UPPER
RS	0.04921631	0.05682122	-0.08982030	0.18825292
A	584.13914158	147.09227405	224.21705322	944.06122995

ASYMPTOTIC CORRELATION MATRIX OF THE PARAMETERS

	RS	A
RS	1.000000	-0.996076
A	-0.996076	1.000000

RESULTS OF ETHYL RED SOLUBILIZED IN BRIJ 35 MICELLES AT pH 5.64

NON-LINEAR LEAST SQUARES SUMMARY STATISTICS DEPENDENT VARIABLE R

SOURCE	DF	SUM OF SQUARES	MEAN SQUARE
REGRESSION	2	0.16997099	0.08498550
RESIDUAL	6	0.00075812	0.00012635
UNCORRECTED TOTAL	8	0.17072911	
(CORRECTED TOTAL)	7	0.01513080	

PARAMETER	ESTIMATE	ASYMPTOTIC STD. ERROR	ASYMPTOTIC 95% CONFIDENCE INTERVAL LOWER	UPPER
RS	0.02924493	0.01136810	0.00142816	0.05706169
A	821.80789248	79.76303253	626.63464204	1016.98114292

ASYMPTOTIC CORRELATION MATRIX OF THE PARAMETERS

	RS	A
RS	1.000000	0.933158
A	0.933158	1.000000

RESULTS OF QUINOLINE BLUE SOLUBILIZED IN OCTYL GLUCOSIDE MICELLES AT pH 4.22

NON-LINEAR LEAST SQUARES SUMMARY STATISTICS DEPENDENT VARIABLE R

SOURCE	DF	SUM OF SQUARES	MEAN SQUARE
REGRESSION	2	42.29746983	21.14873491
RESIDUAL	2	0.02453467	0.01226734
UNCORRECTED TOTAL	4	42.32200450	
(CORRECTED TOTAL)	3	8.93325361	

PARAMETER	ESTIMATE	ASYMPTOTIC STD. ERROR	ASYMPTOTIC 95% CONFIDENCE INTERVAL LOWER	UPPER
RS	0.00000000	0.12410349	-0.53398008	0.53398008
A	98000.00000000	3755.20345164	81842.48610863	114157.51389137

ASYMPTOTIC CORRELATION MATRIX OF THE PARAMETERS

	RS	A
RS	1.000000	0.894805
A	0.894805	1.000000

RESULTS OF QUINOLINE BLUE SOLUBILIZED IN OCTYL GLUCOSIDE MICELLES AT pH 4.94

NON-LINEAR LEAST SQUARES SUMMARY STATISTICS DEPENDENT VARIABLE R

SOURCE	DF	SUM OF SQUARES	MEAN SQUARE
REGRESSION	2	3.15985778	1.57992889
RESIDUAL	2	0.00423056	0.00211528
UNCORRECTED TOTAL	4	3.16408834	
(CORRECTED TOTAL)	3	0.59824501	

PARAMETER	ESTIMATE	ASYMPTOTIC STD. ERROR	ASYMPTOTIC 95% CONFIDENCE INTERVAL LOWER	UPPER
RS	0.00394996	0.05286307	-0.22350397	0.23140390
A	63071.77345823	3767.70055666	46860.48827308	79283.05864339

ASYMPTOTIC CORRELATION MATRIX OF THE PARAMETERS

	RS	A
RS	1.000000	0.900260
A	0.900260	1.000000

RESULTS OF QUINOLINE BLUE SOLUBILIZED IN OCTYL GLUCOSIDE MICELLES AT pH 5.34

NON-LINEAR LEAST SQUARES SUMMARY STATISTICS DEPENDENT VARIABLE R

SOURCE	DF	SUM OF SQUARES	MEAN SQUARE
REGRESSION	2	0.45168913	0.22584457
RESIDUAL	2	0.00051692	0.00025846
UNCORRECTED TOTAL	4	0.45220605	
(CORRECTED TOTAL)	3	0.05407029	

PARAMETER	ESTIMATE	ASYMPTOTIC STD. ERROR	ASYMPTOTIC 95% CONFIDENCE INTERVAL LOWER	UPPER
RS	0.00000000	0.02511496	-0.10806213	0.10806213
A	74074.00000000	5479.48044033	50497.43950938	97650.56049062

ASYMPTOTIC CORRELATION MATRIX OF THE PARAMETERS

	RS	A
RS	1.000000	0.947311
A	0.947311	1.000000

RESULTS OF QUINOLINE BLUE SOLUBILIZED IN BRIJ 35 MICELLES AT pH 4.22

NON-LINEAR LEAST SQUARES SUMMARY STATISTICS DEPENDENT VARIABLE R

SOURCE	DF	SUM OF SQUARES	MEAN SQUARE
REGRESSION	2	28.15264065	14.07632033
RESIDUAL	2	0.00589118	0.00294559
UNCORRECTED TOTAL	4	28.15853184	
(CORRECTED TOTAL)	3	1.24915371	

PARAMETER	ESTIMATE	ASYMPTOTIC STD. ERROR	ASYMPTOTIC 95% CONFIDENCE INTERVAL LOWER	UPPER
RS	0.50149221	0.10542563	0.04787735	0.95510708
A	98634.83473623	4805.45288180	77958.41262170	119311.25685076

ASYMPTOTIC CORRELATION MATRIX OF THE PARAMETERS

	RS	A
RS	1.000000	0.966321
A	0.966321	1.000000

RESULTS OF QUINOLINE BLUE SOLUBILIZED IN BRIJ 35 MICELLES AT pH 4.95

NON-LINEAR LEAST SQUARES SUMMARY STATISTICS DEPENDENT VARIABLE R

SOURCE	DF	SUM OF SQUARES	MEAN SQUARE
REGRESSION	2	1.07655710	0.53827855
RESIDUAL	2	0.00142045	0.00071022
UNCORRECTED TOTAL	4	1.07797755	
(CORRECTED TOTAL)	3	0.02577346	

PARAMETER	ESTIMATE	ASYMPTOTIC STD. ERROR	ASYMPTOTIC 95% CONFIDENCE INTERVAL LOWER	UPPER
RS	0.22014727	0.05176887	-0.00259865	0.44289316
A	123354.17132925	8552.92963439	86553.48099136	160154.86166714

ASYMPTOTIC CORRELATION MATRIX OF THE PARAMETERS

	RS	A
RS	1.000000	-0.776042
A	-0.776042	1.000000

RESULTS OF QUINOLINE BLUE SOLUBILIZED IN BRIJ 35 MICELLES AT pH 5.34

NON-LINEAR LEAST SQUARES SUMMARY STATISTICS DEPENDENT VARIABLE R

SOURCE	DF	SUM OF SQUARES	MEAN SQUARE
REGRESSION	2	0.21386257	0.10693129
RESIDUAL	2	0.00582797	0.00291399
UNCORRECTED TOTAL	4	0.21969055	
(CORRECTED TOTAL)	3	0.03369242	

PARAMETER	ESTIMATE	ASYMPTOTIC STD. ERROR	ASYMPTOTIC 95% CONFIDENCE INTERVAL LOWER	UPPER
RS	0.00000000	0.10489495	-0.45133152	0.45133152
A	64064.00000000	28914.04818132	-60344.47510976	188472.47510976

ASYMPTOTIC CORRELATION MATRIX OF THE PARAMETERS

	RS	A
RS	1.000000	0.966291
A	0.966291	1.000000